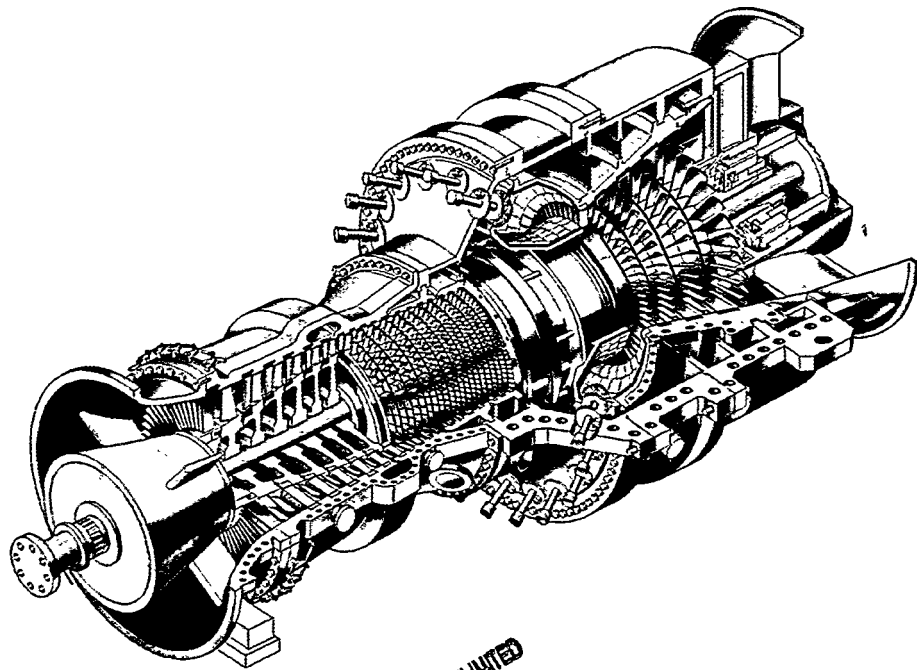


BALTICA IV MASTER

Plant Maintenance for Managing Life & Performance

Vol. 1



DISTRIBUTION OF THIS DOCUMENT IS UNLIMITED
FOREIGN SALES PROHIBITED

al



⚡ Helsinki Energy

IVO
GROUP

 **PVO GROUP**



TECHNICAL RESEARCH CENTRE OF FINLAND

ESPOO 1998

DISCLAIMER

Portions of this document may be illegible in electronic image products. Images are produced from the best available original document.

VTT SYMPOSIUM 184

Keywords:
power plants, maintenance, boilers, turbines,
condition monitoring, life management,
evaluation, performance

BALTICA IV
Plant Maintenance
for Managing Life & Performance
Vol. 1

Helsinki–Stockholm–Helsinki
7–9 September, 1998

Edited by

Seija Hietanen & Pertti Auerkari
VTT Manufacturing Technology

Organised by

VTT Manufacturing Technology



TECHNICAL RESEARCH CENTRE OF FINLAND
ESPOO 1998

ISBN 951-38-4577-X
ISSN 0357-9387

Copyright © Valtion teknillinen tutkimuskeskus (VTT) 1998

JULKAISIJA – UTGIVARE – PUBLISHER

Valtion teknillinen tutkimuskeskus (VTT), Vuorimiehentie 5, PL 2000, 02044 VTT
puh. vaihde (09) 4561, faksi 456 4374

Statens tekniska forskningscentral (VTT), Bergsmansvägen 5, PB 2000, 02044 VTT
tel. växel (09) 4561, fax 456 4374

Technical Research Centre of Finland (VTT), Vuorimiehentie 5, P.O.Box 2000, FIN-02044 VTT, Finland
phone internat. + 358 9 4561, fax + 358 9 456 4374

VTT Valmistustekniikka, Käyttötekniikka, Kemistintie 3, PL 1704, 02044 VTT
puh. vaihde (09) 4561, faksi (09) 456 7002

VTT Tillverknings teknik, Driftsäkerhetsteknik, Kemistvägen 3, PB 1704, 02044 VTT
tel. växel (09) 4561, fax (09) 456 7002

VTT Manufacturing Technology, Operational Reliability,
Kemistintie 3, P.O.Box 1704, FIN-02044 VTT, Finland
phone internat. + 358 9 4561, fax + 358 9 456 7002

Preface

A competitive plant must perform in a changing economical environment without compromising on safe service. This creates an optimisation task in which solutions are shaped by increasingly free market forces both in Europe and elsewhere, future costs of available fuels, the regulatory environment of the plant, and new or emerging technology that could set new standards for the industry.

All this affects not only new but also existing plants – and for both, these turbulent times offer plenty of opportunity to explore the technological basis for new solutions. The BALTICA IV Conference aims to provide state-of-the-art professional experience on current issues in plant maintenance for managing the life and performance of critically important systems and components.

Compared with earlier BALTICA Conferences the volume of combined presentations has again increased, hopefully reflecting the response by the BALTICA conference series to the needs of companies and professional personnel in this field. The first part of the programme and the publication are structured around major processes and subsystems in the plant, and the second part around technological viewpoints for tackling major issues or new trends.

The editors wish to express their sincere gratitude to the authors, referees, organisers and the Board of the Conference for their invaluable contribution in preparing the BALTICA IV Conference. Financial support by the CEC and other sponsoring organisations is also gratefully acknowledged.

Espoo, September 1998

Seija Hietanen

Pertti Auerkari

BALTICA IV Editors

Contents

Preface	3
Opening address	11
<i>H. Kleemola, Research Director, VTT Manufacturing Technology</i>	

Contents of Volume 1

Session 1: New technology for the competitive edge of present and future plants

High efficiency USC power plant - present status and future potential	13
<i>R. Blum & J. Hald</i>	
New ferritic steels for advanced steam plants	29
<i>K. H. Mayer & H. König</i>	
Optimizing power plant cycling operations while reducing generating plant damage and costs	39
<i>S. A. Lefton, P. M. Besuner, G. P. Grimsrud & A. Bissel</i>	
The Thematic Plant Life Assessment Network (PLAN)	65
<i>R. C. Hurst, D. McGarry, & H. H. Pedersen</i>	

Session 2: Gas turbines and combined cycle plants

Degradation of gas turbine coatings and life assessment	79
<i>N. S. Cheruvu</i>	
Cost-effectiveness of combustion turbines: recommendations for reliability, maintainability, supportability and maintenance requirements	93
<i>C. Meuwisse, A. Despujols, B. Givaudan & L. Lafage</i>	
Gas turbine cleaning upgrade (compressor wash)	105
<i>P. Asplund</i>	
Experience with restoration of the EBPVD coatings in stationary power gas turbines	119
<i>A. S. Osyka, A. I. Rybnikov, I. S. Malashenko & S. A. Leontiev</i>	

Structural transformations and temperature state of rotating blades of EI893 alloy under operation <i>G. D. Pigrova, A. I. Rybnikov & I. I. Kryukov</i>	131
 Session 3: Steam turbines	
Turbine maintenance and modernization <i>E. Unga</i>	141
Turbine casing bolts; a life assessment and bolt replacement strategy <i>J. H. Bulloch</i>	149
Super long-term creep tests of advanced HP and IP rotor steels <i>A. A. Tchizhik</i>	163
Effect of composition, heat treatment and processing technologies on the microstructure and properties of HP and IP rotors of large steam turbines from 1CrMoV steels <i>A. A. Tchizhik & T. A. Tchizhik</i>	175
Advances in processing technologies for titanium heat exchanger tubes of fossil and nuclear power plants <i>T. P. Likhareva, A. A. Tchizhik & N. N. Chavchanidze</i>	187
 Session 4: Boilers and steam systems	
Header integrity assessment <i>F. Rotvel, C. Sampietri, L. Verelst, H. van Wortel & L. Ying Zhi</i>	201
Predicting the creep life and failure mode of low-alloy steel weldments <i>J. M. Brear, C. J. Middleton & P. F. Aplin</i>	213
Type IIIa cracking at 2CrMo welds in 1/2CrMoV pipework <i>S. J. Brett & P. A. Smith</i>	225
Recent advances in condition assessment of components based on strain monitoring <i>J. D. Parker</i>	239
Life management of power plant based on structural damage testing <i>H. Tallermo, I. Klevtsov & V. Arras</i>	251

Can the lifetime of the superheater tubes be predicted according to fuel analyses? - Assessment from field and laboratory data <i>K. Salmenoja & K. Mäkelä</i>	261
Neural network for prediction of superheater fireside corrosion <i>P. Makkonen</i>	271
Cracking and corrosion recovery boiler <i>H. Suik</i>	283
Peculiar high temperature corrosion of martensite alloy under impact of Estonian oil shale fly ash <i>H. Tallermo, I. Klevtsov & M. Uus</i>	295
Formation of thermal fatigue cracks in periodic rapid quenching of metal <i>A. Ots</i>	305
Life extension of boilers using weld overlay protection <i>G. Lai, P. Hulsizer & R. Brooks</i>	319
Failure analyses and weld repair of boiler feed water pumps <i>R. van Vulpen</i>	331

Contents of Volume 2

Session 5: Evaluation and management systems

Power plant asset market evaluations: Forecasting the costs of power production <i>S. A. Lefton & G. P. Grimsrud</i>	353
The role of enterprise asset management system in PVO Group's business <i>J. Järvinen</i>	367
Advanced targeted monitoring of high-temperature components in power plants <i>E. Roos, K. Maile & A. Jovanovic</i>	379
An advanced maintenance advisory and surveillance system for boiler tubes - AMASS <i>A. B. Tomkings</i>	397
The role of predictive on-line monitoring systems in power generation industry <i>S. D. Gittings & J. Baldwin</i>	413
A solution for maintenance-related problems in the power generating industry <i>C. Delamarian & H. R. Kautz</i>	427
Integrated vibration-based maintenance: an approach for continuous reduction in LCC, a case study <i>B. Al-Najjar</i>	437
Performance measures for world class maintenance <i>A. W. Labib</i>	449
Methodology for quantitative assessment of technical condition in industrial systems <i>C. Steinebach & A. Sørli</i>	463

Session 6: Miniature specimen methods

- The application of miniature disc testing for the assessment of creep damage in CrMoV rotor steel 477
J. D. Parker, G. C. Stratford, N. Shaw, G. Spink & H. Metcalfe
- The small punch assessment of toughness losses in low alloy steels 489
J. H. Bulloch
- Small punch creep test: A promising methodology for high temperature plant components life evaluation 501
S. Tettamanti & R. Crudeli

Session 7: Developments in NDT and applications for structural integrity

- Computer-aided ultrasonic inspection of steam turbine rotors 511
K. H. Mayer, M. Weber & M. Weiss
- Ultrasonic test of highly stressed gear shafts 523
T. Schreiner, W. Heinrich, J. Achtzehn & G. Hensley
- The application of RBI-concept to ultrasonic measurement of fatigue cracks 535
J. Pitkänen, P. Särkiniemi & P. Kauppinen
- New unified fracture toughness estimation scheme for structural integrity assessment 543
K. Wallin, A. Bannister & P. Nevasmaa
- Towards a more consolidated approach to material data management in life assessment of power plant components 555
A. Jovanovic & K. Maile

Session 8: Developments and applications in evaluation of materials, in-service damage and component performance

- Examination of observed and predicted measures of creep cavitation damage accumulation 575
J. M. Brear, J. M. Church & G. Eggeler
- Modelling of creep damage development in ferritic steels 587
R. Sandström

Development of creep damage assessment system for aged thermal power plant	599
<i>I. Nonaka, H. Umaki, H. Nishida & H. Yamaguchi</i>	
Prediction of material creep behaviour for strain based life assessment applications	613
<i>J. H. Rantala, R. C. Hurst & F. Bregani</i>	
Creep crack growth in a reactor pressure vessel steel at 360°C	623
<i>R. Wu, F. Seitisleam & R. Sandström</i>	
Relaxation cracking in the process industry, an underestimated problem	637
<i>J. C. van Wortel</i>	

Opening address

Dear Colleagues,

On behalf of VTT Manufacturing Technology I have the pleasure of welcoming you to the BALTICA IV Conference on Plant Maintenance for Managing Life & Performance. The Conference, this being already the fourth in the series, has become an important meeting for reviewing the evolving technology.

Management of the life and performance of power plants is of considerable economic, environmental and community value. A reliable, environmentally sustainable and competitive production of energy is one of the cornerstones of modern society. However, attaining good plant performance requires a vast range of knowledge and technologies. This is clearly reflected in the programme of this conference. In addition to the use of materials and inspection technologies for evaluating and maintaining the reliability and safety of power plants, ever stronger emphasis is being placed on maintenance management and the application of information technology in predicting the behaviour of plants and their components. One essential feature of this conference is that the greater part of the work presented is application oriented. We therefore look forward to an interesting exchange of views between researchers and those involved in practical plant maintenance.

The presentations of the BALTICA IV Conference reflect a great variety of topics covering the whole range referred to above. Together with the contributions of the participants, an interesting and fruitful meeting is anticipated. Organising part of the conference on board a cruise ship will provide an easy forum for discussions and getting acquainted with other participants.

I would like to acknowledge the contribution of the International Board of the Conference and the Executive Committee in organising the Conference. It is also my pleasure to thank the authors for their presentations, the session chairmen, and all the participants for their contributions which will make this conference.

Prof. Heikki Kleemola
Research Director

VTT Manufacturing Technology

High efficiency USC power plant - present status and future potential

R. Blum, Fælleskemikerne I/S Fynsværket, Denmark

J. Hald, Elsam/Elkraft/TU Denmark, Denmark

Abstract

Increasing demand for energy production with low impact on the environment and minimised fuel consumption can be met with high efficient coal fired power plants with advanced steam parameters. An important key to this improvement is the development of high temperature materials with optimised mechanical strength. Based on the results of more than ten years of development a coal fired power plant with an efficiency above 50% can now be realised. Future developments focus on materials which enable an efficiency of 52-55%.

1 Introduction

During the last decades environmental issues and concerns about limitations in fossil fuel supply have had great impact on electricity generation. Alternative generation concepts based on biomass, wind, wave and sun energy have been developed, but even though great efforts are invested and major results have been achieved in these areas, generation concepts based on fossil fuels are and will still be the dominating source of electric energy.

In order to improve the performance of the fossil based generation concepts the main tasks over the last decade have been an optimisation of flue gas cleaning, deSO_x and deNO_x and an increase of the efficiency for minimisation of pollution and reduction of the energy consumption. For both gas turbine combined cycle plants and coal fired steam turbine plants an efficiency increase of 10 to 15% have been demonstrated during that time, thanks to the development of new advanced high temperature materials with improved mechanical strength. As coal seems to be the most important energy source world wide for electricity generation, Elsam has chosen the development of optimised coal fired power plants as the most important goal for the future. Optimisation of the thermodynamic process and development and qualification of new high temperature steels were the two main lines in this development. The development work has been performed in international collaboration, and

it consisted of theoretic studies, laboratory testing, in-plant testing and of the actual construction of plants with advanced steam parameters.

2 Materials problems

Basic obstacles to an increase in thermal efficiency of USC power plants are the limitations on steam parameters set by properties of the materials used in the steam cycle. Materials development is therefore of crucial importance to the further development of USC power plants. Through the work on USC plants Elsam have been able to pinpoint the key components in the steam cycle for which materials development is needed to increase steam parameters [1,2]. These components are:

- Thick section boiler components and steam lines
- Turbine rotors, casings, valves and bolts
- Superheaters
- Furnace panels

Descriptions of the nature of materials problems in these components are presented below together with new materials developed to overcome the problems.

2.1 Thick section boiler components and steam lines

Materials for thick section boiler components and steam lines need high creep strength, good thermal fatigue resistance and good fabricability. High creep strength allows reduced wall thickness, which assures good mechanical flexibility and low dead weight of steam lines. High thermal fatigue resistance and high creep strength assure high allowable temperature gradients in steam headers. Bending and welding of thick section materials, without undue degradation of properties, is essential for the construction of the plant.

In Denmark the martensitic 12CrMoV steel X20CrMoV121 has been used for steam headers and steam lines at steam temperatures typically 540°C and at pressures up to the supercritical 250bar. In the power plant Esbjergværket Unit 3 commissioned in 1992 the X20CrMoV121 steel was used to its limit at steam parameters 560°C/250bar.

An increase of steam parameters to USC values above 250bar/560°C required materials with higher creep strength. In the beginning of the 1960's a number of high temperature power plants were commissioned in UK and USA operating with steam temperatures up to 650°C. Construction materials for the thick section high temperature components were high creep strength austenitic steels.

Service experiences from these plants have been rather mixed. The plants were built for base load electricity generation, but due to cycling operation in combination with thick section austenitic components they have suffered a number of fatigue problems. A typical example is the Eddystone power plant in which the steam lines failed due to long term embrittlement and fatigue [3].

These experiences demonstrated that due to the inherently low fatigue strength of austenitic steels further USC development had to rely on the development of new ferritic/martensitic steels. And certainly it has been the development of the new high creep strength martensitic 9-12%Cr steels P91, P92 (NF616) and P122 (HCM12A) for thick section boiler components and steam lines, which has pushed forward the USC development.

2.1.1 P91

In the middle of the 1970s the steel P91 was developed in the USA for nuclear application by Oak Ridge National Laboratories and Combustion Engineering based on the 9Cr-1Mo tube steel P9. By optimization of the alloy composition with small amount of V, Nb and N the creep strength was considerably improved. Later it was realised, that the steel could also be used for conventional steam plant, and it was included in the ASME Code in 1984.

The first large scale application of the steel at USC steam parameters followed in the Kawagoe plants in Japan commissioned in 1988. In 1992 the steel was selected by Elsam to be used in the boilers and steam lines of the Danish USC plants Skærbæk and Nordjylland commissioned in 1997 and 1998. The steam parameters 290bar/580°C of these plants are close to the maximum capability for steel P91. The efficiency of the coal fired Nordjylland plant will be 47% [4].

2.1.2 P92 and P122

The Japanese steels NF616 and HCM12A are 9-12%Cr steels with app. 30% higher creep strength than P91. These steels can be used at USC steam conditions up to app. 325 bar/610°C, or up to 630°C steam temperature at lower pressures. NF616 was invented by Prof. Fujita at Tokyo University in the middle of the 1980's and further developed together with Nippon Steel Corporation [5,6]. HCM12A was developed by Sumitomo Metals and Mitsubishi Heavy Industries around 1990 [7]. The basic new alloying concept in these steels is to replace part of the Molybdenum with app. 1,8% Tungsten.

In the international research project EPRI RP1403-50 with participation of steel makers, boiler makers and utilities from Japan, USA, UK and Denmark, pipe production, pipe bending and welding procedures and long term creep data for the two steels were developed, and this led to ASME Code approval in 1994 as P92 (NF616) and P122 (HCM12A) in Code Cases 2179 and 2180 [8].

To demonstrate the viability of the NF616 steel a 1200 mm long test section of the steel was built into the main steam line at unit 3 of the Danish power plant Esbjergværket, which was commissioned in 1992. Annual inspections of the test section have shown no problems during more than 40,000 hours of operation at 560°C/250bar steam. In the project EPRI WO9000-30, which is the continuation of the EPRI RP1403-50 project, three test headers - two made of P92 and one made of P122 - have been built into the USC boiler at Nordjylland, which was commissioned in spring 1998. The headers were designed and approved according to ASME, and this demonstrates that the materials are now ready for use in large scale projects.

Recently the P122 and P92 have been selected for a number of USC plants in Japan [9] and Denmark. The list of USC plants is given in table 1.

Power Plant company	Tsurunga Hokuriku EPDC	Tachibanawan No.2 EPDC	Avedøre 2 SK-Energi
Manufacturer:			
Boiler	MHI	Babcock-Hitachi	FLS miljø-BWE
Steam line	MHI	Babcock-Hitachi	Stein Industrie
Capacity	700 MW	1050 MW	400 MW
Steam parameters	241bar/ 593°C/593°C	250bar/ 600°C/610°C	300bar/ 580°C/600°C
Materials:			
Headers	P122	P122/P92	P92
Steam lines	P122	P122	P92
Commissioning	2000	2001	2001

Table 1. USC plants under construction using P122 and P92.

2.1.3 E911

In Europe a parallel development of a W-alloyed 9%Cr steel E911 has been made in the COST 501 research project [10], and an installation of a demonstration test pipe bend has been made at the Danish USC power plant Skærbæk. The available creep test results however indicate that E911 is clearly weaker than P92.

An overview of chemical composition and creep properties of the new martensitic steels is presented in figure 1.

2.1.4 Long term creep data

One of the most demanding tasks for the validation of a new high temperature steel is the development of a comprehensive database of creep test results. For approval by the ASME a new steel needs tests with rupture times of at least 10,000 hours to establish allowable stresses. For general approval in Europe the international standard ISO 6303 should be followed. This means that rupture times of at least 30,000 hours for five melts of a new steel is needed to make a valid extrapolation to the 100,000 hour mean rupture strength to be used for design.

In Europe the European Creep Collaborative Committee ECCC is coordinating creep testing to share the testing effort between laboratories in different countries, to avoid duplication and to assure that long term tests are being made. Further, the ECCC has set up recommendations for extrapolation procedures to be followed when establishing creep strength values for steels to be included in new European steel standards and design codes [11].

Recently the ECCC has built up creep rupture databases for steels P91 and P92, and strength values for steel P91 has been established, figure 2. These values will be included in the new European standards. In 1998 European strength values for steel P92 will be established by ECCC.

2.2 Turbine materials

Turbine materials require high creep strength, good thermal fatigue resistance and good creep ductility and toughness through the life. This means that the martensitic 9-12%Cr steels as forged or cast components are used in advanced steam turbines. A number of new alloys have been developed for this purpose in Japan and Europe. In Europe this development has been made in the cooperative COST 501 program, which has resulted in 10%Cr-Mo-(W) steels for large forgings and castings. With these alloys turbines with live steam temperatures up to 610°C can be built, and the first deliveries of turbines with the new steels have followed [12].

In the COST program alloy development for steam turbines operating at steam temperatures up to 625°C is ongoing, and a 10%Cr-Mo-B steel has been developed, with sufficient strength for these conditions. The long term creep strength of this steel is ascertained by creep tests on test melts and on a small scale trial rotor. Recently a large 45 ton demonstration rotor forging has been manufactured [13].

In Japan a 12%Cr-W-Co alloy HR1200 developed by Prof. Fujita and HITACHI is expected to allow steam temperatures up to 650°C. A 80 ton demonstration rotor has been produced, but until now only short term creep tests are available for the HR1200 steel. In four to five years it will be clear if the long term strength of the steel will meet the expectations [14].

2.3 Superheaters

Final superheaters of advanced boilers require steels with high creep strength and good corrosion and oxidation resistance. The design temperature of the superheater is typically 35°C higher than the rated steam temperature and for special applications it might be more than 50°C. This means that austenitic steels must be used at advanced steam conditions. In the UK and in Germany a long service experience with the use of austenitic superheaters exists for steam temperatures up to 650°C [15,16].

In the Danish USC plants Skaerbaek and Nordjylland the austenitic 18%Cr-10%Ni steel TP347HFG - which is a fine-grained version of the well known TP347H steel - is used for the final superheaters at steam temperatures up to 580°C. The TP347HFG steel was developed by Sumitomo in Japan. It has excellent oxidation strength due to the fine-grained microstructure, and it can be used at advanced steam conditions up to app. 620°C steam temperature.

Depending on the design requirements further advanced austenitic steels are available with higher strength such as the 18%Cr-9%Ni-Cu steel Super304H [18] developed by Sumitomo, and the 20%Cr-25%Ni steel NF709 [18] developed by Nippon Steel. For severe corrosive loads the high chromium alloyed 25%Cr-20%Ni steel HR3C [19] developed by Sumitomo can be used.

With the more advanced steam conditions in USC plants, the management of superheater life problems become increasingly difficult. To handle these problems a detailed program for the calculation of superheater tube life has been developed by Elsam. The calculations include effects on creep life of fireside corrosion and of the rising metal temperature due to steam side oxidation [20]. With this program it has been possible to verify the behavior of the chosen candidate materials. Furthermore the calculations indicate that the most important factors for the life of a superheater is the fireside corrosion rate and the internal heat transfer coefficient. This means that more attention must be paid to high temperature corrosion when choosing tube materials for secondary reheaters than for superheaters.

A Brite-Euram research project to obtain long term corrosion data for superheater steels at high steam temperatures has been initiated. At unit 3 of power plant Esbjergværket superheater test loops have been installed with steam temperatures in the range 500-620°C. Test materials include the austenitic steels mentioned above as well as some martensitic 9-12%Cr steels exposed at lower temperatures. Exposure times up to 40.000 hours are foreseen. The project will produce detailed corrosion and oxidation data, which can be used for the design of advanced superheaters [21].

Chemical compositions and creep rupture strengths of new superheater steels are shown in figure 3.

2.4 Furnace panels.

Materials for furnace panels need corrosion and oxidation resistance combined with creep strength, and it is a prerequisite that these materials can be welded without requirement for post weld heat treatment. So far this has made the 1%Cr steel 13CrMo44 (T11) the only choice for furnace panels, and this limits the maximum steam temperature at the furnace outlet to app. 420°C. But due to high heat flux the furnace panel materials experience service temperatures much higher than this, and during service the material temperatures increase due to formation of oxides on the inside of the furnace tubes. In advanced USC boilers it is advantageous to increase the pressure and temperature of the water/steam in the furnace panels, and this means that the temperature increase during service accelerates, so materials with higher corrosion resistance and creep strength are needed.

The 2,25%Cr-W steel HCM2S [22] and the 12%Cr-Mo-W steel HCM12 [23] developed by Sumitomo and Mitsubishi and the 2,5%Cr-Mo steel 7CrMoVTiB1010 [24] developed by Mannesmann have far better strength values than the 13CrMo44. In order to use these materials in boilers it is necessary to demonstrate the fabricability without post weld heat treatment and to demonstrate service exposure during in-plant tests.

In Denmark test panels of HCM2S, HCM12 and 7CrMoVTiB1010 have been built into the nose of a subcritical once-trough boiler. During manufacture of the panels the weldability of the steels HCM2S and 7CrMoVTiB1010 without post weld heat treatment was fully demonstrated, and two years of successful operation with the test panels has recently been completed.

In connection with the in-plant test a computer furnace panel calculation

program has been set up to simulate the service exposure and life consumption of a furnace panel in a USC boiler during operation [25]. These calculations first of all demonstrate that the temperature rise during operation is strongly depending on the rate of self oxidation at media temperatures higher than app. 450°C and of the deposition rate of oxides coming from the feed water. High quality feed water chemistry assuring minimum oxide in feed water is therefore a must for USC plants with advanced steam parameters.

Further, our calculations demonstrated that the properties of the new 2,25Cr and 2,5Cr steels will allow for water/steam temperatures in the range 475-500°C at the outlet of the panels.

Compositions and creep rupture strengths of the furnace panel materials are shown in figure 4.

3 Summary and future aspects

Based on the knowledge achieved by participation in a large number of international materials research projects Elsam is convinced that all materials are now available for the construction of a USC plant with steam parameters 325bar/610°C/630°C/630°C and an efficiency approaching 50%. In table 2 the current status of materials development for USC power plants is summarised by showing the limitations on maximum live steam temperatures set by available materials for the key components. The example is for a 400MW USC power plant with live steam pressure of 325bar.

Material	Composition	Max. live steam temp. for pressure 325bar.
Furnace panels		
HCM2S	0,01C-2,25Cr-0,3Mo-1,6W-V-Nb-N-B	625°C
7CrMoTiB1010	0,07C-2,4Cr-1Mo-V-Ti-N-B	625°C
HCM12	0,1C-12Cr-1Mo-1W-V-Nb-N	650°C
Superheaters		
TP347HFG	18Cr-10Ni-1Nb	app. 620°C
Super 304H	18Cr-9Ni-0,4Nb-Cu-N	app. 625°C
NF709	20Cr-25Ni-1,5Mo-0,25Nb-0,05Ti-N	app. 630°C
HR3C	25Cr-20Ni-0,4Nb-N	app. 630°C
Thick section boiler comp.		
NF616	0,1C-9Cr-0,5Mo-1,8W-V-Nb-N-B	610°C
HCM12A	0,1C-11Cr-0,5Mo-1,8W-1Cu-V-Nb-N-B	610°C
Turbine rotors		
COST E/F	0,12C-10Cr-1Mo/1,5Mo-1W/0W-V-Nb-N	610°C
COST B	0,17C-9,5Cr-1,5Mo-0,01B-V-Nb-N	625°C
HR1200	0,09C-11Cr-0,2Mo-2,7W-2,5Co-V-Nb-N-B	(630-650°C)

Table 2. Materials for key components in USC power plants.

The USC development does however not stop here. Recently the demonstration project "Advanced ("700°C") PF Power Plant" funded by the European Commission under the THERMIE programme, has been initiated. The project involves a large group of major suppliers to the power industry and some of the leading utilities in Europe. Project leader is Elsamprojekt A/S. Aim of the project is to introduce nickel or cobalt based superalloys in the most severely loaded parts of boilers and turbines in order to increase the steam temperature up to 700°C. For the boiler materials group in the project this means that the following materials need to be developed:

- A superalloy with 100,000 hour creep rupture strength 100MPa at 750°C for superheater tubes, steam headers and steam lines.
- An austenitic steel with 100,000 hour creep rupture strength 100MPa

at 700°C for superheater tubes.

- A ferritic/martensitic steel with 100,000 hour creep rupture strength 100MPa at 650°C for steam headers and steam lines.

Development of the austenitic and ferritic steels is to minimise the use of highly expensive superalloys. Such material developments will allow the construction of USC plants with efficiencies of 52-55% depending on cooling water and fuel conditions.

4 References

- [1] Blum R: Materials Development for Power Plants with Advanced Steam Conditions - Utility Point of View, Materials for Advanced Power Engineering 1994, Liège 3-6 October 1994.
- [2] Blum R, Hald, J: Development of High Efficiency Power Plants in Denmark. Int. Conf. Advanced Steam Plant, London 21-22 May 1997, IMechE 1997, 3-16.
- [3] DeLong J F, Siddall W F, Haneda H, Daikoku T, Ellis F V, Tsuchiya T, Masuyama F: Operation Experiences and Reliability Evaluation on Main Steam Line Pressure Parts of Philadelphia Electric Co. Eddystone, Thermal and Nuclear Power 35(11) 1984.
- [4] Thomsen F, Moeller Hansen C, Kjaer, S: Experiences from New USC Plant at Skaerbaek and Nordjyllandsvaerket Power Plants in Denmark, this conference.
- [5] Fujita T: Current Progress in Advanced High Cr Ferritic Steels for High Temperature Applications, COST-EPRI Workshop, Creep-Resistant 9-12Cr Steels, Schaffhausen, Switzerland, October 13-14 1986.
- [6] Masumoto H, Sakakibara M, Sakurai H, Fujita T: Development of a 9Cr-Mo-W Steel for Boiler Tubes, EPRI 1st Int. Conf. Improved Coal-Fired Power Plants, Palo Alto, 1986, 5.203-5.218.
- [7] Iseda A, Sawaragi Y, Kato S, Masuyama F: Development of a New 0.1C-11Cr-2W-0.4Mo-1Cu Steel for Large Diameter and Thick Wall Pipe for Boilers, Proc. Fifth Int. Conf. on Creep of Materials, Lake Buena Vista, Florida, USA, May 18-21, 1992, 389.
- [8] Metcalfe E ed. Proc. The EPRI/National Power Conference: New Steels for Advanced Plant up to 620°C, London, May 1995.
- [9] Miyashita K: Overview of Advanced Steam Plant development in Japan, Int. Conf. Advanced Steam Plant, London 21-22 May 1997, IMechE 1997, 17-30.
- [10] Orr J, Woollard L: The Development of 9%Cr Steels from Steel 91 to E911, Inst. of Materials Conf. Microstructural Development and Stability in High Chromium Ferritic Power Plant Steels, Ed. A Strang, D. Gooch. Institute of Materials 1997, 123-145.

- [11] Thornton D V: The activities of the European Collaborative Creep Committee, Proc. Life Assessment of Industrial Components and Structures, Cambridge 30 September-1 October 1993, ERA Report 93-0690, paper 2.9.
- [12] Scarlin B: Advanced high-efficiency turbines utilizing improved materials, Int. Conf. Advanced Steam Plant, London 21-22 May 1997, IMechE 1997, 33-48.
- [13] Vanstone R W, Thornton D V: New materials for advanced steam turbines, *ibid*, 87-98.
- [14] Hikada K, Fukui Y, Kaneko R, Fujita T: Development of 9-12%Cr steels for all-ferrite steam turbine at target temperature of 650°C, *ibid*, 99-114.
- [15] Waltenberger, G.: 30 Jahre Betrieb der ersten 600°C-Hochtemperatur-Dampfkesselanlage. VGB Kraftwerkstechnik 63.(1983) H. 8, S. 653-660.
- [16] Waltenberger, G. Mattern, P.: Einsatz austenitischer Werkstoffe in Dampfkesseln. VGB Kraftwerkstechnik 70.(1990) H. 1, S. 68-76.
- [17] Sawaragi, Y. Ogawa, K. Kato, S. Natori, A. Hirano, S.: Development of the Economical 18-8 Stainless Steel (Super 304H) having High Elevated Temperature Strength for Fossil Fired Boilers. The Sumitomo Search, No. 48, January 1992 p.50-58.
- [18] Quality and Mechanical Properties of NF709 for Power Plant Boilers. Technical publication, Nippon Steel Corporation, May 1993.
- [19] Sawaragi, Y. Teranishi, H. Iseda, A. Yoshikawa, K.: The Development of new Stainless Steel Tubes with High Elevated Temperature Strength for Fossil Power Boilers and Chemical Plants. The Sumitomo Search, No. 40, December 1990 p.146-158.
- [20] Blum, R. Henriksen, N. Larsen, O.H.: Lifetime Evaluation of Superheater Tubes Exposed to Steam Oxidation, High Temperature Corrosion and Creep. Power Plant Technology 1996. Int. Conf. Kolding, Denmark 4-6 September 1996
- [21] Blum, R. Chen, Q. Scheffknecht, G. Vanderschaeghe, A.: A Project to Determine High-Temperature Corrosion Characteristics of Different Steam Generator Materials under Operating Conditions and Steam Temperatures up to 620°C. VGB Kongress "Kraftwerke 1995", 5. bis 7. September 1995 Essen.
- [22] Masuyama, F. Yokoyama, T. Sawaragi, A. Iseda, A.: Development of tungsten strengthened low alloy steel with improved weldability. Materials for Advanced Power Engineering 1994, Liege October 3-6, 1994.
- [23] Iseda, A. Sawaragi, Y. Teranishi, H. Kubota, M. Hayase, Y.: Development of New 12%Cr Steel Tubing (HCM12) for Boiler Application. The Sumitomo Search, No. 40, November 1989, p.41-56.
- [24] Bendick, W. Ring, M.: Stand der Entwicklung neuer Rohrwerkstoffe für den Kraftwerksbau in Deutschland und Europa. VGB-Konferenz "Werkstoffe und Schweißtechnik im Kraftwerk 1996" 8. - 9. Oktober 1996, Cottbus.
- [25] Henriksen, N. Larsen, O.H. Vilhelmsen, T.: Lifetime Evaluation of Evaporator Tubes Exposed to Steam Oxidation, Magnetite deposition, High Temperature Corrosion and Creep in Super Critical Boilers. (To be published).

Materials for header and steam pipe

Chemical composition:

	C	Cr	Mo	W	Cu	Others:
P91	0,1	9	1			V,Nb,N
P92	0,1	9	0,5	1,8		V,Nb,N,B
P122	0,1	11	0,5	1,8	1	V,Nb,N,B

Creep rupture strength:

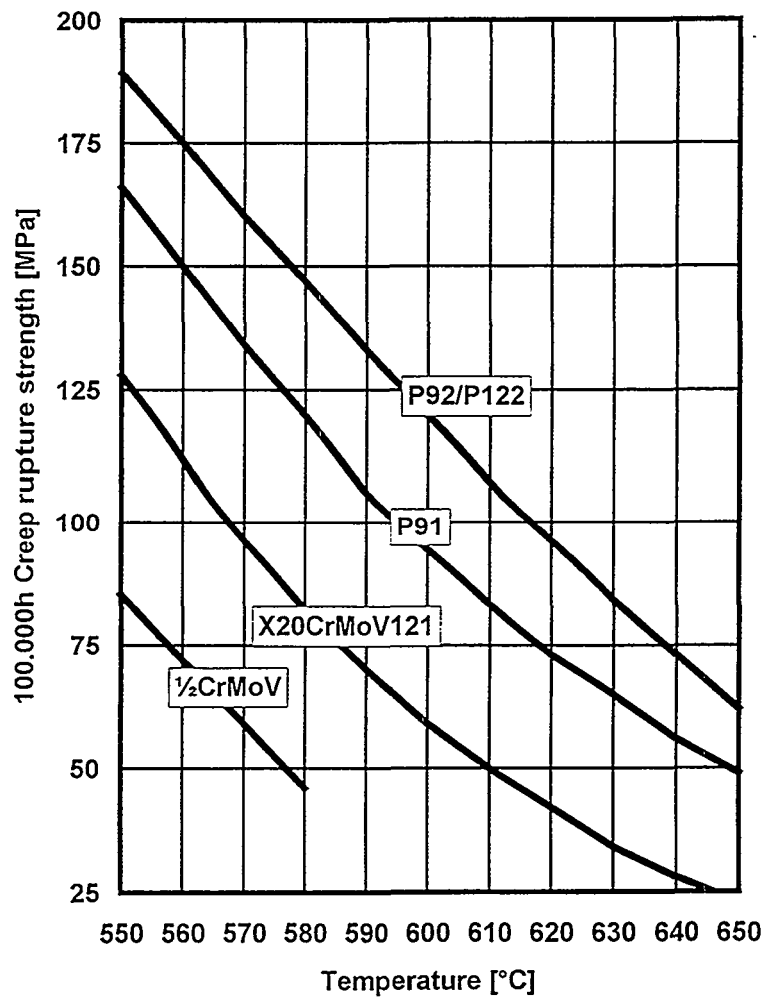


Figure 1

ECCC data sheet

Steel X10CrMoVNb9-1 (1995)

Conditions of steel to which the properties apply

	Details of materials tested		Specified ranges	
			Minimum	Maximum
Chemical composition	C	% (m/m) 0,08 to 0,12	0,08	0,12
	Si	0,11 to 0,49	0,20	0,50
	Mn	0,31 to 0,59	0,30	0,60
	P	0,001 to 0,024	-	0,020
	S	0,0008 to 0,010	-	0,020
	Cr	8,05 to 9,45	8,00	9,50
	Mo	0,85 to 1,09	0,85	1,05
	Ni	0,01 to 0,37	-	0,40
	V	0,18 to 0,25	0,18	0,25
	Nb	0,05 to 0,10	0,06	0,10
	Al	0,001 to 0,035	-	0,020
N	0,030 to 0,069	0,030	0,070	
Heat treatment	*C 1038 to 1090 + 730 to 800 AC		*C 1040 to 1090 + 730 to 780 AC	
Tensile strength at room temperature	N/mm ² Rp0,2 473 to 767 Rmt 648 to 813		N/mm ² 450 min. 630 to 830	

Quantity and duration of data used in assessment

Temperatur	Test Duration						
	h <10.000	h 10.000 to 20.000	h 20.000 to 30.000	h 30.000 to 50.000	h 50.000 to 70.000	h 70.000 to 100.000	h >100.000
	Number of test points available						
*C							
500	66(6)	6(4)	2	-	1(3)	(2)	-
525	6(3)	1	1(2)	-	1(2)	(2)	-
538/540	18	4	(2)	(1)	(5)	1(1)	-
550	194(12)	31(3)	20(4)	7(3)	1(1)	1	-
575	68(1)	12(2)	1	-	-	-	-
593	39(1)	9	3	3(1)	-	(1)	-
600	405(17)	57(2)	13(8)	10(6)	4(5)	(1)	-
625	64(1)	1(1)	-	-	-	-	-
649/650	334(9)	35(4)	11(2)	3	2	-	-
675/677	32	-	1	-	-	-	-
700	34	3	-	-	-	-	-

() Figures in parantheses denote unbroken tests

Average rupture stresses

Temperatur	10.000h	30.000h	100.000h	200.000h
*C	N/mm ²	N/mm ²	N/mm ²	N/mm ²
500	289	273	258*	246*
510	271	255	239*	227*
520	252	236	220*	208*
530	234	218	201	189*
540	216	200	183	171*
550	199	183	166	154*
560	182	166	150	139*
570	166	150	134	124*
580	151	136	120	110*
590	136	122	106	97*
600	123	108	94	86*
610	110	97	83	75*
620	99	86	73	65*
630	89	77	65	57*
640	79	68	56	49*
650	70	59	49	42*
660	62	52	42	35*
670	55	45	36	-

* Values which have involved extended time extrapolation (>3 x and <10 x maximum rupture time)

Figure 2

Materials for Superheater tubes

Chemical composition:

	Cr	Ni	Mo	Nb	Ti	Others:
TP347HFG	18	10		1		
Super 304H	18	9		0,4		Cu, N
NF709	20	25	1,5	0,25	0,05	N
HR3C	25	20		0,4		N

Creep rupture strength:

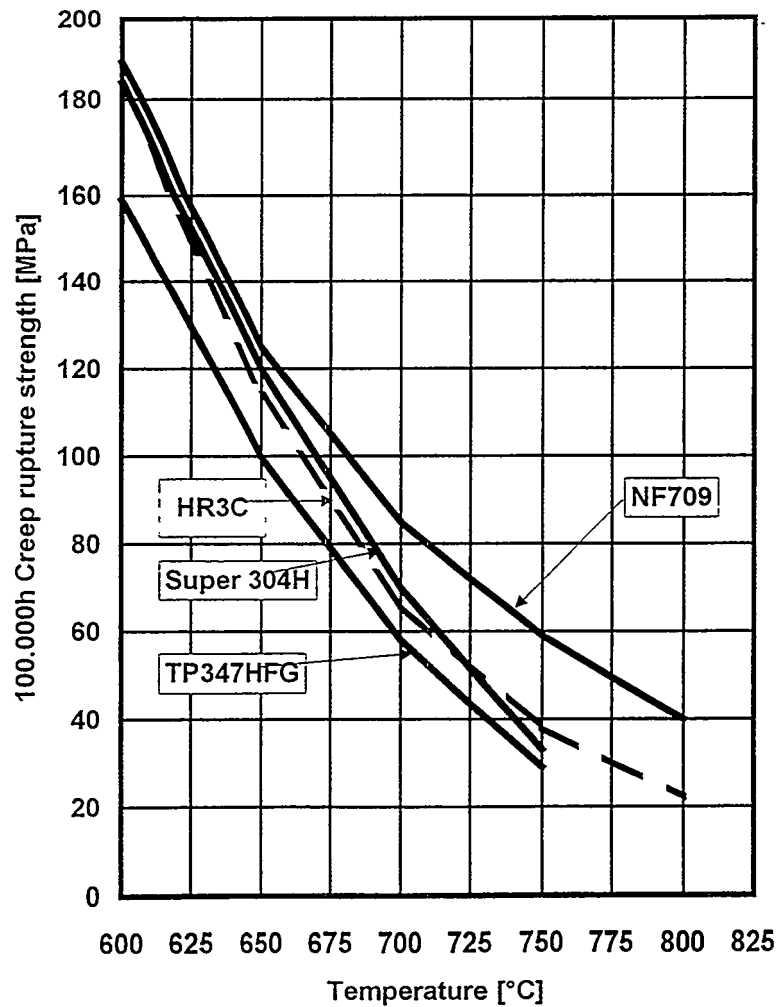


Figure 3

Materials for furnace panels

Chemical composition:

	C	Cr	Mo	W	Others:
1Cr½Mo	0,13	0,90	0,50		
HCM2S	0,06	2,25	0,30	1,60	V, Nb, N, B
HCM12	0,10	12,00	1,00	1,00	V, Nb
7CrMoTiB1010	0,07	2,40	1,00	-	V, Ti, N, B

Creep rupture strength:

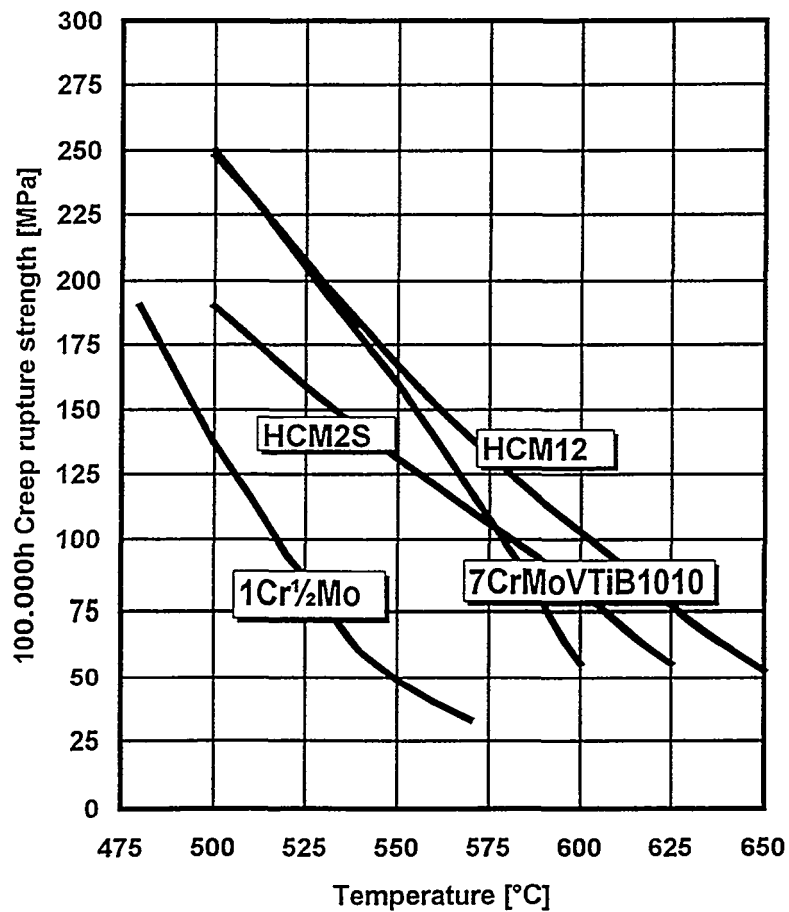


Figure 4

New Ferritic Steels for Advanced Steam Plants

K.H. Mayer and H. König
 GEC ALSTHOM Energie GmbH
 Nuremberg, Germany

Abstract

During the last 15-20 years ferritic-martensitic 9-12% chromium steels have been developed under international research programmes which permit inlet steam temperatures up to approx. 625°C and pressures up to about 300 bars, thus leading to improvements in thermal efficiency of around 8% and a CO₂ reduction of about 20% versus conventional steam parameters. These new steels are already being applied in 13 European and 34 Japanese power stations with inlet steam temperature up to 610°C. This paper will give an account of the content, scope and results of the research programmes and of the experience gained during the production of components which have been manufactured from the new steels.

Introduction

Materials development work over the past 15-20 years has paved the way for large fossil-fired power stations to be built today with live steam temperature of 610°C, reheat temperature of 625°C and supercritical steam pressures. The likely potential for reducing the heat rate by increasing the pressure and temperature of the steam admitted to the turbine on the basis of single and double reheating is shown in Fig. 1 (1). At live steam condition of 600°C and 300bar with double

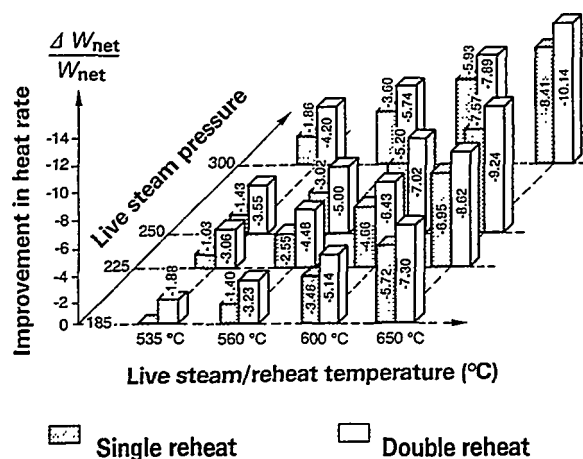


Fig. 1. Improvements in the heat rate with single and double reheating.

reheating, for example, the heat rate can be reduced by about 8% compared with the heat rate of today's standard power stations featuring steam parameters of 540°C/180 bar and single reheat. This improvements in thermal efficiency helps considerably to conserve fuel resources and reduce CO₂ emissions by about 20%.

Research Programmes

Further developments of conventional thermal power stations aimed at increasing thermal efficiencies was essentially prompted by the second oil crisis. The starting point were studies carried out by power plant operators in the USA(EPRI) and in Japan(EPDC). The research programmes focused on developing further the existing high-temperature-resistant ferritic-martensitic 12%CrMoV steels for the production of rotors, casings, chests, pipes and headers capable of operating with inlet steam temperatures up to 593°C(1100°F) as well as the further development of the existing high-temperature-resistant austenitic steels suitable for inlet steam temperatures up to 649°C(1200°F), - Fig. 2. Spurred by the research activities in Japan and USA, European power station builders and steel producer pursued in the 1980's the further development of ferritic steels geared to inlet steam temperatures of up to approximately 625°C in the context of the COST 501(2) European research programme. General speaking, material development work under the COST 501 programme concentrated on the competitiveness of the new generation of fossil-fired thermal power stations compared with existing plants and the combined gas and steam-fired power stations.

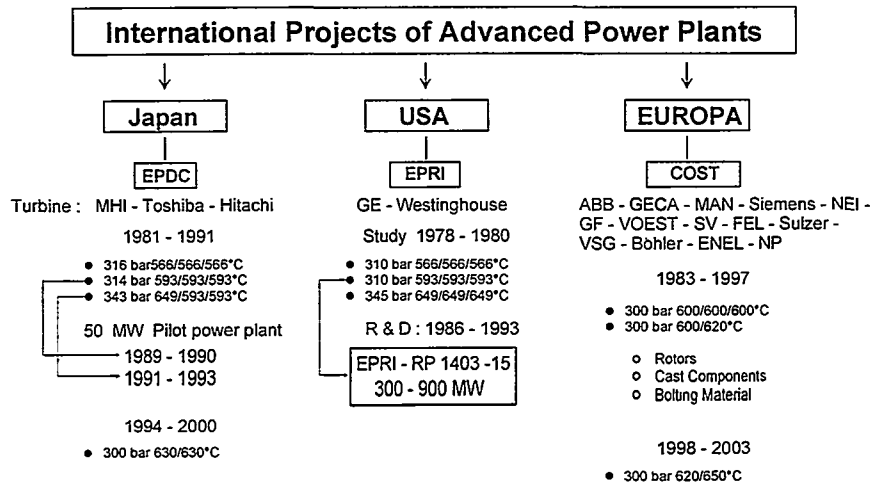


Fig. 2. International research programmes for developing advanced fossil-fired power stations.

Development of Materials

Further development and qualification of ferritic-martensitic steels took place on the basis of decades of research work all over the world aimed at studying the effect of tungsten, niobium, cobalt, nitrogen and boron on the operational

properties of power station steels (3 to 5) and using the constantly progressing electron-optical methods for characterising the microstructure of the metals.

The research programmes focused on improving the creep strength in the 550-650°C temperature range. Investigations also attempted to determine the fracture toughness, long-term toughness behaviour, low-cycle fatigue strength and the microstructure of the test materials as well as the manufacturability of the relevant components. Fig. 3 gives for example an overview of the developed and tested rotor steels in the three rounds of COST 501 based on the conventional European 12%Cr steels X22CrMoV12 1, X19CrMoVNbN 11 1 and the Co alloyed aircraft steel FV 535.

Basic Steels	X22CrMoV 12 1 (SEW 555)	X19CrMoVNbN 11 1 (DIN 17240)	FV 535 (Firth Vickers)
Typ	Boron - Typ	Mo-, MoW-, W- and N-Typ	WNB-, CoB-, CoWNB-, CoWB-Typ
COST 501 Round 1 (83 - 85)	Plus: B(100-180ppm) Nb (0,06%) Mod.: C,Cr,Mo,V B0: X10CrMoVNbB 9 1 B2: X18CrMoVNbB 9 1	↓	↓
COST 501 Round 2 (86 - 92)	B0: X10CrMoVNbB 9 1 B2: X18CrMoVNbB 9 1	Plus: (W 1 - 1,8 %) Mod.: C,Cr,Mo,V,Nb,N F: X12CrMoVNbN 10 1 E: X12CrMoWVNbN 10 1 1 D: X12CrWMoVNbN 10 2 1 N: X8CrMoVNbN 9(12) 1	↓
COST 501 Round 3 (93 - 97)	B0: X10CrMoVNbB 9 1 B2: X18CrMoVNbB 9 1	F: X12CrMoVNbN 10 1 1 E: X12CrMoWVNbN 10 1 1	Plus: (W 1,8 - 2, 6%) Mod.: C,Mn,Ni,Cr,Co,Mo,V,Nb,N,B FB2: X12CrMoCoVNbB 9 1 FN2: X12CrWMoVNbNB 10 2 FN3: X12CrCoWMoVNbNB 10 2 2 FN4: X12CrCoWMoVNbNB 12 2 2 FN5: X12CrCoWMoVNbB 11 2 2

Fig. 3. European 9-12%Cr Rotor Steel Development.

Under the COST 501 programme a total of 65 different test materials have so far been examined in several heat treatment conditions for the purpose of qualifying turbine, piping and boiler steels. The max. testing time of the most promising candidate materials is between 50 000 and 80 000 hours in the case of creep tests, providing a good basis for a reliable extrapolation of the 100 000h creep strength for the steels developed in the round 1 and 2. The steels developed in the round 3 are still in the development stage with a max. test time of about 20 000 hours.

Figures 4 and 5 give details on the creep strength applicable to 100 000 hours and the chemical composition of the newly developed turbine, tube and boiler steels (c to d) as a function of the temperature and in comparison to the previously used steels (a and b). A creep strength of 100 MPa, decisive for the sizing of the components, serves as a guide to assessing the steels. This strength is achieved by the new ferritic-martensitic steels in the 590°C to 625°C range, i. e. they permit an increase in application temperature, depending on the choice of steel, of the order of 25°C to 70°C versus conventional steels.

This alloying development also resulted in an improvement in weldability, ductility, fracture toughness and low-cycle fatigue strength.

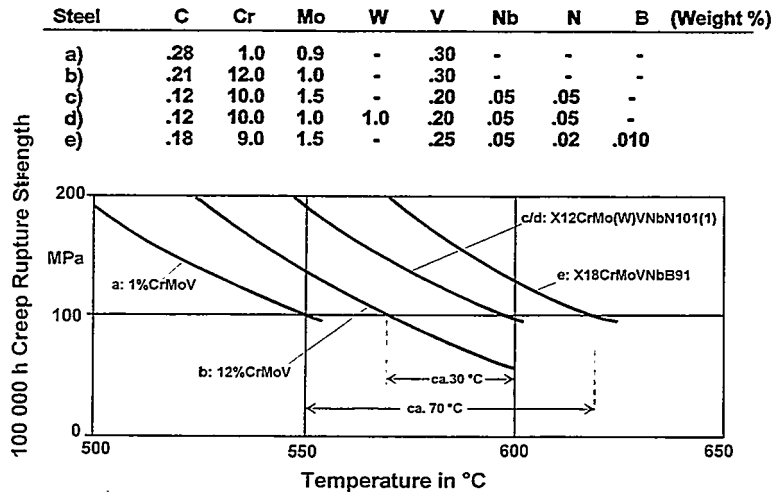


Fig. 4. 100 000 h Creep Strength of Turbine Steels.

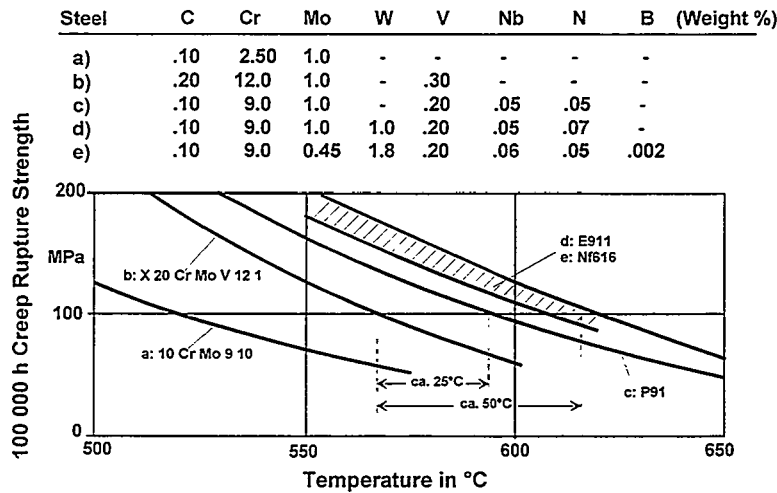


Fig. 5. 100 000 Creep Rupture Strength of Tube and Boiler Steels.

Fig. 6 illustrates, in an exemplary way for the rotor steels, a comparison of the fracture toughness which is of great significance in assessing the resistance to brittle failure. The new HP and IP rotor steels 10%CrMo(W)VNbN feature a substantially greater fracture toughness than the 1%CrMoV and 2%CrMoV HP and IP rotor steels used previously up to approximately 550°C and, in addition, tend to show greater fracture toughness compared with the conventional 12%CrMoV HP and IP rotor steel.

The gain in low-cycle fatigue strength of the newly developed 10%CrMo(W)VNbN versus the 1%CrMoV rotor steel is shown in the left half of Fig. 7. The additional reduced thermal expansion of the 10%CrMo(W)VNbN

steels compared with the low-alloys steels also has beneficial effects on the permissible start-up gradient of the turbine units. The right half of Fig.7 demonstrates the relative gain in permissible rate of temperature change at the rotor surface for a hot start for a specific shaft dimension for both these types of steel (6). The improvements achieved by employing the newly developed 10%CrMo(W)VNbN steel is over 50% in this case.

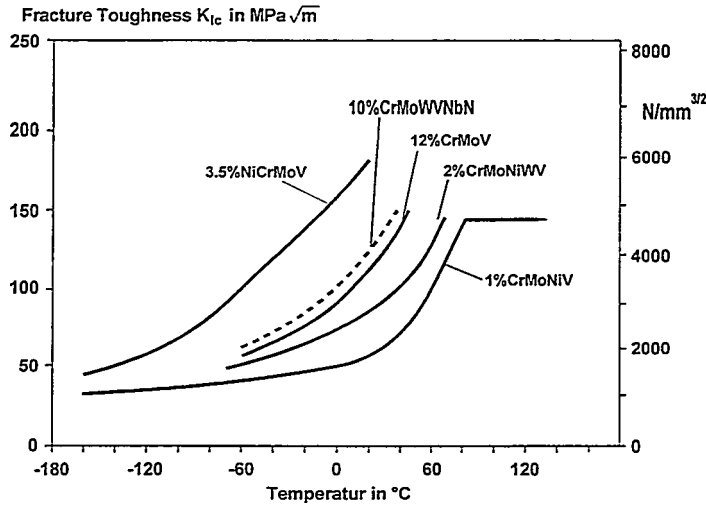


Fig. 6. Fracture Toughness of Turbine Rotor Steels.

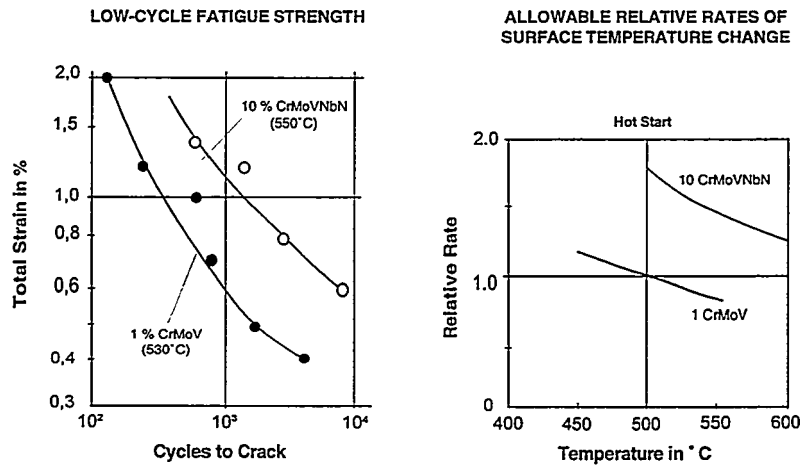


Fig. 7. Low-cycle Fatigue Strength and permissible Rate of Temperature Change of 1%CrMoV and 10% CrMo(W)VNbN HP and IP Rotor Steels.

On the basis of the design criteria of rotor steels, Fig. 8 demonstrates the advances made with the 10%CrMo(W)VNbN rotor steels in comparison to the conventional 1%CrMoV rotor steel in the form of an overview for max. 600 $^{\circ}C$ applications, the range of which has been extended significantly not only at high and low component temperature, but also by means of increased permissible stresses.

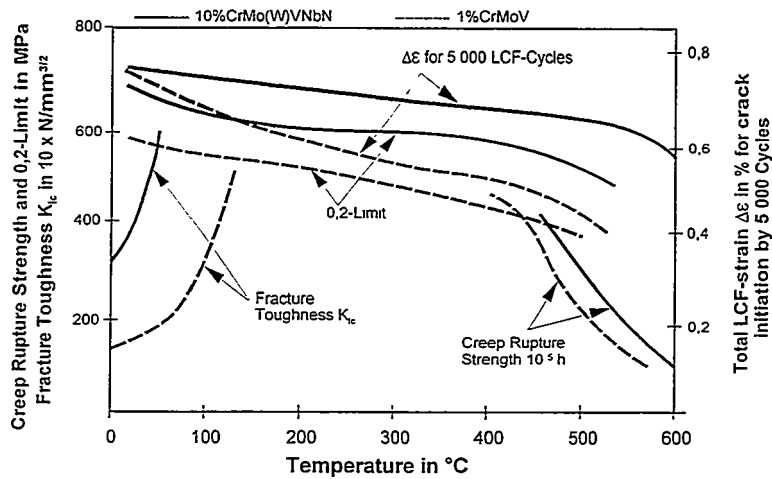


Fig. 8. Comparison of Design Criteria of HP and IP Rotor Steels manufactured by 1%CrMoV and 10%CrMo(W)VNbN Steels.

New Generation Power Stations

The success of material development programmes is already being reflected in the form of new orders for fossil-fired thermal power stations. Table 1 gives an overview of those thermal power stations built in Japan following completion of the initial development phase (7).

Table 1. Japanese super-critical Thermal Power Stations commissioned 1993 to 2003.

	Main Steam		Hot Reheat Steam	Output	Number of Units
	Pressure bar	Temperature °C	Temperature °C	MW	
	240-250	538	593	700	1
	240-250	566	566	350-500-700	3
	240-250	566	593	500-700-1000	4
	240-250	593	593	600-700-900-1000	6
	240-250	600	600	1000	3
	240-250	600	610	600-1050	3

A total of 20 power stations are involved with inlet steam temperatures of between 566°C and 610°C with outputs ranging from 350 to 1050 MW. The first of these, featuring a reheat temperature of 593°C (1100°F), were commissioned in 1993. The turbines with a 610°C reheat temperature and a live steam temperature of 600°C are due to be commissioned from 2001 to 2003. Phase 2 of the materials development programme aimed at further developing the ferritic-martensitic steels is likely to be more or less completed by 2000. Contracts for 630°C inlet steam temperature are most likely to be awarded from this time onwards.

Table 2 shows a list of power stations in Europe in which the newly developed steels are being applied to achieve elevated steam parameters.

Table 2. European Thermal Power Stations with Advanced Steam Parameters.

Steam Plant	Fuel	Output	Life	Reheat	Thermal
		MW	Steam bar/°C	Steam °C	Efficiency %
Skaerbaek	Gas	400	290/582	580/580	49
Nordjylland	Coal	400	290/582	580/580	48
VALA	Coal	260	180/536	570	
Avedore	Biomass,Oil	530	300/580	600	47
Schkopau A,B	Lignite	450	285/545	560	40
Sch.Pumpe A,B	Lignite	800	268/545	565	40,6
Boxberg Q,R	Lignite	818	268/545	583	41,7
Lippendorf R,S	Lignite	900	268/554	583	41,7
Frimmersdorf	Lignite	950	268/580	600	42,3
Westfalen	Coal	350	283/597	618	

The gas- and coal-fired Danish power stations at Skaerbaeck and Nordjylland have a double reheat cycle with inlet steam temperatures of 580°C and a live steam pressure of 290 bar. The Danish plant at Avedore, which is fired on biomass and oil, features a reheat temperature of 600°C and live steam condition of 300 bar and 580°C. 570°C has the reheat temperature of the coal-fired 260MW power station VALA in Finland. The live steam condition are 180bar/536°C.

In the case of the lignet-fired power stations, which only have a single reheat cycle and, with one exception, are located in eastern Germany, the maximum reheat temperature is 600°C at live steam conditions of 270 bar and 580°C. In Germany is planned in addition a 350 MW coal-fired power plant with a reheat temperature of 618°C and live steam condition of 597°C and 283 bar.

Based on the present state of art, a live steam temperature of approximately 610°C and a reheat temperature of about 625°C can be achieved.

Manufacturing Experiences

The experience gained so far in the manufacturing of components for the above mentioned power stations is decidedly positive (8) . 3 European forgemasters were involved in the COST 501 development of the rotor materials and manufacturing of the rotors (9-11) and at least 6 European foundries manufactured the castings of which most originated from two foundries which were also actively involved in the COST 501 development work (12 and 13). One of the two foundries made over 80 castings of between 3 t and 60 t. The spectrum of weight range of the produced castings from the same foundry is given in Fig. 9.

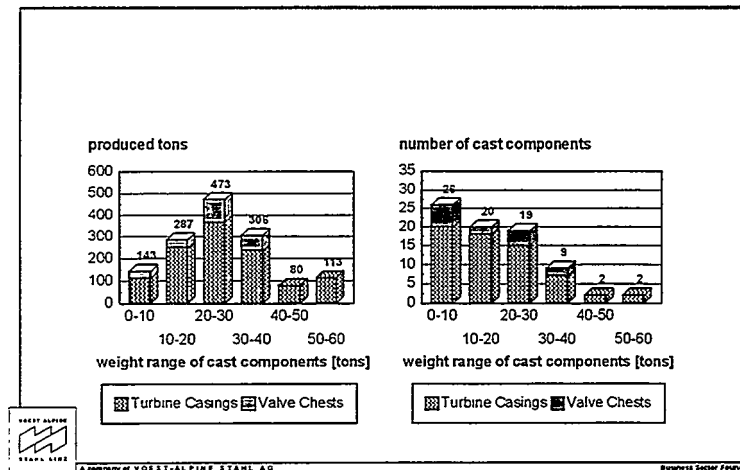


Fig. 9. Spectrum of Weight Range of Castings produced by a large Foundry.

The second foundry gained experience with about 270 castings in the weight range and application given in the following table, not only for steam turbine components, but also castings for stationary gas turbines (13).

Components	Component Weight Range in t	9%CrMoVNbN number	10%CrMoWVNbN number
various	< 1	8	98
Various	1 - 5	9	
Valve chests		4	76
Casings/Bladecar.			18
Valve chests	5 - 10		29
Casings/Bladecar.			16
Valve chests	> 10		12

As opposed to the 1%CrMoV cast steel generally employed, the production period for castings of the new 9 – 10%CrMo(W)VNbN steel grades is 2-4 weeks

longer, depending on the size and complexity of the casting. This is due primarily to the more complex and longer heating during the various thermal treatment cycles, ranging from cooling in the mould, to feeder cutting, tempering and repeated stress relieving(12).

The cost increase from 1%CrMoV steel castings to 9-10%CrMo(W)VNbN steel grades was to be 20-40% depending on the size and complexity of the steel castings.

Summary and Conclusion

During the last 15-20 years ferritic-martensitic 9 to 12% chromium steels have been developed under international research programmes which permit live inlet steam temperature for fossil-fired thermal power stations up to approximately 610°C, pressures up to about 300 bar and reheat temperatures up to about 625°C. The result has been improvements in efficiency of around 8% and a reduction of CO₂ emissions of about 20% versus conventional steam parameters.

The objectives of the European research programme, which today involves 65 partners from 13 different European countries, have been coordinated so that the steam plants of the new generation allow the same flexible and cost effective operation as the conventional units.

The new steels are already being used in 13 European and 34 Japanese power stations with inlet steam temperatures of up to 610°C. The experience which has been gained in the production of components for these power stations is decidedly positive. The properties of the production components correspond almost entirely to those of the pilot components of the research programmes.

Current and future tests will be aimed at achieving inlet steam temperatures up to max. 650°C, using mainly ferritic-martensitic steels for the highly stressed turbine components.

References

- (1) K.H.Mayer, W.Bendick, R.-U.Husemann, T.Kern and R.B.Scarlin: "New Materials for Improving the Efficiency of Fossil-Fired Thermal Power Stations", VGB PowerTech 1/98, pages 22 to 27.
- (2) C.Berger, K.H.Mayer and R.B.Scarlin: "Neue Turbinenstähle zur Verbesserung der Wirtschaftlichkeit von Kraftwerken", VGB Kraftwerkstechnik 71 (1991), Heft 7, Seiten 686-699.

- (3) T.Fujita: „Effect of Mo and W on long Term Creep Rupture Strength of 12%Cr Heat Resisting Steels containing V,Nb and B“, Transaction ISIJ, 18 (1978), pp. 115 – 124
- (4) P.Patriarca et al: „U.S. Advanced Materials Development Programme for Steam Generators“, Nuclear Technology 28 (1976),March, pp.516-537
- (5) P.Ernst: „Effect of Boron on the Mechanical Properties of modified 12%CR Steels“, ETH Zürich, No. 8596 (1988)
- (6) A.N.Patterson, G.Simonin and H.Neft:“Steam Turbines for Advanced Conditions“, GEC ALSTHOM Monte Carlo Conference 1994.
- (7) K.Miyashita:„Overview of Advanced Steam Plant Development in Japan“, International Conference on Advanced Steam Plants, 21-22 May 1997 London, Great Britain,
- (8) M.Taylor and D.V.Thornton:“Experiences in the Manufacture of Steam Turbine Components in Advanced 9-12%Chromium Steels“, International Conference on Advanced Steam Plants, 21-22 May 1997 London, Great Britain,
- (9) M.A.Walsh:“Manufacture of 10%CrMoVNBn Turbine Rotor for super-critical Applications“, 13th International Forgemasters Meeting , Advances in Heavy Forgings, October 12-16, 1997 , Pusan, Korea.
- (10) W. Meyer, G.Zeiler and R.Bauer:“Influence of various Melting Processes on the Properties of 10%Cr Steel for Application at Temperatures up to 600°C“, 13th International Forgemasters Meeting , Advances in Heavy Forgings, October 12-16, 1997, Pusan, Korea
- (11) K.-H.Schönfeld and H. Wagner:“Experiences in Manufacturing and Mechanical Properties of Turbine Rotor Forgings and Discs in Improved 10%CrMoWVNbN Steel“, International Conference „Advanced Heat Resistant Steels for Power Generation“, 27-29 April 1998, San Sebastian, Spain
- (12) K.H.Mayer, R.Hanus, T.Kern, M.Staubli and D.V.Thornton:“High Temperature Cast Components for Advanced Steam Power Plants“, 6th Liege COST Conference 5.-7. October 1998
- (13) Information of J.Stief, PHB Stahlguß GmbH, D-66377 St.Ingbert-Rohrbach, Germany

Optimizing Power Plant Cycling Operations While Reducing Generating Plant Damage and Costs

Steven A. Lefton, Phil M. Besuner, and G. Paul Grimsrud
Aptech Engineering Services, Inc.
Sunnyvale, California USA

Alan Bissell
Electric Supply Board
Dublin, Ireland

Abstract

This paper describes a method for analyzing, quantifying, and minimizing the total cost of fossil, combined cycle, and pumped hydro power plant cycling operation. The method has been developed, refined, and applied during engineering studies at some 160 units in the United States and 8 units at the Irish Electric Supply Board (ESB) generating system.

The basic premise of these studies was that utilities are underestimating the cost of cycling operation. The studies showed that the cost of cycling conventional boiler/turbine fossil power plants can range from between \$2,500 and \$500,000 per start-stop cycle. It was found that utilities typically estimate these costs by factors of 3 to 30 *below* actual costs and, thus, often significantly underestimate their true cycling costs.

Knowledge of the actual, or *total*, cost of cycling will reduce power production costs by enabling utilities to more accurately dispatch their units to manage unit life expectancies, maintenance strategies and reliability. Utility management responses to these costs are presented and utility cost savings have been demonstrated.

1 Introduction

This paper presents the findings from engineering studies that Aptech Engineering Services, Inc. (APTECH) has done for ten major utility systems to quantify the economic effects of unit cycling at over 160 fossil, hydro, pumped hydro, combustion turbine, and combined cycle power plants. These studies included extensive review of failure data, application of methods to predict future reliability, and analysis of past and future predictions of individual power plant capital and maintenance data. Generally these studies identify the costs associated with the effects of a specific type of operation, including unit cycling, derating and uprating (1) (2).

Although most of these studies were done under strict confidentiality agreements, this paper will describe the general techniques used in these and other studies. Two case studies, Electric Supply Board and Florida Power Corporation, also will be discussed. Overall, it has become clear from these studies that each of them must be customized to a specific utility's needs and to its available cost and reliability databases.

2 Background

The following discussion gives the background on how competition is causing changes in utility operating practices, such as increased unit cycling, and why the total cost of these practices needs to be quantified and forecasted.

2.1 Definition of Cycling Operation

In this paper, the term "cycling" refers to various operating modes that occur in response to changes in system load requirements. These modes generally include on/off operation, low-load cycling operations and load following. Frequent low-load cycling, especially at higher rates of megawatt change rate, must have their total impact quantified. On/off operation is further subdivided into cold starts (downtime > 120 hours), warm starts (downtime 24 to 120 hours) and hot starts (downtime < 24 hours). This may be modified based on unit size.

2.2 Competition and Its Effect on Operating Practices

Competition in the utility sector increasingly is being driven by Independent

Power Producers (IPPs), Qualified Generating Facilities (QFs) and Non-Utility Generators (NUGs). Competition from IPPs, QFs and NUGs, and the presence of a utility's own nuclear power plants on the generating system, often results in an overabundance of baseload capacity. Competition has driven many US states, such as California, and other countries to deregulate. Deregulation has required some utilities to predict future costs for long-term power purchase agreements other utilities need to determine costs for bid prices to electricity pools. This situation generally requires fossil units designed for baseload operation to begin some type of cycling operation, as defined above.

2.3 Effect on EFOR

When a utility begins to cycle its fossil plants, it typically observes a significant increase in equivalent forced outage rate (EFOR)(3) due to the increased component failure rate. Figure 1 illustrates this effect. This is a schematic diagram based on data from four types of large, aging, coal-fired units studied by APTECH. The figure compares EFORs for the four types of units. Those under baseload (non-cycling) operation have the lowest EFOR. Under cycling operation, the lowest EFOR is achieved by units in this order: units that were specifically designed for cycling; baseload-designed units that were upgraded for cycling; baseload-designed units that were not upgraded for cycling.

2.4 Effect on Capital and Maintenance Expenditures

Additional capital and maintenance expenditures are another effect of switching to cycling operation. Figure 1 shows schematically how the infusion of capital and maintenance dollars suppresses the increase in EFOR rate. Our studies suggest that increased failures lag behind the switch to cycling operation by one to seven years. When the failure rate increases, capital and maintenance spending then must increase to keep the unit operable. The expenditures may lead to much higher, noncompetitive capital, maintenance and fuel costs for the units that are cycling. The higher capital, maintenance and fuel costs for these cycling units, in conjunction with the reduced generation, yield a higher average generation cost.

The net effect is a perpetual spiral of increased cost, noncompetitiveness, decreased generation and, finally, further increases in cost per megawatt-hour of generation. This may cause the unit to be retired prematurely.

2.5 The Need to Understand Costs and Manage Assets

A noncompetitive cost per megawatt-hour often leads a utility to consider early retirement of the unit and the associated high-cost capacity replacement. Early retirement may also be brought upon a unit by cycling-related increased forced outages and unexpected capital requirements.

Therefore, it is seen that competition from QFs, NUGs, and OTLA makes it necessary for utilities to understand the bases and origins of capital and maintenance costs associated with long-term operation of their power plants, and to manage their power plant assets accordingly. To become aware of the origins of these costs, utility engineers need to understand the influence of different plant operating modes on wear and tear costs. Understanding the origin of these costs can lead to economic controls on the key variables affecting total costs. In response, APTECH has developed a code called COSTCOM that correlates key plant damage parameters, such as superheaters, reheater, and turbine case (T, P, ΔT , MW) and their rate of change, which then calculates in real time the monetary value of cycling related wear and tear costs.

3 Influence of Operation Mode on Wear and Tear Costs

Certain operating modes can either increase or decrease wear and tear costs. These are described below.

3.1 Operations That Increase Wear and Tear

Both cycling and steady-state operations cause wear and tear. Cycling operations typically increase fatigue-related wear and tear. These cycling operations include taking the unit off- and on-line by hot, warm, and cold starts and cycling the unit up and down the load range from maximum continuous rating to minimum loads. Higher unit load change rates cause larger amounts of damage than smaller load changes. Unit shutdowns and unit trips are also especially hard on equipment. Characteristics of the methods used to start up and shut down a plant, including ramp rates, temperature limits and hold times, greatly affect unit reliability and longevity.

Steady-state operations typically increase creep-related wear and tear. Creep damage and reduced service life occur when units operate at steady-state, and this damage significantly increases when the unit is operated above its design rating or operating limit. All these effects put upward pressure on wear and tear costs.

3.2 Operations That Reduce Wear and Tear

Operations that typically reduce unit wear and tear is steady-state baseload operation at or below the design rating. This is generally achieved by derating units about 3% to 5% of rated maximum power. Utility engineers can also reduce wear and tear costs by carefully increasing the time between major overhauls, if there are no major impediments to increasing these times.

3.3 Mission Statements

Once a utility understands the origins and effects of these operations on their unit wear and tear costs, it can begin to reduce these costs by selectively changing its power plant operational modes. This process can and will lead to a "system optimization" and minimization of the total revenue requirements.

For example, Figure 2 shows schematically that by reducing annual cycles on selected power plants, system costs can be reduced and an optimum balance can be achieved. This balance is achieved by first finding the true, or total, cost to cycle each unit, and then by defining the mission of each unit to achieve the targeted lower costs.

Defining the mission of each unit is very important because it must be compatible with economic unit capabilities. For example, the plants identified with lower costs per cycle should have the mission to cycle more than the higher-cost units. APTECH had developed a code CYCLING ADVISOR™ that dispatches a utility fleet of plants over a ten-day period. The code seeks the least cost of the total fuel costs and cycling related costs.

4 Cycling-Related Damage Mechanisms

Personnel estimating cycling costs need to be aware of cycling-related damage mechanisms. These are discussed below.

4.1 Background

Every time a power plant is cycling, the boiler, steam lines, turbine, and auxiliary equipment go through unavoidable thermal and pressure stress cycles. These stress cycles damage the components every time they occur. This damage accumulates over time, eventually leading to increased component failures and forced outages. To preserve the plant's availability, the utility must escalate capital and maintenance expenditures.

There are several material damage mechanisms that are likely to be accelerated by increased cycling. The major ones include creep, fatigue, creep-fatigue interaction, corrosion (especially during out-of-service periods) and other interrelated phenomena that promote accelerated component aging (such as erosion, wear and vibration). Creep, fatigue, and creep-fatigue interaction probably are the most important cycling-related damage mechanisms. These are discussed below in more detail.

4.1.1 Creep and Fatigue

Creep and fatigue are terms commonly used in the field of engineering mechanics. Creep is time-dependent change in the size or shape of a material due to constant stress (or force) on that material. In fossil power plants, creep occurs during *steady-state* (e.g., baseload) operation, and stems from continuous exposure to elevated temperatures and stress levels that result from constant high temperature and pressure in a pipe or tube. Fatigue is a phenomenon leading to fractures and failures when a material is under *fluctuating* stresses. In a fossil power plant, such fluctuating stresses come from large transients in both pressures and temperatures. These transients typically occur during cyclic operation.

4.1.2 Creep-Fatigue Interaction

Since baseload fossil units are designed, almost by definition, to operate predominantly under creep conditions, they experience increased outages when they also are subjected to excess fatigue conditions from cycling operation. This is the origin of the term creep-fatigue interaction.

Materials behave in a complex way when both types of mechanisms occur. The two phenomena (creep and fatigue) are not necessarily independent, but act synergistically to cause premature failure. Creep strains (i.e., mechanical

deformation from applied stress) can reduce fatigue life and fatigue strains can reduce creep life (4).

Figure 3 illustrates how creep and fatigue interact to reduce life. This figure, from the American Society of Mechanical Engineers (ASME), shows how the interaction between creep and fatigue affects the life expectancies (i.e., time to failure) of three types of materials (5). The most important aspect of the ASME curves is the highly nonlinear nature of this interaction.

For example, the high temperature components in most boilers have been built of ferritic steels, such as the 2-1/4% chrome/1% molybdenum steel included in Figure 3. Assume that this material has gone through 50% of its life due to creep damage from baseload operation, as shown by Point "A" in the figure. It will reach the end of its life with only about 10% of its allowable fatigue damage accumulation. This example shows that a material subjected to both creep and fatigue will fail much faster than if it experiences only creep or fatigue by themselves.

5 Implications of Creep-Fatigue Interaction

The key implication is that older units designed for baseload operation and used in this capacity over many years are very susceptible to component failure when they are eventually forced to cycle regularly. For example, assume that an older baseloaded unit undergoes three to six starts per year and has reached 40% to 80% of its life from creep damage alone. If it is suddenly dispatched to operate at fifty starts per year, it may take only two to six years to accumulate the 10% to 20% total fatigue damage needed to cause material and component failures.

Thus, while increases in failure rates due to cycling may not be noted immediately, critical components will eventually start to fail. Shorter component life expectancies will result in higher plant EFOR, longer scheduled outages, and/or higher capital and maintenance costs to replace components at or near the end of their service lives. In addition, it may result in reduced total plant life or more capital to life extend the plant. How soon these detrimental effects will occur will depend on the amount of creep damage that is already present and on the specific types and frequency of the cycling.

5.1 Additional Effects of Cycling Operation

The effects of cycling on power plant components can be dramatic and surprising. One often neglected effect is the increase in operator errors that occur due to the increased personnel involvement that is necessary for cycling activities. Specific component effects can also be identified. Table 1 lists many power plant component problems attributable to cycling. While some of these effects were not initially thought to be the result of cycling operations, our studies have shown that cycling activities are at least partially a cause.

6 Equation for Total Cost of Cycling

During several preceding engineering studies, APTECH developed an equation for the total cost of cycling a fossil power plant. This equation consists of at least seven distinct cost elements, as given below. (The " Δ " symbol refers to the incremental costs due to cycling.)

$$\begin{aligned} \text{Total Cost of Cycling} &= \Delta \text{ Operation, Maintenance, and Capital} \\ &\quad \text{Spending (1)} \\ &+ \Delta \text{ Replacement energy and capacity cost due to} \\ &\quad \text{changed EFOR (2)} \\ &+ \Delta \text{ Cost of long-term heat rate change (3)} \\ &+ \Delta \text{ Cost of heat rate change due to low load and} \\ &\quad \text{variable load operation (4)} \\ &+ \Delta \text{ Cost of startup auxiliary power, fuel, and} \\ &\quad \text{chemicals (5)} \\ &+ \Delta \text{ Cost of unit life shortening (6)} \\ &+ \Delta \text{ General engineering and management cost} \\ &\quad \text{(including planning and dispatch) (7)} \end{aligned}$$

The first cost element is the additional maintenance and overhaul capital costs attributed to cycling. These are typically the long term, wear and tear costs associated with additional maintenance and additional overhauls required on

Table 1. Effects of Cycling on Plant Components.

Boiler	Turbine	Chemistry	Electrical
<ul style="list-style-type: none"> • Fatigue Cracking of: <ul style="list-style-type: none"> — Boiler Tubes in Furnace Corners — Tube to Buckstay/ Tension Bar — Tube to Windbox Attachment — Tube to Header — Tube to Burner — Membrane to Tube — Economizer Inlet Header — Header Ligament • Boiler Seals Degradation • Tube Rubbing • Boiler Hot Spots • Drum Humping/Bowing • Downcomer to Furnace Subcooling • Expansion Joint Failures • Superheater/Reheater Tube Leg Flexibility Failures • Superheater/Reheater Dissimilar Metal Weld Failures • Startup-Related Tube Failures in Waterwall, Superheater, and Reheater Tubing • Burner Refractory Failure Leading to Flame impingement and Short-Term Tube Overheating 	<ul style="list-style-type: none"> • Cracking Due to Water Induction into the Turbine • Increased Thermal Fatigue Due to Steam Temperature Mismatch • Steam Chest Fatigue Cracking • Steam Chest Distortion • Boiling Fatigue Distortion/ Cracking • Blade, Nozzle Block, Solid Particle Erosion • Rotor Stress Increase • Rotor Defects (Flaws) Growth • Seals/Packing Water/ Destruction • Blade Attachment Fatigue • Disk Bore and Blade Fatigue/Cracking • Silica and Copper Deposits • Lube Oil/Control Oil Contamination • Shell/Case Cracking • Wilson Line Movement • Bearing Damage 	<ul style="list-style-type: none"> • Corrosion Fatigue • Oxygen Pitting • Corrosion Transport to Boiler and Condenser • Air, Carbon Dioxide, Oxygen Inleakage (Require NH₃ Countermeasures) • NH₃-Oxygen Attack on Admiralty Brass • Grooving of Condenser/ Feedwater Heater Tubes at Support Plates • Increased Need for Chemical Cleaning • Phosphate Hideout Leading to Acid and Caustic Attack • Silica, Iron, and Copper Deposits • Out of Service Corrosion • Increased Plant Chemistry Upsets/Off Normal Chemistry • Increased Electricochemical Corrosion Potential (ECP) Corrosion During Startup and Off-Load Times 	<ul style="list-style-type: none"> • Increased Controls Wear and Tear • Increased Hysteresis Effects that Lead to Excessive Pressure, Temperature, and Flow • Controls not Responsible • Motor Control Fatigue • Motor Insulation Fatigue • Motor Insulation Failure Due to Moisture Accumulation • Motor Mechanical Fatigue Due to Increased Starts/Stops • Wiring Fatigue • Insulation Fatigue Degradation • Increased Hydrogen Leakage in Generator • Fatigue of Generator Leads • Generator Retaining Ring Failures • Generator End Turn Fatigue and Arching • Bus Corrosion When Cool (i.e., Low Amps) • Breaker and Transformer Fatigue

cycling units. Experience in the industry shows that maintenance and capital spending typically increases, and overhaul times lengthen, with increased cycling. This cost element also may include the capital cost of cycling-related improvements. These improvements would include turbine bypass systems, stress analyzers, and equipment to upgrade automatic operation, such as automatic burner insertion, burner management systems, controls upgrades, chemistry upgrades, and turbine water-induction protection. Overall, capital and maintenance spending typically have been the largest cycling cost elements for most of the units that APTECH has studied.

The second cost element refers to the cost of having to increase the use of less economical generation units. It also includes the cost of possibly needing to purchase of additional short-term firm capacity due to lower availability of the cycled units.

The third cost element relates to long-term unit efficiency changes due to component degradation, such as worn seals and fouled heat exchangers.

The fourth cost element refers to increases in average heat rates caused by the operation of the unit at lower than desired capacity levels, and by dynamic load changes during cycling that may affect operation efficiencies.

The fifth cost element includes the fuel, chemicals and auxiliary fuel needed for startup. Most utilities keep track of these costs, and APTECH has found that they typically are the only costs that most utilities attribute to cycling.

The sixth cost element is system long-term generation capacity costs. This cost results from the acceleration of the need for capital expenditures to build new capacity due to the shortened life of the units being cycled.

The seventh cost element, general engineering and management, includes cycling cost studies, the general engineering study costs associated with modifications and upgrades to plants to make them cycle better, and the management costs associated with optimizing the units to cycle them more efficiently. It also includes the cost of figuring out the optimal dispatch strategy to dispatch the unit in cycling properly. This is a very complex optimization procedure, and this cost element accounts for the development of an appropriate dispatch algorithm for use in system operation.

The specific method used to compute cycling costs for a particular utility depends on how the utility accounts for various cost items, and on which cost

components are the most significant. As mentioned above, in past studies for other utilities, the first term in this equation generally has been the largest quantity in the equation.

7 Cycling Cost Estimation Method

Cost estimates begin with collecting technical, operating, and economic data for specific units. Data on forced-outage hours and actual hourly generation are used to build a general mathematical model of the damage that the units have suffered over the period studied. This "general damage model" is calibrated by plant signature data and by "direct damage modeling" of selected critical components.

The general damage model is based on the unit hourly generation history, and calculates damage per cycle under steady and cyclic loads and loads of any size that interact nonlinearly. It accounts for any combination of load peaks and valleys, time of load peaks, ramp rates, load changes with time, and differences among hot, warm, and cold starts. The damage ascribed to typical shutdowns and unit trips is also included.

For simplicity, the various types of cycling modes and resulting damage are converted to normalized values, defined in units of "equivalent hot starts." The damage model calculates the total damage from both load cycling and on/off cycling in terms of equivalent hot starts per year. Base-load units studied that load-cycle daily to at most 75% of maximum continuous rating (MCR) generally accumulate 40 to 60 equivalent hot starts per year. Cycling units with 100 overnight or overweekend shutdowns that load-cycle daily to 35% MCR may accumulate 200 to 300 equivalent hot starts per year.

Finally, the actual annual costs for maintenance, capital, and forced outages are correlated to the total cycling damage. A multi-variable statistical regression analysis and mathematical techniques are used to calculate the cost of the next incremental load cycle or on/off cycle.

A direct correlation is developed between the active damage mechanisms in critical components and the types of cycling operation that the unit experienced during a particular service period. This is called "direct" damage modeling, as opposed to the general damage model described. Results from this correlation are then used to modify the general damage model, to better apportion the

equivalent hot starts to each actual plant cycling operation, and to improve the estimates of damage.

Input for a direct damage model comes from on-line plant monitoring data. This includes data from strain gages on boiler waterwall tubes, boiler heat-flux monitoring, boiler feedwater chemistry monitoring, heat-rate testing, and failure analysis.

Costs are apportioned to all operations contributing to these starts, based on actual pressure, temperature, and stress-level changes during cycling (Figure 4). The analysis of actual data representing the absolute temperature change during a shutdown, cold start, warm start, hot start, and two load cycles are shown for the reheater only in Figure 5, left, with ramp-rate for these transients in Figure 5, right.

7.1 Data Collection and Review

The first task is the collection and review of all relevant data. Past outage data is broken down into forced and planned outages and the high-impact or critical components are listed with their respective contributions to the EFOR. Plant visits, examination of failure records, maintenance costs, and capital costs, and acquisition of key plant signature data, such as startup, shutdown, and load following data are all key to the development of a usable database. Such data would include pressures and temperatures of the boiler, turbine, feedwater heaters, condensers, and chemistry data and typical data on oxygen levels/corrosion product transport during cycling, as shown for the reheater in Figures 4 and 5. Senior plant personnel fill out a questionnaire to identify current cycling problems and to estimate the future effects of cycling.

7.2 "Top-Down" Statistical Analysis

The next step is to correlate the total equivalent hot starts to both capital and maintenance cost, using multi-variable regression statistical analysis. Regression is also used to correlate cycling (e.g., unit off/on) to heat rate and to EFOR changes and their associated costs.

Figure 6 shows actual data for ten similar 125 MW fossil units with average EFOR correlated to equivalent cycles. The plot includes a "Best Fit EFOR" curve based on nonlinear regression.

Actual EFOR appears to track the annual cycles. Note that peaks in the EFOR occur seven, five and two years after significant cycling begins. This suggests that adding a cycle creates a lag time for EFOR, and therefore spending to correct the cause of outage. Furthermore, this lag time for EFOR suggests that adding a small amount of fatigue damage to older, creep-damaged material leads to component failures. This is consistent with the creep/fatigue interaction curves from ASME as shown previously in Figure 3.

In practice, APTECH has found that the increase in heat rate from cycling is due to such things as turbine seal wear, turbine blade erosion, air heater fouling at low loads, and a host of other cycling-related heat rate impact variables.

7.3 "Bottom-Up" Engineering Accounting Analysis

This independent cost analysis method is used to corroborate the results of the top-down analysis. The bottom-up engineering accounting analysis involves reviewing actual work orders on past capital and maintenance activities and apply experienced engineering judging to what extent these expenditures were related to cyclic operations. Once the total annual capital and maintenance expenditures due to cycling are estimated, they are divided by the cycling-related annual equivalent hot starts calculated by the general damage model. The resulting capital and maintenance cost per hot start is then compared with the output from the top-down method. APTECH has obtained very good correlation between the top-down and bottom-up methods.

8 Summary of Cycling Cost Estimates

A summary of the results of calculations and studies for five major utility systems are shown in Table 2. The cost of cycling conventional boiler/turbine fossil power plants can range from between \$2,500 and \$500,000 per start-stop cycle, depending on the specific unit size, type, fuel, pressure, and design features.

During the projects, it was also discovered that utilities typically estimate these costs at a factor of 3 to 30 *below* actual costs and, thus, often significantly underestimate their true cycling costs. The result would be that their units are cycled far more than they should result in excessive capital and maintenance spending requirements of the power plants.

Table 2. Results of Utility Studies.

Unit Type	Typical Industry Value (Without Consideration of Total Cycling Cost)	Potential Range of Total Costs
Small Drum	\$5,000	\$2,500 - \$100,000
Large Supercritical	\$10,000	\$30,000 - \$500,000
Gas Turbine	\$100	\$300 - \$65,000

9 The Application of Cycling Cost Information

After computing a more accurate estimate of the total cost of cycling, the next step is the practical application of this information. Here are some examples of how best to use this knowledge.

9.1 Lowering Overall System Costs

Table 3 lists some specific measures that may be taken by a utility to lower overall system costs, given better knowledge of the total cost of cycling. Specifically for the "system dispatch" operating area in Table 3, one result of true optimal dispatch (i.e., based on accurate cycling cost estimates) will be that resources with the lowest cycling costs, such as "designed-for-cycling" fossil units and pumped storage units, will tend to be dispatched more. There also will be a tendency for more purchases during peak load hours, and more dump energy sales during nighttime hours to lower cycling costs. Plants with good efficiency and high cycling costs will tend to stay on line longer.

It is recommended that utility management consider all these types of cost reduction measures when evaluating how much effort to devote to estimating total cycling costs, and more important, how to use them.

Table 3. Cost Reduction Measures Afforded by Better Estimates of the Total Cost of Cycling.

Utility Operation Area	Cost Reduction Measures
Plant Operation	Closely monitor and modify startup, shut-down, and ramping protocols to lower component fatigue stresses.
Plant Maintenance	Do predictive maintenance accounting for cycling damage to minimize cycling related forced outages.
System Dispatch	Modify loading order of units to reflect true cycling costs. Modify unit commitment dispatch program to account for true cycling costs and, using short-term load forecasts, do proper tradeoffs between cycling cost and other variable costs.
Medium and Long-Term Transaction Evaluation Costs	Include in the negotiation and accounting of energy and capacity transactions, consideration of the beneficial or adverse impact of the transaction on in system cycling. This is particularly important when evaluating purchase opportunities that are baseload in nature.
System Planning	Account for cycling costs on existing units when evaluating new resources. This will tend to make flexible resources that have low cycling costs be more value to the system.

9.2 Improvement of Production Cost Models and Dispatch Models

There are a number of system dispatch models in use by electric utility dispatchers. These models were developed with the objective of determining optimum hourly dispatch schedules with unit fuel costs, heat rates, and operational constraints the primary factors in determining the optimum

schedules. More recently, with the increases in market interchanges and complex purchase and sales contracts, significant effort has been put into better modeling of energy and capacity transactions. One area that has not been seriously looked at by most utility dispatchers and unit commitment vendors is the damage or wear-and-tear rates caused by varying generation unit operation practices, including on/off cycling, load following cycling, load changes with varying MW ramp rates, load following at varying load depths, higher than rated capacity operation, and minimum load operation. The design of the current system dispatch models does not include capabilities of modeling these damage rate factors other than allowing for "startup costs."

APTECH's CYCLING ADVISOR seeks to find the lowest system cost hourly dispatch schedule taking into account all major cost factors, including generation equipment wear and tear. It is currently set up to run over a ten-day period, which would include at least one low load weekend period. Its output includes hourly load levels of each unit, the number and characteristics of each cycle type (e.g., starts, load follows, equivalent hot starts), total system costs including "wear and tear," fuel, and net purchase/sale proceeds -- all for the lowest cost dispatch schedule found by the program.

Figure 7 shows an example system dispatch output for a hypothetical utility. Other CYCLING ADVISOR outputs include tables of hourly dispatch for each unit and period summaries of all major cost factors (e.g., wear and tear, fuel).

10 Case Studies

Two case studies concerning the cost of cycling are described in this paper.

10.1 Florida Power Corporation

The study for Florida Power Corporation (FPC) was initiated in May 1995. FPC had recognized that cycling would increase maintenance, capital, outage, and loss-of-efficiency expenditures, and wanted to quantify these cycling-related costs. The study focused on the entire fleet of FPC units, but the result of two 500 MW coal-fired units at the Crystal River plant are presented here.

The total cost of cycling was estimated by using several complementary but independent methods. The primary method has been generally described in this paper. Besides the engineering and statistical analysis steps, selected unit data

from past APTECH studies and from NERC GADS were compared. FPC's cycling-related plant expenditures were audited in detail. Also, operators and experts were surveyed to rank and validate the costs between the two units. These multiple and complementary approaches helped to cross-validate the results.

The results of the evaluation of FPC's own operating cost history show that a unit such as Crystal River, Unit 2 can be expected to incur total cycling costs ranging between \$30,000 and \$110,000 for each individual hot start. The corresponding range for a cold start is between about \$70,000 and \$240,000, with a best estimate also more precisely determined. "Best" estimates per hot start were also calculated, but are not disclosed here due to competitive restrictions. When FPC incorporated these data and data from other units in the FPC fleet into its production cost models and dispatch models, the resulting savings were shown to be \$10 to \$25 million per year.

10.2 Electricity Supply Board of Ireland

The Irish Electric Supply Board (ESB), with headquarters in Dublin, Ireland, commissioned a study of three power plants in January 1996 and added five more units in January of 1998. The purpose of the study was to determine the cost of cycling of each unit type in the ESB system, and make operational and equipment recommendations in order to optimize cycling and reduce cycling damage.

The first study of three plants is complete and the later study is currently ongoing.

The salient results from this study are as follows:

1. The coal fired 305 MW subcritical pressure units at Moneypoint are heavily baseloaded and have incurred little cycling related damage. Notwithstanding this, they typically incur some 40 - 80 equivalent hot starts in the few starts and minor load swings in a year. These units are more baseloaded than any units that APTECH knows of in the United States.
2. The oil fired 120 MW subcritical pressure units 1 & 2 at the Poolbeg Station are heavily cycled (two shifted) such that they incur between 200 and 400 equivalent hot starts per year (see Figure 2-10 from ESB Report 2764). Despite this, they handled the heavy cycling well and consequently have relatively low cycling costs compared to other similar US units. The

capital and maintenance costs are not excessive considering the inevitable cycling related damage that these units incur. Future projections of capital and maintenance costs based on future cycling are very close to the future costs that ESB independently estimated using conventional remanent life techniques (see Figure 3-11 from ESB Report 2764).

3. The oil fired 260MW subcritical once through units 3 & 4 at Tarbert Power Station have also been cycled heavily such that they incur 150 to 350 equivalent hot starts per year. These units have incurred heavy cycling damage, out of service tube corrosion/pitting, and their cycling related expenditures were benchmarked to be higher than conventional subcritical units of similar size in the US.
4. The estimates of the cost of cycling made by ESB when compared to the results of the APTECH study were found to be significantly low. APTECH cycling cost estimates for one Unit type ranged from four to five times higher for cold starts and eight to ten times higher for hot starts. Furthermore, ESB had not attributed any cost to the frequent load following required of some units to control generation on the island. The cost of these load cycles (which was not insubstantial) was also estimated by APTECH; and
5. The level of the cycling related costs identified by APTECH study was such that a reappraisal of the system dispatch may be justified. This could involve reducing load on units which were formally always baseloaded to avoid the costs associated with shut down of other units. Some changes to dispatch have already occurred with further modifications currently under consideration.
6. Operational recommendations for various units included reducing start up rates, monitoring the start up furnace gas and superheater metal temperatures, monitoring the furnace waterwall tubing to downcomer differential and especially reducing the shutdown rates at elevated temperatures.
7. Plant chemistry related improvements included extending to all units the nitrogen blanketing (when the units come off line) currently carried out for some units, reducing oxygen during start up, monitoring the air ejector exhaust flow and discontinuing the practice of chemical cleaning the boilers with hydrochloric acid.

The study of the other units is under way but, no other results are available for release at this time.

10.3 Lessons Learned From Case Studies

These case studies are typical of evaluations that should be done before enacting a proposed change from baseload to cycling operating mode. Such evaluations should also be done for all types of new generation and/or long term purchases. When bidding and for long-term cost forecasting, use a future cost equation that includes the effects of cycling.

The primary elements of a future power plant cost equation are as follows:

1. Fixed costs related to the capital purchase – interest, depreciation, taxes, insurance, etc.
2. Fixed costs related to operation and maintenance – mostly base in-house and contract personnel needed no matter whether unit is operating
3. Fuel costs
4. Non-fuel capital, operating and maintenance costs directly related to the amount of energy generated
5. Capital, operating and maintenance costs related to the amount of on/off and load following cycling

APTECH focuses on items two, four, and five, the various components of capital, maintenance, and operation costs. It is believed that these costs should be expressed in the following form:

$$\text{Total COM} = \text{Fixed COM} + A * (E) + B * (\text{EHS's})$$

where:

COM = Annual recurring capital, operation, and maintenance costs

A = A coefficient with units \$/MWH

E = Energy produced in MWH per year

B = Cost per equivalent hot start

EHS's = Equivalent hot starts per year – an indicator of the total

amount of cycling (i.e., cold, warm, and hot starts and load follow cycles)

11 Conclusions

The actual, or total, cost of cycling fossil units that were originally designed for baseload operation is greater than most utilities have estimated and accounted for in their system dispatch programs. The total cost of cycling for each unit type should be carefully assessed by utility management to ensure that their generator assets are used in an optimal way.

The cost estimation method described in this paper uses engineering and statistical analyses designed to help a utility optimally manage its power plant assets. It accounts for past operations and future expected effects of cycling (or other operational plans) on cost, life, and reliability.

The bottom-line effects of such an analysis can lead to cost savings between \$10 and \$200 million when evaluated over the life cycle of a typical 600 MW coal-fired power plant. Even more significant cost savings can be obtained when a complete utility system is analyzed and optimized. Such savings are going to be essential in the future competitive world where low-cost providers, those that best optimize their systems to minimize long-term average cost, are likely to emerge as the preferred electricity suppliers.

12 Acknowledgments

Many people at APTECH contributed their individual knowledge and skills to these projects. They include K.A. Ecoffey, T.A. Kuntz, S.R. Paterson, P.B. Lindsay, M.J. Cohn, T.W. Rettig, and J.J. Yavelak.

ESB personnel that contributed to this project include Alan Bissel, Gerald Caffery, and many plant personnel.

13 References

1. Lefton, S. A., et al., "Fossil Power Plants in Cycling Mode: Real costs and Management Responses," 1996 EPRI Managing Fossil Generating Assets in Emerging Competitive Marketplace Conference, Washington D.C., October 1996.
2. Lefton, S. A., et al., "Managing Utility Power Plant Assets to Economically Optimize Power Plant Cycling Costs, Life, and Reliability," 1994 EPRI Fossil Plant Cycling Conference, New Orleans, LA, September 1994.
3. North American Electric Reliability Council-Generation Availability Data System, "Reporting Instructions," October 1993.
4. "Metals Handbook - Tenth Edition, Volume 1 - Properties and Selection: Irons, Steels, and High-Performance Alloys," ASM International.
5. American Society of Mechanical Engineers, "Class 1 Components in Elevated Service, Section III, Division 1," Cases of ASME Boiler and Pressure Vessel Code, Case N-47, Rev. 29, December 1990.
6. Schreiber, R. J., et al., "Cycling Cost Assessment Project," 1994 EPRI Fossil Plant Cycling Conference, New Orleans, LA, September 1994.
7. Lefton, S. A., Besuner, P. M., et al., "Estimating the Total Cost of Fossil Plant Cycling Operation," Final Report for Electric Power Research Institute, RP 3746-01, December 1995.

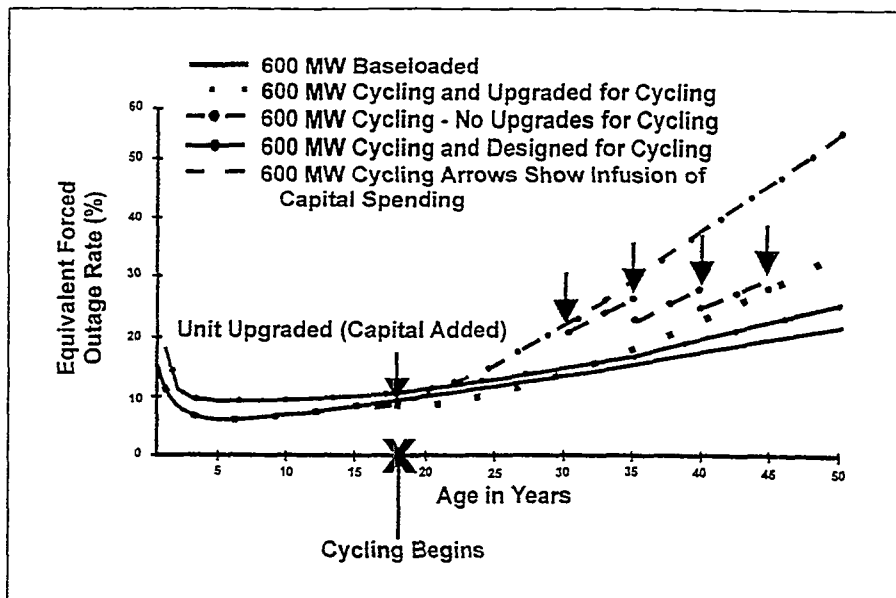


Figure 1. Schematic Diagram of Typical EFOR and Capital Infusion Effects for Large, Aging, Coal-Fired Units Designed or Upgraded for Cycling.

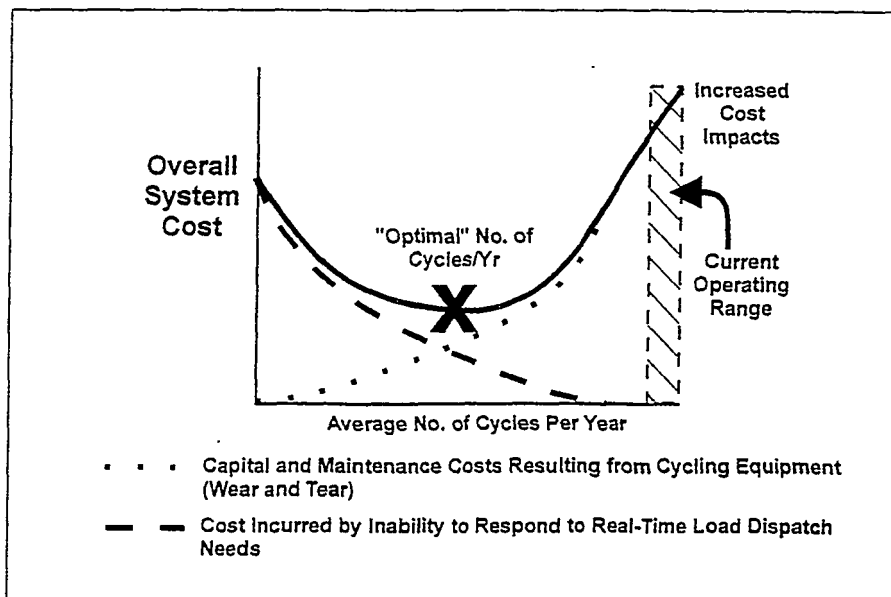


Figure 2. Schematic Diagram of Overall System Costs Versus Average Cycles Per Year for Utility Power Plants.

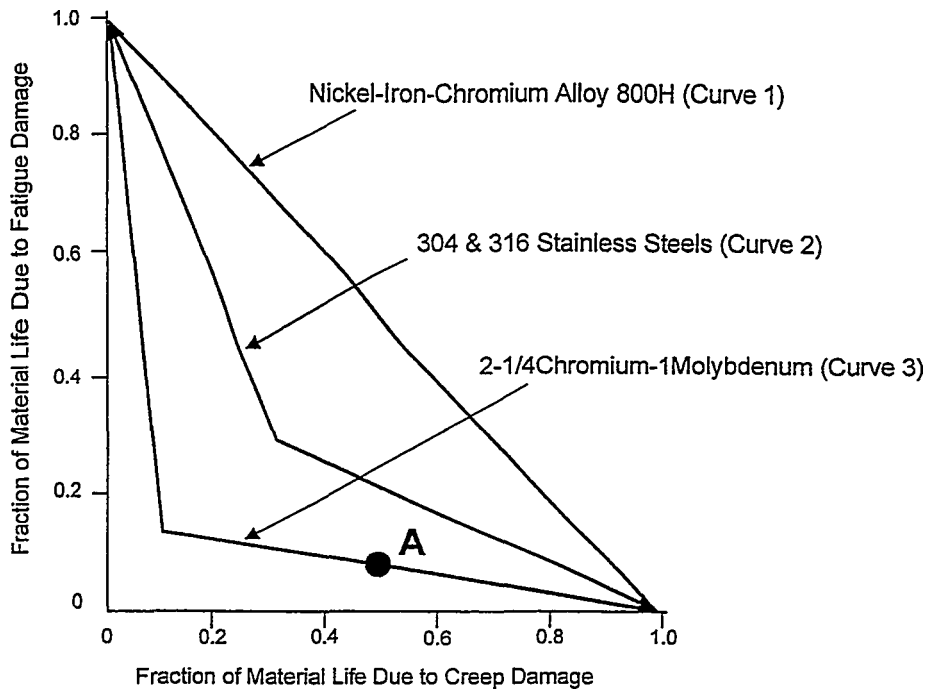


Figure 3. Creep Fatigue Interaction Design Curves for Several Materials.

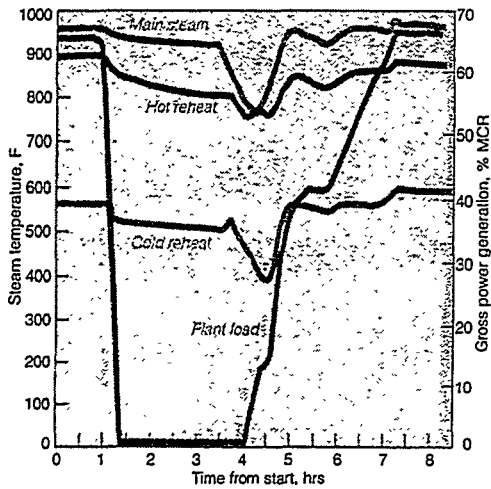


Figure 4. Steam temperature variations during load swings compound aging effect on plant equipment.

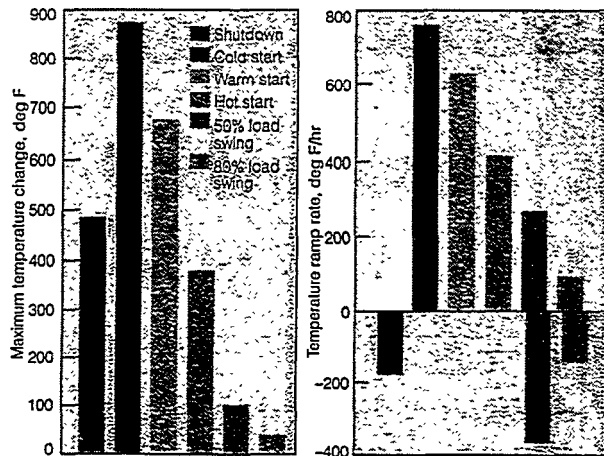


Figure 5. Reheat outlet temperature changes (left) and ramp rates (right) during transients, greatest for cold startup, typify effects of cycling modes. Both are factored into calculations of equipment damage.

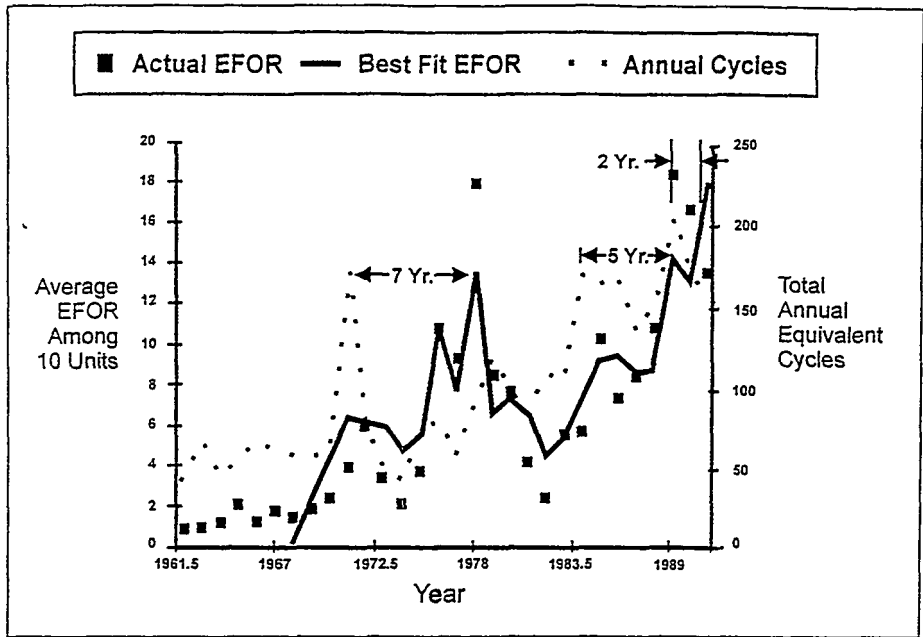


Figure 6. Effect of Cycling on Plant Reliability (EFOR).

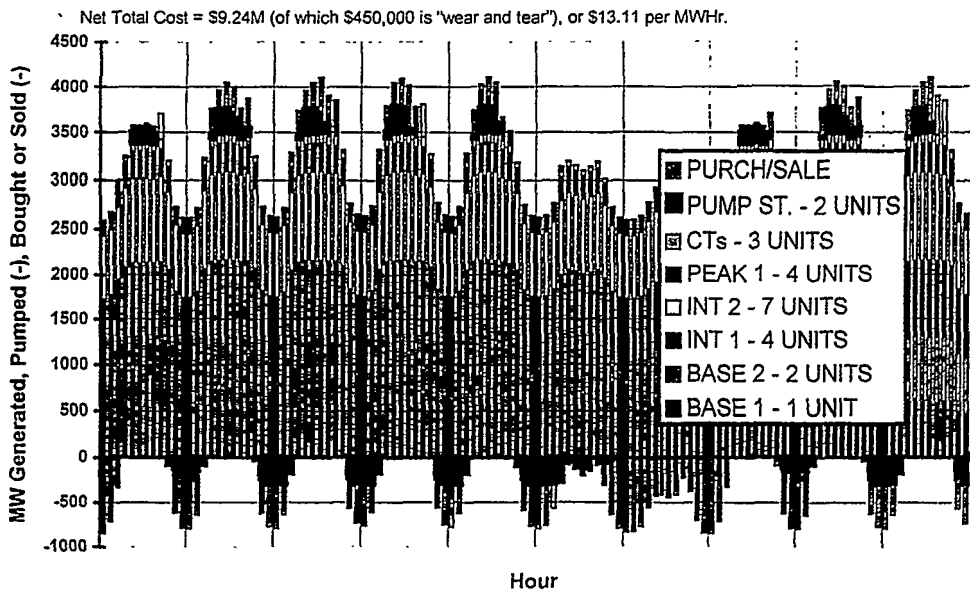


Figure 7. Optimized Hourly Dispatch for High Load Period Using CYCLING ADVISOR and APTECH-Derived Total Cycling Costs.

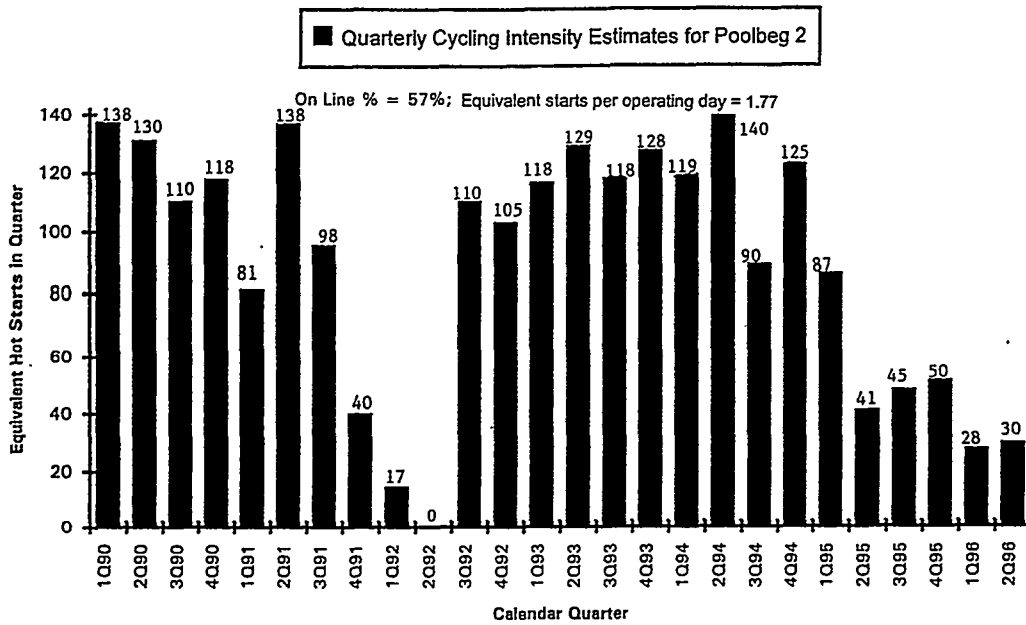


Figure 8. Quarterly Cycling Intensity Estimates for Poolbeg Unit 2.

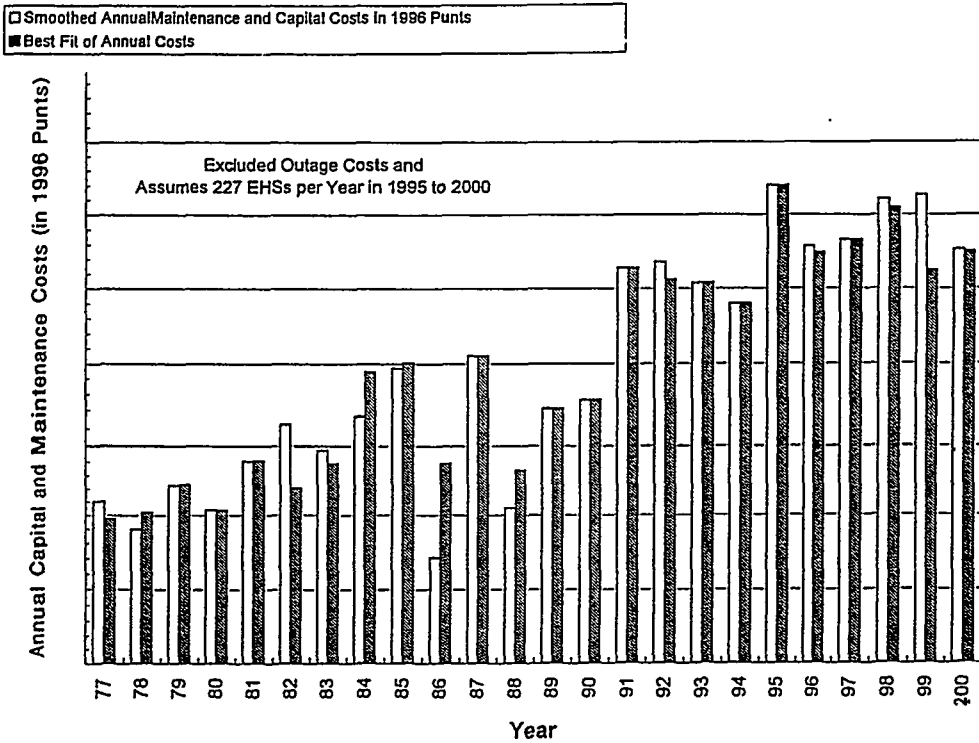


Figure 9. Best Estimate of Smoothed Poolbeg Unit 2 Maintenance Costs Plus 9.7 M Puntis in Nonrecurring Capital Costs in 1991 to 2000.

The Thematic Plant Life Assessment Network (PLAN)

R.C. Hurst, Sector Head
EC/JRC Institute for Advanced Materials
Petten, The Netherlands
D. McGarry, Group Head
EC/JRC Institute for Advanced Materials
Petten, The Netherlands
H. H. Pedersen, Brite Euram
DG XII
Brussels, Belgium

Abstract

The Plant Life Assessment Network (PLAN) is a Brite Euram Type II Thematic Network, initiated by the European Commission to facilitate structured co-operation between all cost shared action projects already funded by the Commission which fall under this common technical theme. The projects involved address a multiplicity of problems associated with plant life assessment and are drawn from Brite-Euram, Standards, Measurement and Testing, Nuclear Fission Safety and Esprit EC programmes. The main aim of the Network is to initiate, maintain and monitor a fruitful co-operation process between completed, ongoing and future EC R&D projects, thereby promoting improved cross fertilisation and enhanced industrial exploitation of R&D results.

As the project is in its infancy, this paper covers the background to the initiative in some detail. In particular two key aspects are highlighted, namely, the requirement of the EC to launch such a network in the area of plant life assessment including its evolution from two small Thematic Research Actions and, secondly, the mechanism for structuring the Network in an ordered and proven way along the lines of the EC/JRC European Networks, PISC, NESC, AMES, ENIQ, ENAIS and EPERC.

The operating and financial structure of the Network is detailed with reference made to the role of the executive Steering Committee, The

Network Project Leader and the Network Financial Co-ordinator. Each of the 58 projects involved in the Network, representing a wide range of industrial sectors and disciplines, is distributed in terms of their efforts between 4 disciplinary Clusters covering Inspection, Instrumentation and Monitoring, Structural Mechanics and Maintenance. For each of these Clusters, an expert has been appointed as a Project Technical Auditor to support the elected Cluster Co-ordinator to define Cluster Tasks, which contribute to the overall objectives of the project. From the Project Representatives, Cluster Task Leaders and Leaders of Horizontal Themes (spanning all Clusters) have been appointed and the Tasks and Themes approved to date are outlined.

Finally, the proposed method of working within the Network, emphasising the strong role of information dissemination using modern informatic tools, is described taking into account the clearly defined objectives, the scope and the agreed deliverables of the project.

1. Introduction

The European Commission supports engineering industry R&D projects either directly through IVth Framework Programme sponsorship of the projects themselves or additionally through Thematic Networks which usually link together like projects either at the initiative of the projects (Type I) or at the initiative of the EC (Type II). There is a well founded view that added value can be obtained by grouping projects or experts in a particular field into networks in order to induce cross fertilisation of information and know-how leading to more effective technology transfer.

In the particular area of Plant Life Assessment, the Brite EuRam Programme Managers have recognised that significant benefit can potentially be obtained by grouping existing and future projects in a multidisciplinary network. Most Type I Thematic Networks concentrate on a specific disciplinary theme which is addressed by experts in that field. In fact two separate Targeted Research Actions (TRAs) on the specific disciplinary themes of Monitoring and Maintenance were the precursors to the PLAN project. Such themed configurations undoubtedly lead to added value due to the knowledge transfer afforded by setting up a structured network as demonstrated for the TRA's. A much more ambitious approach has been taken in the Type II network conceived by the EC which brings together experts from diverse disciplines, albeit with the same goal of enhancing the reliability, safety and efficiency of structural plant components. Such interdisciplinary networks have higher risks than conventional networks but the increased potential for synergism bodes well for benefits beyond those which could be expected for the same investment

of resources. Nevertheless, without some clear structure to the Network, the potential benefits may disappear in the ensuing chaos which frequently prevails in multidisciplinary projects.

In this respect the EC took recourse to a co-ordinator with experienced network management skill for complex structural integrity research networks. Commencing with the Programme for Inspecting Steel Components (PISC), the Joint Research Centre's Institute for Advanced Materials has developed a number of structural integrity based networks based on this successful model. The PISC successor projects, AMES, ENIQ and NESC [1] have real project goals, just as in PISC, with the need for extensive experimental and computational work. As a result, these networks are relatively expensive to run and require contributions in kind and usually some additional sponsorship. Although a fundamentally different base for the network compared to a Brite-Euram Thematic Network, where funding is at a lower gearing for actions and tasks compared to experimental projects, there is, nevertheless, commonality in the co-ordination methodology employed. It was therefore deemed logical for an approach to be made to JRC Petten to assist with the elaboration and to assure the scientific and technical co-ordination of the Thematic Network entitled "Plant Life Assessment Network" (PLAN). As usual for such a network, the structure has been designed around a key mission statement which provides for "a European Network enabling the cross fertilisation of knowledge along with the dissemination and transfer of information, obtained from EC sponsored research, into a form suitable for field use and for consideration by code and standard bodies".

2. Objectives & Scope

The general objectives of PLAN are not dissimilar to other EC Thematic Networks and they cover:

- promoting synergy by identifying like projects.
- ensuring the optimal use of Community funding.
- securing added value by organising the individual projects into research clusters and horizontal themes.
- the co-ordination of research through the clusters, cluster tasks and horizontal themes
- achievement of teamwork via the networking principle
- the exchange and dissemination of information
- technology transfer between different partners and industries and,
- contributing towards the future shaping of EC research priorities and activities.

The specific PLAN objectives are formulated around the core of the Network structure which comprises four key structural integrity research Clusters covering inspection, instrumentation and monitoring, structural mechanics, and maintenance. The Representatives of EC shared cost action projects form the partnership of the Network and are allocated to the most appropriate Cluster covering the field of their project. Each Cluster is expected to define and execute certain Cluster Tasks and Actions within the generic objectives of the Network and to contribute towards trans-Cluster Horizontal Themes which will bridge the disciplines prevalent in the Clusters.

The scope of the proposed network covers life management of industrial plant, the structural integrity of components, and the plant life management infrastructure. This scope includes all industrial plant which fall under the competence of the EC Brite-Euram, Standards, Measurement and Testing, ESPRIT and Nuclear Fission Safety shared cost action research programmes. The Network is conceived to be truly multi-sectorial and multi-disciplinary with a generic relevance for industry, with its participants representing most industrial sectors covering the power generation, chemical and petrochemical, manufacturing and transport industries and addressing a range of problems relating to plant life assessment and management.

3. The PLAN Network Structure and Partnership

The generic functional organisation scheme for PLAN (Figure 1) explains how different projects are expected to participate in Clusters, Cluster Tasks and Horizontal Themes with some examples given of potential activities. Some 58 projects, led predominantly by industrial organisations, representing several 100 industrial enterprises, universities and research organisations are already actively involved. Project Co-ordinators usually represent their projects within the Network but an alternative Project Representative may be mandated from each project consortium. In addition to being a Member of at least one of the four Network Clusters, each Project Co-ordinator /Representative is expected to contribute to at least one Cluster Task, and at least one Horizontal Theme. Funding for participation in the Network covers expenses for attending and contributing to Clusters, Cluster Tasks, and Horizontal Themes, and all other meetings and actions approved by the Steering Committee within agreed maxima. The total funding accommodates the potential for launching up to three Cluster Tasks per Cluster and three Horizontal Themes for the whole Network. A Steering Committee has been created to fulfil the function of executive body of the Network, whereas the JRC/IAM is responsible for the operation and management of the Network as the Scientific and Technical Co-ordinator with the assistance of an independent Financial Co-ordinator. In addition to the Cluster Co-ordinators, the Steering Committee is strengthened through

the involvement of Project Technical Auditors, each specialising in a Cluster field, who carry out the individual project auditing on behalf of the EC and are in a good position able to catalyse the links and synergies between projects.

The professed aims of the Network implicitly include the enhancement of technology transfer and information dissemination between industries, types of organisation, disciplines and organisations in different European countries. Figure 2a exemplifies the diversity of representation from the different projects: Figure 2b the national distribution of all the partners of all 58 projects; Figure 2c the types of industries involved, where the projects are industry specific; Figure 2d the variety of organisations, involved as Project Co-ordinators/Representatives; and, finally, the number of projects in each disciplinary Cluster is portrayed in Figure 2e.

4. Goals and Deliverables of the PLAN Network

With the aim of assuring information dissemination across EC sponsored projects, their participant organisations and industrial sectors and of providing added value to their output, the PLAN Network has set out a comprehensive list of expected deliverables for the Thematic Network.

The four separate Clusters will form the engine of the Network, with their role to facilitate exchange of information between partners from similar disciplines but from a variety of industrial sectors. This role will be facilitated through:

- Cluster Seminars and Workshops
- 3 Themed Cluster Tasks per Cluster
- Cluster State of the Art reviews
- Participation of Cluster Projects in International Conferences and Seminars in the technical field of the Cluster.

The deliverables from these actions will be in report form, prepared under the responsibility of the appointed Cluster Co-ordinator and Cluster Task Leaders. These reports are expected to address the dissemination of mutual technical information to identify the shortcomings in a particular field or approach, to propose the way forward and identify the means and resources required to tread this path and, finally, to indicate the aspects, common to all Projects in a Cluster or not, which are relevant or can be developed to be so, for promoting Codes and Standards at a European or global level.

Dissemination of information and co-operation across the 4 Clusters is crucial to the success of the Network, as the multi-disciplinary interactions which occur in actual plant life assessment and management must be reflected and evaluated. The actions foreseen cover:

- 3 trans-Cluster Horizontal Themes

- Structured actions and discussions in and from plenary Network meetings
- Joint meetings or seminars of 2 or more Clusters on topics of common interest
- The organisation of a dedicated International Conference covering all key issues involved in plant integrity and operation

Again the deliverables from these actions will be meeting minutes, reports and conference proceedings, prepared by the Horizontal Theme Leaders and the Network Scientific and Technical Co-ordinator. Likewise, the reports will address information dissemination, identification of shortcomings and proposals for the way forward, in particular in advising the EC on the priorities for funding in the Vth and VIth Framework Programmes. The potential relevance for new Codes and Standards development, where benefit can be obtained from a multi-disciplinary, cross sectorial approach, must be emphasised.

The final group of deliverables which are to be extracted from the input of the Partners under the responsibility of the Network Co-ordinator cover:

- Auditing of those Projects which are allocated to the PLAN network by the EC, with the added advantage to PLAN of an independent assessor who has a broader overview of like projects and should be able to pinpoint additional common interests
- The establishment of a PLAN partner Catalogue
- Preparation of a WWW Homepage updated at least 4 times/annum, facilitating access for all Project partners to evaluate the continually updated output of the Network.
- Incorporation of a specific, publicly accessible, section to the Homepage for dissemination of the function of the PLAN Network and information concerning the general progress achieved to a wider audience
- 6-Monthly and Annual Progress Reports on the Network for the Partners and for the EC.

5. Current Status

At the time of preparation of this paper, the PLAN Network is only 6 months along the road towards its 4 year goals. Although, and perhaps not surprisingly, considerable time and effort was required to establish basic participation agreements and funding contracts for the initial 64 member PLAN consortium, considerable progress has been achieved with installing the Cluster based structure of the Network, defining and approving the first tranche of Cluster Tasks and Horizontal Themes and setting up the first version of a central information collection and dissemination system. Two key plenary meetings have been held along with Cluster and Cluster Task meetings in order to inject a rapid start to the actions of the Network.

Figure 3 gives the current specific functional organisation of PLAN, all Projects having been allocated to their appropriate Clusters (Table 1) and Cluster Co-ordinators elected. Further the already approved Cluster Tasks are indicated with their actual titles and the responsible Cluster Task Leader. Some latitude still exists for new Tasks although, as indicated, some prospective tasks are quite close to approval. For each of the approved Tasks, a detailed proposal has been prepared with a clear indication of the participants from each Cluster. Also agreed are the first two of the planned Horizontal Themes, indicated with their titles and Theme Leaders, again corresponding to detailed proposals and participation agreement. Planning and timescales have already been agreed for all the approved Cluster Tasks and Horizontal Themes and the Network is primed for action. The WWW Homepage has been firmly established in a prototype form, containing information about the Network along with the possibilities to link through the page to both the EC Cordis data base for all EC projects as well as the Homepages for the individual projects where they are available.

6. Conclusions

The multi-disciplinary, multi-sectorial PLAN Thematic Network has been devised for information dissemination, improved co-operation, and derivation of added value between similar plant reliability and operation based EC Shared Cost and Concerted Action Projects. In its first semester, a rigid framework has been established for meeting the professed objectives and achieving the defined goals of the Network, based on establishing clustered groups of projects of similar background, identifying Cluster Tasks, devising trans-Cluster Horizontal Themes and setting up a central information collection and dissemination point. Progress is on schedule and augurs well for the future of the PLAN Network.

7. Reference

- [1] U.von Estorff, S.Crutzen, R.Hurst, P.Lemaitre, D. McGarry
JRC of the EC-Institute for Advanced Materials, P.B.2, NL-1755 ZG Petten
AMES,ENIQ, NESC: Three European Networks in the Field of Structural Integrity
TOP SAFE'98 Valencia (Spain) -15-17 April 1998

Table 1. Project allocation per Cluster (Cluster A - Inspection, Cluster B - Instrumentation/Monitoring) .

Proj. N°.	Project Title	Project Leader	Institute Company
<i>Cluster A - Inspection</i>			
BE-1042	Nex X-ray imaging sensors	Mr. C. Fröjd	Regam Medical Systems AB
BE-1164	Development of a portable remote controlled real-time radioscopy system for quantitative industrial inspection of large thickness	Dr. J. Rheinlander	RISO NATIONAL Labo.
BE-1389	Rapid quality weld inspection without surface preparation	Dr. B. W. Shepherd	MITSUI BABCOCK
BE-3038	Compact wall and ceiling climbing robotic vehicle with dexterous manipulator arm for low cost remote nondestructive inspection in hazardous environments	Prof. Bryan Bridge	Univ. South Bank London
BE-3482	Multi-sensor inspection system for component testing : towards more reliable NDT applications	Mr. V. Just	EDF
BE-3681	Fast film replacement system for high resolution X-ray weld inspection with ultrasonic data fusion	Dr. V. Kaftandjian	INSA
BE-3743	On-line quality control, production process assessment and tracking system for mechanical parts	Prof. C. Fernandez	Univ. Pol. Madrid
BE-5935	Inspection and maintenance of power plant components	Mr. K. Lieven	MIT GmbH
BE2-0522	Development of a photothermal measuring technique for the determination of hardness profile in steel	Dr. H. Stamm	JRC/IAM
BE2-0525	Training industry in neutron strain scanning	Dr. M.W. Johnson	Rutherford Appleton Laboratory
BE2-0546	A thematic network on climbing & walking robots including the support technologies for mobile robotic machines	Dr. G.S. Virk	University of Portsmouth
BE2-0557	Advanced tomographic sensors for industrial multiphase imaging	Dr.B.S.Hoyle	University of Leeds
SMT-2022	Effect of ultrasonic scattering on inspection of austenitic welds	Dr. M. Bieth	JRC / IAM

Proj. N°.	Project Title	Project Leader	Institute Company
<i>Cluster B - Instrumentation / Monitoring</i>			
BE-1147	Pulsed digital holography and shearography	Ms O. Petillon	AEROSPATIALE
BE-1372	Magnetostrictive actuators for damage analysis and vibration control	Prof. L. Lecce	Univ. Napoli
BE-1432	Fibre optic strain monitoring at elevated temperatures	Mr. B. Hildenwall	Vattenfall AB
BE-3116	Multi-Wavelength Shearography	Dr. H. R. Schubach	Eitemeyer Qualitätssicherung
BE-3246	Remote monitoring strain/extension using novel sensing element	Mr. R. Shipton	ERA Technology Ltd
BE-3471	Continuous corrosion surveillance of process equipment by new (electrochemical) sensing techniques and devices	Prof. W. Bogaerts	KU Leuven
BE-3833	Two-dimensional acoustic imaging arrays	Dr. C. Millar	GEC-Marconi
BE-5535	Advanced material non destructive testing using high resolution dual energy tomography (DUALETO)	Miss P Tappo	Iso TEST Eng. SRL
BE-6056	On-line acoustic monitoring of structural integrity of critical power plant components operating at high temperature	Mr. C.G. De Michelis	CISE SpA
BE-7289	Protection and monitoring systems for hydroelectric generating sets	Mr. F. Arregui	IBERDROLA
BE-7567	Fibre optics for remote monitoring of structural integrity of elevated temperature insulated systems (FORMS)	Mr. M.Gomes	ISQ
CR-1625	Non destructive real-time control of the quality of electrical spot welding	Mr. J. Catty	CETIM

Table 1 (continued). Project allocation per Cluster (Cluster A - Inspection, Cluster B - Instrumentation/Monitoring) .

Proj. N°.	Project Title	Project Leader	Institute Company
<i>Cluster C - Structural Mechanics</i>			
SMT-2070	Development of creep crack growth testing and data analyses procedures for welds	Dr. B. Dogan	GKSS
BE-1426	Structural integrity assessment procedures for European industry	Mr. E. S. Webster	British Steel PLC
BE-1702	Validation, expansion and standardisation of procedures for high temperature defect assessment	Dr. I. Shibli	ERA Technology Ltd
BE-1835	Prediction of pressure vessel integrity in creep hydrogen service	Mr. P. Balladon	Creusot Loire Industrie SA
BE-3019	A methodology for life prediction and condition assessment for welds of refurbished and new steam cycle plants	Mr. A.A. Batista	EDP SA
BE-5245	Optimization of methodologies to predict crack initiation and early growth in components under complex creep-fatigue loading (C-FAT)	Dr. S. Holdsworth	GEC ALSTHOM Ltd
BE-6021	Development of an understanding of materials properties under the combined influence of creep, fatigue and oxidation.	Mr. G. Koenig	Daimler-Benz Aerospace
BE-7301	Life optimization of dissimilar metal welds for high temperature components	Mr. V. Bicego	CISE SpA
BE-7463	Creep crack growth in carbon- manganese steel at 300 - 420°	Dr. R.V. Maskel	MITSUI BABCOCK
BE-7500	A novel creep resistant tin strengthened 9-12%CR ferritic steel for advanced steam power plant.	Mr.G. Shrimpton	AEA Technology
BE-7913	Superheater materials testing for ultra supercritical boilers	Dr. A Vanderschaeghe	GEC Alsthom -Stein Ind.
BET2-0509	European collaboration in creep data development for welds "weld-creep"	Dr. D. Robertson	ERA Technology Ltd
FI-0073	Relation between different measures of Exposure-Induced Shifts in Ductile-Brittle Transition temperatures-Validation of surveillance practice & mitigation methods for ageing reactor materials	Dr E. G. Taylor	Magnox Electric Plc
FI-0181	Evaluation of techniques for assessing corrosion cracking in dissimilar metal welds	Dr D. Tice	AEA Technology
FI-0312	Structural integrity of Bi-metallic components	Mr. C. Faidy	Electricité de France
FI-0344	Reconstitution techniques qualification and evaluation to study ageing phenomena of nuclear pressure vessel materials	Dr E. Van Walle	Studiecentrum voor kernenergie
FI-0357	Variation of residual stresses in aged components	Dr R.H. Leggatt	The Welding Institute
CR-5084	Inspection and surveillance of metallic pressure vessels during proof testing	Dr. C. Herve	CETIM

Proj. N°.	Project Title	Project Leader	Institute Company
<i>Cluster D - Maintenance</i>			
SP-249	Implementation of power plant component life assessment	Dr. A. Jovanovic	MPA Stuttgart
20598	ESPRIT - MATES	Mr. R. Campo	Dassault Electronique
20874	ESPRIT - REMAFLEX	Mr. J. Pinoteau	SEMA Group
BE-1313	Vibration interpretation using simulations and the intelligence of networks	Mr. I. Jennings	MONITION Ltd
BE-1524	Monitoring On-line integrated technologies for operational reliability	Mr. A. Ball	British Aerospace Ltd
BE-1732	Human factors in aircraft dispatch and maintenance safety	Dr. N. Mc Donald	Univ. Dublin Trinity College
BE-1843	Condition monitoring and predictive maintenance of high voltage rotating machines :European insulation diagnosis criteria and equipment	Mr. J.P. Gemeau	ELECTRABEL SA
BE-2015	Model based diagnosis of rotor systems in power plants	Dr. J. E.T. Penny	Univ. Aston Birmingham
BE-3044	Extending the economic lifetime of aging plants by systematic engineering	Mr Reunanen	VTT
BE-3491	The monitoring of reciprocating plant & machinery for improved efficiency & reduced breakdown	Mr. A. Khan	MITEC International Ltd
BE-5525	Advanced Maintenance advisory surveillance system for equipment operating in hostile environments (AMASS)	Mr. V. Mendes Martins	EDP S.A
BE-7120	Reliability based decision support system for the maintenance management of the underground networks of utilities.	Dr. D. Kalles	Computer Tech. Institute Patras University
BE-7405	The development of a PC artificial intelligence system for the diagnosis and prognosis of machine condition using acoustic emission and acceleration monitoring (PC-COMMON)	Mr. J.I. Hormaeche	COINPASA
BE-8104	Intelligent equipment process monitoring for consistent finished product quality (IMPROQ)	Mr. P. Kitson	British Steel PLC
BE2-0545	Intelligent forecasting system for refineries and power systems	Prof.B. Bitzer	Univ-gesamthoch-schule Paderborn

NETWORK COORDINATION

		NETWORK CLUSTERS																							
		A: INSPECTION						B: INSTRUMENTATION/ MONITORING						C: STRUCTURAL MECHANICS						D: MAINTENANCE					
Participating Projects/Partner No		1	22	43	14	9	Pn	27	38	16	58	50	Pn	49	32	12	6	21	Pn	56	42	19	35	51	Pn
Cluster Tasks:	Task 1:							Task 1:						Task 1:						Task 1:					
	Task 2:							Task 2:						Task 2:						Task 2:					
	Task 3:							Task 3:						Task 3:						Task 3:					
		HORIZONTAL THEMES																							
Horiz. Theme 1:																									
Horiz. Theme 2:																									
Horiz. Theme 3:																									

Figure 1. Generic Organisation of PLAN.

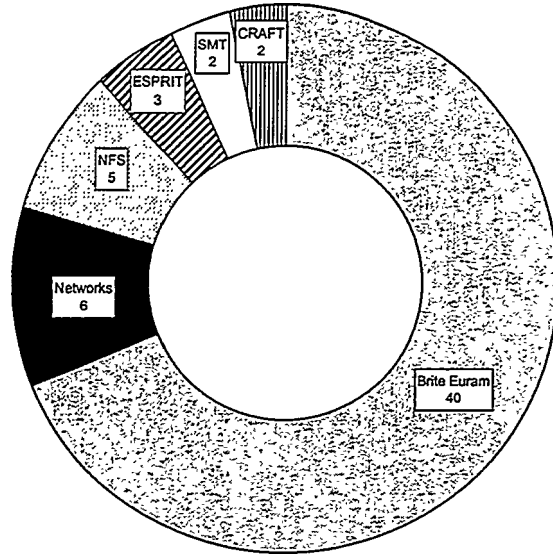


Figure 2a. The representation of different projects within PLAN.

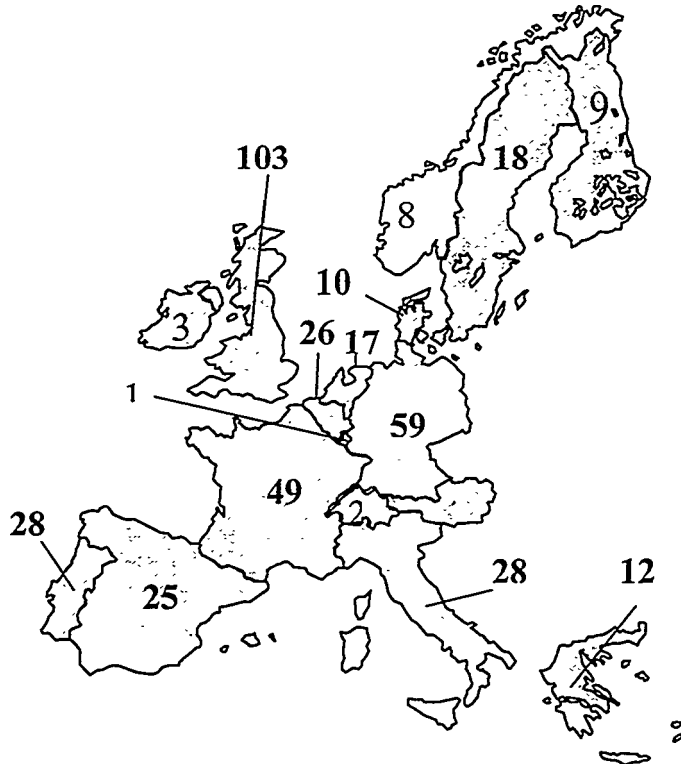


Figure 2b. The national representation of project partners within PLAN.

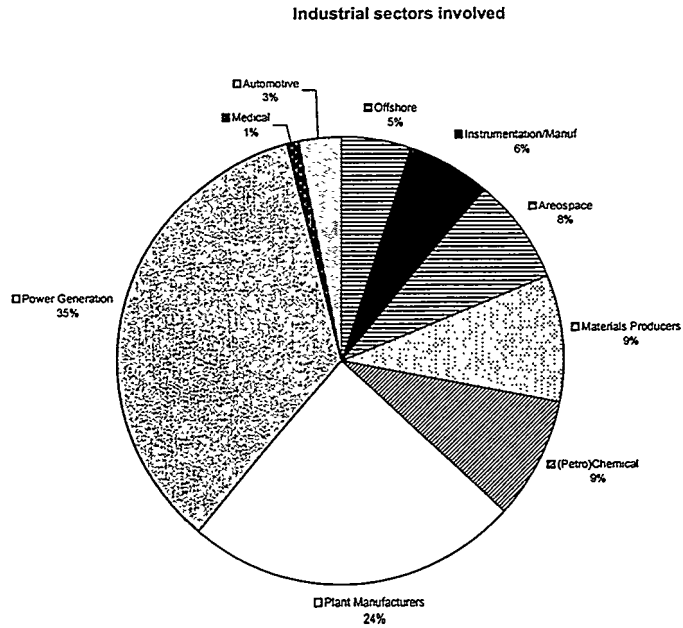


Figure 2c. Industrial sectors involved in the PLAN Network.

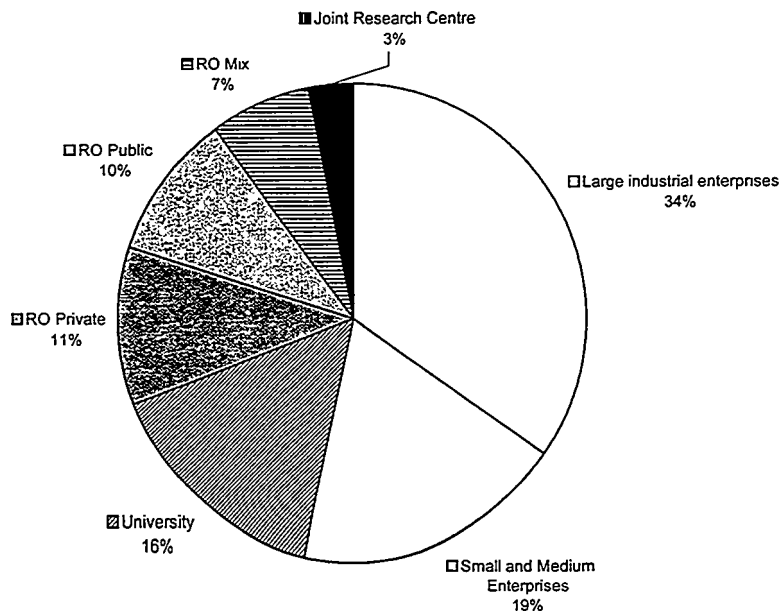


Figure 2d. Organisations participating in the PLAN projects.

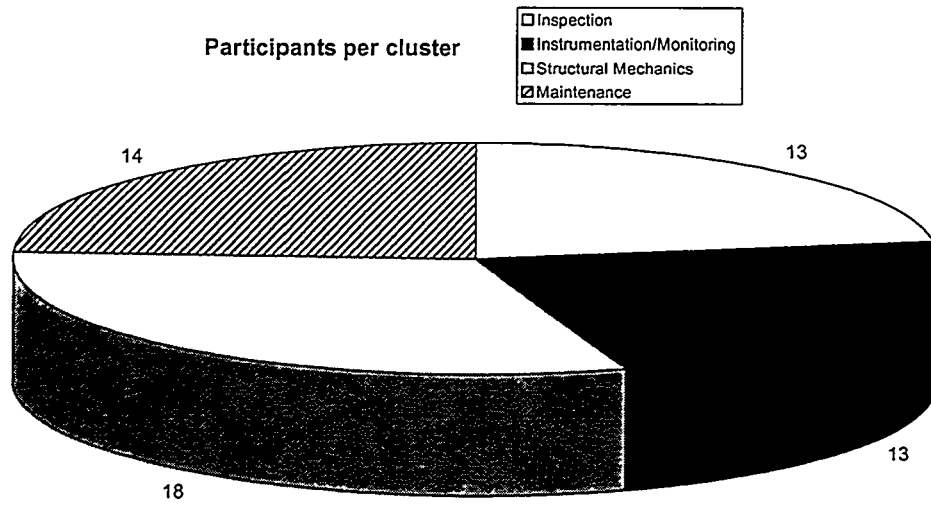


Figure 2e, Project participation per cluster.

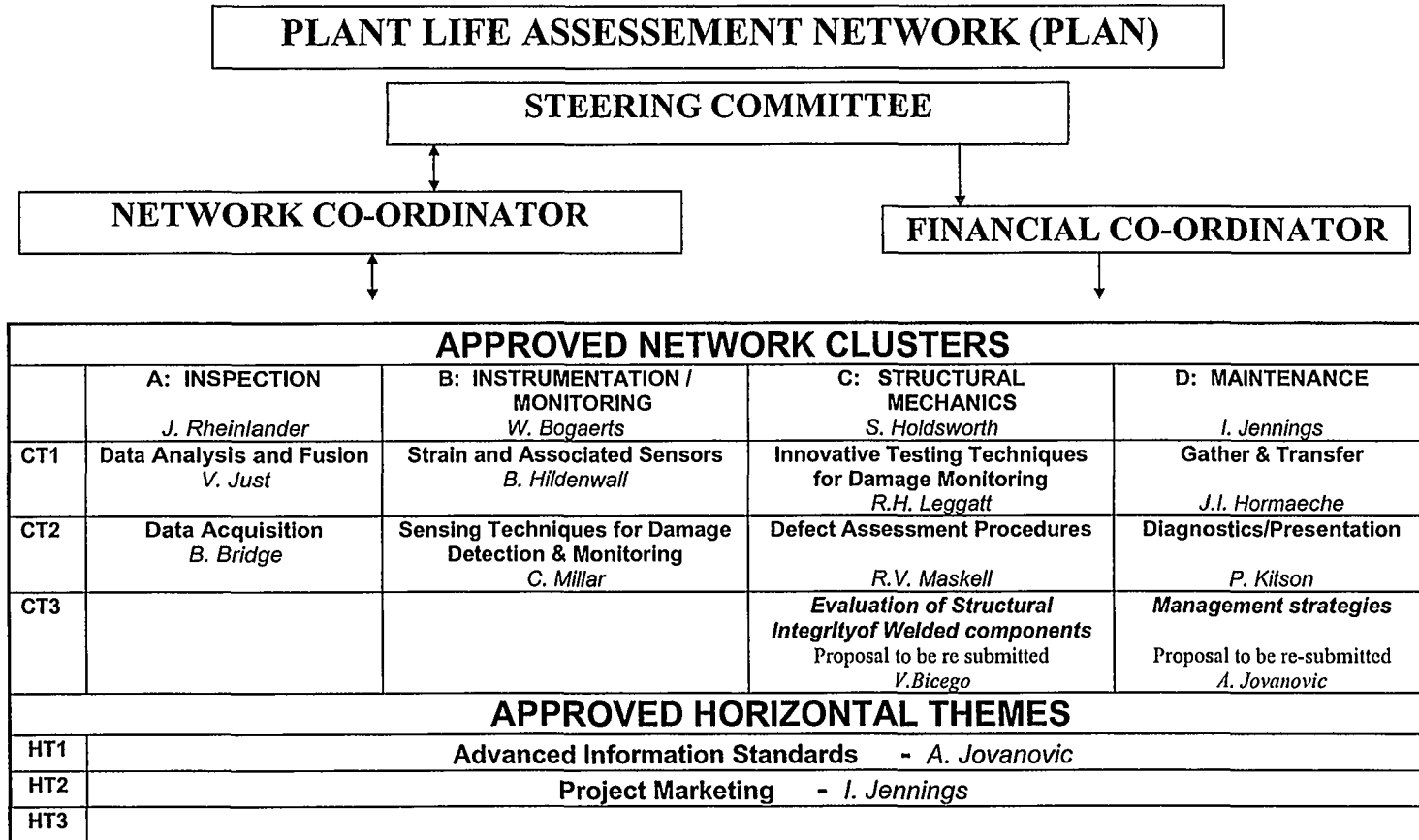


Figure 3. The current specific functional organisation of PLAN.

Degradation of Gas Turbine Coatings and Life Assessment

N. S. Cheruvu, Staff Engineer
Southwest Research Institute
San Antonio, Texas, USA

Abstract

MCrAlY coatings are widely used on hot section components of gas turbines to provide hot corrosion and/or oxidation protection by formation of an oxide layer on the surface. As the protective oxide scale exfoliates during service, aluminum from the coating diffuses outward for reformation of the protective scale. Aluminum may also diffuse inward due to the differences in composition between the coating and the substrate. Thus, the coatings degrade due to oxidation, oxide scale spallation, and inward and outward diffusion of aluminum. Service life of these coatings is controlled by the aluminum content in the coating, operating temperature and start-shutdown cycles. In-service degradation of CoCrAlY and CoNiCrAlY coatings is presented in this paper. A procedure to predict the remaining service life of coatings under oxidizing conditions is discussed.

1 Introduction

To improve the efficiency of land-based gas turbines, all of the major equipment manufactures have been introducing advanced turbines that are designed utilizing improved design techniques/materials and coatings. These turbines are fired at higher firing temperatures and utilize optimum cooling of hot section components to increase efficiency of a turbine. As a result, these components experience higher operating temperatures. Because of the higher operating temperatures encountered in these designs, the performance and durability of the coating system has now become one of the prime life limiting factors of hot section components. Among these components, turbine blades are the most critical parts since reliability and availability of a gas turbine depend on the integrity and life of these blades. As the operating metal temperature increases, kinetics of base material and coating degradation increases with the metal temperature [1], which in turn lowers the coating service life.

In the mid 1960's, coatings were introduced in land based turbines to provide hot corrosion protection of turbine blades. Both blade alloys and the coatings are susceptible to hot corrosion (type I or II) at operating temperatures ranging from 620° to 930°C. The severity of hot corrosion increases with temperatures up to 870°C and then decreases with increasing temperatures above 870°C [2]. At temperatures above 925°C, oxidation supersedes hot corrosion. In addition, hot corrosion problems are normally encountered in turbines that are fired with contaminated fuels. Advanced turbines are fired with relatively clean natural gas and operate at a temperature range where oxidation supersedes hot corrosion [3,4]. Therefore, oxidation is the primary concern in these designs.

To prevent or minimize oxidation, turbine blades are coated with overlay (MCoCrAlY) or diffusion type (aluminide or Pt-Al) coatings. However, an overlay (CoCrAlY or NiCoCrAlY) coating with or without a top aluminide is widely used on rows 1 and 2 turbine blades of modern turbines. Coatings provide protection by formation of a thin, adherent alumina (oxide scale) layer on the surface. The β -phase particles (CoAl or NiAl) in these coatings act as a reservoir for aluminum and supply aluminum to form the protective surface alumina layer. Both coatings and substrate materials degrade during long-term service. Degradation of coating adversely affects durability and remaining service life of a turbine blade or vane. The degree of degradation is sensitive to operating temperature. In this paper, in-service degradation of CoCrAlY and NiCoCrAlY coatings is presented. Field data have been used to demonstrate the effect of service temperature on coating degradation. A procedure for predicting the remaining service life of coatings under oxidizing conditions is discussed.

2 In-Service Coating Degradation

Prolonged service exposure of CoCrAlY and NiCoCrAlY coatings leads to coarsening of β -phase particles, formation of β -phase depleted zone, and enlargement of interdiffusion zone below the coating. The degradation is diffusion controlled and, therefore, the change in β -phase depleted and interdiffusion zone widths can be used to estimate the condition and metal temperature of a blade. The β -phase depleted zone widths have been used as an indicator of coating condition of NiCoCrAlY type coatings [5] and to predict the operating temperature [6] of service run blades. The interdiffusion zone widths have been used to correlate the service temperature of Stage 1 turbine blades operated on a GE Frame 6001B engine [7]. These blades were coated with GT 29+ (over aluminized CoCrAlY).

2.1 In-Service Degradation of CoCrAlY Coating

GE applies either CrCoAlY (GT 29) or CoCrAlY with an over aluminized layer (GT 29+) coating on row 1 and row 2 turbine blades for hot corrosion and/or oxidation resistance. The CrCoAlY coating is applied using either Vacuum Plasma Spray (VPS) or Low Pressure Plasma Spray (LPPS) processes. In the as-coated condition, the microstructure of CoCrAlY coating exhibits approximately 50% of β -phase (CoAl) particles, by volume in the γ matrix. The top aluminide is a single (β) phase coating and is applied using pack cementation or the over-the-pack process. Figure 1 shows undegraded microstructure of over aluminized CoCrAlY coating on a GTD-111 blade. Nominal composition of CoCrAlY and top aluminide coatings is given elsewhere [7,8]. Nominal aluminum content in the GT 29 coating is 6%.



Fig. 1. Microstructure of un-degraded CoCrAlY with a top aluminide coating layer (GT 29+).

Condition of CoCrAlY (GT 29) coating on an un-cooled GTD-111 DS blade after 58,000 hours of operation in a MS 5002 engine is shown in Figures 2 and 3. The engine was fired at 927°C (1700°F). In-service degradation of coating included localized oxidation of coating (Figure 2) and formation of a β -phase depleted zone at the outer surface of the coating (Figure 3). In some areas, the localized oxidation has progressed through the thickness of the coating. At the localized oxidation front, there is an area that has been depleted of the β -phase particles, suggesting that aluminum from β -phase diffused to the surface to form oxide. The β -phase particle depletion at the coating/substrate interface was observed only at

sporadic locations. No continuous depleted zone was observed at the coating/substrate interface. A small change in the interdiffusion zone was noted at the 50% blade height compared to the zone width at the 10% height. Since the operating metal temperature at the 10% blade height is significantly lower than at the 50% blade height, it can be assumed that the coating at the 10% blade height does not degrade and represent an as-coated condition.

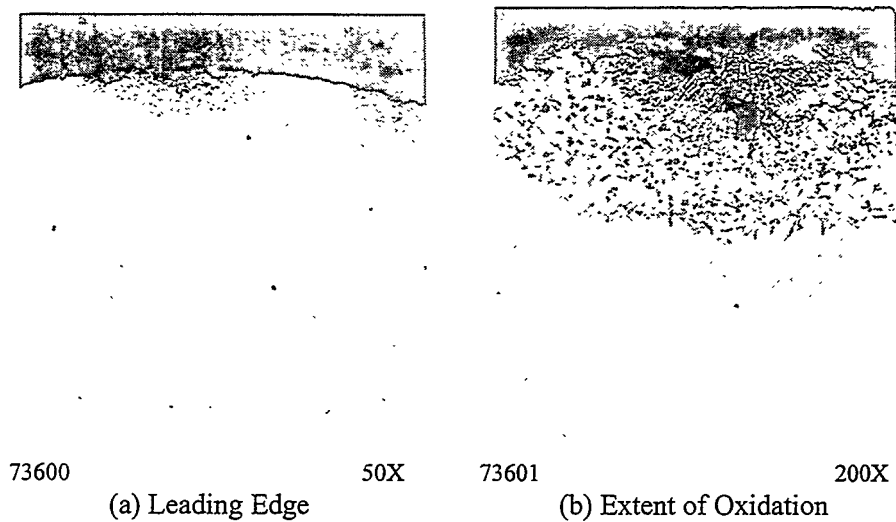


Fig. 2. Condition of leading edge of a CoCrAlY (GT 29) coated GTD-111 DS blade after 58,000 hours of operation on GE's 5002 engine. The coating was locally oxidized and in some locations the oxidation extended through the thickness of the coating.

Condition of an over aluminized CoCrAlY (GT 29+) coating on two cooled GTD-111 row 1 blades (#25 and #28) was evaluated after 25,834 hours of operation on an MS 6001B engine. These two blades were operated on the same engine and reported to have operated at different temperatures [9]. The operating history and metal temperatures of the blades, along with chemical composition of the blades and coatings, are described in a paper by Cheruvu and Leverant [7]. The metal temperatures of blades 25 and 28 at the 70% blade height were reported to be approximately 896° and 876°C, respectively [7,9].

Service exposure of 25,834 hours led to transformation of β -phase in the aluminide into γ -phase at the outer surface of the coating in both blades. The β to γ transformation was discontinuous as shown in Figure 4. The

discontinuous white layer, γ -phase, was reported to contain approximately 3 wt%.

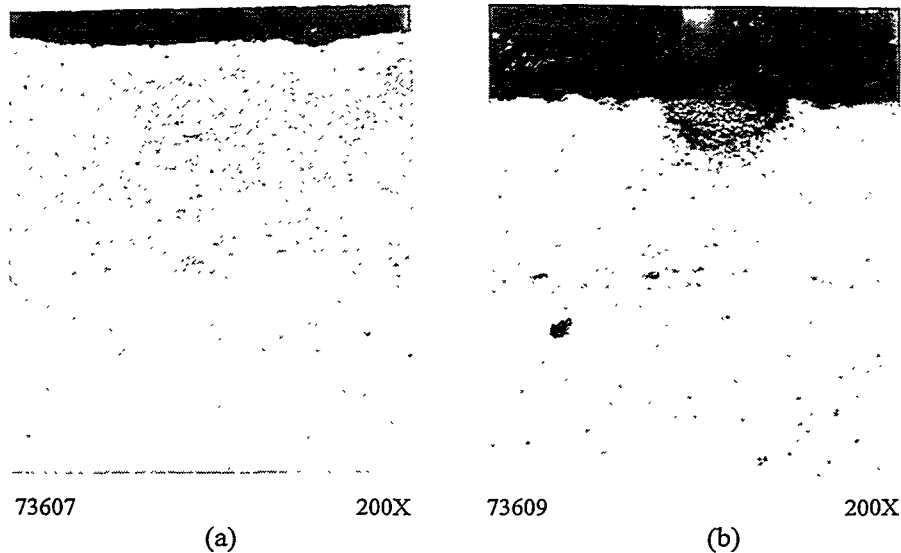


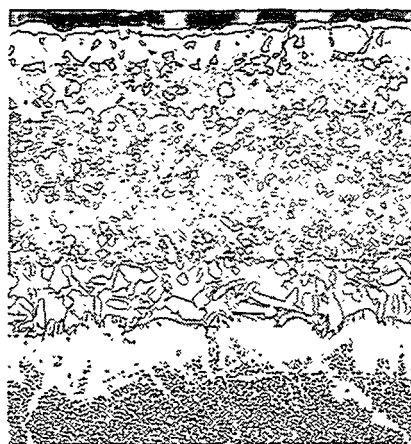
Fig. 3. Microstructure of in-service degraded CoCrAlY coating after 58,848 hours of operation. Note β -phase depleted regions at the vicinity of the localized oxidation area and the outer surface of the coating.

Below this white layer, β -phase in the aluminide, in isolated areas, was transformed into γ' containing 18% Al. Loss of aluminum in β -phase resulting from spallation and reformation of a protective oxide scale during service is responsible for the β to γ or γ' transformation. Due to the presence of top aluminide coating, service exposure did not produce a β -phase particles depleted zone at the CoCrAlY/aluminide coating interface. Consistent with results of GT 29 coating, no continuous β -phase depleted zone was formed at the coating/substrate interface of these blades.

However, the interdiffusion zone width below the CoCrAlY coating in the substrate varied from location to location and between the two blades, Figures 5 and 6. Among the locations examined in a transverse section, the trailing edge had the largest interdiffusion zone in both blades. At all locations, blade 25 exhibited wider interdiffusion zones than did blade 28.



Fig. 4. In-service degradation of CoCrAlY with a top aluminide coating (GT 29+) on a GTD-111 Blade after 25,834 hours of operation on a GE's 6002 B engine. The β -phase was transformed into γ on the coating outer surface (white layer).



88247

200X

(a)



88253

200X

(b)

Fig. 5. Variation of interdiffusion zone widths among various location on blade 25.

coating and base metal were oxidized [6]. In other areas, in-service degradation of coating resulted in formation of a β -phase depleted zone at the outer surface and the coating/substrate interface. The β -phase depleted zone width was wider at the trailing edge than at the leading edge of the blade.

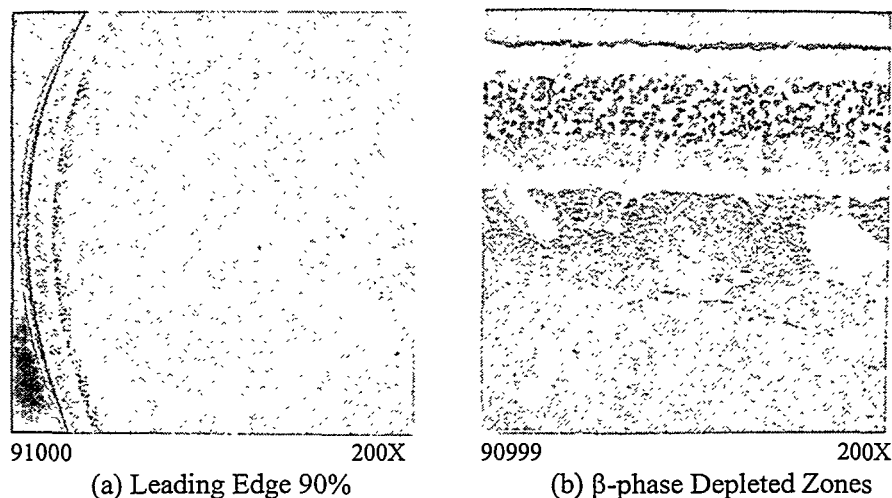


Fig. 7. Condition of leading edge of a NiCoCrAlY coated U-520 blade after 20,000 hours of operation on a W501 D5 turbine.

To lower the metal temperature, the cooling hole design was modified from a camberline to a peripheral cooled blade design. In a peripheral cooled blade the cooling holes are drilled in two rows closer to the concave and convex surface of the airfoil, as opposed to a single row of holes as in a camberline cooled blade. Cheruvu et al. have investigated the effect of this design modification on an in-service coating degradation [1]. In-service degradation of coating at the leading and trailing edges of camberline and peripheral cooled blades of 501 D5 is shown in Figure 8. The coating at the leading and trailing edges of the peripheral cooled blade is in good condition after 16,700 hours of operation. A small β -phase depleted zone was noted at the outer surface and the coating/substrate interface. The coating on the leading edge of the camberline cooled blade was oxidized and no β -phase particles were seen. The oxidation was extended into the base metal. The coating on the trailing edge was locally oxidized. The β -phase particle depleted areas were seen at the coating outer surface and the coating/substrate interface. The β -phase depleted zones in the camberline cooled blade were significantly wider than those in the peripheral cooled blade. The coating degradation results confirm that the peripheral cooled blade had operated at a lower temperature than did the camberline cooled blade.

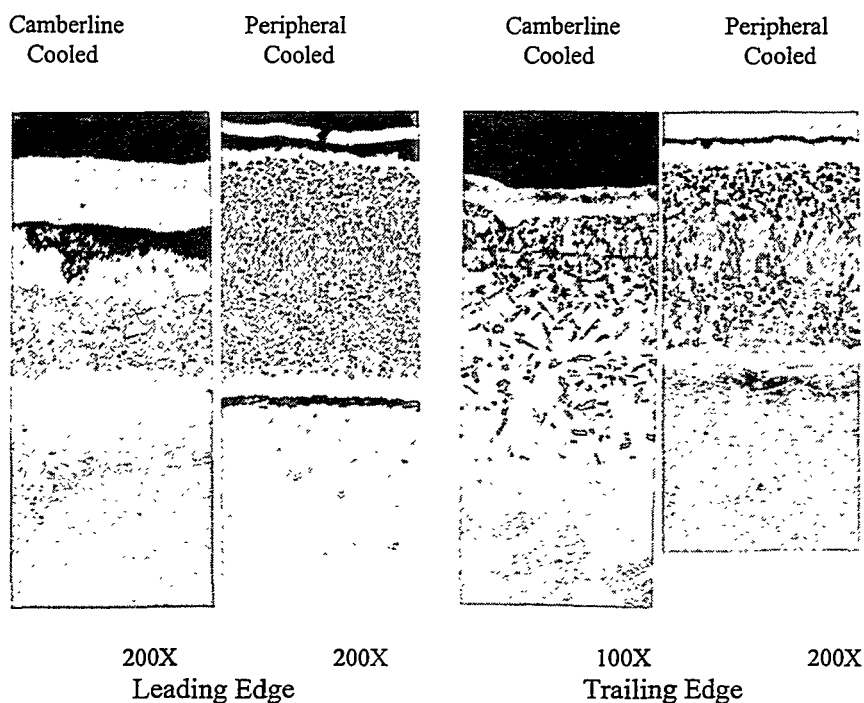


Fig. 8. Variation of coating degradation at the leading and trailing edges of camberline and peripheral cooled blades after 16,700 hours of operation.

3 Life Assessment Model

The results presented in the previous section show that long-term service exposure leads to degradation of coatings. The mechanisms of degradation include oxidation, oxide spallation and loss of aluminum due to outward and inward diffusion during service. The blade metal temperature, chemistry of coating and substrate, and number of start-shutdown cycles control loss of aluminum in the coating due to inward and outward diffusion. Higher operating temperatures and larger number of start-shut down cycles promote oxide scale growth and spallation and thus, increase aluminum loss during service. The service life of a coating depends on either the aluminum content or volume fraction of β -phase particles. The coating loses its ability to provide oxidation protection to the base metal when the aluminum content in the coating falls below a critical value. The critical aluminum content depends on the chemistry of the coating and is dictated by the minimum amount of aluminum required in the coating to form a continuous protective oxide scale. Hence, all the coating degradation

mechanisms that result in loss of aluminum should be considered in developing a lifing model for a coating.

A coating life model, using critical aluminum criterion considers loss of aluminum due to cyclic oxidation and spallation [10], and outward [11] and inward diffusion [12] of aluminum. The cyclic oxidation model was described by Chan in Reference 10. This model was extended to account for aluminum loss due to outward and inward diffusion by Chan et al. [11,12] for predicting the service life of a coating. The model was validated using laboratory and field data [12]. The essential features of this model include oxidation kinetics, oxide spallation, inward and outward diffusion, overall kinetics of cyclic oxidation and life prediction methodology. The mathematical treatment can be found in detail in References 10-12. A computer program was written to calculate aluminum content and the volume fraction of β -phase in a coating on a cycle-by-cycle basis for predicting useful life of a coating. The model was applied to predict the useful life of the CoCrAlY coating on laboratory GTD-111 specimens subjected to cyclic oxidation conditions. The experimental details were presented elsewhere [12]. A comparison of the calculated and measured weight change curves for CoCrAlY coatings at 954° and 1066°C is presented in Figure 9(a). The Al content and volume fraction of the β phase have been calculated; the result of the Al content is compared against experimental data in Figure 9(b), which shows good agreement between model and experiment.

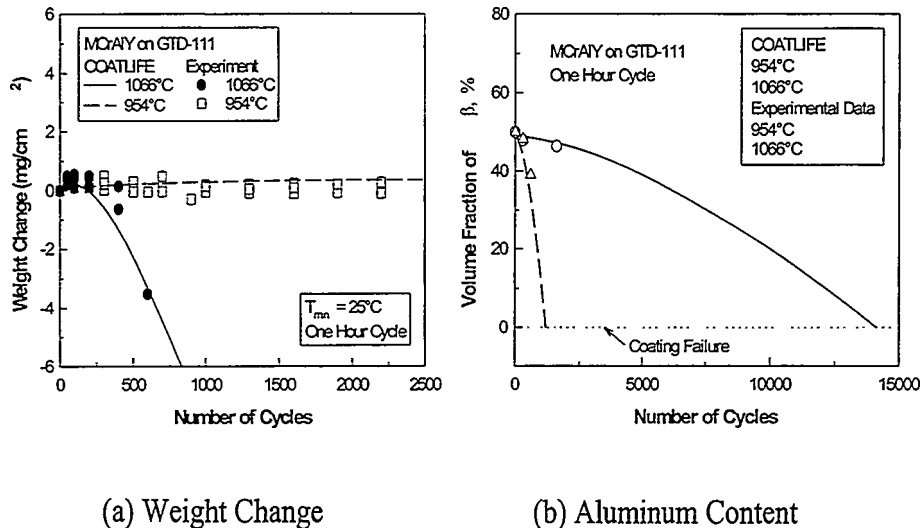


Fig. 9. Comparison of experimental and life prediction model calculated values.

The model was then used to calculate the time to failure of the coating as a function of cycle time. The calculated values of the times-to-failure are then divided by the cycle time to obtain the number of startup cycles to coating failure. A coating life diagram is then obtained by plotting the number of startups as a function of cycle time in a log-log plot. As an illustration, a coating life diagram calculated for CoCrAlY coatings subjected to cycling between 25°D and 1066°C is presented in Figure 10.

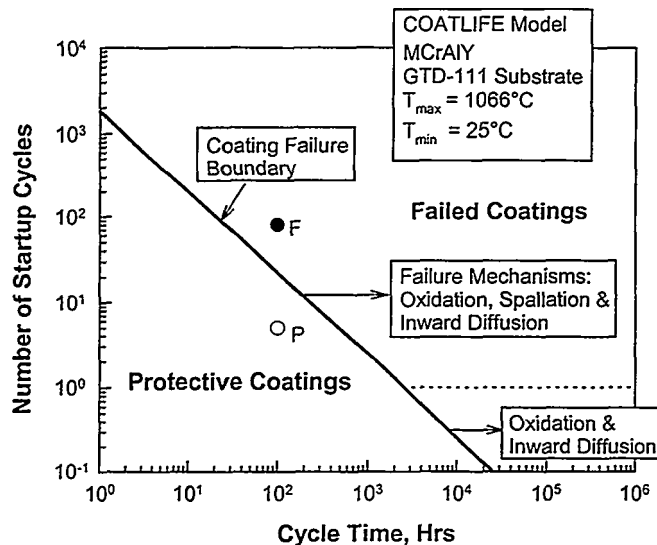


Fig. 10. Coating life diagram showing failure and no failure regions.

The solid line, calculated using the model, represents the failure boundary for the coating under the imposed temperature. The coating is protective when the number of startup cycles at a given cycle time, e.g., point P, is less than that of the failure boundary. Conversely, the coating has failed if the number of startup cycles exceeds the coating failure boundary, as illustrated by point F in Figure 10. The coating life diagram thus provides a simple and rigorous means for forecasting the remaining life of a coating after it has been in service. The controlling failure mechanism along the coating failure boundary varies with cycle time and temperature. In general, oxidation and spallation dominate at short cycle times while oxidation and inward diffusion dominate at long cycle times. At intermediate cycle times, coating failure involves oxidation, spallation, and inward diffusion, as shown in Figure 10.

4 Conclusions

- Long-term service exposure at high temperatures experienced in gas turbines leads to degradation of CoCrAlY, aluminide and NiCoCrAlY coatings.
- Degradation of CoCrAlY coating (GT 29) is evidenced by oxidation, coarsening of β -phase particles, formation of a β -phase depleted zone at the coating outer surface, and an enlargement of interdiffusion zone in the substrate below the coating.
- Degradation of top aluminide coating is evidenced by transformation of β -phase (CoAl) into γ or γ' .
- Degradation of NiCoCrAlY coating is evidenced by oxidation, coarsening of β -phase particles, formation of a β -phase depleted zone at the coating outer surface and the coating/substrate interface.
- Transformation of β -phase (CoAl) into γ or γ' in the aluminide coating, formation of β -phase depleted zone regions in the CoCrAlY and NiCoCrAlY coatings is due to loss of aluminum, resulting in oxide spallation and inward and outward diffusion of aluminum during service.
- The degree of degradation depends on service temperature. Kinetics of coating degradation increases with the operating metal temperature of a blade. Lower metal temperature extends coating service life.
- A coating life prediction model that was developed by Chan and Chan et al [10-12] considering all the coating degradation mechanisms, i.e., spallation and inward and outward diffusion of aluminum is discussed. This model can be used to predict the remaining service life of coatings.

5 References

1. Cheruvu, N. S, Carr, T.J, Dworak, J., and Coyle, J: "In-service Degradation of Corrosion Resistant Coatings," ASME International Gas Turbine and Aero Engine Congress and Exhibition, Paper 96-GT-429, Birmingham, UK, June 1996.
2. Viswanathan, R.: "Damage Mechanisms and Life Assessment of High Temperature Components," *ASM International*, pp.438, 1989.
3. Dallio, J. A. and Boone, D. H.: "Failure Mechanisms of Coating Systems Applied to Advanced Turbines," ASME International Gas Turbine and Aero Engine Congress and Exhibition, Paper 97-GT-486, Orlando, Florida, USA, June 1997.

4. Wood, W. I.: "Internal Damage Accumulation and Imminent Failure of an Industrial Gas Turbine Blade Interpretation and Implications," ASME International Gas Turbine and Aero Engine Congress and Exhibition, Paper 96-GT-510, Birmingham, UK, June 1996.
5. Czech, N., Schmitz, F., and Stamm, W.: "Thermal Mechanical Behavior of Advanced Overlay Coatings," *Materials and Manufacturing Processes*, Vol. 10, pp. 1021-1035, 1995.
6. Srinivasan, V, Cheruvu, N. S., Carr, T. J., and O'Brien, C. M.: "Degradation of MCrAlY Coatings and Substrate Superalloy During Long-term Thermal Exposure," *Materials and Manufacturing Processes*, Vol. 10, pp. 955-969, 1995.
7. Cheruvu, N. S and Leverant, G. R.: "Influence of Metal Temperature on Base Material and Coating Degradation of GTD-111 Buckets," ASME International Gas Turbine and Aero Engine Congress and Exhibition, Paper 98-GT-511, Stockholm, Sweden, June 1998.
8. Rairden III, J. R.: U.S. Patent, RE 30.995, Reissued July 1982.
9. Rooth, R. A, Agema, K. S., and Hiemstra. P.: "Metallurgical Analysis of Temperature Monitored Gas Turbine Blades," ASME International Gas Turbine and Aero Engine Congress and Exhibition, Paper 97-GT-212, Orlando, FL, USA, June 1997.
10. Chan, K. S, "A mechanics based Treatment of Cyclic Oxidation," *Met. Mat. Transactions*, Vol. 28, pp. 411-422, 1997.
11. Chan, K. S., Cheruvu, N. S, and Leverant, G. R: "Coating Life Prediction Under Cyclic Oxidation Conditions," Transactions of the ASME, *Journal of Engineering for Gas Turbines and Power*, Vol. 120, pp. 608-614, 1998.
12. Chan, K. S., Cheruvu, N. S, and Leverant, G. R: "Coating Life Prediction for Combustion Turbine Blades," ASME International Gas Turbine and Aero Engine Congress and Exhibition, Paper 98-GT-478, Stockholm, Sweden, June 1998.

Cost-effectiveness of combustion turbines: recommendations for reliability, maintainability, supportability and maintenance requirements

M. MEUWISSE C., research engineer
M. DESPUJOLS A., research engineer
Électricité de France, Research and Development Division
6, quai Watier
78401 Chatou
FRANCE

M. GIVAUDAN B., head of Diesel and Combustion Turbine Group
Électricité de France, Engineering and Construction Division - SEPTEN
12/14 avenue Dutriévoz
69628 Villeurbanne
FRANCE

M. LAFAGE L., senior engineer
Électricité de France, Engineering and Construction Division - CNET
Les collines de l'Arche - Immeuble Concorde
92057 Paris La Défense
FRANCE

ABSTRACT

The profitability of combustion turbines intended for export is of extreme importance for Electricité de France. It is principally during the development phase of a project that one can ensure respect of two indissociable factors, essential to the per-kWh production cost: global operating costs and performance in terms of reliability and availability.

The approach proposed here advocates the global acquisition of the installation and its logistic support. Generally applicable recommendations are given. They enable integrating in the future plant specifications all requirements relative to plant reliability, availability, maintainability and logistic support. They are structured according to type: expression of needs and management factors.

1. Introduction

The profitability of electric power plants designed for export is of extreme importance for Electricité de France. It is principally during the development phase of a project that one can ensure respect of two indissociable factors, essential to the per-kWh production cost: life cycle costs and performance in terms of safety and availability [Degrave *et al.*, 1996]. In the case which is of interest to us here, of combustion turbines intended for export, this phase is essentially a process of acquisition of “off-the-shelf” products.

During this process, rigorous respect of the target objectives of **operating availability** and **global cost** is decisive for subsequent efficient and competitive use of the installations; “use” involves operation, maintenance and logistic support. Adhering to these objectives requires a qualitative and quantitative expression of needs in a wide range of domains: use of the power plant, maintenance, dependability, safety, training, documentation, spare parts, etc. It also presupposes that a system be set in place to verify and measure achievement of the objectives during the acquisition process.

The purpose of this study is to draw on concrete cases to establish certain **recommendations** which can improve the means by which logistic support is taken into account and availability and cost objectives are defined when calls for tenders are put out.

Our study was conducted in three steps:

1. First, Call for Tender files for previous contracts were reviewed. Analysis pointed up their strong points as well as potential improvements concerning availability, maintenance and logistic support for the installation.
2. The files were then compared so as to highlight the specific features of each contract.
3. Finally, recommendations were proposed enabling integrating in the user requirement specifications all demands related to availability, maintenance and logistic support for the installation.

The recommendations formulated here concern means for providing for all availability, maintenance and logistic support with a major impact on the operating and economic efficiency of the installation. *They do not bear on technical aspects related to power generation.*

“Support” in a power plant is a result of a combination of a number of elements, in particular the maintenance program, spare parts and tools. To be exhaustive, this list should also include: transfer of equipment (handling, packaging, storage, transportation), human resources, training, documentation, supplies (including spare parts, in particular), facilities and computer resources. Optimizing these elements requires a simultaneous study of the “Reliability - Availability - Maintainability” features of the equipment [NAVESEAINST 5000.39, 1987] & [MIL-STD-1388-1A, 1983].

Experience shows that the major proportion of the life cycle cost of a system is irreversibly determined by decisions made in the design phase. The curve in Figure 3 illustrates the principle of this impact of initial decisions on global costs. A study of the curve of actual costs (i.e. real expenditure) shows that while Conceptual and Basic Design studies are relatively inexpensive, the choices resulting from these studies are considerably less so.

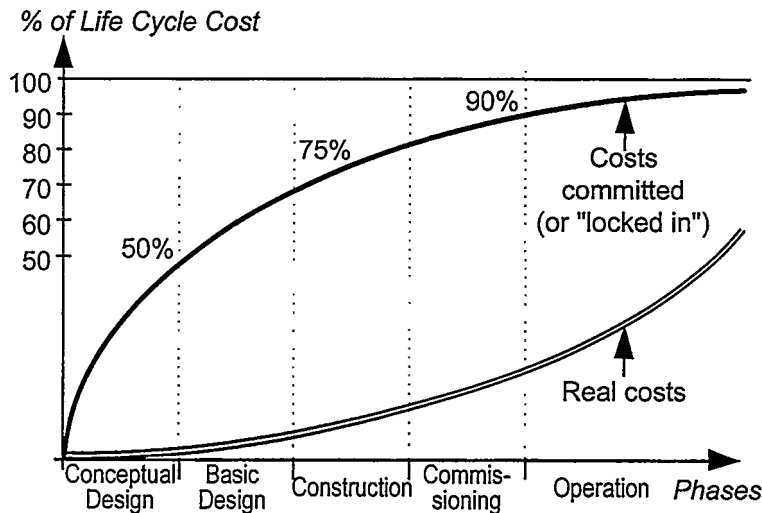


Figure 3 - Committed and real costs.

For all these reasons, control over the operating availability characteristics of a system presupposes that all demands related to both equipment and logistic support be simultaneously and coherently defined in the call for tenders.

3. Feedback analysis

3.1 The approach

The approach taken in analyzing Call for Tender files for previous contracts was based on the objectives of ensuring availability and controlling global costs, as shown in Figure 4:

- analysis of the **expression of needs**
- analysis of how the acquisition process is **managed** in the phases of *consultation* (evaluation and selection of bids) and *project management* (verification and measurement of objectives met as work proceeds).

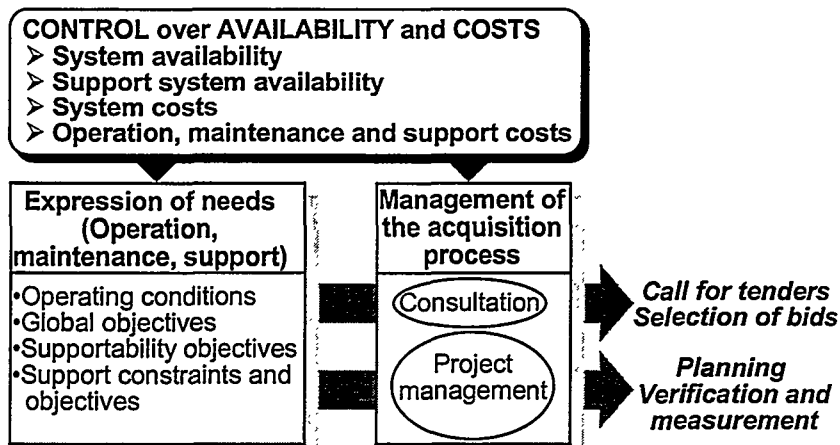


Figure 4 - The analytical approach.

The acquisition process generally consists in two distinct phases, each of which breaks down into several steps:

- Consultation, which is to say: call for tenders, evaluation and selection of bids, purchase contract;
- Project management (carrying out of work), involving installation, commissioning, testing, effective acceptance and transfer of ownership.

3.2 Drawing up of Call for Tender files

Call for Tender files consist in five types of documents:

- documents describing the project,
- documents expressing the needs,
- documents on management of the consultation phase,
- documents defining the contract,
- documents on project management.

3.3 Analysis of the expression of needs

The expression of needs is analyzed to point up all elements with an impact on the availability and global cost objectives for the installation, which is to say:

- requirements in terms of mission (or operating conditions),
- requirements in terms of availability and global cost,
- requirements in terms of supportability,
- requirements in terms of support constraints and objectives.

3.3.1 Operation profile

The system operational profile is defined by operating data, which is indispensable to the manufacturer if he is to:

- prepare the preventive and corrective maintenance program (definition of maintenance adapted to the objectives of the installation),
- define and quantify the appropriate support resources (such as staff, training, documentation, spare parts and consumables, tools).

3.3.2 Cost and availability objectives

It is necessary to formulate requirements in terms of operating availability and global cost, which, in the case of power generation, can be expressed as a global per-kWh cost.

3.3.3 Supportability objectives

The design of the installation has great impact on its supportability, which is defined by its characteristics of reliability, maintainability, testability, accessibility, safety, ergonomics and by human factors. The supportability of an installation must be viewed in both qualitative and quantitative terms.

3.3.4 Support constraints and objectives

Support constraints and objectives reflect the user's expectations, and his needs must be taken into consideration. Support constraints essentially stem from operating conditions and maintenance organization, as well as staff constraints.

Support objectives involve all those elements (information, resources and services) needed by the user to operate and maintain the installation. The most important are information (in particular, the detailed maintenance program and the operating, maintenance and supply manuals) and resources (i. e. personnel, tools and spare parts).

3.4 Management of the acquisition process

Management of the acquisition process relates to the project objectives and the conditions under which it is conducted. The two phases identified above must be analyzed:

- consultation phase, from the call for tenders to signing of the contract for the bid selected,
- project management phase, in which work is carried out and terminated by the transfer of ownership.

3.4.1 Management of the consultation phase

The objective of the consultation phase is to select the bid which best satisfies the criteria specified in the call for tenders. This phase can be considered well managed when the selection criteria and the means by which bids are reviewed are clearly made explicit (general, technical and economic criteria).

It appears, however, that call for tender criteria do not generally lay sufficient stress on the "support" aspects, which nonetheless provide good grounds for selecting or rejecting bids.

3.4.2 Project management

The aim here is to check progress and verify that the set objectives are met. This implies careful planning of operations and checking of objectives at each step; this phase is completed with the commissioning of the installation and transfer of ownership.

During this phase, the objectives which must be verified and measured generally relate to the technical performance of the installation and to the reliability required of the installation under the operating conditions specified in the call for tenders.

3.5 Comparison of different types of contracts

The purpose of comparing different processes of acquisition of combustion turbines is to broaden the scope of the recommendations by identifying differences between different types of projects: those conducted in line with international directives and those internal to EDF. Not only does this highlight certain deficiencies in the fields of interest to us, but it also points up positive elements from which much can be learned.

3.6 Conclusions from this feedback

Generally speaking, the acquisition process does enable taking into account the “support” aspects with an impact on availability and cost objectives. Moreover, in the case of the most recent calls for tenders reviewed:

- data relative to the target use of the installation are extremely explicit;
- the technical expression of needs clearly and sufficiently describes the aspects of logistic support related to training, documentation, tools, spare parts, packaging, handling, storage and transportation.

On the other hand, availability and cost objectives are generally not defined with sufficient precision. Economic criteria with an impact on global cost (such as per-kWh production cost) are sometimes defined as selection criteria during the consultation phase.

All too frequently, the “maintenance strategy and organization” aspect is only superficially treated: while “supportability” is reasonably well handled in that the purchaser refrains from more or less indirectly imposing technical solutions on the manufacturer, the need still remains to obtain precise information characterizing the supportability of the installation (e.g. maintainability features).

Calls for tenders are generally structured in a global enough way to enable good control over acquisition of the plant: they deal with management of both the consultation phase and the ultimate project. There nonetheless remains room for improvement in managing the acquisition process: essentially, selection criteria must be exhaustive and support resources, measurement procedures and the conditions for inservice validation of support elements must be clearly broken down and provided for.

Comparison of various processes of acquisition reveals one general trend: the definition of the cost/availability objectives, the conditions under which they are evaluated, and exchanges of information with the supplier are most well formalized in the framework of international contracts.

4. Preliminary recommendations

The recommendations fall under two main headings:

- **expression of needs** in the fields of RAM (Reliability, Availability, Maintainability), maintenance and logistic support;
- **management** of the acquisition process: both the consultation and project management phases.

4.1 Expression of needs

The resources needed for operation and maintenance account for a significant proportion of the overall cost of the life cycle of an installation, and are a major factor in operating performance. For this reason, it is essential that the expression of needs also take into account the user's needs in terms of *logistic support*. This first helps the manufacturer to identify the best maintenance and support configuration to be proposed; in addition, it enables the client to compare the solutions proposed so as to select the one best suited to his needs.

Needs must therefore be expressed in terms of desired *results* and imposed *constraints*, rather than in terms of *solutions*. However, all aspects related to RAM, maintenance and support must be exhaustively expressed. Furthermore, "results" must be quantifiable and measurable, a precondition for verifying that the target results are achieved.

Data on logistic support is necessary to express the needs, exchange information with manufacturers and enable checking or measuring objectives. The expression of support needs must include the following in order to be exhaustive:

- installation operational profile,
- target global performance,
- objectives of the installation,
- support constraints,
- support objectives.

The definition of the **operational profile** of the installation describes its operating characteristics, the number of units needed and their geographical environment.

Definition of **global performance** depends on the type of project and includes such aspects as operating availability and global per-kWh cost. Performance targets must be realistic in light of acquired experience, for example. The way in which performance is calculated must be made explicit.

The definition of **supportability** requirements and of the type **information** needed to describe these (in particular, reliability, maintainability, accessibility, testability, safety) must not impose demands with an impact on design choices.

Definition of the support **constraints** involves the operating conditions of the plant, the maintenance organization (levels of maintenance and types of tasks) and personnel constraints.

For each element in logistic support, **objectives** must be expressed:

- the **maintenance** plan, clearly setting forth the support data required;
- **training** of staff (category and prerequisites of staff to be trained, objectives and conditions of training, evaluation);
- technical **documentation** (conditions of use, processes of validation and criteria for acceptance, types);
- **tools** and **equipment** needed for logistic support: the expression of needs must not prejudice technical solutions. It must bear essentially on requirements in terms of standardization and the use of specific existing tools. It must also define the conditions for acceptance and maintenance of tools and equipment;
- the obligatory and recommended **spare parts** and **consumables**; the procedure for acquiring spare parts must be defined, as must that for exchanging information at the time of their acquisition;
- **computer resources support**; the expression of needs relates to what is needed to run the software and on the resources needed for its maintenance and evolution;
- the **facilities** for the installation; commissioning of a new unit can require new infrastructure or modifications in existing infrastructure (for operation, maintenance, training, etc.); the expression of needs must allow for this;
- for **packaging, handling, storage and transportation**, the expression of needs essentially relates to standards to be respected and to safety requirements to be met in view of the conditions of storage and transportation, especially for dangerous products.

4.2 Management of the acquisition process

4.2.1 Consultation phase

Documents used in the consultation phase must enable the manufacturers contacted to understand the objectives and organization of the project clearly, and to know the documents and information to be provided in their bid, the criteria and means of selection of bids, and the conditions and mandatory clauses of the contract. To this end, the following in particular must be integrated:

- a structuring of the bids, clearly distinguishing responses relating to the proposal of an *installation* from those relating to its *logistic support*, so as to simplify analysis;
- any additional selection criteria based on the cost or availability objectives, supportability requirements, or support system objectives (these may, for example, be parameters relating to evaluation of training);
- a breakdown of prices, clearly distinguishing sales prices for the *installation* from those for its *support*.

4.2.2 Project management phase

The following be provided for in the project management phase:

- **overall planning** of the acquisition process, integrating the supply of all support elements,
- the conditions and processes of **evaluation**, or measurement of the degree to which set objectives have been met (system and support system),
- the **conditions** for global operational acceptance (system and support system), transfer of ownership and guarantee.

5. Conclusion

Acquiring electric power generation installations implies acquiring the resources needed for their operation and maintenance. These resources represent an initial investment at the time of acquisition. In the course of plant operation, they induce recurrent costs throughout the service life of the installation. In addition, they contribute significantly to the operating performance of the plant.

The recommendations proposed here are structured under two headings: **expression of needs** and **management factors**. An exhaustive and pertinent expression of needs formulates both qualitative and quantitative objectives for the installation and its support system; good management enables verifying the degree to which the set objectives have been met.

The approach proposed here encourages the buyer to consider two indissociable aspects from the very early phases of a project: operating performance and global cost, and advocates the global acquisition of the installation and its logistic support.

References

Blanchard, B., 1992, "*Logistics engineering and management*", 4th Edition, Prentice Hall, Englewood Cliffs, NJ 07632.

Degrave, C., Martin-Onraet, M., and Meuwisse, C., 1996, "Integrated logistic support concept in the design of nuclear power plants", *Proceedings, 4th JSME/ASME joint international conference on nuclear engineering* - vol 2, pp 27-31, New Orleans, LA / USA.

MIL-STD-1388-1A, 1983, "*Logistic Support Analysis*", DOD, Washington DC, 11 April 1983.

NAVESEAINST 5000.39, 1987, "*Acquisition and management of ILS for ships, systems and equipment*", DOD, Washington DC, 21 March 1987.

GAS TURBINE CLEANING UPGRADE (compressor wash)

Peter Asplund
GAS TURBINE EFFICIENCY,
175 62 JARFALLA, SWEDEN

ABSTRACT

The influence of gas turbine degradation on operating costs is high. Gas turbine cleaning is one of many actions taken for power recovery and is to consider as preventive maintenance. It is generally performed within the industrial field and occasionally within the aero sector. In order to meet the gas turbine development with high blade loads and ever-increasing temperatures, together with emission taxes and environmental regulations, more efficient and careful cleaning methods are needed. Following a survey about potentials for cost reduction in gas turbine operation a new man-hour and water saving cleaning method has been evaluated for a standard process.

Compared with traditional cleaning methods, the new method is water, - cost, - weight and space saving due to a new washing technique. Traditional methods are based on using different nozzles for ON and OFF-line cleaning, which rise the demand for complicated systems. In the new method the same nozzle installation, same liquid flow and pressure is used for both ON and OFF-line cleaning. This gives a cost reduction of appr. 20.000 - 30.000 USD per gas turbine depending on installation and size. Evaluation of the new method shows significantly improved ON -line cleaning performance and thus OFF -line cleaning is required only during scheduled stops.

INTRODUCTION

Gas turbines draw huge amounts of air per unit of time and are thus subject to particles forming an undesirable coating, primarily in the compressor. This reduces compressor efficiency and disturbs the airflow through the engine, causing increases in fuel consumption, temperatures, and harmful emissions. Gas turbine cleaning is carried out in the fields of aviation, industry and other applications, and the need for compressor wash varies. The object is to clean the compressor and gas path. The procedure contributes to minimize the degradation and losses as well as giving a number of other positive effects such as lowered heat rate and emissions for a given power setting.

BACKGROUND

A great variety of turbine cleaning systems are currently in use. They are common in their relatively low level of engineering with often poor cleaning efficiency and large amounts of washing fluids. Many of the fluids used are hazardous to the environment and to the health of personnel. Engine manufacturers, in their manuals, often recommend chemicals in direct contradiction to existing or notified environmental regulations.

This paper describes the difference between existing and a new cleaning method and what savings can be obtained with the new method.

ENGINE CLEANING STUDY

The study revealed that :

- Stationary gas turbine users (incl. marine and offshore) generally have systems and methods, but there is a large potential for efficiency improvements.
 - The systems available are complex, expensive and often ineffective in cleaning (low value for money).
 - In the view of dwindling water resources and detergent cost, more efficient, water saving methods are needed.
 - Many cleaning fluids used are hazardous to the environment and personnel.
- During last 20 - 30 years the engines have gone through extensive development. The cleaning methods do not correspond to this development.

GAS TURBINE CLEANING OPTIMIZATION

Gas turbine technique objectives :

- Ultra high efficiency
- Environmentally superior
- Cost competitive

Gas turbine operation affected by :

- Emission taxes
- Environmental regulations
- Development : Ever-increasing temperatures due to Advanced Turbine Systems (ATS) with ultra high efficiency and high blade loadings gives sensitivity to surge and vibrations. Also Thermal Barrier Coatings (TBC) are affected by air borne impurities.

POTENTIAL PROBLEMS WITH EXISTING CLEANING CONCEPTS :

- Abrasive cleaning is more and more prohibited due to engine coatings and cooling arrangements (this asks for effective ON-line alternatives).
- Complex and expensive nozzle installations (affects maintainability, extensive workload during engine overhaul).
- Tailored and complex systems for every gas turbine plant (expensive, affects maintainability, long delivery time, documentation etc.).
- Large quantities of liquid used (heavy loads on bladings, inefficient use of good water and detergent). Fig 1.
- Extensive engine preparation before wash (due to large amounts of liquid).
- Use of hazardous liquids (environment and health considerations).
- A lot of hazardous liquid waste to dispose of (expensive and cumbersome).

NEW METHOD

Trials have been performed 1988 - 1996 with a new water /detergent saving method on a large number of gas turbines - aero - industrial and marin applications in all power segments. (Table 1 and table 2). Depending on GT size, with up to 90% reduction in liquid usage. The new concept is based on use of a higher injection pressure.

The cleaning concept operates with relatively small amounts of liquid compared with old-generation systems. This is accomplished by a high degree of atomization gained by liquid pressurisation as earlier discussed, which means that less liquid is used per wash, which is cost saving for the operator and beneficial to the environment. It also means less strain on starting systems and engine parts. The system is designed for both ON and OFF - line cleaning, using the same nozzle installation.

Evaluation of new method for gas turbine cleaning.

Various are and stationary engine sizes tested, from 100 kW to 50 Mw. The trials have been done in cooperation with Volvo Aero, Saab Aircraft, Swedish Airforce, Swedish Navy, Neste, Finnair and IVO. Table 1 and table 2.

Table 1. Trials and results from various aero engine applications.

AIRCRAFT	ENGINE TYPE	AIR FLOW	LIQUID FLOW	GAIN
VIGGEN (Swe. Airforce)	Gas turbine starter	0,75 kg/s	0,6 L/min.	Torque recovery 3 %.
VIGGEN	RM8 A/B	140 kg/s	34 L/min, Crank- soak wash 2 x 30 sec.	10-15° C. Efficient cleaning after bird strike for reliable damage assessment.
SAAB 105 (Swe. Airforce)	RM 9 Aubisque	23 kg/s	8 L/min, crank	ITT 2 - 4 % (~ 20° C).
JAS 39 GRIPEN (Swe. Airforce)	F404/RM12	68 kg/s	20 L/min, crank	~1% thrust, effective cleaning after robot fire.
SAAB 340	GE CT7	5 kg/s	7,6 L/min, crank	ITT 6 - 15° C.
SAAB 2000	GMA 2100	16,3 kg/s	- " -	ITT 9 - 30° C.
FOKKER 50	PW 100		- " -	ITT 12° C.
MD 80 (Finnair)	JT8D - 200	145-220 kg/s	30L/min, crank	ITT 10 - 15° C.
Helicopter	Allison 250	1,5 - 2,5 kg/s	~ 2,5 L/min, crank	ITT 4 - 10° C.

Significantly reduced strain on starting systems and compressor blades compared to old method.

ITT = Inlet Turbine Temperature

Table 2. Trials and results on various stationary turbine applications with new cleaning method.

Stationary gas turbine applications (industrial & marine).

OPERATOR	ENGINE TYPE	MW/ AIR FLOW	LIQUID FLOW	GAIN
NESTE	FRAME 6	45 MW /130 kg/s	40 L /min, OFF-line, 2000 H between wash with deterg.	1-2 MW typical. Recovery to nominal output.
IVO	- " -	- " -	30 L/min, ON-line with dem. water daily.	Recovery to nominal output.
IVO	- " -	- " -	30 L/min, ON-line with dem. water, 2-3 times/week, OFF-line with deterg.	- " -
IVO UK	FRAME 9 E	124/410	37 l/min, On-line dem. water daily. OFF-line on cond. deterg.	- " -
LAHTI ENERGY	- " -	- " -	40 L/min, OFF-line with deterg. every 200 h	- " -
VATTENFALL	RR AVON	14,5 / 77	22 L/min, OFF-line with deterg.	- " -
GÄRSTAD	ABB GT 10	25 / 79	30 L/min, OFF-line with deterg.	- " -
SWEDISH NAVY	RR PROTHEUS	4000 shp / 15	10 - 12 L/min, ON-line with deterg.	10 % shp recovery 39°C red. ITT.
- " -	MTU 6022	115 /	OFF and ON-line, with deterg.	Significant reduction in smoke emissions. 10°C red. ITT.
SVANEMÖLLE Denmark	SIEMENS V64.3	62 / 192	40 L/min, ON-line with deterg. OFF-line every on cond.	Recovery to nominal output
Porvoo Energy	SOLAR CENTAUR - H	4,3/ 19	8 L/min, ON-line (3 min.) deterg.	Increased power output ≈ 3 %

ITT = Inlet Turbine Temperature

SUMMARY AND CONCLUSION :

The new cleaning method has been found to have following advantages :

- It is effective in cleaning of the whole engine, i.e. not only the compressor but the whole interior.
- Considerable reduction in the amount of fluid used at each wash; thus reduced spillage/wastage and consumable cost.
- Considerably reduced loads on compressor and turbine blades and starting systems due to reduced flow rates. Fig. 1.
- Minimal surface erosion.
- Enables the use of same nozzle installation for ON-line and OFF-line washing, thus drastically reducing hardware installation costs (nozzles, valves etc.) Ref. Fig. 2.
- Elimination of hazardous chemicals.
- Easy and economical to retrofit in operational installations.
- Workload saving, specially during service and overhaul (due to nozzle installation).

Thus, the new cleaning method performs well regarding cleaning effect, and is superior from cost effectiveness point of view.

BLADE AND STARTER STRAIN COMPARISON
BETWEEN TRADITIONAL AND NEW WASH METHOD

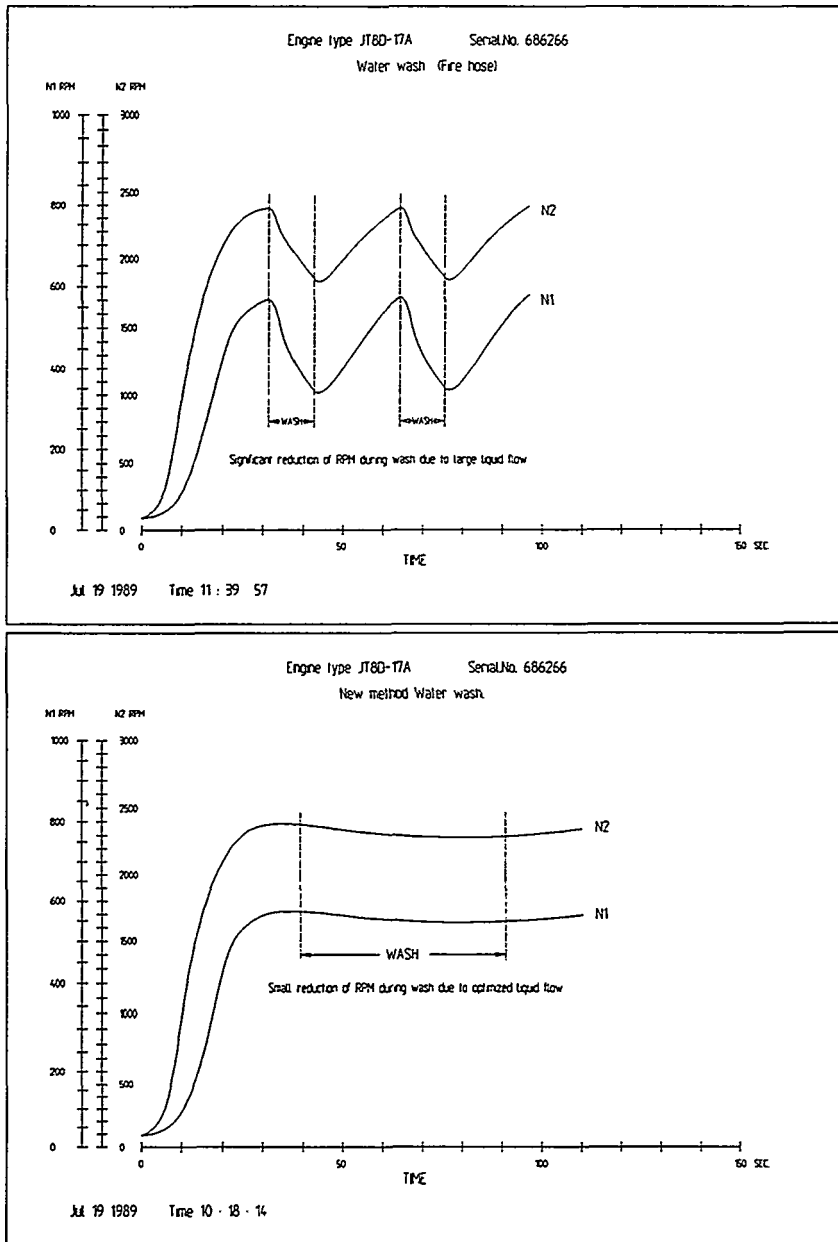
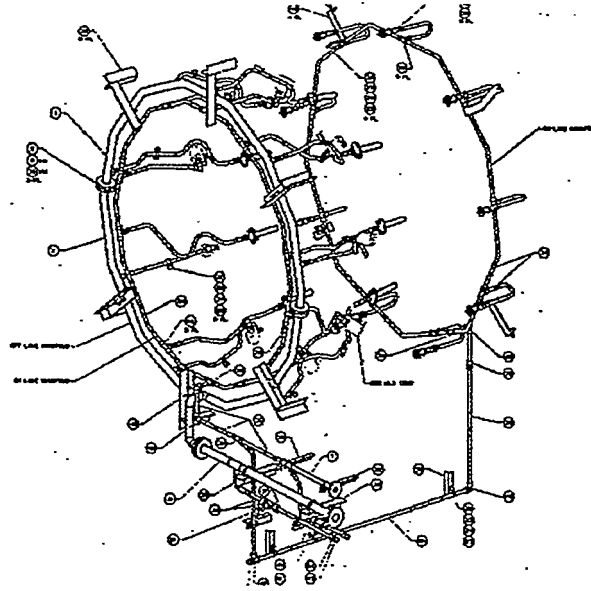
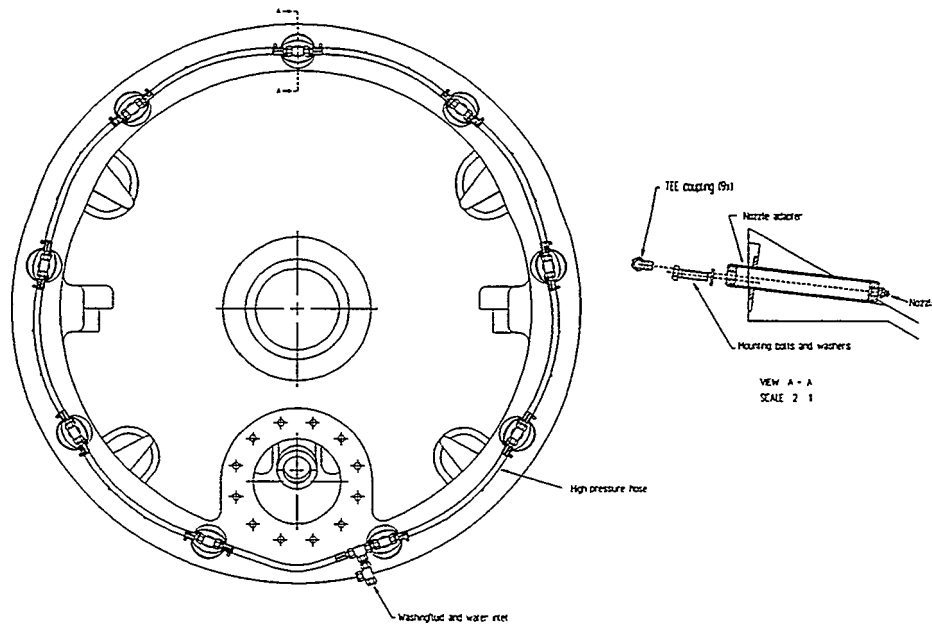


Figure 1. Comparison of compressor load during wash with old and new method.

Comparison between nozzle installations with traditional contra new cleaning method on Frame 6 FA.



Traditional nozzle installation with two different manifolds for ON and OFF line cleaning.



Typical nozzle installation with the new cleaning method for ON and OFF - line cleaning.

Figure 2.

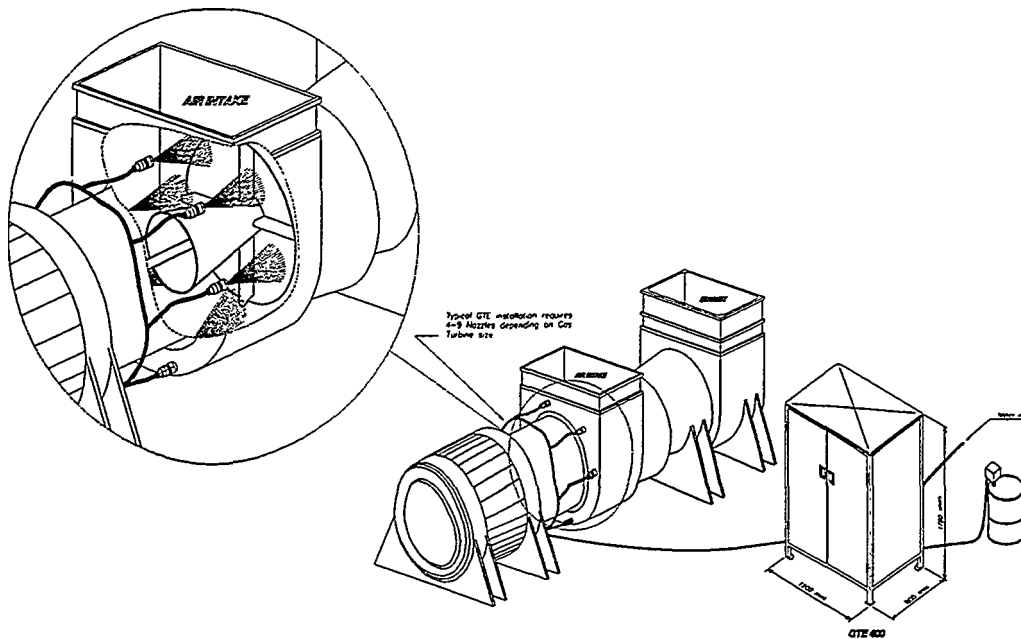
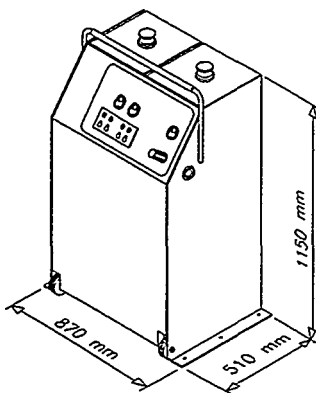


Figure 3. Typical new cleaning system with same nozzle installation for ON and OFF - line cleaning.

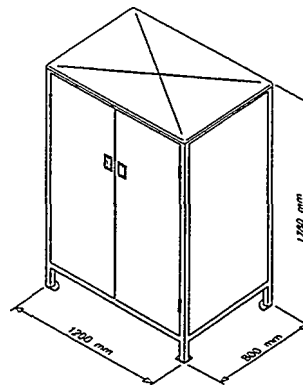


GTE 160

1 - 45 MW

Dry weight : 200 kg.

Figure 4.



GTE 400

1 - 250 MW

Dry weight : 320 kg

Figure 5.

Figure 4. Typical size of cleaning system for turbines up to 45 MW.

Figure 5. Typical size of cleaning system for turbines up to 250 MW+.

Cost savings

Example : The new cleaning method enables a hard ware cost reduction to be achieved by 20 - 30.000 USD in a typical 20 - 40 MW gas turbine installation, mainly due to simplified nozzle installation.

ENGINEERING DISCUSSIONS

DROPLET SIZE

There is always an aim for small droplets for a given liquid flow, which can be achieved by :

1. Low pressure (4 - 6 bar) with many small size nozzles.
2. Low pressure mixed with air.
3. High pressure.

Particle size and speed are the crucial factors deciding whether the fluid will be peripherally dispersed by the centrifugal force or whether it will be able to follow the airflow through the engine. Particle size is also of importance considering impact force against compressor and turbine blades, especially during ON-line washing. The use of different pressures, flow rates and temperatures etc. and how the droplet size is affected, is discussed as follows :

Liquid cleaning is affected by following characteristics :

Droplet size (atomization)

Impact

Viscosity

Temperature

Surface tension

Specific gravity

Pressure

Droplet size

Beside the liquid characteristics there are three major factors affecting drop sizes :

1. **Pressure** - low pressure provides larger drop sizes, than high pressure for a given liquid flow rate.
2. **Nozzle capacity** - large capacity provides larger drop sizes and vice versa, for a given liquid flow rate.
3. **Spray pattern**

Impact

The spray angle affects the impact of the droplets. The impact is decreased with increased angle. The greatest impact in kg/cm^2 is obtained by a solid stream. See figures below (at distance = 30 cm from nozzle outlet).

Spray angle flat fan :	Percent impact per cm^2 of theoretical tot. impact :
---------------------------	--

15°	30 %
25°	18 "
40°	12 "
50°	10 "
65°	7 "
80°	5 "

Theoretical total impact spraying
water :

$$0,024 \times (\text{l/min at spraying pressure}) \times \sqrt{\text{spraying pressure kg/cm}^2}$$

Viscosity

High viscosity liquids provide narrower spray angles compared to water.

Temperature

Liquid temperature affects viscosity, surface tension and specific gravity which have influence on nozzle performance. An increase in liquid temperature improves the spray pattern quality, increases the spray angle and decreases the drop size.

Surface tension

An increase in surface tension increases the drop size and decreases the spray angle.

Specific gravity

An increase in specific gravity decreases the nozzle capacity and the velocity.

Pressure

Generally the pressure affects capacity, velocity, impact and wear, increasing them with increased pressure. The drop size decreases. See the table below. Factors affecting nozzle performance :

	Increase in operating pressure	Increase in spec. gravity	Increase in viscosity	Increase in fluid temperature	Increase in surface tension
Pattern quality	Improves	Negligible	Deteriorates	Improves	Negligible
Capacity	Increases	Decreases	*	**	No effect
Spray angle	Increases, then decreases	Negligible	Decreases	Increases	Decreases
Drop size	Decreases	Negligible	Increases	Decreases	Increases
Velocity	Increases	Decreases	Decreases	Increases	Negligible
Impact	Increases	Negligible	Decreases	Increases	Negligible
Wear	Increases	Negligible	Decreases	**	No effect

* Full cone and hollow cone increase; flat spray decreases.

** Depends on fluid and spray nozzles used.

According to engineering discussions above regarding achievement of small droplets for a given liquid flow the conclusion is :

Low pressure : This requires a large number of small capacity nozzles for a given liquid flow per unit of time. This means disadvantages like :

1. High nozzle installation costs.
2. Space and weight demanding.
3. Poor maintainability due to risk of nozzle blockage.
4. Man - hour demanding during overhaul.
5. Difficult to retrofit due to space requirement.

Low pressure mixed with air :

This would also require a large number of nozzles for a given liquid flow per unit of time, and the system complexity increases.

High pressure : The number of nozzles needed for a given liquid flow is considerably lower, with advantages like:

1. Same nozzles for ON and OFF-line cleaning.
2. Considerably reduction in nozzle installation cost.
3. Easy to retrofit.
4. Lower risk for nozzle blockage.
5. Man-hour savings during overhaul due to less installed hardware.
6. Better function maintainability.
7. Less system complexity due to use of the same nozzles for ON and OFF-line cleaning.

REFERENCES:

ASME 92-GT-360, Performance of Gas Turbine Compressor Cleaners.

ASME 94-GT-452, On-line detergent fluid evaluation.

ASME 90 P-4, Boyce Engineering, Gas Turbine Axial Compressor Fouling

FFV Aerotech M 58-37:396, Washing tests on a/c 37 Viggen starting system.

FMV M225-08:23183, Evaluation of new washing method for the RM 8 engine.

GE C 92-JCS-27, Washing effect comparison - BB3100 and Rivenaes R-MC.

VAS, Feb 10-89, Washing tests, RM 9 engine.

VAS M225:253 and 1990-02-19 S411, Washing effect of different washing fluids.

VAS MF95:152, Tests of new compressor wash system at Swedish Navy 21. Missile Vessel squadron.

Wärtsilä Diesel 931217 R8/R-MC, On-line cleaning tests on exhaust turbo units.

EXPERIENCE WITH RESTORATION OF THE EBPVD COATINGS IN STATIONARY POWER GAS TURBINES

A. S. Osyka

State Area Power Station N 3 of Mosenergo (GRES-3)
142530, Electrogorsk, Russia

A. I. Rybnikov

Polzunov Central Boiler and Turbine Institute (NPO TsKTI)
Polytechnicheskaya, 24, 194021, St. Petersburg, Russia

I. S. Malashenko

E. O. Paton Electric Welding Institute
Bozhenko st., 11, 252005, Kiev, The Ukraine

S. A. Leontiev

Leningradsky Metallithesky Zavod
Sverdlovskaya nab., 18, 195009, St.Petersburg, Russia

Abstract

The use of electron beam physical vapour deposition (EBPVD) technology for CoCrAlY protective metal coatings improved the resource of power gas turbine blades in 2-4 times. After 7000 h operation the pitting corrosive attack is observed by the mechanism of hot low-temperature corrosion. The technology of removing and redeposition for coating layer has been developed. Blades with redeposited layer after the specified reductive heat treatment have operating time over 3000 h. Coatings on blades are in good states.

1 Introduction

The use of EBPVD coatings for protection of large-size rotating blades of peak load power GT-100 gas turbine running on liquid fuel improved the resource of rotating blades in 2-4 times [1]. It is more effective to use the EBPVD coating having the ceramic surface layer [2,3].

The main obstacle preventing the further use of the metallic coating is hot low-temperature corrosion which shows itself more evident in gas turbines operating in the south of Russia (Krasnodar heat-and-electric power plant) that at the power plants in the north part of Russia (GRES-3, Moscow and Ivanovo-GRES) Another factor decreasing the coating effectiveness is the disturbance of the deposition technique. In both cases it is necessary in due time to remove of the coating and the damaged layer of the base metal and to redeposit of the coating.

At present article are being investigated the subject of removing the redeposition of metal or metal-ceramic coatings and the results of operation of the rotating blades with redeposited coatings.

2 Experimental details

The subjects of study were large-size uncooled rotating blades (Table 1) of the first and the second stages of the high pressure turbine (HPT) and the ones of the first stage of the low pressure turbine (LPT) of the peak load power GT-100 gas turbine manufactured by JSC "Leningradsky Metallichesky Zavod". The blades are made of the superalloy EI 893 (Ni base, Cr 15%-17%, W 8%-10%, Ti 1,2-1,6%, Al 1,2%-1,6%, Mo 3,5%-4,5%). Electron beam coatings of different types were deposited at rotating blades at E.O.Paton Electric Welding Institute (Kiev, Ukraine) (Table 1,2). At the first stage rotating blades of the LPT of GT-100 gas turbine at GRES-3. Mosenergo (Table 1) the coating was deposited after 5295 operating hours.

Table 1. Parameters of moving blades of superalloy EI 893 for the GT-100 gas turbine.

Power plant	Stage	Dimensions, mm	Number of blades needed repair	Temperature of blade metal, °C	Coating before repair	Operation, hours before repair	Coating after repair
Krasnodar heat-and-power station	1 HPT	250	98	740	SDP8	4137	SDP8
	2HPT	290	57	650	SDP8	5017	SDP8
	1 LPT	420	128	650	SDP8	7021	SDP8
GRES-3 Mosenergo	1 HPT	250	15	740	SDP3A	5903	SDP8
	2 HPT	290	10	650	SDP3A	6903	
	1 LPT	420	62	650	SDP3A ¹⁾	7381 ²⁾	

Note:

- 1) Coating consolidation by microballs didn't conduct.
- 2) After operation of blades without coating.

Table 2. Chemical composition of evaporated alloys used in power engineering for producing corrosion- and heat-resisting coatings.

Alloy (coatings)	Mass fraction, %				
	Co	Ni	Cr	Al	Y
SDP-3A	bal	-	22-24	11-13	0.2-0.5
SDP-8	bal	0-2	25-28	9-11	0.2-0.5
SDP-11A	bal	0-2	24-26	3-5	0.3-0.6
KDP-1	ZrO ₂ + 8% Y ₂ O ₃				

Before the coating deposition the blades were put through the heat treatment according the following mode: 1020°C, for 1 hour + 1160°C, for 3 hours + 1000°C, 4 hours + 900°C, 8 hours + 820°C, 15 hours. As the coating deposition is performed on the blade heated up to 850-900°C and then a two stage homogenizing annealing is carried out at 1030°C for 2 hours (in the interval a surface treatment by microballs is being conducted) and the two-stage heat treatment in vacuum is being applied at 900°C for 8 hours + 820°C, for 15 hours for restoration of metal properties [4].

The GT-100 gas turbine is running on liquid fuel (Table 3).

Table 3. Impurity content inn liquid fuel for GT-100 gas turbine (mass fraction %).

Content	Na + K	Ca	S	Particles
Real	up to 0.0006 ¹⁾	satisfied	satisfied on the whole	satisfied
Specifications Demand 38.101-858-80 ²⁾	no more than 0.0002	no more than 0.0005	no more than 1.88	no more than 0.02

Note :

- 1) in some cases
- 2) Vanadium and Plumbum content doesn't settled in specifications

3 Results and discussion

3.1 The blade coating condition after operating.

After operation the coating has evidence of the pitting corrosive damages to some extent. The formation of pits on the trailing edge is the most typical for the blades of the first and the second stages of the HPT and of the first stage of the LPT (Fig.1). The number of pits are seen as ones of unity, as the other merged together along extended area which occupied the considerable part of the trailing edge surface. Pitting is being observed on the blade airfoil, mostly on the convex surface. Number of pits varies from the separate ones up to the pits, merged into the whole zones which are covered of the significant part of the airfoil (Fig. 1).

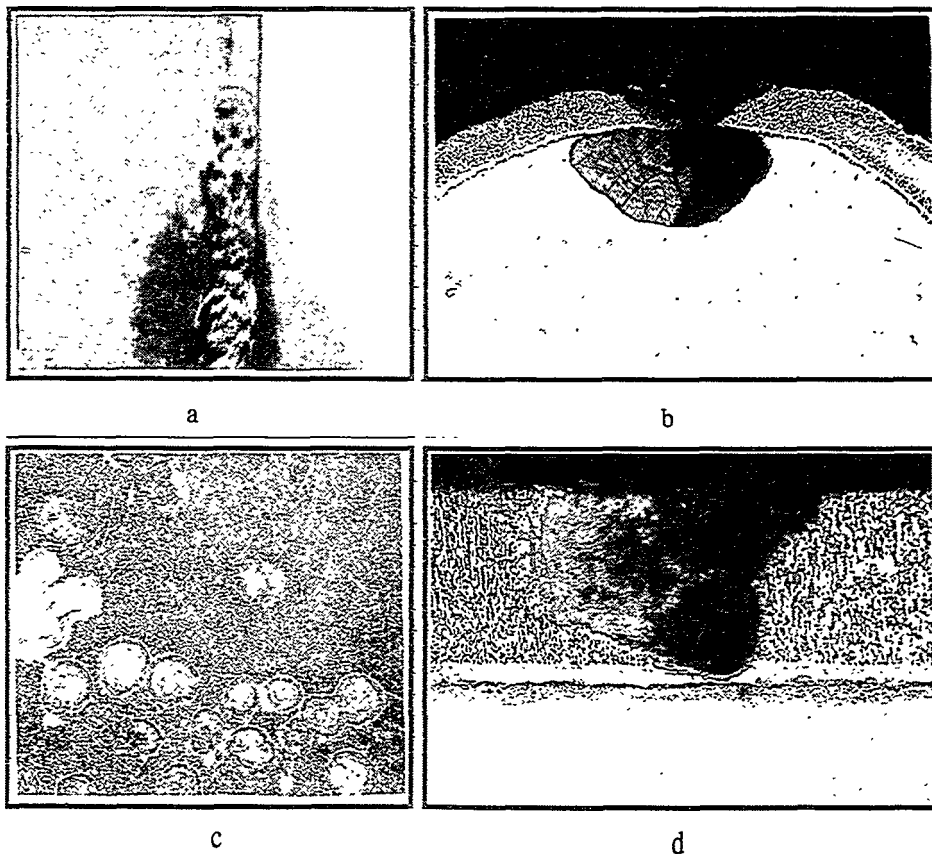


Fig.1. Corrosion damage on trailing (a,b) and convex side (c,d) of the first stage blades of HPT of GT-100 gas turbine.

Metallographic examination of the coating areas with pitting indicates that at the pitting region can be seen the full damage of the coating and the penetrating of the corrosive damage into the base metal (Fig. 1). The depth of the base metal damage is 150 mm. The investigation of the phenomenon of pitting damage of the coating and of the base metal displayed that the damage is run through the mechanism of hot low-temperature corrosion [5, 6].

Lack of treatment by microballs (intended primarily to densify the surface layer of the coating and to eliminate channels of crystal growth) for the set of rotating blades of the first stage of the LPT (Table 1) caused a corrosive damage of the coating (Fig. 2). But the corrosive damage of the base metal has not observed practically in this case.

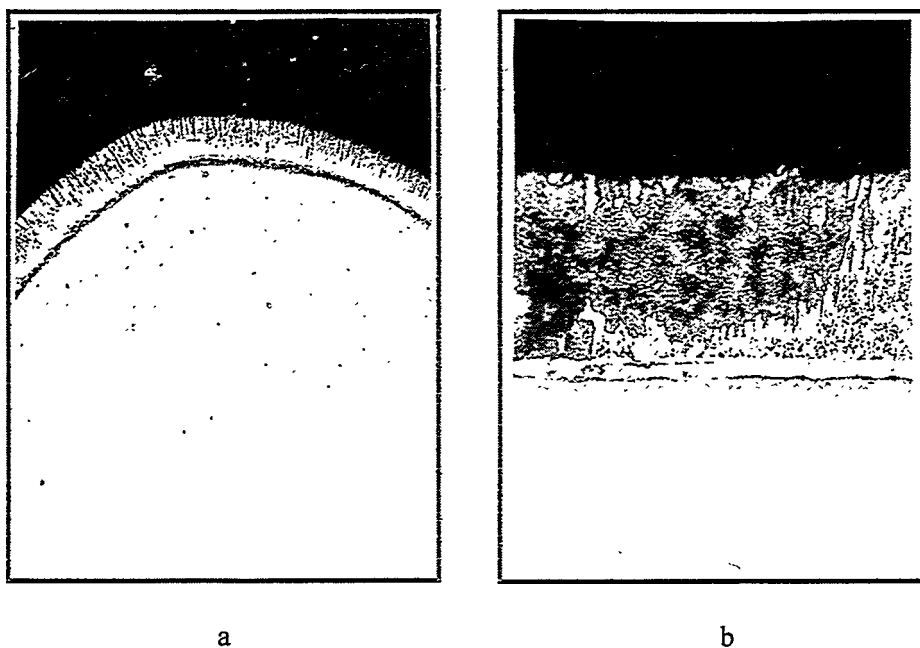


Fig. 2. Corrosion damage EP PVD SDP-3A coating on the first stage blade of LPT of GT-100 gas turbine after 7381 operating hours.

At all rotating blades at the areas without corrosive damages the coating has the depth close to the original one. The spinel layer $(\text{Fe, Ni, Co})_3\text{O}_4 + \text{Al}_2\text{O}_3 \text{ Cr}_2\text{O}_3$ of different depth has observed on the coating surface. The chemical composition of the coating changes insignificantly under operation.

Chromium and aluminium content in the coating doesn't change from the original one and nickel content increased due to diffusion from the base metal (Table 4). The coating constitutes a two-phase structure, i.e. ϵ -matrix and intermetallic β -phase. Diring operation takes place the complete transformation of the γ -mode of the matrix (which is presented in the initial condition) into ϵ -mode. This transformation promotes a distinct increasing of the coating microhardness (Table 4).

Table 4. Chemical and gas composition and microhardness of the electron beam coating of moving blades of the GT-100 gas turbines before and after operation.

Stage	Operation hours	Coating	Content of chemical elements (mass %)			Phase composition	Micro-hardness (Mpa)
			Cr	Al	Ni		
HPT	5903	SDP-3A	<u>21.9</u>	<u>11.8</u>	<u>4.1</u>	ϵ, β	<u>6300</u>
			22.9	12.3	4.4		7150
2 HPT	6972	SDP-3A	<u>22.1</u>	<u>12.1</u>	<u>1.4</u>	ϵ, β	<u>5700</u>
			22.6	12.4	1.9		6580
1 LPT	7381	SDP-3A	<u>21.7</u>	<u>12.1</u>	<u>3.7</u>	ϵ, β	<u>6780</u>
			22.8	12.7	4.2		7350
	after operation	SDP-3A	<u>22.0</u> 24.0	<u>11.5</u> 12.9	<u>0.5</u> 0.9	ϵ, γ, β	<u>4800</u> 6300

3.2 The blade metal condition after operation

Under operation the main changes of the blade metal are related to the basic alloy hardening γ' -phase. According to the stage number (which determines the temperature) an extra precipitation of γ' -phase in amount of 2 % to 6% is observed (Table 5). The structure of grain boundaries remains practically unchanged (Fig. 3). The modifications of the alloy microstructure are accompanied by changes of the blade metal properties (Table 6, 7). According to the amount of the extra precipitated γ' -phase the growth of the hardness and strength and the reduction of the plasticity is observed as at 20°C as at 750°C. But nevertheless, as it can be seen at Table 6, the whole complex of the blade metal properties is at high level and doesn't limit the further use of the blades.

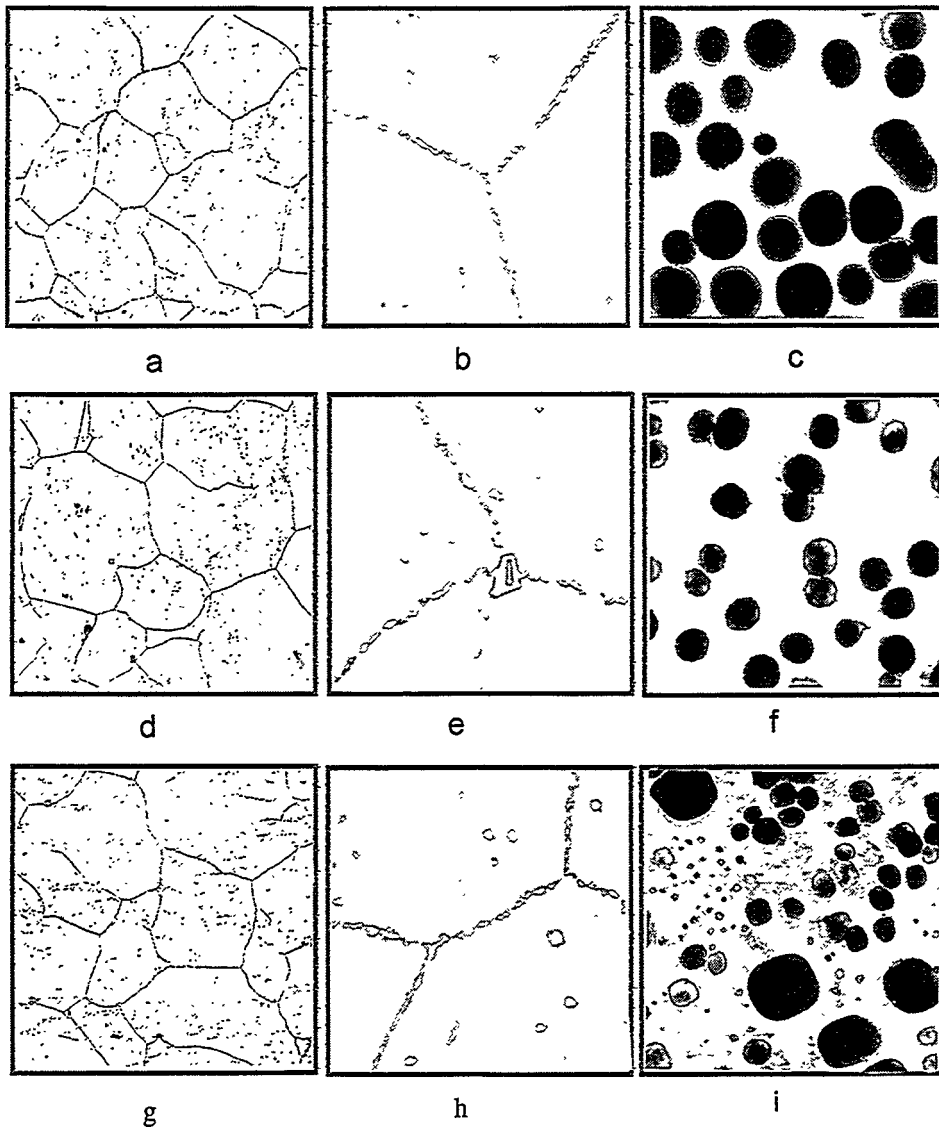


Fig. 3. Microstructure of EI 893 alloy:
 (a-c) after coating deposition and reheat treatment
 (d-f) after (a) + 7381 operating hours
 (g-i) after (a) + 5903 operating hours
 (a, d, g) optical image x 100
 (b, e, h) optical image x 100
 (c, f, i) electron microscope image x 50000.

Table 5. Structural and phase characteristics of the metal of rotating blades.

Heat treatment	Service period (n)	Phase composition of the alloy*	Amount of carbide and borid phases (%)	Amount of γ' -phase, (%)	Characteristics of γ' -phase		
					Mean particle size (μm)	Mean particle distance (μm)	Distribution of particles (μm^{-2})
1	2	3	4	5	6	7	8
Standard: heating 1020°C, 1h + 1160°C, 3 h + 1000°C, 4 h + 900°C, 8 h + 820°C, 15 h	-	γ, γ' , M_6C , $M_{23}C_6$, MC, M_5B_3 , M_3B_2	0.4... 0.6	10... 12	0.07... 0.12	0.08... 0.12	45...60
Standard + RHT (1030°C, 4h + 1160°C, 3 h + 900°C, 8 h + 820°C, 15 h)	-	γ, γ' , M_6C , M_3C_6 , M_5B_3 , MC	0.5... 0.8	10... 12	0.07... 0.12	0.08... 0.12	45...60
Standard + RHT	5903	γ, γ' , M_6C , MC, M_3B_2 , M_5B_3	0.7... 0.8	13... 16	0.06... 0.09	0.07... 0.09	55...65
Standard + RHT	6972	γ, γ' , M_6C , MC, M_3B_2 , M_5B_3	0.6... 0.7	12... 14	0.07... 0.09 0.01... 0.03	0.07... 0.09 0.12... 0.16	50...55 10...15
Standard + RHT	7381	γ, γ' , M_6C , M_3B_2 , MC, M_5B_3	0.8... 0.9	12... 16	0.12... 0.14 0.03... 0.05	0.12... 0.16 0.07... 0.09	25...40 50...70

1	2	3	4	5	6	7	8
Standard + RHT+ service period + RHT	-	$\gamma, \gamma',$ $M_6C,$ $M_3B_2,$ $M_5B_3,$ MC	0.6... 0.8	10... 12	0.08... 0.12	0.07... 0.12	45...60

*- phases are given in order of their amount decreasing.

Table 6. Mechanical properties of GT-100 gas turbine blades made of EI 893 alloy (test temperature 20°C).

Group of blades	Service period (n)	HB (MPa)	$\sigma_{0.2}$ (MPa)	σ_B (MPa)	δ (%)	Ψ (%)	KCU (kJ/m ²)
uncoated (standard heat treatment)	-	<u>2360</u>	<u>530</u>	<u>960</u>	<u>27</u>	<u>31</u>	<u>680</u>
		2500	580	1040	37	39	1120
(standard + RHT)	-	<u>2360</u>	<u>530</u>	<u>970</u>	<u>25</u>	<u>27</u>	<u>680</u>
		2500	570	1040	37	38	1010
1 stage HPT	5903	<u>2760</u>	<u>630</u>	<u>1100</u>	<u>23</u>	<u>20</u>	<u>570</u>
		2850	650	1140	25	23	840
2 stage HPT	6972	<u>2640</u>	<u>610</u>	<u>1060</u>	<u>23</u>	<u>22</u>	<u>590</u>
		2710	630	1130	27	24	760
1 stage LPT	7381	<u>2590</u>	<u>620</u>	<u>1070</u>	<u>29</u>	<u>25</u>	<u>640</u>
		2840	690	1090	36	30	720
Specification	-	<u>2100</u>	<u>490</u>	≥ 830	≥ 20	≥ 22	≥ 590
		2700	670				

Table 7. Mechanical properties of GT-100 gas turbine blades made of EI 893 alloy (test temperature 750°C).

Group of blades	Service period (n)	$\sigma_{0.2}$ (MPa)	σ_B (MPa)	δ (%)	Ψ (%)	Creep test $\sigma = 270$ MPa	
						τ (h)	δ (%)
uncoated (standard heat treatment)	-	<u>450</u>	<u>735</u>	<u>24</u>	<u>26</u>	<u>550</u>	<u>9</u>
		490	860	37	48	1250	23
(standard + RHT)	-	<u>430</u>	<u>740</u>	<u>26</u>	<u>30</u>	<u>608</u>	<u>10</u>
		490	840	36	36	1307	28
1 stage HPT	5903	<u>470</u>	<u>790</u>	<u>23</u>	<u>30</u>	<u>703</u>	<u>19</u>
		540	930	28	33	1130	23
2 stage HPT	6972	<u>440</u>	<u>760</u>	<u>25</u>	<u>23</u>	<u>907</u>	<u>21</u>
		540	840	27	25	984	24
1 stage LPT	7381	<u>410</u>	<u>760</u>	<u>28</u>	<u>29</u>	<u>893</u>	<u>17</u>
		490	790	32	32	1101	19
Specification	-	-	≥ 640	≥ 20	≥ 22	> 500	-

3.3 Removing of the coating layer from the blades after operation.

In spite of the fact that the base metal of blades and the coating on the undamaged areas have the structure and the properties which allow their further use the presence of the corrosive damages need the remove of the coating and of the surface layer of the base metal and the redeposition of the coating. Stripping only the coating layer or both the coating layer and the surface layer of the base metal depending on the depth of pits was performed by aerosol gas-dynamic cleaning [7]. The principle of the process is the treatment of the blade surface by high-speed finely divided aerosol particles of working fluid accelerated by gas flows up to 200...500 m/s. By collision of aerosol particles of the working fluid of fine size $[(1.5...5) \cdot 10^{-5} \text{ m}]$ and the blade surface under treatment the high values of the unit pressure are being developed at the zone of contact of the particles and the surface which are destroying intensively of the surface layer. The blade surface condition is checked for the presence of the residual pits. The process terminates by the

absence of pits on the blade surface and the last one is being prepared for redeposition of the electron beam coating.

3.4 The structure and properties of the redeposited coating.

Two variants of electron beam coatings have been deposited at blades after removing the coatings with the corrosive damages i. e. a three-layer coating of SDP11A/SDP8/KDP1 and a one-layer coating of SDP8.

Check of the blade coating allows to reveal the three-layer and one-layer coating microstructure as being typical one and the variants of these coatings deposited on the remained layers of the original coating (Fig. 4). The coatings have the typical microstructure. The chemical composition, the depth and the microstructure of the coating layers conform the specification.

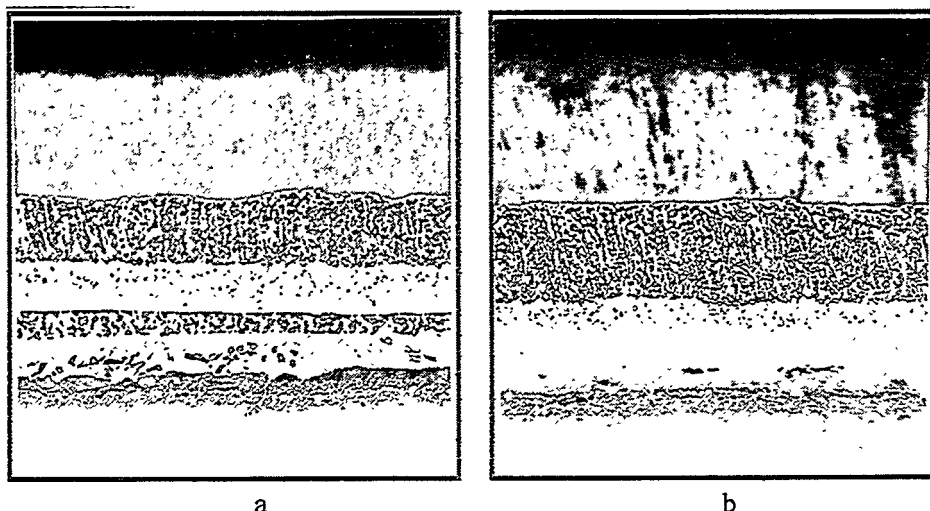


Fig. 4. Microstructure of the three-layers EB PVD coating SDP11/SDP8/KDP1 on the first stage blade LPT of GT-100 gas turbine.

(a) with remained layer of the original coating x 320

(b) without remained layer of the original coating x 320

3.5 Blade metal after the coating redeposition and after reheat treatment.

The microstructure and the phase composition, the mechanical properties of the blade metal after coating redeposition and after reheat treatment match those before the operation (Table 5, 6).

3.6 Experience of service of the restored blades.

Use of the blades with metal coatings of SDP8 type (Table 1) at GT-100 gas turbine at Krasnodar heat-and-power plant for 3000 h after repair hasn't been followed by corrosive damages of the restored coating. It should be noted that by now the after-repair operation time doesn't exceed the operating hours of the blades with one-layer coating before the repair.

The use of the repaired blades with the metal-ceramic coating at GRES-3 of Mosenergo (Table 1) is also characterized by the absence of the corrosive damage of the coating. But this phenomenon can't be explained by the more effective coating compound due to the very short time of operation compared to the operating time before the repair.

4 Conclusion

1. The removing at the proper time of the damaged coating and of the damaged surface layer of the blade base metal gives the opportunity of their further use.

2. The developed repair technique allows to restore of the coating and to eliminate the structural change of the blade material which have taken place under operation and during the redeposition of the coating.

3. The use during repair of more efficient compounds of the coatings corrected according to operation results permits to increase in 2 times of operation life of the blades up to the next (the second one) repair.

List of references

1. A. I. Rybnikov et al. Surf. Coat. Technol., 68-69 (1994) 38-44.
2. A. S. Osyka et al. Surf. Coat. Technol., 76-77 (1995) 86-94.
3. B.A.Movchan et al. Surf Coat Technol., 67(1994) 55-63.
4. B.A.Movchan et al. Probl.Spets. Electrometall., (1) (1985) 3441.
5. D.I.Wortman et ai. Thin Solid Films, 64 (2) (1979) 281-288.
6. K.L.Luthra. Metallurgical Transactions, A, v13A, Get (1982) 1853-1864.
7. M. L Zadkevich et al. Tiazeloe Mashinostroenie, (2) (1993) 34-36.

Structural transformations and temperature state of rotating blades of EI893 alloy under operation

Pigrova G.D.
Rybnikov A.I.
Kryukov I.I.
Polzunov Central Boiler and Turbine Institute (NPO CKTI)
Polytechnicheskaya, 24, 194021 , St. Petersburg, Russia

Abstract

The composition and quantity of different phase component of EI893 alloy after long term operation as base metal for rotating blades of gas turbines GT-6, GTN-9, GTK-10 and GT-100 types were studied. The obtained data were analysed with regard to the chemical composition of alloys and of initial condition of heat treatment. Data of metal phase analysis obtained after operation can provide the basis for evaluation of temperature field of rotating blades in the course of operation since structural condition of phase components and redistribution of alloying elements are being specified by temperature and in-service time.

1. Introduction

The EI893 alloy is widely used for the manufacture of different stage rotor blades in GT-6, GTN-9, GTK-10, GT-100 and other turbine units. The blades made from EI893 and operating under different temperature-stress conditions in various corrosive environments both with and without protective coatings.

NPO CKTI has gained a lot of data in experimental studies of metal phase composition after various heat treatment procedures for the length of laboratory test aging at temperatures in the range from 500 to 700°C, as well as after alloy operation in different units.

For better insight into the process of phase-formation taking place in a heat treatment zone, a phase diagram has been constructed for temperatures between 850 and 1050°C. The major strengthening phase in the alloy is a

Ni₃(Al,Ti)-based γ' -phase in which all metal alloying elements are dissolved. The amount of γ' -phase varies with temperature; and is typically about 9% at 850°C, 5% at 900°C and 2% at 950°C. The γ' -phase composition changes moderately with the temperature.

Beside γ' -phase, the so-called secondary phases (carbides and borides) form in this alloy. Carbide phases of the MC (titanium -), M₂₃C₆ (chromium -) and M₆C (nickel, molybdenum and tungsten - based) types are most typical for this alloy. Boride phases are represented by the M₃B₂ (chromium, molybdenum and tungsten - based) and M₅B₃ (chromium and tungsten - based) type structures.

2. Experimental details

The subjects of study were specimens and rotating blades of the gas pumping gas turbines GT-6, GNT-9, GTK-10 and of the peak load power GT-100 gas turbine. The specimens and blades are made of the superalloy EI893 (Table 1).

Table 1. Chemical composition of EI893 alloy.

Mass fraction, %									
C	Ni	Cr	Mo	W	Ti	Al	Fe	Mn	S
≤ 0.07	bal.	<u>15.0</u>	<u>3.5</u>	<u>8.5</u>	<u>1.2</u>	<u>1.2</u>	≤ 3.0	≤ 0.6	≤ 0.02
		17.0	4.5	10.0	1.6	1.6			

A method of physical-chemical analysis was used in the studies. Phase extracts were prepared by anodic dissolution of the matrix in 10 pct HCl-methanol electrolyte. The resulting specimens were analysed by X-ray diffraction method using cobalt radiation. The composition of the extracted phases was evaluated by chemical analysis with photometry.

3. Results and discussion

3.1 Heat treatment procedures

The formation process study of secondary phases under various heat treatment conditions shows that the secondary phase formation is greatly

affected by the homogenization temperature at subsequent tempering stages. The higher is the homogenizing temperature, the greater is the probability of stable phase formation. The M_6C and M_3B_2 phases have been found after heat treatment at the homogenizing temperature of 1200°C . These phases have been found during material studies of a blade from EI893 alloy after long-term operation (40 000 to 60 000 h) independent on the initial heat treatment conditions. Consequently, these phases may be considered as characteristic of a stable EI893 alloy state.

The most commonly used heat treatment procedure for the EI893 alloy in industrial service is a multistage aging process involving a number of successive exposures to high temperatures: 1000°C - 4 h, 900°C - 8 h, 820°C - 15 h. The amount of γ' -phase is determined by the last stage temperature and is usually 10 to 12%. The analysis of secondary phase transformations during staged heat treatment with homogenisation at 1200, 1600 and 1100°C reveals some regular features. A distinguishing feature of borides is the $M_5B_3 \rightarrow M_3B_2$ transition. In the event of full homogenisation occurrence at 1200°C , the stable M_3B_2 boride will precipitate during subsequent heat treatment.

If borides are partially dissolved at 1160°C , then M_3B_2 is observed to form during tempering, and X-ray diagrams show a progressive transition from M_5B_3 to M_3B_2 . The same reaction also occurs at over 1100°C , but it is less pronounced, and the predominant boride after a full heat treatment procedure is M_5B_3 .

Carbide phases also form in various ways, depending on the homogenising and tempering temperature. After homogenisation at 1200°C , some balance in carbide formation is observed: the predominant precipitate at 1000°C is M_6C and at 900°C - $M_{23}C_6$.

Similar carbide reaction occur under 1160°C during a multistage heat treatment. Exposure to 1100°C will intensity M_6C precipitation. The subsequent stage at 1000°C also shows the additional formation of M_6C . The vigorous M_6C precipitation in the temperature range from 1000 to 1100°C will suppress the formation of $M_{23}C_6$ at the next stage at 900°C because the most of carbon content is associated with M_6C . If homogenization is followed by the treatment stage at 800°C , then only the $M_{23}C_6$ carbide and boride phases contents after this heat treatment are from 0.15 to 0.25%.

The carbon content within 0.01—0.03% has only a slight effect on the course of carbide reactions, but it determines the quantities of carbide phases.

Thus the above study shows that the homogenizing and tempering conditions produce various combinations of M_6C , $M_{23}C_6$, M_3B_2 and M_5B_3 phases. Homogenization at 1200°C provides almost full dissolution of carbides

and borides. At 1160°C MC and M_5B_3 are still present and additional M_6C is observed to form at 1100°C. During later heat treatment stages at 1000°C, the M_6C and M_3B_2 phases are precipitating and at 800 to 900°C - the $M_{23}C_6$ phase. The MC carbide is stable only at early heat treatment stages. The $M_5B_3 \rightarrow M_3B_2$ reaction is established and its feasibility depends on heat treatment conditions.

The use of coatings for gas turbine blades has brought some changes in the EI893 heat treatment conditions because a diffusion annealing at 1030 to 1050°C for 4 to 6 h is performed as the coatings are being applied. During annealing the γ' -phase fully dissolves, leading to metal strength losses, as well as to some changes in the secondary phase structure. When the metal is at temperatures between 1030 and 1050°C, a partial $M_{23}C_6 \rightarrow M_6C$ transformation may occur. Hence, additional heat treatment involving stages at 900 and 820°C should be carried out after coating application. This heat treatment procedure uses two cooling methods for the metal after exposure to high temperatures:

1. 1030°C - 4 h, vacuum cooling; 900°C - 8 h, vacuum cooling; 820°C - 15 h;
2. 1030°C - 4 h, furnace cooling up to 900°C at the rate of $\sim 15^\circ\text{C}/\text{min}$; 900°C - 8 h, furnace cooling up to 820°C at the rate of $\sim 15^\circ\text{C}/\text{min}$; furnace cooling.

A great deal of phase analysis data for EI893 alloy after standard three-stage heat treatment is available in NPO CKTI. It has been shown that the γ' -phase amount is determined by the last stage temperature, the γ' -phase formation in the region of high temperatures is observed to be very intensive and exposure for several hours produces γ' -phase in quantities typical for the given temperature. A temperatures in the range from 815 to 830°C, γ' -phase usually amounts to 10-12%.

The γ' -phase study on coated blade metal for which a complicated heat treatment procedure involving various cooling methods was recommended showed that γ' -phase amount was a usual level, which was quite natural, because the temperature at the last heat treatment stage remained unchanged (Table 2).

Table 2. γ' -phase amount in GT-100 turbine blade material.

Heat treatment	γ' -phase amount, %
1) 1170°C - 3 h; 800°C - 12 h + EBC* + + 900°C - 8h; 820°C - 15 h;	11.6
2) Three-stage procedure + EBC + + 900°C - 8h; 820°C - 15 h (rapid cooling);	10.8-12.0
3) Three-stage procedure + EBC + + 900°C - 8h; 820°C - 15 h (slow cooling).	10.0-12.0

The comparison of γ' -phase composition in the investigated blade metal with previously obtained data suggests that the γ' -phase composition is not different from that obtained for EI893 alloy after standard three-stage heat treatment.

As it has been shown earlier, the three-stage heat treatment procedure is characterised by the formation of M_6C (mainly at the 1000°C stage) and $M_{23}C_6$ (at 900°C). Additional heat treatment when coating is used provides an exposure to 1030°C, during which the M_6C carbide is usually formed. This carbide is therefore a predominant phase in the material of all blades regardless of the methods of cooling from this heat treatment stage (Table 3). The $M_{23}C_6$ carbide is present in much smaller quantities. At heat treatment when EBC is used, the amount of secondary phases is increased at the expense of M_6C formation with a higher M/C ratio than that of $M_{23}C_6$.

Table 3. The phase composition of GT-100 turbine blade metal after heat treatment.

Heat treatment	Secondary phases
1) Three-stage procedure	$M_{23}C_6$, M_6C , M_3B_2 , M_5B_3 , MC
2) Three-stage procedure + EBC + + 900°C, 820°C (rapid cooling);	M_6C , $M_{23}C_6$, M_3B_2 , M_5B_3 , MC
3) Three-stage procedure + EBC + + 900°C, 820°C (slow cooling).	M_6C , $M_{23}C_6$, MC, M_3B_2 , M_5B_3

A more stable carbide structure can be considered as produced during heat treatment of electron-beam coated metal, and this reduces the probability of carbide reaction occurrence during later operation. Boride phases are present in the form of M_3B_2 and M_5B_3 . It should be noted, however that the $M_5B_3 \rightarrow$

M_3B_2 reaction is somewhat slowed down in case of heat treatment of electron-beam coated metal, which is likely to be attribute to the formation of molybden-containing M_6C .

3.2 EI893 alloy service in turbines.

There is a great body of experimental data accumulated in NPO CKTI, concerning the phase transformation study on EI893 alloy when it is used as a gas turbine blade material. The detailed phase analysis has been carried out for the blade metal in GT-75-6 and GTK-10 turbines after operation for 20000 to 30000 h and GTN-9 turbines after 65000 h. Data on γ' -phase amounts in different blade parts (Table 4) correspond to the operating temperature values in these regions. There is additional phase precipitation in blade parts with temperatures of 600 to 610°C. The identical condition is observed in high-temperature regions of a blade air foil. The γ' -phase amount data for blade parts heaving different operating temperatures and the laboratory test results given earlier enable to plot the temperature dependence of γ' -phase amount in EI893 alloy in the range of 550 to 950°C (Fig.1). In the low-temperature region (550 to 600°C) no full γ' -phase precipitation is likely to occur even for 65000 h, while at temperatures above 650°C a rather rapid γ' -phase formation is observed and after aging for 1000 h there is, as a rule, a balance in γ' -phase amounts.

Table 4. The phase composition of EI893 alloy in blades after operation.

Unit	Service life	Stage	Blade region	Secondary phase	γ' -phase amount, %	Second phase amount, %
1	2	3	4	5	6	7
GT-750-6	30165	1RB*	locking piece	M_6C , $M_{23}C_6$, M_3B_2 , MC	9.0	1.0
			air-foil	M_6C , $M_{12}C$, $M_{23}C_6$, M_3B_2	16.6	1.4
		2 RB	locking piece	M_6C , $M_{23}C_6$, M_3B_2 ,	9.0	1.1
			air-foil	M_6C , $M_3B_2C_6$, MC	12.0	1.4

1	2	3	4	5	6	7
GT-750-6	22430	1 RB	locking piece	M_6C , $M_{23}C_6$, M_3B_2 , MC	9.5	1.4
			air-foil	M_6C , M_3B_2 , MC	14.0	1.4
GTK-10	11300	1 RB	locking piece	M_6C , $M_{23}C_6$, M_3B_2 , MC	11.4	1.2
			air-foil	M_6C , M_3B_2 , MC	17.0	1.3
	20500	1 RB	locking piece	M_6C , $M_{23}C_6$, M_3B_2 , MC	9.4	1.1
			air-foil	M_6C , M_3B_2 , MC	15.9	1.3
GTN-9	65000	1 RB	locking piece	M_6C , $M_{23}C_6$, M_3B_2 , MC	11.4	0.9
			air-foil	M_6C , M_3B_2 , MC	16.5	1.0
		2 RB	locking piece	M_6C , $M_{23}C_6$, MC	11.0	0.7
			air-foil	M_6C , $M_{12}C$, $M_{23}C_6$, MC	15.8	0.8
		1 FB**	locking piece	$M_{23}C_6$, M_5B_3 , MC	15.0	0.4
			air-foil	M_6C , $M_{23}C_6$, M_5B_3 , M_3B_2 , MC	12.0	0.5
		2 FB*	locking piece	M_6C , $M_{23}C_6$, M_5B_3 , M_3B_2 , MC	16.0	0.7
			air-foil	M_6C , $M_{12}C$, $M_{23}C_6$, M_5B_3	16.2	0.8

* RB - rotor blades

** FB - fixed blades

The chemical composition of secondary phases after long-term service (Table 4) features the presence of carbide and boride structures identical to

those as stabilised after heat treatment and aging, except for the $M_{12}C$ η -type carbide fixed in a high-temperature region in some blades. This is a carbide of the same type as M_6C , but with a higher M/C ratio. Perhaps, it can be considered as the next stage of a metal carbide stage. The above data on the phase composition for different units are distinguished by a prior metal heat treatment: a three-stage procedure used for GT-750-6 and GTK-10 units and a simple single-stage one (800°C - 12 h) for GTN-9. During service, the metal after a three-stage heat treatment exhibits the presence of the M_6C and $M_{12}C$ carbides in high-temperature blade regions, and M_6C and $M_{23}C_6$ in the low-temperature ones while after a simple (single-stage) heat treatment an increase in the M_6C amount is observed, and $M_{23}C_6$ is still retained. The distinction between boride phases compositions consist in the presence of the M_3B_2 type after a three-stage heat treatment and M_5B_3 after a single one. The operating temperature appears to be insufficient for the boride reaction progress, and the boride structure in metal is retained after heat treatment. The quantity of secondary phases is also different: 1.0 to 1.4 % in operation after a three-stage and 0.5 to 1 % after a single-stage procedure.

4 Conclusion

Thus, additional temperature-dependent γ' -phase precipitation occurs during EI893 operation, and the $M_{23}C_6 \rightarrow M_6C \rightarrow M_{12}C$ carbide reaction is developing. It should be noted, that this reaction is a characteristic of the metal after any heat treatment procedure, and in a state of equilibrium the alloy will have η -type carbides and M_3B_2 boride. Nearest this state are the high-temperature blade regions after long-term operation with a prior three-stage heat treatment.

Based on a great volume of phase analysis data for the EI893 alloy, it can be concluded that the phase transformation of this metal under time-temperatures effects involve a γ' -phase precipitation, and $MC \rightarrow M_{23}C_6 \rightarrow M_6C \rightarrow M_{12}C$ carbide and $M_5B_3 \rightarrow M_3B_2$ boride reaction development.

Using a proper heat treatment procedure for the alloy, various steps of metastable state can be provided depending on the required quality level of properties and manufacturing techniques. During long-term aging or operation, the alloy goes through the stages approaching the balanced state which is characterised by the presence of γ' -phase, η -carbide of the M_6C and $M_{12}C$ types and the M_3B_2 type boride.

Turbine Maintenance and Modernization

Esa Unga, Manager of Production Services
Teollisuuden Voima Oy (TVO)
FIN-27160 Olkiluoto, Finland

Abstract

The disturbance-free operation of the turbine plant plays an important role in reaching good production results. In the turbine maintenance of the Olkiluoto nuclear power plant the lifetime and efficiency of turbine components and the lifetime costs are taken into account in determining the turbine maintenance and modernization/improvement program. The turbine maintenance program and improvement/modernization measures taken in the plant units are described in this presentation.

1 Introduction

Teollisuuden Voima Oy's (TVO) Olkiluoto nuclear power plant generates approximately 20 % of Finland's electricity. The country's largest generation location, Olkiluoto, has supplied electricity to customers reliably and cost-effectively about twenty years. Average load factors have typically been 90 % or higher.

TVO's two BWR units were delivered by the Swedish AB ASEA ATOM (nowadays ABB Atom). Olkiluoto 1 (OL1) has been in operation since 1978 and Olkiluoto 2 (OL2) since 1980. Reactor pressure is 70 bar, steam flow to turbine is 1080 kg/s (at 710 MWe) and feed water temperature 180 °C. Originally the net power level was 660 MWe (2000 MWth) but in 1984 it was increased by 8 % to 710 MWe (2160 MWth). Because of modernization project carried out in 1994-1998 power uprating from 710 MWe to 840 MWe (2500 MWth), about 15 percent, became possible. The main goals of the modernization are to ensure plant safety, to increase electricity production, to extend the plant life time and to improve the expertise as well as productivity of the TVO staff. The goals are supporting each other. The modernization of the turbogenerator was one part of this project.

The turbine is a single turbine-generator unit. The turbine was designed and manufactured by the Swedish STAL-LAVAL (nowadays ABB STAL) under a licence agreement with BROWN BOVERI & CIE (nowadays also ABB). It is a 3000 rpm tandem-compound, single shaft, machine with one high pressure (HP) cylinder and four low pressure (LP) cylinders. The generator was designed and manufactured by the Swedish ASEA AB (nowadays ABB Generation). All main parts where electrical losses occur are directly water cooled. The generator is equipped with a brushless excitation system with an A.C. exciter and rotating rectifiers. Turbine plant has 3 low pressure and 2 high pressure feed water heating stages, four HP steam inlet control/stop valves, two reheater steam inlet control/stop valves, two bypass steam control/stop valves (100 % bypass capacity) and special MOPS/SCRUPS-moisture separators between the HP-turbine and moisture separator/steam reheater.

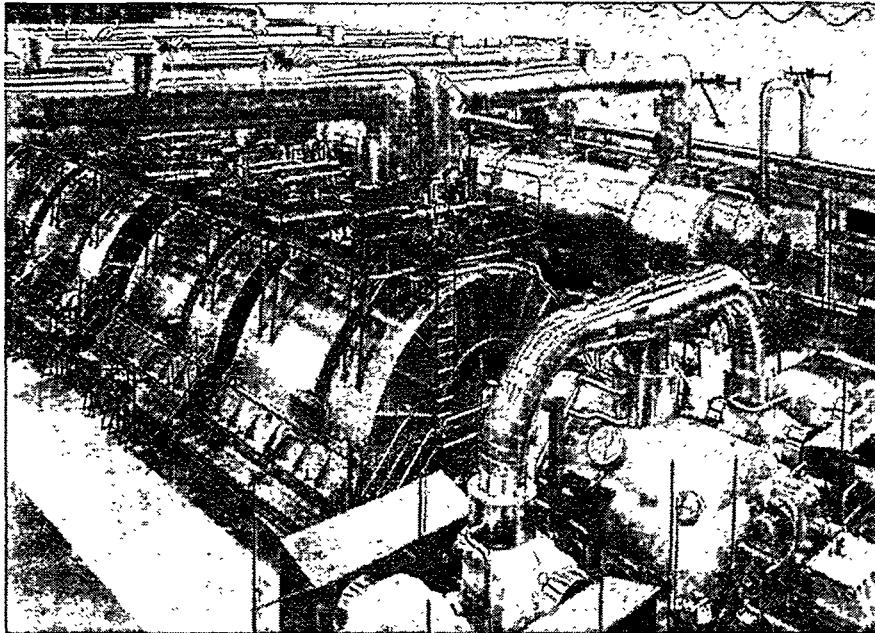


Fig.1. The turbine hall of Olkiluoto 1 after 1998 outage. The last works of the modernization project were completed during 1998 outages at both plant units.

2 Maintenance Philosophy

TVO's maintenance philosophy is to keep both power plant units in modern, up-to-date condition to avoid unplanned shutdowns and to operate them at high efficiency. To achieve this goal, good condition monitoring and

maintenance are needed. Good trend supervision and detection of failures at an early stage is one of the main principles. Identifying existing or potential problem areas by advanced vibration monitoring, a careful follow-up of process efficiency, chemistry and other process parameter and the use of other predictive methods (thermography, oil analysis, motor operated valve testing etc.) are essential to determine the condition of the power plant units.

Today the main part of maintenance is, however, based on periodical inspections and services. The intervals between major services can be extended and the availability of a unit improved by using predictive maintenance methods and adopting the concept of condition based maintenance. Various analyses are used to optimize and to allocate maintenance measures to right objects.

3 Modernization program of Olkiluoto NPP

An extensive modernization programme is currently finished at the Olkiluoto site, designed to guarantee a long service-life and enhanced safety and generating capacity. The programme was started in 1994 with extensive prestudies and safety analyses. The main part of the modifications on the power plant units were made in 1996-1998 (the generator exchange of OL2 was made in 1994). The programme includes, for example, a revamp of the turbine control/safety system and improved turbine efficiency, an upgrade of the reactor core monitoring system, modernization of the fuel loading machinery and increased reactor output.

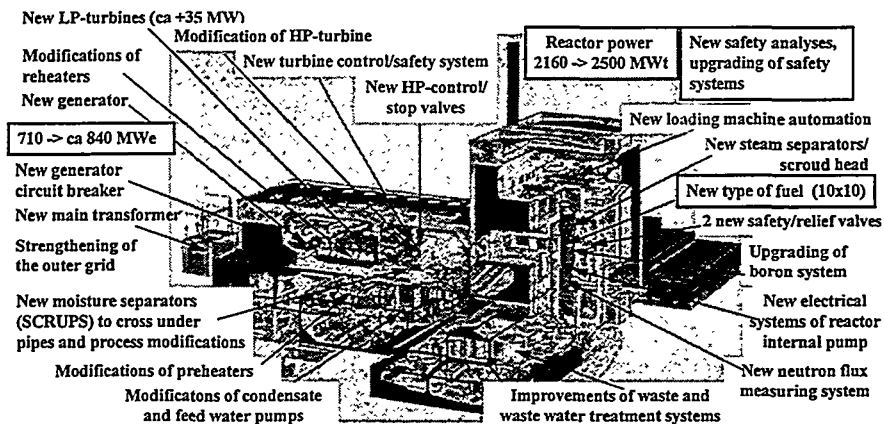


Fig.2. During the modernization project of Olkiluoto NPP in 1994-1998 the output power was uprated from 710 MWe to 840 MWe.

4 Modernization of the turbine plant

Before the modernization project TVO has made continuously improvements/modifications at the turbine plant. Erosion corrosion on carbon steel piping and components (reheaters, flash boxes) was a big problem in the initial years of operation. Systematical inspections since 1980 were made in the systems of the turbine plant to manage the risk areas for erosion corrosion and to avoid operation problems. The material has been changed to stainless steel in extraction steam lines, the flash boxes of all preheaters, low pressure preheaters, some valves, some details in moisture separators/steam reheaters and a lot of drain pipes. The cross-under pipes from the HP-turbine to the moisture separators/steam reheaters have been sprayed with a metal which is not sensitive to erosion corrosion. Also some parts of the moisture separators/steam reheaters and the HP-turbine outer casing have been sprayed with the same method and the results have been succesful.

The original tube material of the main sea water condensers was aluminium brass but after corrosion problems the condenser was replaced at OL2 in 1985 and at OL1 in 1986. The new tube material is titanium, which has excellent corrosion resistance even under brackish water conditions. The sea water side of the tube plates is also titanium coated. The heat surface of the condenser was increased from 22 000 m² to 27 700 m², thus increasing the electricity output particularly during the warm sea water period. New problem with titanium tubes was the drop erosion on the steam side. This is avoided in the future by replacing the outermost tubes with special hard stainless steel (SMO) tubes (made during the 1996-1998 outages).

The sea water is used to cool the main condenser as well as the several auxiliary systems and air coolers; therefore the plant has an extensive sea water pipeline systems made of rubber lined carbon steel. These pipelines have been changed to carbon steel pipes with powder epoxy coating as a means of eliminating damages that appear in the rubber liner. Fibreglass and plastic pipes have also been used in appropriate places. The programme is still going on.

The moisture content of the steam after the HP-turbine is about 15 %. This moisture causes erosion corrosion in the cross-under pipes and moisture separators/steam reheaters, and it lowers the efficiency of steam reheaters. As a remedy, extra moisture separators (so called MOPS/SCRUPS = moisture preseparator/special cross-under pipe separator) were erected to the cross-under pipes directly after HP-turbine at OL1 in 1987 and at OL2 in 1988. The moisture content dropped down to about 2 % and this improved the plant efficiency by about 4 MW.

The HP-turbine was modified using a modern blade profile to have better efficiency at OL2 in 1985 and at OL1 in 1986.

In the initial years of operation, many defects on the generator rotors due to design weaknesses were noted. The generator supplier delivered new rotors with better design and the new rotors have been operating well. The material of the rotor retaining rings was also replaced by stress corrosion resistant materials (18/18). To carry out the basic maintenance and modernization of the generators, a new generator (stator and rotor) was purchased for OL2 and the exchange was made during the annual outage in 1994. The old OL2 generator was modernized and it has been installed to OL1 during the annual outage in 1996. The exchange of generators enables the increase of the electrical output of the plant units.

During the modernization project the turbine plant vendor made studies of possible improvements on the turbine plant to improve the efficiency of the turbine plant and to enable the plant power increase. New low pressure turbines (4/unit) gave about 35 MW because of a better efficiency. The exchange of LP-turbines were made during the annual outages 1996-1998 and it included new rotors and new blade carriers and blading with new design. Also modifications of inner casings due to bigger exhaust area, erosion resistant materials and erosion resistant plating on blade carriers, inner casings and better axial sealings between steam chambers were included. To keep short outage times the LP-turbines were exchanged "in packages: old parts out and new complete parts in".

The HP-turbine was needed to be modified to enable increasing the plant power level (changing/taking off some blade stages). Also exchange of HP-steam control/stop valves were made in 1998 to decrease the pressure drop over the valves. By having new 2-flow reheaters it is possible to increase efficiency by some megawatts; this requires also the exchange of HP-turbine (will be made perhaps in 2004-2005). Cost-benefit studies of these modifications are not yet finished. Some improvements of reheaters and installing new moisture separators (SCRUPS) before reheaters were made in 1998.

Turbine control and safety system was exchanged to a 3 channel computer based system at OL1 during the annual outage in 1996 and at OL2 in 1997. This will increase the plant units' availability as single failures can be better tolerated and the new system fulfills the new demands of control requirements. As so far the experience of new systems have been very positive. Also the need of maintenance (and costs) will be reduced remarkably.

5 Service programs and intervals

Service programs are based on the recommendations of the plant vendors and equipment suppliers. Operation experience is used to optimize maintenance periods and programs. Programs are evaluated continuously. Sharing experience with other power plants (having the same type of power plants/turbogenerators and using the same plant vendors/contractors for outage works) is an essential part of experience exchange. By modifications of components and having more simplified and maintenance friendly design can service intervals be increased and costs reduced remarkably.

LP-turbines have been normally opened about every 6 years but the new LP turbines make possible to increase the opening interval to 10 years. Total inspection of the rotor and rotor blades are done by modern NDT-methods when opened (not opened LP turbines can also be inspected through inspection holes if needed). The last stage of rotor blading are normally disassembled for inspection. Turbine casing and stator vanes are inspected visually and by NDT-methods if needed. The position of the rotor in relation to the stator is measured by laser. The main reason for opening the turbines has been the inspection of rotor blades, because some blades with cracks have been found. Also the erosion of the turbine inner casings and blade carriers caused a lot of repair and some decrease in the turbine efficiency (internal leakages). All problem areas have been taken into account in the design of the new LP-turbines to avoid similar problems in the future (for example erosion protection of all risk areas and careful material selection). The opening interval of HP-turbine is about 7 years and that of bearings 3-4 years.

LP turbine outlet blades are inspected every second year by special eddy current instrument, also the alignment control of the turbine shaft is planned be done every second year with the new strain gauge method.

The main steam valves and servomotors are overhauled at a 4-6 year periods. Preheaters are inspected according to special program for pressure vessels.

Components which are of great importance for operation and which can be easily inspected at reasonable cost are inspected every year. They are, for example, turbine condensor, LP- and HP-turbine outlets, cross-under pipes and special steam dryers after the HP-turbine, moisture separators/steam reheaters, flash boxes etc. Also functional testing of vital regulating components are made every year.

The generator rotor is planned to be taken out every 6 years. An inspection of the main generator by KUDAR-equipment or other methods without dismantling the rotor is planned to be made every 2 years. KUDAR-equipment is used for checking the tightness of stator slot wedges, inspecting the stator laminations to detect shortcircuits and hot spots, visual inspecting of air gap surfaces (rotor and stator surfaces) and ultrasonic testing of rotor retaining rings, rotor wedges and rotor teeth.

The maintenance measures, intervals and execution are specified in special maintenance and service instructions, which are basically based on the instructions of the plant vendors and equipment suppliers. TVO has made their own instructions (including training material like video tapes etc) for the most important equipments. All service works, modifications and repairs are planned according to the special routines/instructions specified in the quality assurance program.

6 Investments to short outages

Some improvements have been made to make overhauls and inspections easier and less time consuming. For example turbine couplings and HP turbine casings have got new hydraulic bolts. A new alignment method of the turbine/generator shaft has been taken in use some years ago; the method is based on the strain gauge measurements directly on the couplings (no opening of couplings for measurement are needed) and the time needed to check the alignment is reduced to about 15 hours (12 hours barring + 3 hours measurements). LP-turbines are equipped with inspection holes to make it possible to inspect some parts of the turbine with an endoscope or a small camera without opening it. Also installing more local hoists, permanent platforms for maintenance, having proper spare part policy with replacement units etc. help to keep short outage times. Outage times for turbine overhauls have decreased from 6 weeks to the present about 2 weeks by developing working methods and making improvements all the time. The turbine balance at start-up after outages has been good because of the good balance of new rotors and balance indication (and balancing before run-up). At balance indication the couplings are indicated and possible position changes at couplings are compensated by weights (rotors has only one bearing).

By means of an optimal spare parts policy it is possible to keep up the quality of maintenance work done during the relatively short outages. The number of complete component replacement units, such as turbine blades, servomotors, various pumps and valves etc. has increased over the years. During the outage components are replaced and they are overhauled after

the outage in workshop conditions. This together with risk studies helps to avoid major unexpected repairs during outages.

7 Execution and personnel

The main part of maintenance is done during outages and by contractor personnel. Getting competent resources is assured by having some own key persons and by having long term contracts with plant vendors and main contractors. Normal service outage at turbine plant takes about two weeks, also the modernization measures (for example exchange of 2 LP-turbines, modification of HP-turbine and exchange of HP-control/stop valves) were made during annual 15-19 days outages. One reason for this is having a detailed and early planning and good cooperation with plant vendors (an experienced service engineer on site through the year) and working together with contractors to reach common goals. Reaching short outage times with good quality is the benefit of both parts in the long-term.

8 Future

How can we keep the high availability and good plant efficiency at competitive costs in the future when the plant units became older? One way is to use more predictive maintenance methods to optimize the needed maintenance measures, to make improvements/modifications and to develop working methods, tooling etc. continuously. The cost-benefit considerations must not be based only on short-term but also on long-term values.

TURBINE CASING BOLTS; A LIFE ASSESSMENT AND BOLT REPLACEMENT STRATEGY

J.H.BULLOCH , MATERIALS SPECIALIST
ESB, POWER GENERATION
DUBLIN, IRELAND

ABSTRACT

The present paper describes a detailed study concerning the life assessment and replacement strategy of large turbine casing bolts in a 120 MW steam raising unit. After 122000 hours service, circa 1991/92, the Cr-Mo-V steel casing bolts, involving a total of 184 bolts, from two identical 120 MW units, termed Units 1 and 2, were examined to establish the extent of Reverse Temper Embrittlement, RTE, and creep damage suffered during service.

The bolt replacement plans for the two units were as follows; Unit 1 bolts were completely replaced with new bolts while Unit 2 embrittled bolts were withdrawn from service and replaced with Non- Embrittled bolts from Unit 1; basically Unit 2 bolts were made up from a mixture of Unit 1 and 2 Non- Embrittled bolts which had been in service for 122000 hours.

Remnant life assessments, concerning both embrittlement and creep damage aspects, were carried out on this series of casing bolts at service times 122000, 150000 and 200000 hours. These assessments involved the use of general embrittlement and creep damage laws which were empirically derived and concerned such parameters as microstructural grain size, bulk phosphorus content and accumulated service strain.

INTRODUCTION

A wide variety of critical engineering parts under stress function in steam raising plants and can undergo both mechanical and material property changes during real service conditions. Indeed one specific sizeable plant component which can experience such changes, which can cause failures to occur, is the steam turbine. The remnant life assessment of steam turbine components with over 100000 hours

service at numerous operating temperatures is of vital importance with respect to both plant reliability and availability(1-3).

The present paper describes the various life assessments and replacement strategy of a series of large turbine casing bolts over a period of 200000 hours. These remnant life assessments have been conducted using a general embrittlement law and a creep damage law which have been empirically derived for low alloy steels. The derivation of these laws is also discussed at length.

HISTORICAL DETAILS

In 1991/92 routine turbine inspections were conducted on two sister 120MW Units, termed Units 1 and 2. Each Unit consisted of a total of 92 IP and HP casing bolts, fabricated from a 0.2-0.25%C,1.3%Cr,0.8%Mo,0.3%V low alloy steel, which had been in service for 122000 hours at 490⁰ C. The length ranges of the IP and HP casing bolts were 0.4 to 0.8m and 0.5 to 1.4m respectively.

During these inspections a series of studies were carried out in an effort to identify the actual extent of creep damage and embrittlement, caused by RTE, suffered by these casing bolts during service. A detailed account of these studies are given in References 4 and 5. Basically it was found that no creep cracks were observed in the threaded regions of the casing bolts and that only minor damage ,in the form of isolated cavities, was evident at the first load bearing thread root location.

The service embrittlement characteristics of the casing bolts indicated the existence of two discrete and separate regions, viz., an Embrittled region, at coarse grain sizes and high %P levels, and a Non-Embrittled region, which corresponded to an area of fine grain sizes and low %P levels. From these grain size- %P trends it was clear that the divide between these two regions could be simply described by the following expressions;

$$d . (\%P) = 0.28 \quad (\text{UNIT 1}) \quad (1)$$

$$d . (\%P) = 0.18 \quad (\text{UNIT 2}) \quad (2)$$

where d was expresses in μm and the %P in wt.%.

In terms of actual numbers it was established that only around 9% of the casing bolts from Unit 1 were embrittled while about 30% of the casing bolts from Unit 2 suffered similar toughness losses caused by the occurrence of RTE during service. As a result of these studies that the casing bolt replacement strategy for the two Units would be as follows; (a) to replace all Unit 1 casing bolts with new ones and (b) to re-introduce the Non-Embrittled Unit 2 casing bolts back into Unit 2 and replace the Unit 2 embrittled casing bolts with Non-Embrittled casing bolts from Unit 1.

In terms of creep damage it was established that the casing bolts which had exhibited creep damage, ie, isolated cavities at the thread root of the first load bearing thread, were also embrittled, and as such, no creep damaged casing bolts were found in the revised series of casing bolts of Unit 2. Grain size, bulk

phosphorus content and accumulated service strain details of this revised series of Unit 2 IP and HP casing bolts are given in Tables 1 and 2 respectively. Note that when these casing bolts were re-introduced back into service in 1992 they already had been subjected to 122000 hours of service at operational temperatures of 490⁰ C.

In 1997 after a further service of some 30000 hours, total service of 150000 hours, the Unit 2 turbine casing bolts were re-inspected in an effort to ascertain (a) the existence of any creep damage at the bolt threaded locations and (b) the amount of accumulated service strain, %ε. It was observed that no creep damage, in the form of cracks, were found in the bolt threads and the results of the individual casing bolt length measurements are listed in Table 3.

DERIVATION OF THE GENERAL EMBRITTEMENT LAW

A detailed account describing the experimental data and the generation of the General Embrittlement Law for low alloy steels will be published at a later date(7). Essentially a variety of turbine casing bolts, fabricated from Cr-Mo and Cr-Mo-V low alloy steels, were removed from service after service times which ranged from 60000 to over 200000 hours. It was shown in each case that the dividing line between Embrittled and Non-Embrittled casing bolts could be consistently described by the following expression;

$$d \cdot (\%P) = C \quad (3)$$

where d was the grain size expressed in μm, %P was the bulk phosphorus content of the steel in wt% and C was a scaling constant.

During these studies it was clear that the value of this constant C, which characterised the extent of embrittlement, ie low C much embrittlement, high C less embrittlement, was strongly related to the degree of accumulated service strain, %ε. The relationship between C and %ε for six different series of low alloy steel casing bolts together with an earlier linear trend indicated that the trends could be adequately described by the expression;

$$C = A (\%ε)^{-B} \quad (4)$$

where A and B are scaling coefficients.

As a result of the commonality exhibited between equations (3) and (4) it was clear that an expression, which related grain sized, bulk phosphorus content, %P, and accumulated service strain, %ε, could be derived which best described the threshold condition, or dividing line between Embrittled and the Non-Embrittled condition, for embrittlement in low alloy steels in high temperature service; viz,

$$d \cdot (\%P) \cdot (\%ε)^B = F \quad (5)$$

where F and B were constants with values of 0.0772 and 0.64 respectively. This expression represents the General Embrittlement Law which was applicable to

low alloy steel components operating at elevated temperatures. Essentially when the product of the parameters of the LHS are greater than F embrittlement occurred; when less zero embrittlement was envisaged. In terms of remnant life the ratio of the LHS to F was taken as a measure of the amount of embrittlement life used up during service.

DERIVATION OF THE CREEP DAMAGE LAW

The results of a detailed creep damage assessment carried out on a selection of embrittled casing bolts taken from Units 1 and 2 in the 1991/92 studies and it was clear that the microstructural grain size exerted a large influence on the existence of creep damage, which was typically isolated cavitation, inasmuch that at average grain sizes of 20 to 30 μm cavitation was only present at accumulated stains of 0.4% or greater while at 60 to 70 μm creep damage was evident at 0.2% strain. The dividing line which separated the creep damage and the zero creep damage regions could best be expressed as;

$$(80 - d)(\% \varepsilon)^{-1} = G \quad (6)$$

where d is expressed in μm , $\% \varepsilon$ in terms of the total bolt length and G is a scaling constant of numerical value 154. Although this creep damage law was established after a time of 122000 hours service at 490⁰ C it should also apply at longer service times since the isoductility time-temperature C-curve results reported by Etienne et al (6) for a CrMoV steel suggested that the creep ductility was approaching a minimum after over 100000 hours at 490⁰ C. Hence this particular creep damage law can be regarded as somewhat conservative in nature.

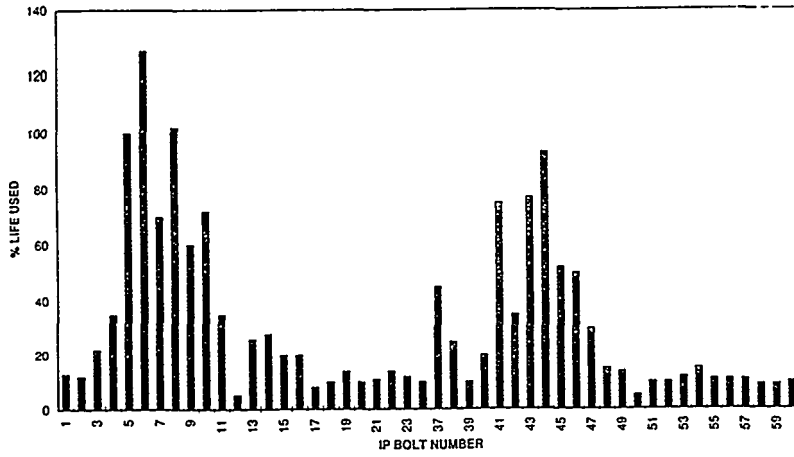
Basically the equation represents the Creep Damage Law which indicated that when the product of the LHS was greater than the value of G then creep damage was observed, when less no such damage was expected. A % probability of creep damage, based on the simple ratio of the LHS to G, was taken as a measure of the creep damage life used up during service. Although it could be said that this creep damage criteria was somewhat conservative in nature because no macro- defects were present, since the time required for cavitation to progress to macrocrack type damage was less than the time between outages, the adoption of this criteria was thought prudent.

EMBRITTLMENT AND CREEP DAMAGE ASSESSMENTS

THE 122000 HOURS ASSESSMENTS

Using these two laws, which were really threshold conditions that were pertinent to embrittlement and creep damage, the life assessments conducted on the Unit 2 IP casing bolts after 122000 hours service are illustrated in figure 1. The % embrittlement life used indicated that the vast majority of the casing bolts exhibited high remnant life levels of around 80%. However, the casing bolts which were located around the "hotter" inlet zones exhibited higher used life

Embrittlement



Creep

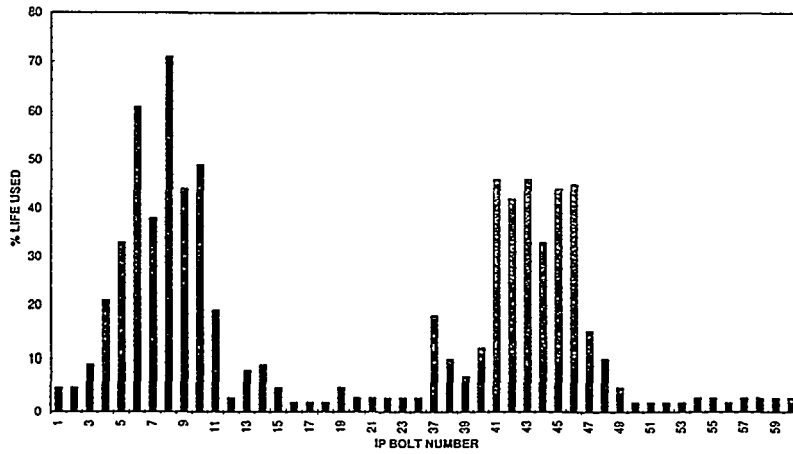
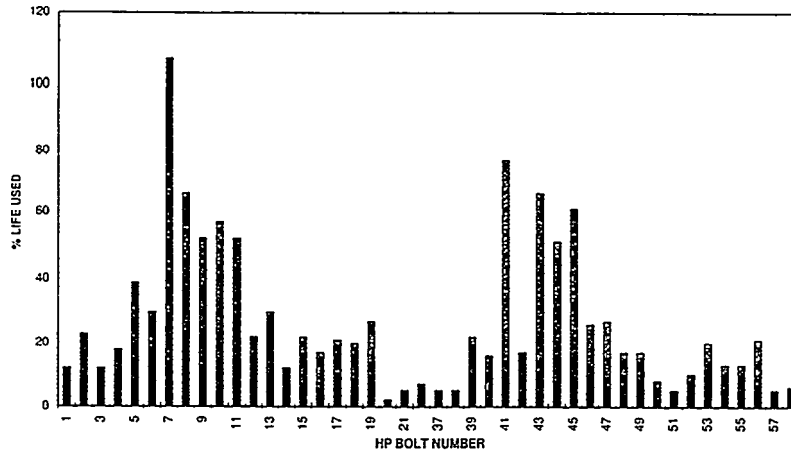


Figure 1. Life assessments of IP bolts after 122,000 hours service.

Embrittlement



Creep

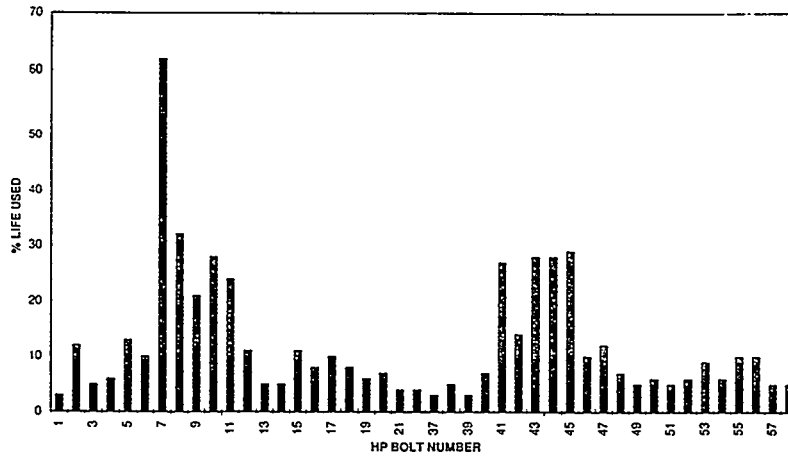


Figure 2. Life assessments of HP bolts after 122,000 hours service.

values which varied from 50 to 100%. Ideally, casing bolts IP5, 6 and 8, and probably IP44, should have been withdrawn from service during the 1991/92 outages since they were effectively already embrittled, ie the % embrittlement life used approached 100%. However, since (a) in a few instances embrittlement occurred in the identical IP casing bolt in both Units, (b) three different IP bolt lengths existed and (c) the general embrittlement law was not known at the time of these outages, the replacement strategy was compromised and a few embrittled casing bolts had to be used to make up numbers in the revised series of Unit 2 bolts.

The creep damage life details of the IP casing bolts after 122000 hours service, see figure 1, demonstrated that the majority had remnant creep damage lives of about 90%. The IP bolts surrounding the inlet zone exhibited higher used life levels which varied widely between 20 to 70% and indicated that no creep defects were present. This fact helped ameliorate the integrity question posed by the inclusion of a few embrittled casing bolts in the revised Unit 2 series of bolts.

The embrittlement and creep damage life assessments conducted on the HP casing bolts are portrayed in figure 2. Only one embrittled bolt was identified, viz., HP7, while the vast majority of the HP casing bolts exhibited very high embrittlement and creep damage life values of about 80 and 90% respectively. Again the highest levels of life used were around the 'hotter' inlet zone regions.

THE 150000 HOURS ASSESSMENTS

Through using the bolt length measurements of the Unit 2 turbine IP bolts recorded during the 1997 outage the various life assessments after 150000 hours service were calculated and both the embrittlement life used and the creep damage life used are given in figures 3 and 4 respectively. Figure 3 indicated that six IP casing bolts exhibited zero life left in terms of embrittlement, viz, IP5,6,7,8,43 and 44. Effectively three of these casing bolts had become embrittled during the some 30000 hours service since 1992 because the others were already in the embrittled condition in 1992.

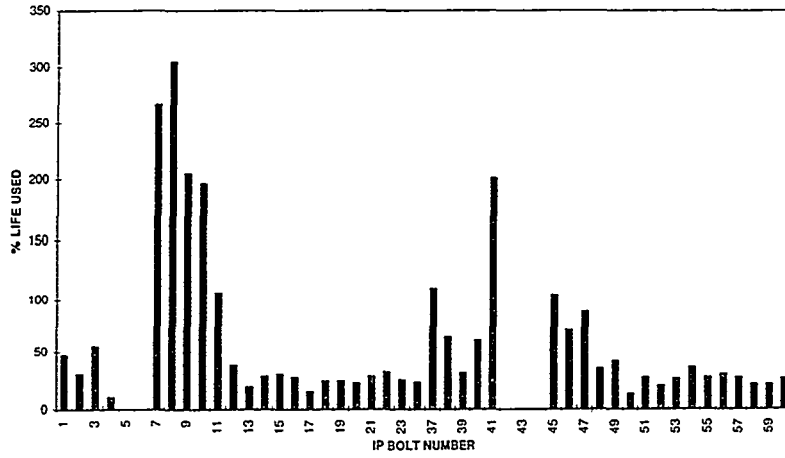
In terms of the creep damage life assessment it was evident that these particular embrittled IP casing bolts had remnant life values which ranged from zero to 60% while the others exhibited very high levels of remnant life values of about 90%. From these details a decision was made to withdraw these six casing bolts from service and replace them with new casing bolts.

The life assessments involving the HP casing bolts, see figure 4, indicated that the majority had remnant embrittlement life values of between 70 to 90%. Only two HP casing bolts, viz, HP7 and 41, were deemed to have been approaching, or reached, the embrittled condition and it was decided to replace them with new casing bolts.

It was clear that (a) the majority of the HP casing bolts exhibited high remnant creep life levels of approaching 90% and (b) the embrittled HP casing bolts had intermediate remnant creep life values with ranged from 40 to 60%.

Considering all the Unit 2 IP and HP casing bolts, which numbered 92, it was decided to withdraw only around 9% of the bolts from service and replace them with new ones; this represented a significant cost saving exercise.

Embrittlement



Creep

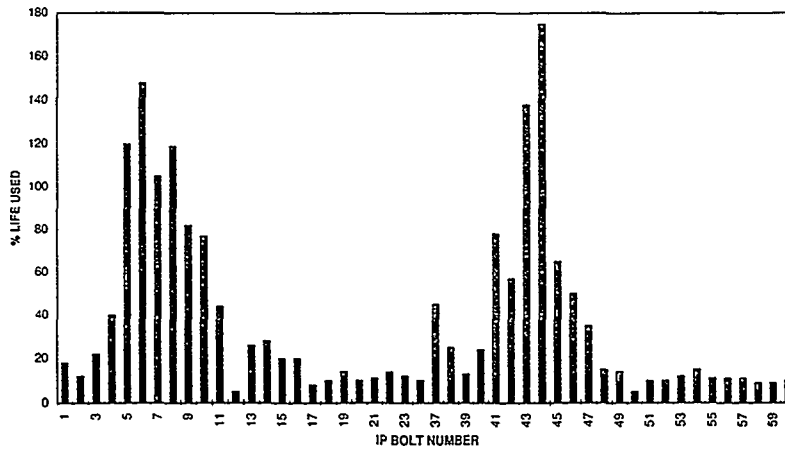
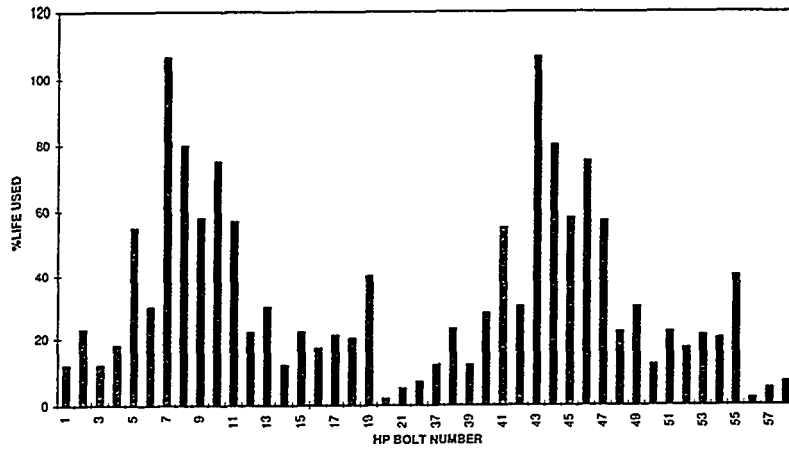


Figure 3. Life assessments of IP bolts after 150,000 hours service.

Embrittlement



Creep

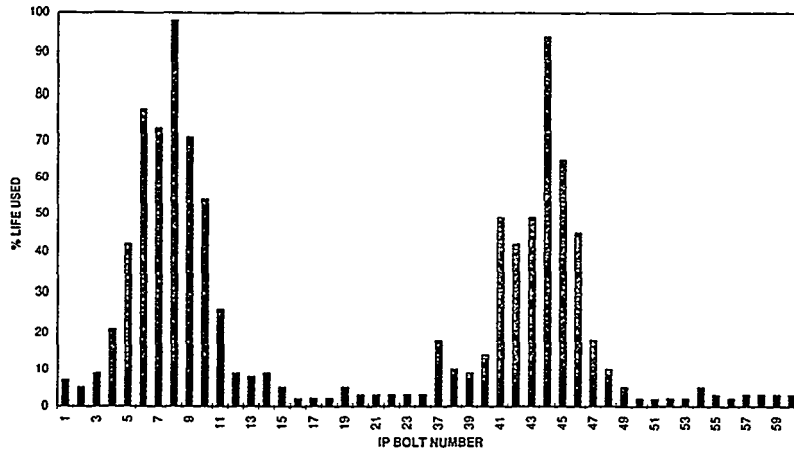


Figure 4. Life assessments of HP bolts after 150,000 hours service.

THE PROJECTED 200000 HOURS LIFE ASSESSMENTS

The next inspection outage planned for Unit 2 turbine casing bolts was 2005 which would extend their service lives to about 200000 hours. The accumulated strain values used in the 200000 hours life assessments were the extrapolated values taken from a general accumulated service strain, $\% \epsilon$, versus service time plot. In the majority of cases the most pessimistic (highest) value of strain was used in the projected life assessments and it was noted that the wide variations in accumulated strains in individual bolts was indicative of variations in the bolt tightening procedures and care should be exercised during future tightenings.

The various life assessments of the IP casing bolts are shown in figures 5 and 6. In terms of service induced embrittlement, ie RTE effects, it was evident that only two IP casing bolts were embrittled, viz., IP9 and 41, while the remaining bolts exhibited high remnant life levels of between 70 to 90%.

Regarding creep damage it was clear that only two bolts exhibited around zero remnant creep damage life figures, viz, IP9 and 45, while the rest indicated a very low probability of creep damage. Note that casing bolt IP9 was deemed to have suffered both embrittlement and creep damage and it could be expected that this bolt could fail during service.

From the resulting remnant life assessments it was judged that, even after 200000 hours service, only three IP casing bolts needed to be withdrawn from service and replaced by new casing bolts.

In the case of the HP casing bolts, see figures 6, it was evident that four HP casing bolts, viz HP8,10,43 and 45, were considered to be embrittled while one casing bolt, HP10, was deemed to have approached the end of its creep damage life. Thus a total of four HP casing bolts needed replacing.

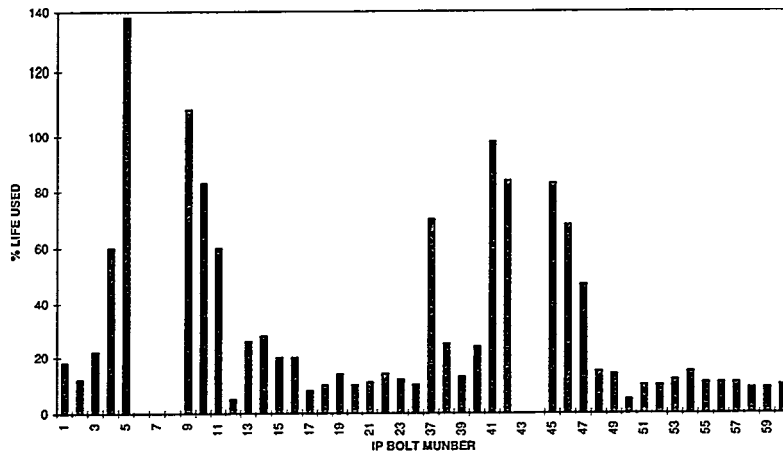
Considering both the IP and HP casing bolts it was projected that only about 8% of the Unit 2 casing bolts were required to be withdrawn from service and replaced with new bolts. Interestingly, this figure was similar to that of the 150000 hours service replacement strategy which again represented a significant cost saving exercise.

CLOSING REMARKS

It has been demonstrated that the use of empirically derived general embrittlement and creep damage laws can make the remnant life assessment and extension turbine casing bolts a relatively simple exercise. Indeed all that is required is a knowledge of the important material properties, such as microstructural grain size, d , and bulk phosphorus content, $\%P$ and the accumulated service strain, $\% \epsilon$. After these properties have been established only periodic bolt length measurements, taken during outages, are required to monitor remnant life details.

Remnant life assessments, in terms of service embrittlement and creep damage, have been conducted on a series of CrMoV steel turbine casing bolts after 122000,150000 and 200000 hours service. It has been demonstrated that the 150000 and 200000 hours assessments indicated that only a small proportion of the casing bolts, typically between 8 to 9%, needed to be withdrawn from service and replaced with new casing bolts. These represented significant cost saving exercises. Indeed after 200000 hours service it was evident that a massive 83% of

Embrittlement



Creep

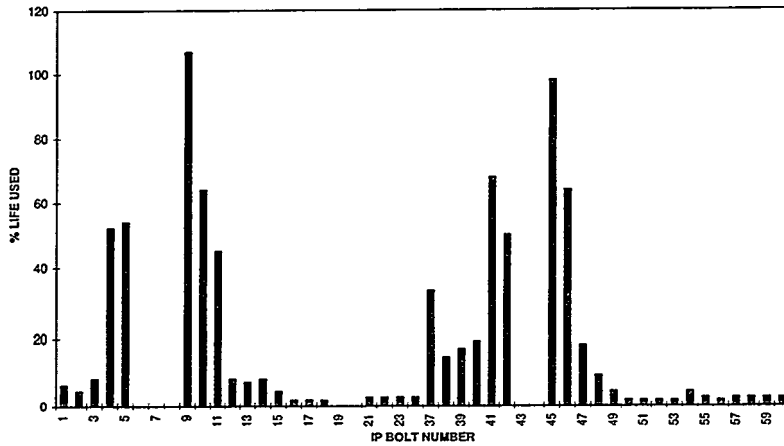
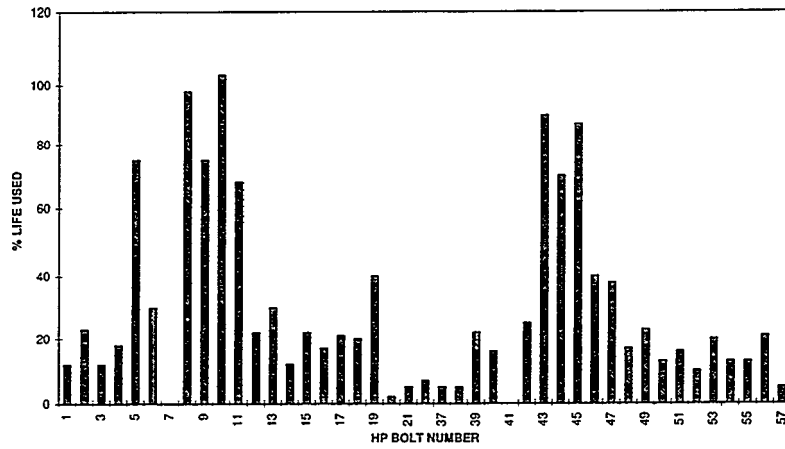


Figure 5. Projected life assessments of IP bolts after 200,000 hours service.

Embrittlement



Creep

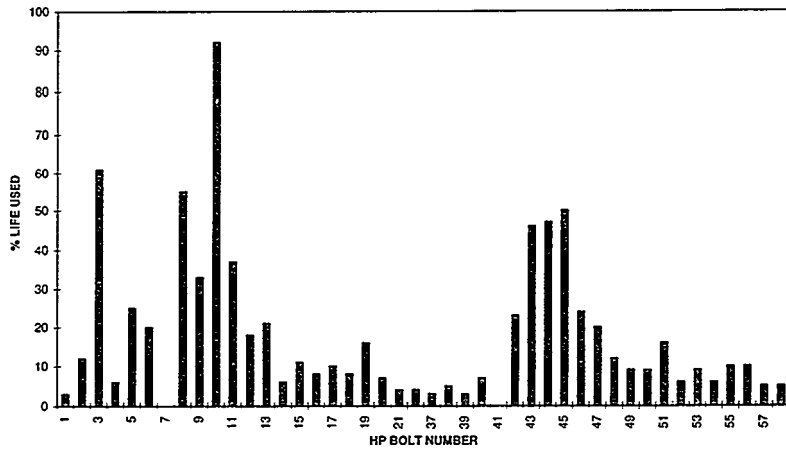


Figure 6. Projected life assessments of HP bolts after 200,000 hours service.

the original casing bolts would still be fit to be safely re-introduced back into service.

The threatened casing bolts were all located around the "hotter" inlet zones of the IP and HP compartments of the rotor. Effectively, a continuous loss of life situation was prevalent only in these casing bolts since the majority of the other casing bolts resided within the cooler locations such that no significant progressive build-up of accumulated strains were possible.

REFERENCES

1. R.D. TOWNSEND, In Procs. First Inter. Conf. "Microstructure & Mechanical Properties of Ageing Materials" (Eds. Liaw, Viswanathan, Murty, Simonen and Frear) TMS Warrendale, PA, 1992, p 1.
2. J. BOLTEN, in Procs. Inter. Conf. "Life Extension of Thermal Power Plants" Vol 2, 1994, Paper L17.
3. K.H. MAYER, C. BESIGK & H. NEFT, *ibid.* Paper L13.
4. J.H. BULLOCH & J.J. HICKEY, Procs. First Inter Conf. "Microstructure & Mechanical Properties of Ageing Materials" (Eds. Liaw, Viswanathan, Murty, Simonen & Frear) TMS, Warrendale, PA, 1993, p41.
5. J.H. BULLOCH & J.J. HICKEY, *Maters. at High Temps.*, 12, 1994, p 15-24.
6. C.F. ETIENNE, H.C. VAN HELST & P. MEIJERS, *Creep of Engineering Materials and Structures*, Eds. G. Bernasconi & G. Piatti, Allied Science Pub. London, 1979, pp 149-193.
7. J.H. BULLOCH, Unpublished ESB Results.

Table 1. IP bolt details from 122,000 hours service outage.

BOLT NUMBER	GRAIN SIZE(UM)	%P (WT%)	% STRAIN	BOLT NUMBER	GRAIN SIZE(UM)	%P (WT%)	% STRAIN
1	14.7	0.009	0.02	37	20.2	0.009	0.07
2	12.2	0.009	0.02	38	16.6	0.009	0.04
3	14.4	0.009	0.04	39	9.1	0.008	0.03
4	16	0.009	0.07	40	13.9	0.008	0.05
5	43.7	0.009	0.08	41	16.9	0.01	0.19
6	39.4	0.008	0.16	42	9.5	0.009	0.14
7	23.2	0.008	0.14	43	16.9	0.01	0.19
8	19.2	0.008	0.28	44	29.2	0.01	0.11
9	17	0.008	0.18	45	14	0.008	0.19
10	20	0.008	0.19	46	14.7	0.008	0.17
11	14.7	0.009	0.08	47	18.3	0.008	0.06
12	9.8	0.009	0.01	48	9.2	0.009	0.04
13	20.2	0.009	0.03	49	14.9	0.008	0.02
14	14.4	0.011	0.04	50	5.3	0.014	0.01
15	14.1	0.012	0.02	51	12.2	0.012	0.01
16	14.1	0.011	0.01	52	9.5	0.012	0.01
17	8.5	0.01	0.01	53	9.8	0.015	0.01
18	9.3	0.015	0.01	54	13.6	0.015	0.01
19	9.3	0.015	0.02	55	12.6	0.012	0.01
20	8.4	0.015	0.01	56	10.7	0.016	0.01
21	9.9	0.016	0.01	57	9.7	0.016	0.01
22	12.1	0.015	0.01	58	9.9	0.012	0.01
23	9	0.016	0.01	59	8.6	0.014	0.01
24	10.3	0.012	0.01	60	9.7	0.015	0.01

Table 2. HP bolt details from 122,000 hours service outage.

BOLT NUMBER	GRAIN SIZE(UM)	%P WT%	% STRAIN	BOLT NUMBER	GRAIN SIZE(UM)	%P WT%	% STRAIN
1	17.6	0.01	0.01	37	19.6	0.008	0.01
2	15.3	0.008	0.05	38	12.4	0.008	0.02
3	21.5	0.009	0.01	39	31.7	0.01	0.01
4	15	0.009	0.02	40	11.2	0.01	0.03
5	30	0.009	0.04	41	27.9	0.01	0.09
6	18.1	0.01	0.04	42	9.3	0.009	0.06
7	20.4	0.01	0.24	43	20.8	0.01	0.11
8	22.2	0.009	0.12	44	10.2	0.015	0.12
9	19.5	0.01	0.08	45	21.5	0.009	0.11
10	20.5	0.009	0.11	46	15.4	0.01	0.04
11	17.6	0.01	0.1	47	16.6	0.009	0.05
12	11.7	0.01	0.05	48	14	0.009	0.03
13	21.5	0.01	0.03	49	16.4	0.01	0.02
14	16.9	0.01	0.02	50	11.8	0.01	0.01
15	12.5	0.009	0.05	51	10.5	0.008	0.01
16	13.6	0.009	0.03	52	12.8	0.008	0.02
17	13.9	0.009	0.04	53	8.1	0.019	0.03
18	15.5	0.009	0.03	54	17.1	0.007	0.02
19	11.8	0.018	0.02	55	16.6	0.007	0.03
20	12.2	0.007	0.02	56	18.2	0.008	0.03
21	12	0.007	0.01	57	11.2	0.007	0.01
22	15.2	0.008	0.01	58	11.5	0.008	0.01

Table 3. Accumulated average bolt strains recorded after 150,000 hours service.

IP BOLT NUMBER	% STRAIN	IP BOLT NUMBER	% STRAIN	HP BOLT NUMBER	% STRAIN	HP BOLT NUMBER	% STRAIN
1	0.03	37	0.07	1	0.01	37	0.01
2	0.02	38	0.04	2	0.01	38	0.01
3	0.04	39	0.04	3	0.17	39	0.01
4	0.09	40	0.06	4	0.01	40	0.01
5	0.1	41	0.2	5	0.05	41	0.11
6	0.2	42	0.09	6	0.04	42	0.07
7	0.27	43	0.2	7	0.16	43	0.13
8	0.37	44	0.31	8	0.16	44	0.15
9	0.29	45	0.28	9	0.1	45	0.14
10	0.21	46	0.07	10	0.2	46	0.06
11	0.11	47	0.07	11	0.11	47	0.06
12	0.04	48	0.04	12	0.05	48	0.01
13	0.03	49	0.03	13	0.01	49	0.03
14	0.01	50	0.01	14	0.01	50	0.02
15	0.01	51	0.01	15	0.01	51	0.05
16	0.01	52	0.01	16	0.01	52	0.01
17	0.01	53	0.01	17	0.01	53	0.01
18	0.01	54	0.01	18	0.01	54	0.01
19	0.01	55	0.01	19	0.04	55	0.01
20	0.01	56	0.01	20	0.01	56	0.01
21	0.01	57	0.01	21	0.01	57	0.01
22	0.01	58	0.01	22	0.01	58	0.01
23	0.01	59	0.01				
24	0.01	60	0.01				

Super Long-Term Creep Tests of Advanced HP and IP Rotor Steels

Andrei A. Tchizhik, Prof., D.Sc.
The Polzunov Central Boiler and Turbine Institute (PCBTI),
Department the Fatigue Life of Materials for Power Plant Equipment
24, Politekhnicheskaya St., 194021, St - Petersburg, Russia

Abstract

A creep model has been developed for predicting the long-term creep behavior, in excess of 200,000 h for advanced materials. The new creep theory is based on a continuum microdamage model and is used to calculate the fields of stress and strain and wedge and cavities damage in critical components of steam and gas turbines. The application of this new model increases the reliability and service life of modern turbines. The accuracy of the model to predict long-term creep behavior, creep ductility was verified using the data bank of super long-term creep tests of advanced materials.

1 Introduction

To provide an efficient design of creep loaded components it is necessary to study the evolution of deformation and exhaustion of real materials under very long-time conditions. Not enough data exist for long-term creep resistance and creep fracture of rotor materials for the modern steam turbine. In Russia, the creep data bank includes more than 6 billion hours of investigation for the «Russia (R, R2M, R2MA)» grade steels from the HP and IP rotors of steam turbines with unit capacity from 200MW to 1200MW. This data bank was obtained during 34 years of uniaxial loading for the batch of 1CrMoV rotor R-grade steel and demonstrate: the influence of the degradation of properties and microdamage on the long-term creep resistance, creep fracture and long creep ductility data; legitimacy of the different new prediction methods of long-term creep and creep fracture data; necessity of the use of new creep theory with multi-structural damage parameters for the assessment of long-term predictions; and possibility of utilizing steel manufacturing programs for evaluating the remaining life of HP and IP steam turbine rotors.

2 Experiments

The bath of steel chosen for the present investigation was selected to represent the lower bound creep strength properties anticipated for the batch 1CrMoV

(R2MA) rotor grade steels . The sample of this steel used in this investigation was taken from a full scale virgin IP rotor (1050 mm body diameter) for a 200MW steam turbine , which was manufactured in 1964 from 70 Mg duplex (basic + acid) Martin process ingot .The chemical composition of the present steel melt (in wt %) was determined as C=0,29 , Si=0,32 , Mn=0,58 , S=0,010 , P=0,010 , Cr=1,79 , Ni=0,23 , Mo=0,97 , V=0,28 , Cu=0,10 , Al=0,008 and Sn <0,012. Following duplex normalizing at 980° and 960°C and tempering at 600°C , the room-temperature tensile properties were follows :

Yield strength , (Rp0,2)	504 - 553 MPa
Tensile strength , (Rm)	695 - 715 MPa
Elongation , (A 5)	19,6 - 20,6 %
Reduction in area , (Z)	66,0 - 69,8 %

Test pieces ,with gauge length of 100 ,150 and 200mm and diameter of 10mm , were tested in tension at 500° , 525° and 550°C using high-sensitivity constant -load tensile creep machines (calibration errors : loading < 0,5 % ; displacement < 5µm ; temperature < 1,5°C). Up to 50,000 creep strain readings were taken during each test . Normal creep curves were observed under all test conditions studied , as illustrated by the curves presented in Fig. 1 for 550°C test temperature , where : 1) data points represent the measured creep strain / time readings ; 2) solid lines represent the fit obtained by using the basic constitutive equations on this paper . The preliminary constant - load creep curves were analyzed using the New Projection Concept Micro-mechanical Modeling [1,2] to forecast long - term behavior . The predicted values of the creep limits and the minimum creep rates and proposed level of creep strain and times to fracture were then compared with measured long - term data obtained independently at 500° , 525° and 550°C for the batch of 1CrMoV rotor steel (R2MA).

3 Results

3 . 1 Super Long Term Creep Behaviour

The data obtained from the batch of 1CrMoV rotor steel (R2MA) demonstrates the following :

- the preliminary creep stage is very long and lasts 40,000 - 50,000 h at 500°C and 20,000 - 30,000 h at 550°C.All procedures for extrapolating the shape of creep curves with creep data less than 40,000 h have not worked. The very long time of preliminary creep stage is related to the dissipation of the initial density of dislocations and the long process formation stability substructure as well as the allocation of the dispersible carbide Mo₂C , with particle dimensions ranging from 1200 to 2500 nm. The carbide reactons in this rotor

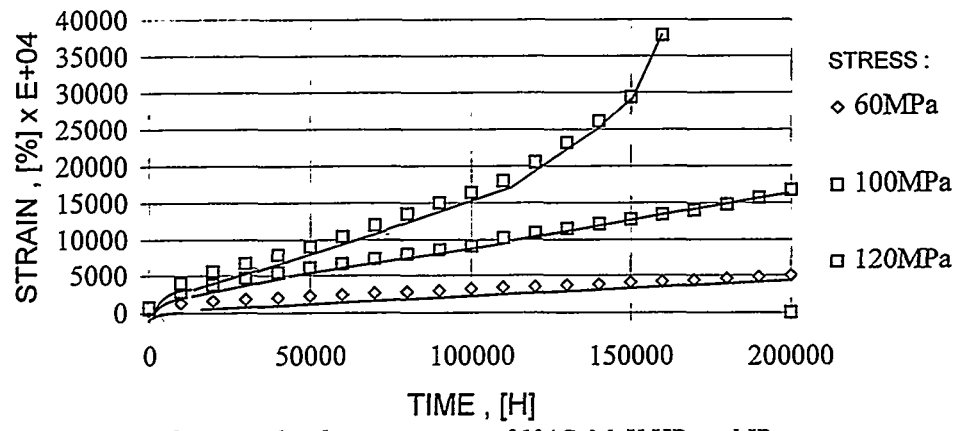


Fig. 1 Constant load creep curves of 1%CrMoV HP and IP rotor steel grade (R2MA) at 550 C.

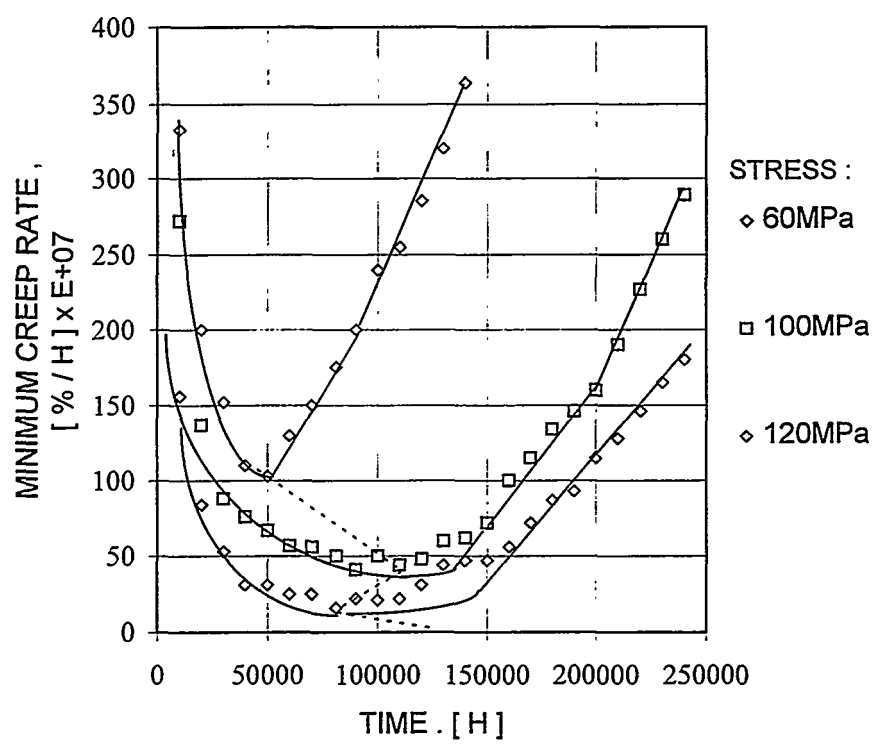


Fig. 2. Minimum creep rate curves of 1%CrMoV HP and IP rotor steel grade (R2MA) at 550 C.

steel batch depended on the tempering response. For low temperature tempering the preliminary creep stage is longer. The maximum scatter of creep strain between different rotor forging was found in the preliminary creep stage. This analysis is very essential for the operating control of rotor's central hole;

- the third creep stage is very long too and usually exceeds half the creep fracture time. Creep curves for this stage are not usually available. The third creep stage permit the use of simple mathematics creep fracture damage theories "without the effect of hardening". This creep stage demonstrates that extrapolating the creep fracture ductility for the 1CrMoV steel from secondary creep stage data is not valid and can predict very low values which are inappropriate for real creep fracture ductility levels ;
- the creep exponent 'm' (Norton parameter) increases at the preliminary creep stage. The calculation this parameter from creep data requires no less than 20,000 up to 30,000 h for 1CrMoV rotor steels. The Norton parameter varies linearly with the absolute temperature "1/T". This equation takes the form $m = A/T + B$ (where the "A" and "B" are constants and T is absolute temperature in Kelvin), and can be used for interpolating Norton parameter for practical applications [3] ;
- the diversity of creep strain values for different rotor forging is related to the scatter of creep strain on the preliminary creep stages. This factor is very important for operating creep control on conventional power stations ;
- the minimum creep rate time (MCRT) increases at inside area of the similar mechanism of long-term creep fracture. The change of creep microdamage mechanisms at transition from creep ductile rupture (cavities inside grains by all the volume) to brittle ruptures (wedge microcracks and cavities on the grain boundaries) decreases the sharply MCRT every change time Fig. 2.

The data obtained for 1CrMoV rotor steel demonstrate the need for calculation of a newly Projection Concept Micro - mechanical Modeling technique with minimum state constants. The θ Projection Concept [4] usually includes at least 20 state constants. Very large creep data bank must be available for correctly determining the constants. Some years ago the author with co-authors had suggested the newly Projection Concept Micro-mechanical Modeling (PCMM) for high-temperature steels and alloys [1,2,5]. This newly PCMM is based on a method of analysis similar to the continuum fracture damage mechanics adopted by L.Kachanov and Y.Rabotnov. In the proposed scheme the number of structural parameters is equal to the number of creep micro-mechanisms.

A detailed approach for the description of the material behavior can be made using a theory involving two scalar parameters. The value of the first parameter depends on the principal stresses (σ_1) and the second parameter on the intensity of shear stress, von Mises stress (σ_j).

3.2 Creep State Micro-mechanical Modeling

We will deal with certain thermodynamic features of deformation and fracture under creep conditions in a general form. In this case, we will conventionally distinguish between "ductile" fracture of grain body and "brittle" fracture through grain boundaries due to formation of discontinuity ensembles as wedge cracks at the boundary joints of grains or microcavities. For ductile fracture of the grain body, the thermodynamic system is generally considered as «closed». The thermodynamic system should be considered as «open» under conditions of microdefect generation through volume or boundaries of grains, and chemical potentials for a defect $\mu_{L,i}$ (*i*-type defects) and for a source μ should be introduced [6]. It is obvious that chemical potentials increase as a function of discontinuity density and also depend on creep rate and level of macro- and micro-stresses. Furthermore, let the weight of *i*-type microdefect be v_i , and a chemical variable for the system be λ . Then, the condition for mass conservation in the «open» system may be written as $\nabla^2(\mu - \mu_{L,i}) = 0$ [6]. Let « f » is designated as the density of free energy [7], « q » as the density of heat received by element from environment, « s » as the entropy density, « k » being the module of volume compression, « θ » the volume expansion, « Γ » the intensity of shear deformation and « T » as temperature, the following relations will be obtained for the free energy density:

for «closed» system (CS)

$$df = k\theta d\theta + H(\Gamma)d\Gamma - Tds - sdT + dq;$$

for «open» system (OS)

$$df = k\theta d\theta + H(\Gamma)d\Gamma - Tds - sdT + dq - \sum v_i \mu_i d\lambda, \text{ where } (i=[1,L])$$

Thus, confirming that the discontinuity in the «OS» leads to a decrease in the « f » of fracture. Using traditional forms of relations between stresses and deformations $\varepsilon_{ij} = \varepsilon_{ij}^e + \varepsilon_{ij}^c$ (*e* - elastic, *c* - creep component) and introducing the inner parameter for the system $d\lambda = p_{ij} d\varepsilon_{ij}^c$ [8], we can easily obtain the inequality for irreversible system state transformations:

$$\begin{aligned} & (\sigma_{ij} - \partial f / \partial \varepsilon_{ij}^e) d\varepsilon_{ij} + (\sigma_{ij} - \partial f / \partial \lambda \cdot p) d\varepsilon_{ij}^c - (s + \partial f / \partial T) dT > \\ & > (\sum v_i \mu_i + \partial f / \partial \lambda) d\lambda, \text{ where } (i=[1,L]; ij=1,2,3) \end{aligned} \quad (1)$$

and for reversible transformations of system state ($d\varepsilon_{ij}^c = d\lambda = 0$):

$$\begin{aligned}
& (\sigma_{ij} - \partial f / \partial \varepsilon_{ij}^e) d\varepsilon_{ij}^e - (s + \partial f / \partial T) dT = 0 \Rightarrow \\
& \Rightarrow \sigma_{ij} = \partial f / \partial \varepsilon_{ij}^e \text{ and } s = -\partial f / \partial T \quad (2)
\end{aligned}$$

This thermodynamic relation in a damageable media takes the form :

$$(\sigma_{ij} - \partial f / \partial \lambda \cdot p) d\varepsilon_{ij}^c \geq (\sum v_i \mu_i + \partial f / \partial \lambda) d\lambda \quad , \text{ where } (i=[1,L]) \quad (3)$$

Hence it follows that under conditions of developed creep damage, it is necessary to consider the history of loading. The equations determining the state must include «structural parameters of damages». Accordingly, we will assume the density change as a measure of material loss due to creep [7]. Accepting « p_0 » as being the density of undamaged material, « p » for material with creep damage and $\varepsilon_v = (p_0 - p)/p$ as loosening for isothermic deformation under condition of incompressibility, we shall obtain the following relation, characterizing the system equilibrium ($df = 0$):

$$\sigma v_0 d\varepsilon_v = 3 \sum v_i \mu_i d\lambda \quad , \text{ where } (i=[1, L]) \quad (4)$$

A number of conclusions of major concern follows from this relation. Firstly, the ‘loosening’ measured by density is an integral index and does not depend on the nature of microdamages. Secondly, this relation demonstrates the necessity for supplementing the basic equations determining the state by additional equations; the number of which must be consistent with one of the mechanisms of microdamages. Thirdly, the inner parameters of OS must be increased according to the chemical variables of the system. Finally, this relation follows a linear principle for summing up damage relative to chemical potentials for microdefects. All creep damages can be divided into three general groups: pores distributed uniformly through the volume of the deformed body, wedge cracks in joints of three grains and cavities through a volume is determined by the value of accumulated deformation and a damage parameter $\omega = \ln(1 + \varepsilon_v) / \ln(1 + \varepsilon_{*v})$, and the fact that the chemical potentials have a power dependency on damage, we can easily get that:

$$\omega = k \sum v_i \omega_i^{n_i} + (1 - k) \sum (\varepsilon_i / \varepsilon_{i*})^{p_i} \quad , \text{ where } (i=[1,L]) \quad (5)$$

and therefore, at the moment of fracture it will be true that the principle of damage summation, representing the generalization of an earlier principle, where $\omega = 1$ is applicable. Based on the above stated equations with ω as the parameter in the Kachanov - Rabotnov formulation, we can utilize the simplest Kachanov-Rabotnov model with $k = v_i = n_i = 1$, $v_{i-1} = 0$; Lepin model

with $p=i=1$ and $k=0$ [9]; Schesterikov model with $k=v_1=1, v_{i-1}=0, n_1=\text{const}$ [10]; the Tchizhik-Petrenja model with $k=v_1=v_2=n_1=n_2=1, v_{i-2}=0$ [5]; or the Tchizhik model at $n_1 = p \Rightarrow \infty$, using the concept of independence of fracture creep damages (ω Projection Concept [11], etc.).

3.3 Basic Constitutive Equations of New Project Concept

Micro-mechanical Modeling are :

for rate of creep $\xi = d\varepsilon/dt$:

$$\xi = B(t)\sigma^m \exp\left\langle \frac{-H}{RT} \right\rangle, \text{ where } B(t) = a(1-\omega)^{-q} \text{ and } \omega = \omega(t/t_{*1}, t/t_{*2}) \quad (6)$$

for rate of wedge microdamage $\zeta = d\omega_1/dt$:

for $\sigma_1 > 0$

$$\zeta = C(t)\sigma^{n_1} \exp\left\langle \frac{-U}{RT} \right\rangle, \text{ where } C(t) = b(1-\omega_1)^{-r} \text{ and } \omega_1 = \omega_1(t/t_{*1}) \quad (7)$$

for $\sigma_1 \leq 0 \Rightarrow \zeta = 0$

for rate of cavities microdamage $\upsilon = d\omega_2/dt$:

$$\upsilon = D(t)\sigma^k \exp\left\langle \frac{-Q}{RT} \right\rangle, \text{ where } D(t) = c(1-\omega_2)^{-h} \text{ and } \omega_2 = \omega_2(t/t_{*2}) \quad (8)$$

For uniaxial tensile creep ductility from (5 - 7) we obtain for intergranular fracture with formation of wedge cracks :

$$\varepsilon^* = \frac{a}{b(r-q+1)} \sigma^{m-n} \exp\left\langle \frac{U-H}{RT} \right\rangle, \quad (9)$$

where from (6,7) $a, b, r, q = \text{const}$; m -the Norton parameter; n -the brittle creep fracture exponent for areas with formation of wedge cracks; H -the activation energy of creep; U -the activation energy of the brittle creep fracture for areas with formation of wedge cracks; R -universal gas constant; T -temperature, K.

For uniaxial tensile creep ductility from (5,6,8) we obtain for integranular fracture for areas of cavity formation :

$$\varepsilon^* = \frac{a}{c(h-q+1)} \sigma^{m-k} \exp\left\langle \frac{Q-H}{RT} \right\rangle \quad (10)$$

where from (6,8) $a, c, h, q = \text{const}$; k -the exponent of brittle creep fracture for areas of cavity formation ; Q -the activation energy of fracture be formation mechanisms of cavities .

For intergranular fracture with wedge crack formation, 'm' is always greater than 'n' and $U > H$. Hence long-term creep ductility ($CD = \varepsilon^*$) decreases with time and with increasing temperature . For area of formation of cavities, the following cases can take place : for $m = k$ and $Q = H$, in this case CD is independent of time and temperature , for $m > k$ and $Q > H$, in this case CD decreases with time and with rising temperature ; $m < k$ and $Q < H$ in this case CD increases with time .

The relations from (5-10) demonstrate the necessity for having maps of creep deformation and creep fracture mechanisms .Long time creep tests and fractographical analysis of fracture facilitates drawing up maps in relative coordinates up to values of yield strength ($R_{p0,2}$). Thus intergranular fracture for the 1CrMoV rotor steel grade (R2MA) takes place at 550°C and at $\sigma / R_{p0,2} = 0,28-0,30$; and for 525°C it takes place at $\sigma / R_{p0,2} = 0,30 - 0,32$. The data indicates that the time for bending time point in creep fracture curve is the earlier than the higher the yield strength . Hence it also follows that the dependency of creep fracture strength on $R_{p0,2}$ must be maximum for HP and IP steam turbine steel rotors .

3. 4 Creep Fracture of Steam Turbine Rotors

Six HP and IP rotors were investigated in their virgin state ,four of which were for metal from the axial core . To date , six rotors have been investigated with service lives from 55,000 up to 197,000 hours .

The Newly Projection Concept Micro-mechanical Modeling technique stated above was used for analysis of the data . Relations (set-3.3) and maps were used as governing state equations .Norton exponent 'm' ,creep fracture exponent 'n' and other constants were estimated based on interpolation of direct data of long-term creep tests . The m , n and k parameters outside the point of bending were estimated by data from long-term creep tests and creep fracture tests . Figures 3 and 4 show the relationship between creep fracture strength based on direct tests with duration of loading ranging from 56,000 to up 200,000 h at temperature 550°C . On the basis of the presently available data, optimum creep fracture strength can be obtained as yield strength ($R_{p0,2}$) of 580-620MPa .This relation of creep fracture strength with $R_{p0,2}$ is entirely estimated using structural factors .

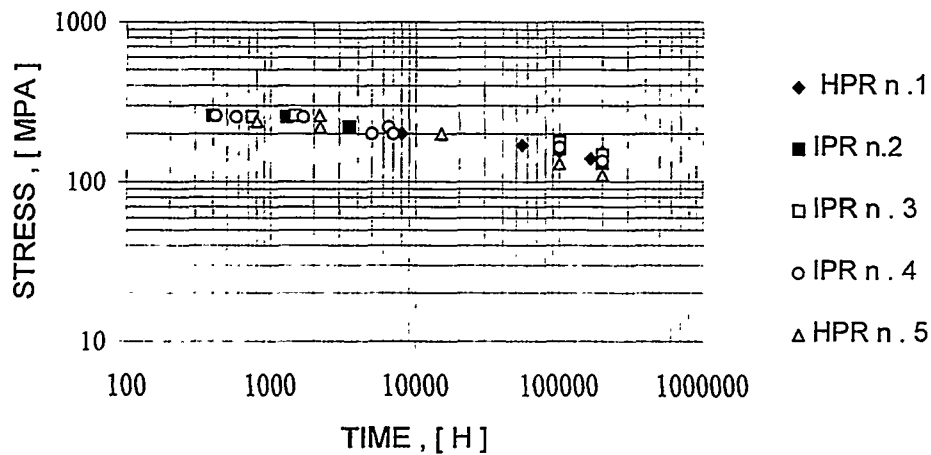


Fig. 3. Creep rupture of 1%CrMoV rotor steel (R2MA) at 550 C from full size HP and IP rotors manufactured in 1963 - 1975.

Note : HPR n.1 - YS 500MPa (near surface body-tang) ;
 IPR n. 2 and n. 3 - YS 500MPa (axial cores) ;
 IPR n. 4 - YS 600 MPa (near surface body-tang) ;
 HPR n.5 - YS 700 MPa (near surface body-tang) .

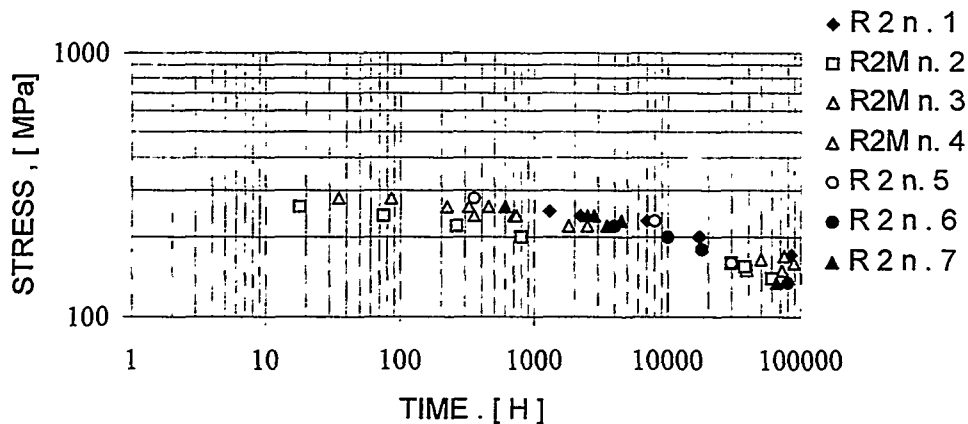


Fig. 4. Creep rupture of 1%CrMoV rotor steels (R2, R2MA) at 550 C from HP and IP rotors after long-term operation times (55,000 - 166,000 h).

Note : n.1-ST 80MW after 80,000h at 565C; nn. 2 and 3 -ST 200MW after 55,000h at 540-565C; n.4 - ST 200MW after 114,000h at 540-565C; nnn. 5, 6 and 7 - after 166,000h at 540-565C.

Samples from the first steam turbine rotors (SVK - 150) is structurally different from the samples prepared from the axial core of modern HP and IP rotors, which is subjected to double normalization. This difference in structure consists mainly of upper bainite and ferrite-carbide mix, formed in a temperature interval for pearlite transformation. Similar structures are characterized by lower level of high temperature strength and lie on the lower boundary of scatter for creep fracture strength of R2 and R2MA steel grades. Similar structures have creep fracture strength 10–12% lower than upper bainite structures as suggested by the available data. As a rule, the presence of similar structures leads to lower values of short term strength properties and consequently lower stability during operation. Values ranging from yield strength of 500 to 600MPa is typical of bainite structures, meeting the maximum values of high temperature strength. Unfortunately, tests for rotors with yield strength above 600 MPa were carried out for martensite structures having also lower characteristics of creep fracture. In this connection one may suppose that optimal level of short-term properties which can provide maximum high temperature strength may correspond to a yield strength of 600–800 MPa. This conclusion certainly requires experimental validation. For the range of yield strength of 440–620MPa, the curve is properly determined by power law dependency and it is used for checking calculations of creep fracture for conventional power stations.

The scatter of the yield strength for LMZ HP and IP rotors lay in the range of 500–620 MPa. The increasing branch of the curve of creep fracture dependency on yield strength was used in forecasting steam turbine resources with application to methods for individual forecast of the second generation. Analysis data for creep fracture strength on the base of 200,000 hour tests are: 180–225MPa at 550°C; 175–185MPa at 525°C; 112–143MPa at 550°C (The lower levels are design levels [12]). Using third generation forecast methods it should be possible to distinguish between creep fracture strength of near-surface body and near-central parts. On the basis of 200,000 h creep tests, the following values of creep fracture strength may be accepted for the central zones: 175–225MPa at 500°C; 170–185MPa at 525°C; 105–115MPa at 550°C.

3.5 Creep Resistance

Reliability of the creep tests which were carried out is confirmed by measuring creep deformation for sufficient number of HP and IP rotors of 200MW LMZ steam turbine. Results of creep tests are summarized on [5,12]. The influence of original mechanical properties on creep characteristics is different. At relatively low deformations (up to 0,5–0,7%

limit creep strength) shows linear dependency on the yield strength . With creep strains over 1% , the influence of the yield strength is slight .

Creep curves for the present batch of «R2MA» steel in different zones of rotor forging in virgin state and after operation show that the creep resistance is higher for samples taken from peripheral zones of forging , where martensite–bainite structure is formed . For central zones , where ferrite is present , creep strains are always higher . Operation increases the creep rate at the second stage in some cases and in a series of cases it leads to an earlier transition into the third stage of the creep process . However , total level of deformation under operating stresses and service life of 200,000–220,000 h is estimated by the first stage of the creep process , i.e. mostly by the structure resulting from the initial thermal treatment .

4 Conclusion

High–precision constant–load creep curves obtained for 1CrMoV rotor steel grade «R2MA» over a range of stress at 500° , 525° and 550°C were analyzed using the New Projection Concept Micro–mechanical Modeling technique .This Concept includes three state equations with two scalar structure parameter of microdamage (ω_1 and ω_2), nonlinear principle of creep damage summation , maps of creep fracture and have near 12 independent constants for calculation of the creep rates . It is also applicable to brittle and ductile fracture and long–term creep ductility . The design creep and creep fracture properties determined from ω data obtained in tests with a maximum duration of 200,000 h accurately predicted the behavior HP and IP rotors of 50–800MW steam turbines operating at stresses giving creep lives of over 220,000–270,000 h at the service operating temperature .

Acknowledgment

The author wishes to express his gratitude to Prof.S.A.Mequid and Mr.Perti Auerkari for editing this paper and LMZ–The Turbine–Building Production Association «Leningradsky Metallichesky Zavod» .The author gratefully acknowledges the Prof.L.M.Kachanov for scienceful support the two scalar damage theory of creep fracture and for develops the new methods of modeling the creep and creep fracture based on his knowledge during a period of more than quarter of a century . The author also grateful to Prof. D. Francois , Prof. B. Wilshire and Prof. R. Evans for beneficial discussion of the long–term creep problems and Ing. L. Werkina for helping to obtain the long–term creep data .

References

- [1] Tchizhik, A . A . , Petrenja , J . K . : ‘Fracture due to creep and micro-fracture mechanisms’ J.Dokl.Akad.Nauk SSSR, **297**, n . 6 , 1987 , p. 1331 .
- [2] Tchizhik, A . A . , Petrenja , J . K . , Rantala , J . H . : ‘Creep damage in materials with homogeneous and heterogeneous structures’, Proc.Fifth Inter. Conf. on ‘Creep and Fracture of Engineering Materials and Structures’, (Ed. B . Wilshire and R . W . Evaans) , The Institute of Metals , London , 1993 , pp. 117 –127 .
- [3] Tchizhk , A . A . : ‘The influence of different factors on creep exponent’, J. Energomashinostroeniye , n . 2 ,1969 , p . 28 – 31 .
- [4] Evans , R . W . , Willis , M . R . , Wilshire , B . , Holdsworth , S . , Senior , B . , Fleming , A . , Spindler , M . , Williams , J . A . : ‘Prediction of long–term creep and creep fracture data for a 1CrMoV rotor steel’, Proc. Fifth Inter . Conf . on Creep and Fracture of Engineering Materials and Structures , (Ed . B . Wilshire and R . W > Evans) , The Institute of Metals , London , 1993 , pp . 633–640 .
- [5] Tchizhik , A . A . , Tchizhik , T . A . : ‘Material aging and life extension of main components for steam turbines ’. Proceeding . ‘Materials aging and component life extension’, Milan , Italy ,Vol.11, 1995 , pp. 813–820 .
- [6] Puarje , Zh . P . : ‘High temperature ductility of crystal bodies’ M . , Metallurgia , 1982 .
- [7] Novozhilov , V . V . : ‘About ductile loosing’ . J. Applied mathematics and mechanic .(Akad .Nauk SSSR) , n . 4 ,1965 , pp. 681–689 .
- [8] Vakulenko , A . A . : ‘ About relations between stresses and deformations in inelastic media’. In book : ‘Research on elasticity and ductility’. LGU . , issue 1 , 1961 , pp. 3–35 .
- [9] Lepin , G . F . : ‘ Creep of metals and criteria of high–temperature resistance’. M. ,Metallurgia , 1976 .
- [10] Schesterikov , S . A . , Melnikov , G . P . , Arshakuny , A . L . : ‘ About construction basic constitutive equations of creep’. J . Problems of Strength, n . 6 , 1980 , pp. 77–81 .
- [11] Tchizhik , A . A . : ‘ Micromechanical Modeling and Verification of Long Term Behavior of Advanced Materials’ . , Proc. Inter . Symposium on .Mechanics in Design , (Ed . S . A . Mequid) ,University ofToronto,Canada, v . 2 , 1996 , pp . 893–902 .
- [12] Tchizhik , A . A . , Tchizhik , T . A . : ‘Effect of Composition , heat treatment and processing technologies on the microstructure and properties of HP and IP rotors of large steam turbines from 1CrMoV steels’.In this Proceeding .

Effect of Composition , Heat Treatment and Processing Technologies on the Microstructure and Properties of HP and IP Rotors of Large Steam Turbines from 1CrMoV Steels

Andrei A. Tchizhik , Prof., D.Sc.

The Polzunov Central Boiler & Turbine Institute (PCBTI),
Department the Fatigue Life of Materials for Power Plant Equipment
24, Politekhnikheskaya St., 194021 , St - Petersburg , Russia

Tatiana A. Tchizhik , Ph.D.

The Turbine-Building Production Association «Leningradsky Metallichesky
Zavod» (LMZ), Central Plant Laboratory
18, Sverdlovskaya nab., 195009 , St - Petersburg , Russia

Abstract

In the paper there is analyzed the evolution of the technology manufacturing of the large forging from the 1CrMoV steels and the results complex of the long time investigations rotors on virgin state and after different operation times. Among the information there are the criterion of the optimization of the composition steel, service properties , especially super long - term creep resistance , creep fracture and long time cracks resistance . Two safety coefficients: stress (SSC) and time safety coefficient (TSC) must be used for calculations of the possibility prolongation service life of HP and IP rotors for large steam turbines.

1 Introduction

Russian research investigations on development 1CrMoV grades of steels for steam turbine rotors at service metal operating temperatures from 540° up to 565°C were begun at LMZ in 1948 [1, 2]. This class of rotor materials was given the tentative name «Russia» (R- letter). Before 1964 the composition optimization for these grades of steels is realized with application first criterion creep resistance generation. Since 1964 the complex research investigations on development 1CrMoV grades of steels had founded on fine optimization of chemical composition , heat treatment and long-term service properties of large steam turbine forging. Beginning from 1964 the fine optimization of chemical

composition is performed by second criterion creep properties generation. This inside Russian (USSR) research program in frame joint CBTI - LMZ network cooperation was allowed to put into practice the life extension of HP and IP steam turbines rotors up to 220,000 h and more.

2 Methods

2.1 The Criteria of Chemical Composition Optimization of 1CrMoV Rotor Grade Steels

Many time the quest of the criteria of chemical composition optimization (CCO) of 1CrMoV rotor steels was the major problem of optimal alloying these creep resistance conventional grade steels. The investigations on CCO were carried out with the same C-content and V/C ratio ($C \approx 0,25\%$, $V/C \approx 1,0$)

The rotor steel properties after chemical composition optimization aimed at were specified :

- 200,000 h creep rupture strength at 550°C of about 110 MPa ,
- good creep rupture ductility ($\geq 10\%$ reduction in area) ,
- acceptable creep crack resistance (C.C.O.D. $\geq 0,1$ mm) ,
- through-hardening up to at least 1280 mm diameter ,
- minimum yield strength of 500 or 630 MPa ,
- acceptable FATT(50) and fracture toughness.

The first criterion of optimal alloying for 1CrMoV rotor steels was offered in [1], named by $Mo_{\text{equivalent}} = (Mo + W)$ atomic % or $(Mo + 0,5W)$ wt. % [4]. This simplest criterion allowed to reveal optimum by creep resistance with total atomic percentage composition of Mo and W at 0,5-0,7% [1,5]. On the basis of these data it was drawn a conclusion that optimum Mo_{Eq} provides the best solid solution strengthening with given content of other alloying elements in steel. The newly - developed criterion of optimal alloying for 1CrMoV steels was established under the screening contribution of chemical elements at summary of the characteristic strengthening mechanisms (solid solution and grain boundary strengthening, carbide reactions). This criterion « α » presented the ratio of $Cr_{\text{eq}} = (Cr + Mo + V + 1,5 Si)$ wt.% to $Ni_{\text{eq}} = (Ni + 30C + 0,5 Mn)$ wt.%. The best results by creep and toughness properties take place for compositions at $\alpha = 0,32 - 0,45$ (Fig. 1).

On the basic of works performed on optimization of 1CrMoV rotor steels by now five main variants of steel compositions were offered among which only three had been widely spread (Table 1). The type of steel with tentative name R-1 was developed simultaneously with R - 2 steel for HP and rotors for LMZ SVK-150-1 steam turbine (170bar/565°C/535°C, 1952

year of comm.). Considerations for adaptability to manufacture gave prior direction for use of R-2 types steels without W and correctness of optimal composition chosen was confirmed by positive long service and laboratory experiences. Further works on optimization of 1CrMoV steel composition were directed to improving of hardening up to at least 1280 mm diameter with keeping creep properties under required level. These works were performed mainly owing to raising of Mo-content up to 1% for steel with tentative name R-3 and up to 1,05% for R-4 steel. Both steel contents were given general name R2MA steel, which was denoted in specifications. The difference between these two contents of rotor steels however must be considered in forecasts for resource of power utility equipment, particularly in analyzing of metal of rotors after long time service. R-5 steel with higher hardenability and brittle fracture resistance used only for experimental forging. In developing this steel composition it was established that optimal hardenability may be achieved with given for this type of steels Cr-content at the level of 1,6% at the expense of alloying by Ni up to 0,6-0,7% to receive a combination of acceptable creep strength and FATT(50) with high creep ductility and creep crack resistance of steels.

Table 1 : High-temperature steels of R-type used for HP and IP rotors.

Steel grade	Chemical composition (wt.%)						
W-Nr.	C	Cr	Mo	W	Ni	V	α
1. R-1 type steel (1948-1950)							
R	0,22	1,50	0,50	0,60	max.	0,20	0,32
	030	1,70	0,70	0,80	0,30	0,30	0,57
2. R-2 type steel (1953-1959)							
R2	0,21	1,40	0,60	-	max.	0,20	0,26
	0,29	1,80	0,80	-	0,30	0,30	0,48
3. R-3 type steel (1959-1963)							
R2M	0,21	1,40	0,80	-	max.	0,20	0,27
	0,29	1,80	1,00	-	0,40	0,30	0,50
4. R-4 type steel (1963-present time)							
R2M	0,21	1,50	0,90	-	max.	0,22	0,31
	0,29	1,80	1,05	-	0,40	0,32	0,54
5. R-5 type steel (1980-present time)							
R2M	0,21	1,50	0,90	-	max.	0,22	0,30
	0,29	1,80	1,05	-	0,70	0,32	0,54

Now the OCC of 1CrMoV rotor steels of R - type carries on at direction the application this steel for manufacturing of newly generation steam turbines with improved the temperature and pressure .

2.2 Features of Manufacture Technology for Rotors

In manufacturing conventional HP and IP rotor forging from 1CrMoV five grades steels of R-type three types melting are used :

- the duplex Martin process (basic + acid Martin steelmaking furnaces) with «Si-killed» deoxidization;
- the basic Martin process with extra-furnace refining on ASEA (RH) with combined Si / C deoxidization;
- the BEA steelmaking process with «Si-killed» deoxidization.

The conventional HP and IP rotor forging had manufactured from 38 Mg up to 105 Mg ingots.

The quality heat treatment was performed with double normalizing on 980° and 960°C with the cooling on air (before 1953), air by fans (1953 - 1973) , combined two - medium cooling water - air step by step (since 1973) and tempering at 660° - 690°C (minimum yield strength is 500 MPa). After quality heat treatment for large forging the yield strength , tensile strength , impact and creep rupture specimens taken from outer (tangential testing) and central (axial testing) positions.

3 Results

3 . 1 Properties of Conventional HP and IP Rotors Steam Turbine from 1CrMoV steel of R-type

Complex of design and service properties of 1CrMoV rotor steels of R-type developed more than once was considered in overviews [1-3 , 5-7]. In this paper the mechanical and impact properties in virgin state of 16 IP rotors the steam turbines with unit capacity 800Mw (diameter 1280mm) at rim and center position are compared in Table 2. The mechanical and impact properties at rim and center position are good and homogeneous and same in comparison to conventional 1CrMoV rotor steel according Russian and European standards. In virgin state of HP and IP rotors from 1CrMoV steel manufactured before 1973 FATT(50) is 60°- 90°C for near-surface and not over 105°C for near - central positions. For large IP rotor the steam turbines with output 800Mw since 1973 from 1CrMoV steel grade R-3 and R-4 with combined medium cooling after double normalizing the FATT(50) is very stable and much higher in comparison to conventional 1CrMoV rotor steels grade R2 manufactured before 1973.

Table 2: Tensile and impact properties of IP rotors steam turbines with output 800Mw at virgin state and 20°C.

Mechanical properties	rotor neck		rotor body	
	Top	Bottom	Top	Bottom
1. Near - surface position (tangential)				
Yield Strength (Rp0,2), MPa	540	550	550	540
	560	650	620	650
Tensile Strength (Rm), MPa	700	700	710	710
	780	780	770	770
Elongation (A 5),%	18 - 22	19 - 33	18 - 24	20 - 24
Reduction in Area(Z),%	65 - 74	64 - 78	59 - 74	56 - 72
Impact Energy (Au), J	86 - 196	102 - 180	78 - 156	63 - 156
2. Near - center position (axial core)				
Yield Strength (Rp0,2), MPa	560	530	560	460
	620	630	630	620
Tensile Strength (Rm), MPa	710	670	720	570
	770	750	780	720
Elongation (A 5), %	20 - 23	20 - 24	20 - 23	18 - 26
Reduction in Area(Z),%	61 - 68	67 - 75	61 - 69	67 - 75
Impact Energy (Au), J	78 - 149	110 - 196	78 - 149	39 - 196

Parameters of fatigue crack growth near center of rotors completely coincide with ones for 1CrMoV steels according to EPRI data (RP1343) .

Investigation results of properties degradation of rotor metals during long service up to 200,000 h show that :

- at the operating temperatures 500°-525°C reducing of yield strength for 1CrMoV steel grades R2 - R5 may be expected up to 5% , tensile strength up to 3-5%,raising FATT(50) by 15°-25°C, decreasing K1c by 10-15%;
- at the operating temperature 550°C reducing of yield strength for 1CrMoV steel grades R2 - R5 may be expected up to 15-16% , tensile strength up to 10-12% , raising FATT(50) by 20°-40°C and decreasing K1c by 25%.

Estimation results of basic creep properties of IP rotors , manufactured after 1973 are shown in Table 3.

Table 3 : Design creep properties of 1CrMoV rotor steel R3-R5 grades
(Specimen position: Middle of Ingot, Half Radius rotor body, tangential).

Creep properties	Design service time , hour	Design service temperature , °C		
		500°	525°	550°
Creep Fracture Strength , MPa	100,000	195	190	130
	200,000	180	175	112
Creep Stress Limit, (1% for design time) , MPA	100,000	170	130	105
	200,000	160	120	96
Norton Parameter	100,000	3,25	2,80	2,20
	200,000	3,80	3,75	2,70
Reduction in Area, %	100,000		65 - 85	16 - 66
	200,000		63 - 85	11 - 58
Creep C.O.D. , mm			0,25	0,15
	100,000		0,35	0,35
	200,000		0,22	0,10
			0,32	0,25

3 . 2 Problems of Raising Residual Life for HP and IP Rotors from 1CrMoV steels

The assessment of residual life of HP and IP steam turbine rotors the usage of traditional calculations by safety stress coefficient (SSC) is necessary but insufficient condition, determining forecast truthworthness . As additional criterion safety time coefficients (STC) must be considered, indicating the effect of composition and technology on the residual life of rotor metals . Long-term creep resistance tests up to 200,000 h allow to analyze the effect of different features on this safety index.

3 . 2 . 1 Composition and Liquation Heterogeneity Effects

Trough investigations of creep fracture for 16 IP rotors from 1CrMo(R3 - R4 grades) steels the dependence STC on the parameter of $\alpha = Cr_{eq} / Ni_{eq}$ is revealed, shown in Fig.2.,in which there are STC curves during 100,000h at 550(C. Received data testify to the necessity for consideration of specific rotor content in the development of individual forecast methods of residual life for steam turbine HP and IP rotors. Keeping SSC at the given level (for example SSC=1,5 , Fig.2) STC can be varied with content of rotor steels within wide range of values from 2,8 to 8.

Low values of α parameter depended on unfavorable carbide reactions in high-temperature tempering of double normalized steel with higher bainite structure at which the carbide formation $M_{23}C_6$ takes place. For analysis of actual (values scatter in regular rotors from 1CrMoV steel (grades R3-R4) the results of melt chemical analysis shown that with α changes from 0,3 to 0,54 according to steel type the most favorable interval of compositions, having higher creep resistance (Fig.1) , creep fracture (Fig. 2) and creep ductility (Fig. 3) meets to these α - values. It follows directly from Fig.2 :

- possibility for further raising of STC thank to alloying optimization;
- possibility for investigations of optimal steel composition employed for high-loaded rotors with lower SSC , but not reducing STC (Design STC and SSC define individual chemical composition with allowable $[\alpha]$ Fig.2. For STC = 4 , SSC = 1,5 the minimum allowable value of parameter of optimum alloying is $[\alpha] = 0,32$. For STC = 6, SSC = 1,5 this allowable value is $[\alpha] = 0,35$. For STC = 4, SSC = 1,3 this value is $[\alpha] = 0,37$ etc.);
- indelicacy for statistical estimations of high-temperature strength ;
- parameters on base of test results not considering the parameter of optimum alloying.

Assessment of complex design and service creep properties of HP and IP rotor steels must be systematic, there are details of regular technology for rotors to be considered at individual methods life extension of turbines.

In analysis the liquation of basic alloying elements must be considered. For this purpose variations in α was investigated for different locations in regular IP rotor of steam turbine with output 200Mw from 1CrMoV steel grade R3. At $\alpha=0,368$ from melting analysis results the actual values of this parameter are : bottom of ingot - near-surface rotor body $\alpha=0,4$,middle of ingot -near-surface rotor body $\alpha=0,36$ and near-center rotor body $\alpha=0,46$, top of ingot near-surface rotor body $\alpha=0,36$, near- half radius $\alpha=0,428$ and near-center rotor body $\alpha=0,458$.The melting analysis results were close to the lower level of α -values all around the ingot volume. If you know the field of α -parameter all around the rotor body you can to calculate minimum STC - SSC for the given HP or IP rotor from 1CrMoV steel and assessment of individual residual life it.

3 . 2. 2 Structure and Properties Effects

The cooling rate on double normalizing of HP and IP rotor from 1CrMoV steels considerably effects on STC [8 , 9] . When carbides of $M_3 C$ are formed during cooling on normalizing in further tempering the character of

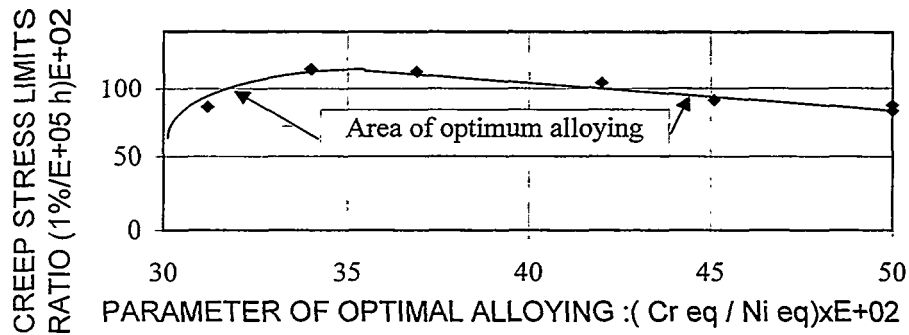


Fig. 1. Relation between creep stress limits ratio (1%/100,000 h) and parameter of optimum alloying for 1CrMoV rotor steels at 525 C.

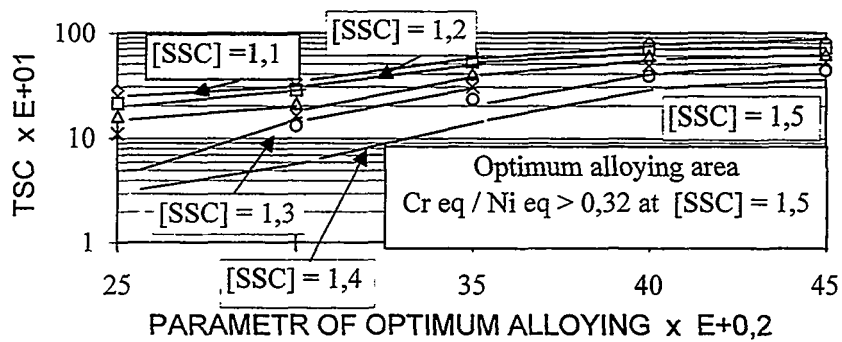


Fig. 2. Relation between creep fracture TSC and parameter of optimum alloying at 550 C.

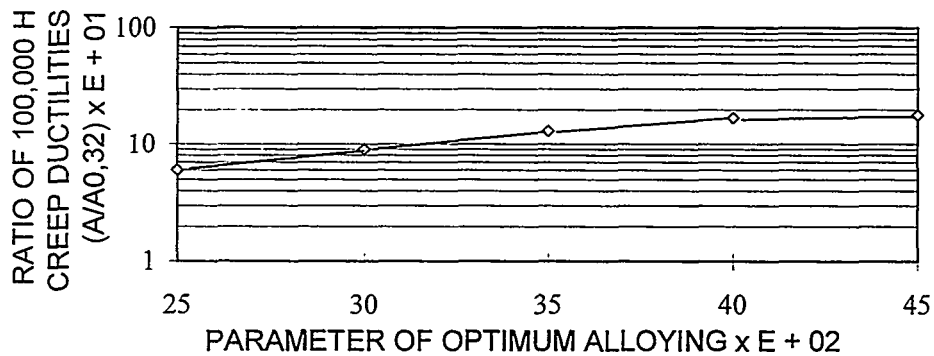


Fig. 3. Relation between ratio of 100,000 h creep ductilities $A / A_{0,32}$ and parameter of optimum alloying at 550 C.

proceeding carbide reactions practically suppresses the process of $M_{23}C_6$ carbide formation even at low α -parameter. Thus at $\alpha=0,23-0,37$ quenching in oil and tempering are used for suppression of $M_{23}C_6$ carbide formation.

The optimum microstructure for HP and IP rotors is tempered upper bainite. Near-surface rotor body the microstructure consists of combined tempered lower bainite and martensite (high creep ductility, acceptable creep strength, low FATT, no notch sensitivity). Near-center rotor body (diameter 1280mm) the microstructure consists of combined tempered upper bainite and up to 20-28 % ferrite after cooling on air (before 1953), up to 8-12 % ferrite after cooling by fans (1953-1973), acceptable creep properties, high (FATT), up to 5 % ferrite after combined cooling on two-medium (since 1973, acceptable creep properties and FATT). Near-center rotor body ferrite in microstructure obtains only at liquation zones of ingots with low C-content.

The tempering parameters (temperature, duration etc.) have a large influence on residual life HP and IP rotors from 1CrMoV steels grades R2-R5. Decreasing of tempering parameters leads to suppression of $M_{23}C_6$ carbide formation and increasing of initial strength properties. Rise in yield strength from 500-550MPa to 600-650MPa at 20°C is fairly effective for metal temperatures up to 540°C (Fig.5). The real values of yield strength the regular HP and IP rotors must be used for fine individual assessment the residual life these main elements steam turbines across calculation real individual values of SSC and STC for actual α -parameter of ingot, carbide reactions (initial and under operation) and all around microstructures.

3.2.3 Effect of Operating Temperature. Control of Rotor State

The super long-term creep test 1CrMoV steel (R-3) [10] allow to determine essentially enough STC according to metal temperature and values of actual SSC. The change of STC with change of metal temperature for 1CrMoV steel grade R4 with $\alpha=0,32$ and different SSC on base of 100,000h is shown in Fig.4.

It follows from Fig.4:

- the clear temperature dependence of STC at $SSC = 1,5$ takes place in temperature range of 500°-550°C. Thus, with metal temperature change by 50°C STC decreases by order;
- the intensity of decreasing STC is reduced with decreasing of SSC;
- the designing of main elements of steam turbines from 1CrMoV steel is possible at lower SSC. In this case maximum temperatures for steel usage must be reduced. Thus for securing no less than tenfold STC on base of 100,000 h maximum temperatures must be not exceed:

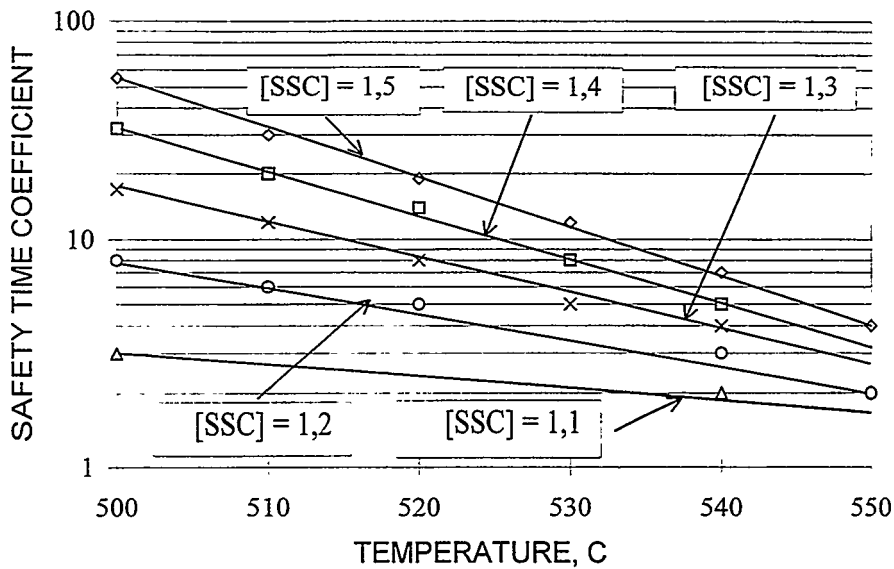


Fig. 4. Relation between safety time coefficient (STC) and opening temperature for different stress safety coefficient (SSC) for lower bound optimum alloying area Cr eq. / Ni eq. = 0,32.

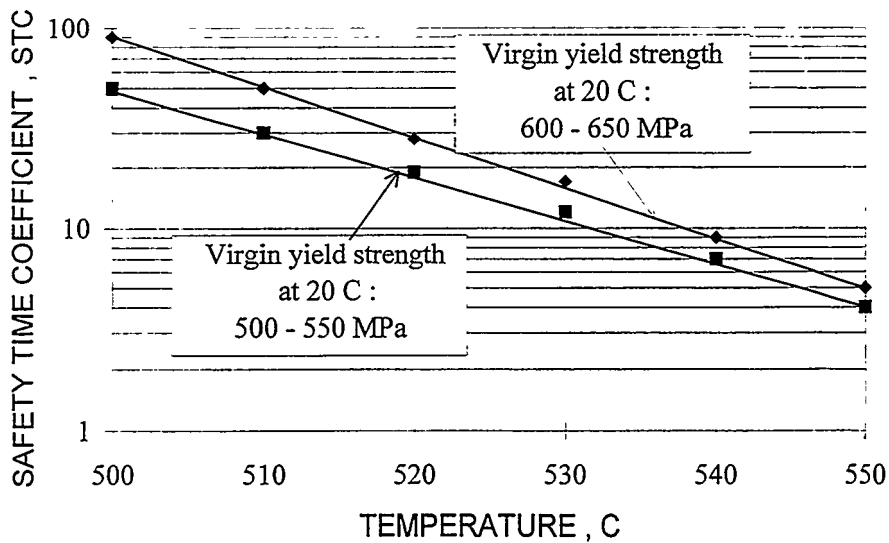


Fig.5. Relation between safety time coefficient (STC) and temperature for different virgin yield strengthes (Cr eq / Ni eq = 0,32 and SSC = 1,5).

- 535°C at SSC = 1,5 ;
- 525°C at SSC = 1,4 ;
- 512°C at SSC = 1,3.

STC estimation enables also to define the control procedure of service state for high-loaded parts under long service. For example, if STC exceeds its tenfold value at the moment of state analysis there will be probable the prolongation for resource of parts till next capital repairs without this state control. If STC is in range from 6 up to 10 there should be proceeded the control of service conditions and also control calculation for residual life. If STC is in the range from 4 up to 6 it is necessary to proceed the through control of the actual state with the individual estimation of residual life . If STC is in the range from 2 to 4 it is necessary the usage of special methods for state control (microdamage control , small punch tests , newly methods of life assessment techniques [11] etc .) and the development of special diagnostic systems for state service control. Of course , enumerated levels of state control by STC are needed in further elaboration and clarification. In recent years however the differential control of the actual state must find an application under conditions when the volume of necessary work on life extension for operation equipment's is greatly increased.

4 Conclusions

Now a days advances in materials of steam turbine rotors are determined by the development of newly methods for system analysis of equipment safety. Fine calculations and grounds of strength and resource by two safety SSC and STC are the basis of system safety analysis for steam turbines. STC enable to define safe periods of service for HP and IP rotors of steam turbines , a system of operating control of rotor state and to develop individual forecast methods of turbine services considering steel composition and technology of rotor manufacturing. STC system enables to formulate new requirements for a composition and production technology of HP and IP rotors of steam turbines from 1CrMoV steel considering the necessity of extension for rotor service life over 200,000 h with simultaneous improving of availability and steam turbine parameters . These requirements can be met by means of simultaneous modernization of used steel composition for securing the given level of safety by basic criteria of creep strength and local criteria of crack resistance of 1CrMoV steel grades. On a base of investigations carried out considering state control of HP and IP rotors for steam turbines of fossil power plants they prolongation of resources for 200 and 300Mw steam turbines of LMZ up to 220,000 h and for steam turbines of lower output up to 270,000 h.

References

- [1] Tchizhik A.I.- «About LMZ works in advances of turbine materials»// Journal Metal Science and Heat treatment of metals (Metallovedenie i termicheskaya obrabotka metallov) (on Russia) , 1957 , N 11;
- [2] Tchizhik A.I., Hein E.A. - «Investigation of regular rotors from R2-steel»// In book: «Properties of materials used in turbomachinery and methods of their investigations», Mashgiz, Moscow-Leningrad ,1962 ,v. 9 ,pp.26-36;
- [3] Tchizhik A.A.- «Individual methods life extension main elements of power plant equipment» // Journal of machine building problems and reability machines (Problemy mashinostroenija i nadjezhnosty mashin) (on Russia), Russian Acad.Sci.,1990, N 5 ,pp.31-35;
- [4] Fujita T., Sato T.,Takahashi N.- «Effect of Molybdenum and Tungsten on the Long Term Creep Rupture Strength of 12 % Chromium Heat Resisting Steel Containing Vanadium, Niobium and Boron»//Transaction of the Iron and Steel Institute of Japan , 1978 , 18 , pp.115-124 ;
- [5] Tchizhik A.I.- «Creep resistance steel for rotors of steam turbines»//In book: «The properties of materials used on turbomachinery and methods of their investigations»,Mashgiz ,Moscow-Leningrad, v.9, 1962 ,pp.7 -25 ;
- [6] Tchizhik A.A.,Tchizhik T.A. - «Materials ageing and life extension of main components for steam turbines»//Proceedings of an International Symposium on Materials Ageing and Component Life Extension, Milan, Italy,10-13 October 1995,v.11,pp.813-820 ;
- [7] Tchizhik A.A.,Tchizhik T.A.- «Residual life assessment methods of large steam turbines»,Proceedings of the Ninth International Symposium on Creep resistance metallic materials, Hradec nad Moravici, Czech Republic,23-26 September 1996,pp.425-429;
- [8] Pigrova G.D., Tchizhik T.A. - «Phase composition of 1,5Cr-1Mo-0,3V rotor steel as a factor of cooling rate from austenitic region»//Proceedings of the Fifth C. R. M. Conference on Materials for Advanced Power Engineering 1994,October 3-6,1994 Liège,Belgium,Abstracts,p.5 ;
- [9] Tchizhik A.I., Tchizhik A.A., Tchizhik T.A. - « The problems of optimization of composition and structure state creep resistance steels for steam turbine rotors»//Memorial Special Report PCBTI(The Polzunov Central Boiler & Turbine Institute) N 270,St-Petersburg, 1992, pp.18-29;
- [10] Tchizhik A.A.- «Super long-term creep tests of advanced HP and IP rotor steels»// In this proceedings;
- [11] Viswanathan R. - « Life assessment of high temperature components »//Proceeding of International Symposium on Materials Ageing and Component Life Extension, Milan, Italy, 10-13 October 1995,v.1.,pp.49-62.

ADVANCES IN PROCESSING TECHNOLOGIES FOR TITANIUM HEAT EXCHANGER TUBES OF FOSSIL AND NUCLEAR POWER PLANTS

T.P. Likhareva
A.A. Tchizhik
N.N. Chavchanidze
Polzunov Central Boiler and Turbine Institute
St.-Petersburg, Russia.

Abstract

The advances in processing technologies for titanium heat exchangers with rolled and welded tubes of fossil and nuclear power plants in Russia are presented in this paper.

The special methodology of investigations with constant small strain rate have been used to study the effects of mixed corrosion and creep processes in condensers cooled by sea or synthetic sea waters. The results of corrosion creep tests and K1scc calculations are given.

The Russian science activities concerning condensers manufactured from titanium show the possibilities for designing structures with very high level service reliability in different corrosion aggressive mediums with high total salt, Cl-ion and oxygen contents.

1 Introduction

Research works on high corrosion-erosion resistance of α -Titanium alloys were begun at Polzunov Central Boiler and Turbine Institute in late 1972. It is known that α -Titanium alloys show highest corrosion-erosion resistance during long service time in condensers cooled by sea water as compared with ordinary austenitic steels when operating in corrosive mediums of nuclear and fossil power plants. These α -Titanium alloys are used in Russia for manufacture of heat exchangers, desalinating

installations and condensers cooled by sea water. The restriction of application of α -Ti alloys in heat exchangers is connected with processes of hydrogen absorption at elevated temperatures. The specimens from their alloys haven't the weight losses during 3,000 h at 20 C° in flowing water. However in this case it is very important that this class of materials have highest impingement corrosion resistance in the range of water flow rates up to 8-12 m/s. The investigations show that the impingement corrosion resistance of α -Titanium alloys is 8-10 times higher than for the austenitic stainless steels.

Recently in Russia grades of technical pure β -Ti for the manufacture of electric-welded tubes at competitive costs with longitudinal uniform welds and cold-deformed tubes were worked out. However the non-destructive methods of quality control for the tubes by ultrasonic and eddy current analysis don't guarantee the full lack of small longitudinal microcracks which can growth during long operation time under mixed creep-corrosion conditions. In this connection special methodology of investigations was performed for the developed production practice of electric-welded titanium tubes for real service conditions of nuclear and fossil power plants.

2 Characteristics of Investigated Tubes and Experimental Details

Investigations of electric welded and cold-rolled tubes from α -Ti alloys were performed as applied to their abundant range of rolled products made at Tube Electro-welding UNIT (TEMU) as well as at Cold-rolled Tube Mill (CRTM). As billets were used cold-rolled strips from VT1-0-titanium alloy (pure technical titanium) composition of which was developed in the middle of 60's years. Chemical composition, mechanical properties and technical requirements for strips from VT1-0 titanium alloy has been developed in order to meet ASTM B 338 requirements for cold-rolled and welded tubes from grade 3. For welded tubes at condensers of nuclear power plants the Fe-content is max. 0,05% no more .

The principal manufacturing technology and methods of quality control of cold-rolled and welded tubes from VT1-0 titanium alloy we used are identical to "Kobe Steel Ltd." Company (Japan) for the KS 70 (JIS Class 3). The strips from VT 1-0 titanium alloy were produced from unalloyed technical titanium sponge after simple Vacuum-Arc Remelting (VAR). The mass of round ingot was near 6 t. The VAR ingot was plasma roughed before the forging strips.

The density of VT1-0 strips is 4,52 g/cm³. The physical properties of strips from VT 1-0 titanium alloy are following in the Table 1.

The emissivity factor of strips from VT1-0 during direct air heating is following: for etched strips are 0,22 at 100 °C and 0,37 at 500 °C, for cold-rolled strips are 0,10 at 100 °C and 0,22 at 500 °C. The specific electrical resistance at 20 °C is $47 \times 10^{-6} \Omega \text{ cm}$. The hardness of the strips from VT1-0 as delivered is (145-175 HV10).

Before the welding each strip had special computer aided ultrasonic examination and evaluation of natural defects .

To produce high-quality electric-welded tubes at mill we had used the special TIG-welding technology in highest pure argon (no technical argon) which was cleaning by pure titanium powder. After the welding each tube had special double-computer aided ultrasonic + eddy current examination and evaluation of natural defects.

Table 1. The general physical properties of VT1-0 Ti-alloy.

Property	Temperature °C				
	20	100	200	300	350
Thermal conductivity, Kcal/m ² hour °C/metre	18,5	18,1	17,7	17,3	17,2
Heat capacity, C, cal/(g- °C)		0,120	0,131	0,135	0,137
Coefficient of linear expansion, $\alpha \times 10^6/^\circ\text{C}$	8,8	8,9	9,3	9,8	
T °C	20-100	100-200	200-300	300-400	

2.1 Requirements Property

The VT1-0 titanium alloy properties of cold-rolled and welding tubes with wall thickness 0,5-1 mm were specified:

- Or 10,000 hours-test weight losses for impingement corrosion at water flow rate.
- Of 8,2 m/s in synthetic water with 3% NaCl at 20 °C are of about 0,0003 mg/cm².
- Uniform welded tube manufacturing technology is the same as for cold-rolled tubes.
- Minimum yield strength is 360 MPa.

- Good ductility (> 18 % elongation).
- Good creep ductility in aggressive corrosion medium (3% NaCl solution).
- Good fatigue properties and stress corrosion cracks toughness (K1scc).

2.2 Materials Investigated

The program of these investigations included:

2.2.1 Production Practice Selection

Potential production practice technologies were identified after a critical review of existing service conditions of condenser at fossil and nuclear power plants with different cooling schemes by flowing river and sea waters, life extension of this units up to 40 years and over. Ti thin walled tubes in Russia and technological advances elsewhere in the world; tube competitive costs. Two principal production practices were investigated: cold-rolled and welded tubes as delivered and after annealing.

2.2.2 Trial Components

The most promising technical pure titanium in Russia (VT1-0 grade) was selected to gain experience in the manufacture of full size components for condensers of fossil and nuclear power plants with tube wall thickness of 0,5-1 mm, outside diameters from 14 mm up to 30 mm, length 9m and over. To date two tubes production practice (cold-rolled and welded tubes) have been developed. They were subjected to detailed destructive examination to determine the corrosion-erosion properties at high rate of water flow, the creep-corrosion ductility, fatigue and stresscorrosion-crack toughness (Kiscc).The use of very long-term impingement stream corrosion tests up to 10,000 h and over and creep-corrosion ductility tests are most important for service Life assessment for condensers of fossil and nuclear power plants.

2.2.3 Non-destructive Quality Control Assessment

This quality control assessment of some quantity of test welded tube samples taken from rejected tubes after double computer aided ultrasonic + eddy current non-destructive control has been undertaken to gain a better understanding of influence of microdefects on processes of creep-corrosion deformation and fracture Ti-grade welded tubes. Three lots of welded tubes were investigated. The first lot of welded tubes was selected for investigations as delivered without heat treatment. That lot was marked by letter "A". The second lot of welded tubes was selected from tubes with good results of non-destructive quality control assessment and after vacuum annealing at 640 °C. That lot was marked by letter "B". The third lot of

welded tubes was selected from rejected tubes after vacuum annealing at 640 °C and double computer aided ultrasonic + eddy current non-destructive quality control. That lot was marked by letter "C". A detail metallographic study of welded joints of rejected tubes hadn't shown the visible defects in root of welds and other zones of welding joints. To date two lots of cold-rolled tubes with good results of non-destructive quality control were selected for investigations. The first lot of ° cold-rolled tubes marked by letter "D" had been produced with annealing on electrocontact installation at 660 °C. The second lot of cold-rolled tubes marked by letter "E" had been manufactured with vacuum annealing at 640 C.

2.3 Preliminary Tests

The preliminary test include :

- Tensile tests at room temperature.
- Core flaring of cold-rolled and welded tubes.
- Flattening of cold-rolled and welded tubes.

Mechanical characteristics at room temperature are following:

1. Welded tubes "A"(as delivered):

$R_{P02} = 400 \div 420$ MPa; $R_m = 520 \div 530$ MPa; $A = 13,5$ % (length 50 mm).

It isn't good result! $Z = 42,0$ % (length 50 mm).

2. Welded tubes "B"(after vacuum annealing):

$R_{P02} = 330 \div 340$ MPa; $R_m = 453m \div 465$ MPa; $A = 19,0$ % (length 50 mm).

$Z = 44,0$ % (length 50 mm).

3. Rejected Welded tubes "C"(after vacuum annealing):

$R_{P02} = 330 \div 340$ MPa; $R_m = 435 \div 455$ MPa; $A = 18,0 \div 18,5$ % (length 50 mm).

$Z = 50 \div 53$ % (length 50 mm).

4. Cold-Rolled tubes "D" (after electrocontact annealing):

$R_{P02} = 295 \div 305$ MPa; $R_m = 460 \div 470$ MPa; $A = 23,0 \div 25,0$ % (length 50 mm).

$Z = 50 \div 52$ % (length 50 mm).

5. Cold-Rolled tubes "E" (after vacuum annealing):

$R_{P02} = 275 \div 305$ MPa; $R_m = 470 \div 480$ MPa; $A = 25,0 \div 26,0$ % (length 50 mm).

$Z = 50 \div 52$ % (length 50 mm).

The core flaring and flattening tests for cold-rolled tubes ("D", "E") and welded tubes ("A", "B", "C") shown the good results for Russian technical requirements and ASTM B 338 for grade 3.

3 Experiments

3.1 General Corrosion Stand Resistance

The general corrosion resistance was studied using special techniques.

The general corrosion test installation consists from three steps with tube drainage and throttling systems. On the first step the stream water rate is 8 m/s; on the second - 4 m/s and on the third 2 m/s.

The tube specimens had been installed on each step of corrosion installation. The weight losses had been measured periodically by taking down the tube specimens with subsequent assessment of weigh losses using comparison test techniques.

General corrosion stand tests were performed on tube specimens (cold-rolled and welding tubes) , exposed to controlled environments, namely:

1. Fresh flowing water from Neva river at room temperatures at rates 2m/s, 4m/s and 8m/s.
2. Synthetic sea water (Mixed solution of fresh flowing water from Neva river and 3%NaCl).

Exposure duration was 1000 h, 2500 h, 3500 h, 7000 h and 10000 h.

3.2 Impingement and Corrosion-Erosion Tests

The impingement and corrosion-erosion tests of the flat specimens from strips of cold-rolled and welded tubes was studied on special rotating bench.

The specimens were located along the rotating acrylic plastic disks. In this case we hasn't chemical reactions between material of disk and metal of the flat specimens and between different metals of the specimens and the water. Along the flat specimens the liner velocity was changed from 2m/s up to 9 m/s.

The corrosion-erosion tests were performed on the specimens from condenser cold-rolled and welded tubes in fresh flowing water and synthetic sea water(Mixed solution of fresh flowing water and 3% NaCl).

3.3 The Creep-Corrosion Resistance (CCR)

The creep-corrosion resistance of the cold-rolled and welded tube specimens was studied on special test machines with small constant rate of

uniaxial displacement tension grips on creep testing machines (0,1 mm/h and 1 mm/h) on the round specimens from tubes.

The tension grips of creep testing machines are two cylindrical movable supports from high strength α -Ti alloy with the same electro-chemical potential. The welds were located at angle of 90 ° or 270 ° to a direction of loading.

The two stages of creep deformation have taken place during the testing of the round specimens:

- 1 -st stage was creep bending around the two cylindrical movable supports;
- 2 -nd stage was eccentric tension creep after the end of specimen bending on movable supports.

On this stage inside bend tension of specimens had taken place.

The full deformation of the round specimen had been calculated by the following relation:

for inside surface in points located at angle of 90° and 270° (weld root for welded tubes)

$$\varepsilon = \left\{ s \left[\frac{1}{D_0} + \frac{1}{D_1} \right] + \frac{2\Delta}{\pi(D_0 - d_0)} \right\} \times 100\% \quad (1)$$

for outside surface in points located at angle of 90° and 270 ° (weld surface for welded tubes)

$$\varepsilon = \left\{ s \left[\frac{1}{D_0} - \frac{1}{D_1} \right] + \frac{2\Delta}{\pi(D_0 - d_0)} \right\} \times 100\% \quad (2)$$

specimens with constant width (10 mm) in air, in flowing synthetic sea water (Mixed solution of fresh flowing water and 3% NaCl) at where ε - local creep ductility in % ; s - wall thickness ;

D_0 - middle diameter of tube before test; d -diameter of cylindrical movable support; $D_1 = 2R_1$;

R_1 -radius of curvature (of a space points are located at angle of 90 and 270); Δ -uniaxial creep displacement between cylindrical movable supports during test.

This test method of round specimens from cold-rolled and welded tubes is very simple for investigations of creep-corrosion resistance in different water mediums. It is important that for the test of round specimens from welded tubes this method permit to determine local creep/creep-corrosion ductility for weld root.

The strain (time) diagram of loading for the round specimens consisted of two parts. The first part with small level of loading had taken place for 1-st stage of creep deformation by bending. After this stage the 2-nd stage of eccentric tensile creep deformation had begun. On this second part of the strain(time) diagram the level of loading increased up to value R on smooth specimens. Constant slow strain rate creep-corrosion tests were performed on the round room temperature.

3.4 Stress Corrosion Cracking Susceptibility

The stress corrosion susceptibility of VT1-0 titanium alloy was studied using constant displacement test techniques from the simple and welded strips with thickness 15 mm. These strips were subjected passed to the electrocontact and vacuum annealing together with cold-rolled and welded tubes.

The tests were performed on C(T) specimens, wedge loaded at different starting K levels. The same K level was imposed to a specimen of each strips. The specimens from strips were submerged in fresh flowing water and synthetic sea water (Mixed solution of fresh flowing water and 3% NaCl) at room temperature.

4 Obtained Results and Discussion

4.1 General Corrosion Resistance (GCR)

Test results of GCR corrosion resistance of cold-rolled and welded tube specimens are summarized in Table 2.

The comparison of common corrosion resistance materials showed:

- Highest general corrosion resistance for the cold-rolled and welded tubes.
- The general corrosion resistance for welded was the same as for cold-rolled tubes.
- Influence of water flow rate on general corrosion resistance wasn't large.

The comparison of GCR for the cold-rolled tubes with annealing in electrocontact installation ("D") and vacuum annealing ("E") in this investigation has not shown large difference. Really for manufacturing technology we must apply only vacuum annealing, because we must formatted the high safe stability thin oxide three-layer on surface of tubes. Outside first polymolecular layer had absorbed by different gas, including hydrogen.

Usually after vacuum annealing this layer is absent. The middle second layer was uncontinuity metal layer with rutil crystal structure. The inside third metallic layer was continuity metal layer with amorphous structure at low operating temperatures of condensers. This layer defines electrochemical properties of passivity titanium.

Table 2. GCR test results.

Material grade	Type of tube produce	Time, h	Weight Loss, mg/cm ²	
			synthetic sea water	
			stagnant (0 m/s)	blowing (8 m/s)
VT1-0 Ti- alloy	Cold-rolled ("D", "E")	10,000	0	0,0003
	Welded ("A", "B")	6,000	0	0,0001
Steel A304L	Cold-rolled	10,000	0,0005	0,8
Cu-Ni alloy (85%Cu, 15%Ni)	Cold-rolled	10,000	2,5	4,5 - 16

After the electrocontact annealing on surface of tubes oxide three-layer and the inside third layer can have the anatase crystal structure. After the short vacuum annealing on surface of tubes is oxide double-layer (without gas absorbed outside first layer) and good amorphous structure. The thickness of oxide layer after vacuum annealing was $60 \div 120$ nm, after service life duration of 100,000 h is Max. $600 \div 800$ nm. The oxide surface layer after vacuum annealing was shown highest stability between the different water-chemical operating conditions for fossil and nuclear power stations.

The authors think that the vacuum annealing cold-rolled and welded tubes is better than electrocontact annealing tubes for long operating time up to 40 years and over.

4.2 Impingement corrosion-erosion tests (ICET)

The results of ICET are summarized in Table 3.

The obtained results showed:

- The titanium cold-rolled and welded tubes have highest ICET properties.

- The comparison of ICET didn't show large difference between cold-rolled and welded tubes.

• It is important to have highest stability of ICET properties for titanium tubes. In pre-item it is shown that this problem must be decided by using only vacuum annealing, because in during impingement corrosion-erosion test it is possible to damage the inside third amorphous layer if the outside first and middle second layers have hydrides-effective stress(strain) concentrations.

Table 3. ICET tests results.

Material grade	Type of tube produce	Time, h	Weight Losses, mg/cm ²	
			synthetic sea water water flow rate	
			(2,4 m/s)	(8,2 m/s)
VT1-0 Ti- alloy	Cold-rolled ("D", "E")	10,000	8,0 E-05	8,9 E-05
	Welded ("A", "B")	6,000	9,1 E-05	9,5 E-05
Steel A304L	Cold-rolled	6,000	1,5 E-03	2,2 E-03
Cu-Ni alloy (85%Cu, 15%Ni)	Cold-rolled	> 10,000	4,2 E-03	5,3 E-02 (Limit for rate)

4.3 Creep-Corrosion Tests (CCT)

The results of CCT are shown in Fig. 1-2. On the different parts of loading diagram it is taken place different results of CCT.

On the first part of diagram corresponded to bending the comparison of loading diagram does not show large difference between the different manufacturing technologies for cold-rolled ("D", "E") and welded ("A", "B" and even "C") for different water mediums (fresh and synthetic sea waters). The obtained results show no substantial difference regarding to the behavior of cold-rolled and welded titanium good and rejected tubes at small creep deformations.

On the second part of diagram corresponded to eccentric tension the comparison of loading diagram showed:

- Large difference between creep loading diagram and creep-corrosion ductility for good cold-rolled and welded tubes passed through the double-computer non-destructive quality control (ultrasonic + eddy current). In this case the ductile creep-corrosion fracture across the base metal was seen. The form of the round specimens before the fracture was octal .
- Large difference between creep loading diagram and creep-corrosion ductility for good ("A", "B") and reject ("C") welded tubes. For rejected welded tubes it was obtained the low max. load and min. creep-corrosion ductility levels. The fracture had begun in weld roots. The form of the round specimens before the fracture was oval or stretched shackle.
- Difference between creep loading diagram and creep- corrosion ductility for welded tubes after electrocontact annealing and vacuum annealing. The obtained results were better for tubes after vacuum annealing. It is possible that the thin plastic amorphous metal layer can arrest small corrosion damage in the thin layer of rutil, but cannot arrest corrosion damage in the first and second layer after the electrocontact annealing.

The creep-corrosion test is very good additional quality control test of welded tubes. This test showed that for welded titanium tubes it is necessary to include the vacuum annealing and double computer non-destructive quality control technology.

4.4 Stress Corrosion Cracking Susceptibility

The results of constant displacement tests were very good. We had obtained for cold-rolled and welded tubes values $K_{1\text{ sec}} = 90 \div 105 \text{ MPa } \sqrt{\text{m}}$ at synthetic sea water (Mixed solution of fresh water and 3% NaCl). Some years ago for tubes from steel grade 304L we had obtained values $K_{1\text{ sec}} = 10 \div 16 \text{ MPa } \sqrt{\text{m}}$ at synthetic sea water.

During the long term operation of condensers of fossil and nuclear power plants vibration of tube bundles had taken. In this case we must develop the new criterion of fracture mechanics for life assessment of these units. Because of the vibration stress level depended on logarithmic decrement "θ" the new criterion of fracture mechanics , must be written in next form $K_{\theta} = K_{1\text{ sec}} \times \theta$.

The comparison of K_{θ} showed large difference in life assessment of condenser tube bundles from VT1-0 Ti-alloy

($K_{\theta} > 0,451 \div 0,53 \text{ MPa } \sqrt{\text{m}}$) and from Cr-Ni steel

($K_{\theta} > 0,1-0,16 \text{ MPa } \sqrt{\text{m}}$)

This criterion shows that in real construction of condensers the Ti-alloys have higher stress corrosion cracking susceptibility than the Cr-Ni grade steels. This conclusion is correct if we haven't absorb hydrogen during long operating time because the absorb hydrogen process can increase the rate crack growth.

5 Conclusion

For manufacturing condenser tubes of fossil and nuclear power plants with long service time and reliability level it needs to use cold-rolled or welded tubes from technical pure titanium (VT1-0 alloy grade). These tubes have the complete highest corrosion-erosion properties for cooling by sea water and flowing water with high Cl level.

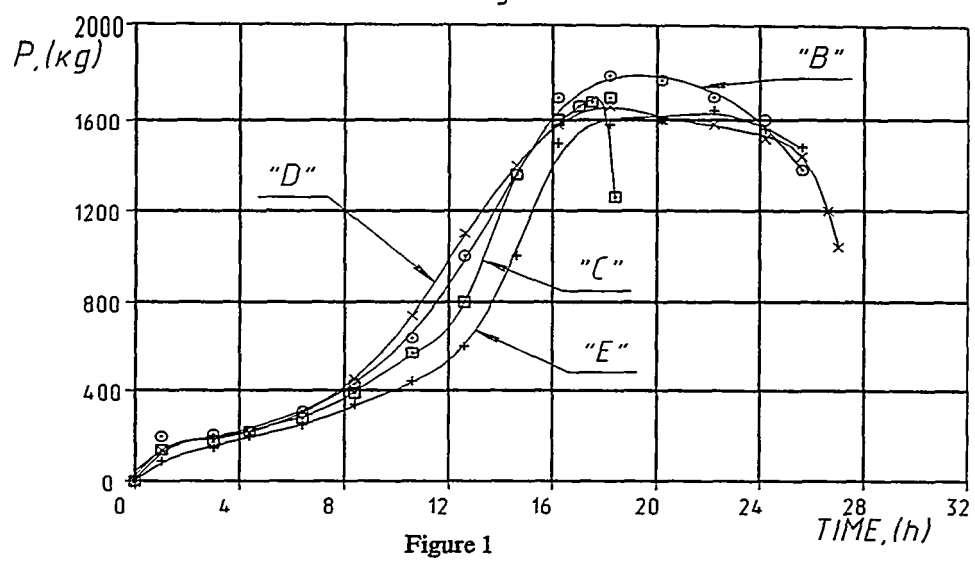
The technology of these tubes must include the vacuum annealing and double-computer non-destructive quality control welded tubes (ultrasonic + eddy current). The quality control welded tube must include the additional creep-corrosion test of the round specimen with full duration 18-24h at room temperature.

For the correct life assessment of condenser tube bundles it needs to use new criterion of mechanical fracture for real constructions.

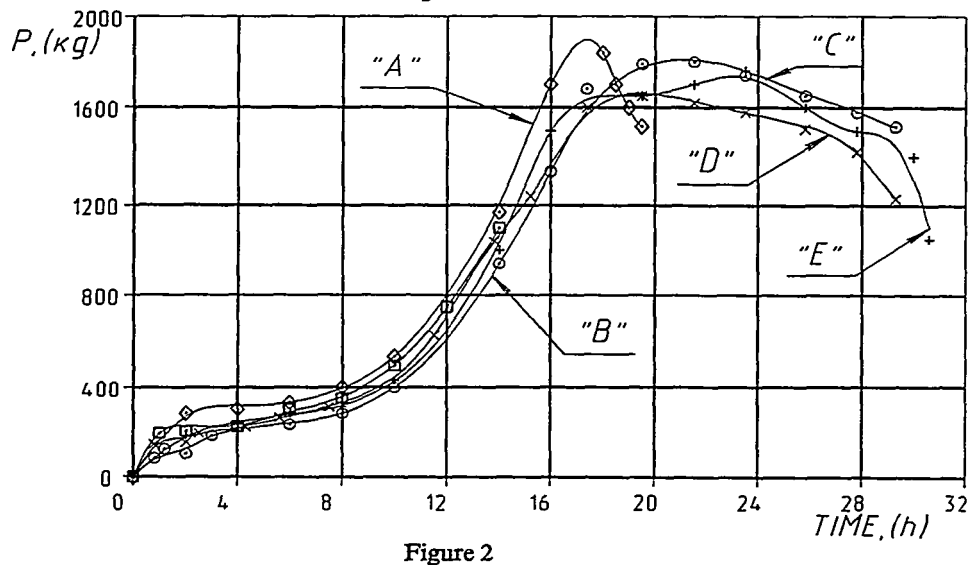
ACKNOWLEDGMENTS

The authors grateful to Prof. V. Regis (ENEL) and Mr David K. Peacock (Titanium Metals Corporation) for beneficial discussion the corrosion-mechanical properties of the condensers thin titanium tubes for the newly large steam turbines of fossil and nuclear power stations.

Tensile diagram of specimens
from VT 1-0 alloy in air at 20 °C



Tensile diagram of specimens
from VT 1-0 alloy in water solution at 20 °C



Header Integrity Assessment

Find Rotvel, ELSAMPROJEKT, Fredericia, Denmark
Claudio Sampietri, ENEL, Milano, Italy
Lieve Verelst, LABORELEC, Linkebeek, Belgium
Hans van Wortel, TNO, Apeldoorn, Holland
Li Ying Zhi, KEMA, Arnhem, Holland

Abstract

In the late eighties creep cracks in the nozzle-to-header welds of high temperature headers became internationally recognized as a problem in older steam power plants. To study the problem a 2¼Cr1Mo service-exposed header, which was scrapped due to creep damage, was made available for testing. A full-scale model was fabricated with partly repaired nozzle to header welds and then tested at increased temperature. Loads included internal pressure and system loads. Damage accumulation and creep crack initiation and growth were predicted and experimentally verified. Conclusions and the practical implications for power plant operation are described.

1 Introduction

In the late eighties creep cracks in the nozzle-to-header welds of high temperature headers became internationally recognized as a problem in steam power plants with more than 100.000 hours of operation. When cracks due to creep life exhaustion are diagnosed in nozzle-to-header welds the strategy is either to remove the cracks by grinding, to weld-repair the region cracked or to replace the complete component. Such strategies can be expensive in terms of repair and replacement costs, as well as in terms of loss of production and an increasing inspection frequency. A header integrity assessment programme (HIAP) was started to address these questions and to provide quantitative data to be used in assessments.

2 Header Investigated

The header shown on Figure 1 had been in operation for 130.000 hours in Unit 2 Boiler 5 at Fynsværket in Odense when it was decided to scrap it in 1990. The header was inspected for the first time in 1987 at the annual overhaul and creep damage was found in the welds between the nozzles and the header body. At nozzle 1 and 2 microcracks (Class 5 according to TRD

508) had developed. At nozzle 3 the damage was characterized as Class 3-4 and at nozzle 4 the damage was only Class 2. An inspection interval of 15.000 hours was recommended.

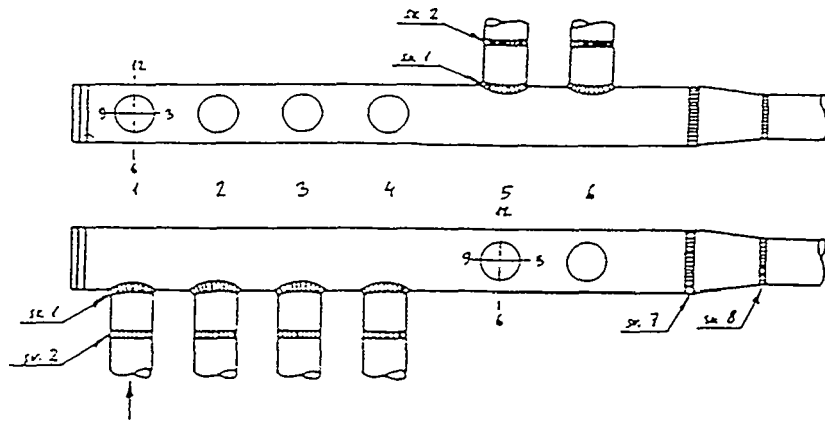


Figure 1. Header used for testing.

In the same couple of years, inspections on similar headers gave the impression of rapidly increasing creep damage and this information together with the observed creep damage on Fynsværket resulted in the decision to replace the header.

3 Header Cutting and Weld Repair

The header was cut between nozzles 2 and 3 (Figure 1). The section containing nozzles 1 and 2 was used to fabricate a full-scale model (Figure 2), while the other parts were used for materials testing. Nozzle 1 was left unrepaired, while nozzle 2 was repair-welded 360° using standard welding procedure. Groove design and groove position is shown on Figure 3. The repair weld was tested with MPI and US.

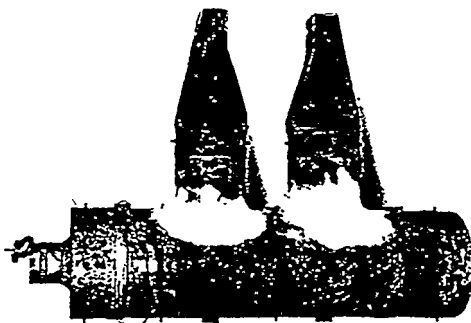


Figure 2. Overview of full-scale component with the loading arms on the nozzles to apply system loads.

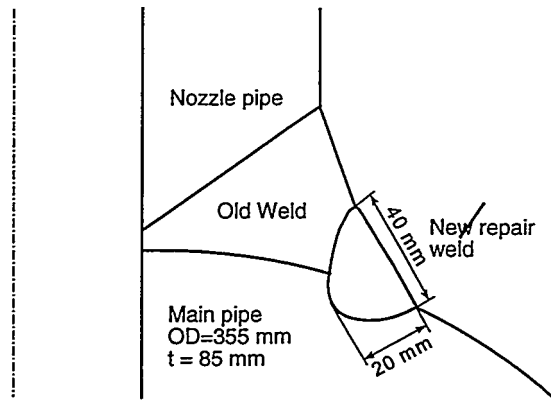


Figure 3. Repair weld groove design and position in the old weld.

4 COMPONENT EXPOSURE

4.1 Test conditions and inspections

The test conditions and the inspection intervals are presented in Table 1.

A total of 11 inspections were performed including:

- * Diameter measurements of the header body and the nozzles;
- * Displacement measurements between the nozzles;
- * Replication of the welded areas;
- * Magnetic Particle Inspection of the welded areas;
- * Potential drop measurements;
- * Final destructive inspection.

The system loads were generated by a cylinder placed between the nozzles. A constant force of 33.5 kN was applied, resulting in an extra stress of 24.5 MPa at the right angle points. The displacement between the 2 nozzles was continuously monitored during testing.

Table 1. Test conditions and inspection intervals of the component.

<p><i>Exposure period from 0 up to 8.000h:</i> Loads: T=620°C, p_i=185 bar (service pressure), no system loads Inspections at 0 - 2.000 - 4.000 - 6.000 and 8.000 hours</p>
<p><i>Exposure period from 8.000 up to 21.000h:</i> Loads: T= 620°C, p_i=185 bar, force between nozzles=33.5 kN Inspections at 9.750 - 11.500 - 13.000 - 15.000 - 18.000 and 21.000 h</p>

4.2 Results of component test

Deformation measured with creep pips. The deformation rate of the nozzles was more than double that of the header body (Figure 4). At the end of the test period (21.000h) the maximum deformations were:

Header body: 0.88%. Unrepaired nozzle: 1.5%. Repaired nozzle: 1.9%.

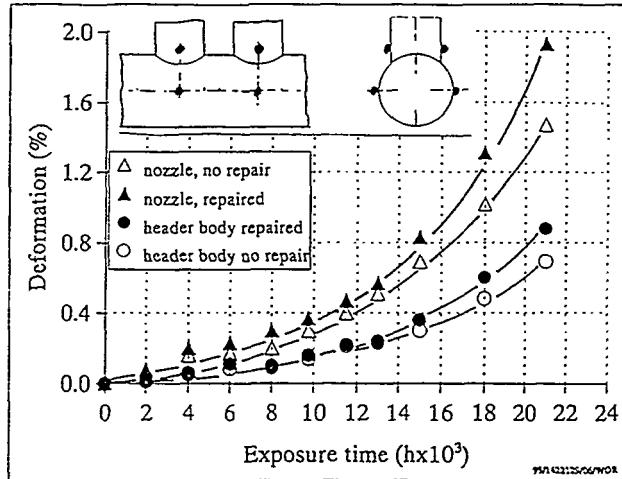


Figure 4. Deformation behaviour of the header body and nozzles at the locations of maximum deformation.

Deformation measured between the nozzles. The displacement behaviour between the 2 nozzles, as a consequence of the system stresses, is presented in Figure 5. Beyond 15.000h the displacement rate increases, as a consequence of the appearance of severe creep damage (cracks) in the right angles.

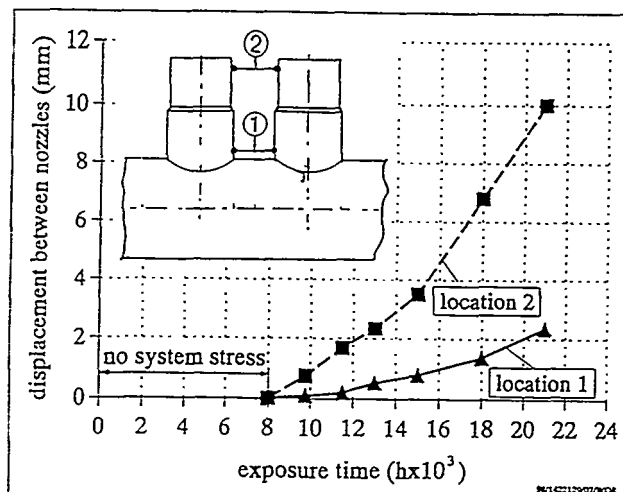


Figure 5. Displacements between the two nozzles during exposure. Locations 1 and 2 are 50mm and 220mm from the header body respectively.

Creep damage evolution measured with replicas. In the unrepaired T-joint the maximum creep damage for the base metal was class 2A and for the fine and coarse grained HAZ class 3A. Moreover, some small cracks were present in the weld metal and coarse grained HAZ. The length of these cracks was <5 mm and the depth <1mm. They were mainly located in the saddle point area. In the repaired T-joint the maximum creep damage was class 2 for base metal and class 3 for the unrepaired weld metal. In the repaired regions no cavitation was present. During the first 8.000h of exposure, without system stresses, the creep damage evolution was neglectable. The small already existing cracks did not grow and were even grinded out during the intermediate inspections. The cavitation evolution in depth between inspections was lower than the oxidation rate.

In the period 8.000-21.000h the creep damage evolution was, due to the applied system loads, remarkable enhanced. In the right angles, where the system stresses were the highest, the damage was more pronounced. The first visible cracks, detected after totally 11.500h, were located at the right angles. In the unrepaired T-joint the damage was predominant in the old weld metal and in the Fine Grained Heat Affected Zone (FGHAZ) of the nozzle. In the repaired T-joint the damage was predominant in the FGHAZ between the old metal and the repair weld and also in the FGHAZ of the nozzle. During further operation the creep damage progress constantly increased and moved towards the saddle points. The damage evolution is summarized in Table 2.

Table 2. Evolution of damage class according to VGB-TW 507.

Replica location:	Right angle, tensile side						Saddle points					
	unrepaired			repaired			unrepaired			repaired		
Nozzle:												
Inspection at (10 ³ h)	8	15	21	8	15	21	8	15	21	8	15	21
Base metal header	2A	2A	2A	2A	2A	2A	2B	2B	2B	2A	2A	2A
FGHAZ header	3A	3A	3B	2A	2B	3A	3A	3A	3B	2A	2A	2B
CGHAZ header	3A	3A	3A	2A	2B	3A	3A	3A	3B	2A	2A	2B
Repair weld	-----			2A	2A	2A	-----			2A	2A	3A
FGHAZ in old weld	-----			2A	5	5	-----			2A	5	5
Old weld metal	3A	5	5	3A	3A	5	3A	5	5	3A	3B	5
CGHAZ nozzle	3A	3A	3B	3A	3A	3B	3A	3A	5	3A	3A	3B
FGHAZ nozzle	3A	3B	5	3A	5	5	3A	3B	5	4	5	5
Base metal nozzle	2B	2B	2B	2B	2B	2B	2B	2B	2B	2A	2B	2B

Crack evolution determined with MPI. In both the unrepaired and the repaired T-joints the first macrocracks were detected after 11.500h exposure. In the repaired regions they were situated in the Fine Grained Heat Affected Zone (FGHAZ) of the old weld metal opposite to the new weld metal. In the unrepaired T-joint they were situated in the old (existing) weld metal. In the repaired T-joint more cracks were generated than in the unrepaired T-joint. After 15.000h exposure the first saddle point cracks were detected in the repaired T-joint, location FGHAZ of existing weld metal. In the unrepaired T-joint the first saddle point cracks were present after 18.000h, locations FGHAZ of the nozzle and old weld metal. During exposure the individual cracks were growing in length and finally grew together (Figure 6). They were predominantly situated in the tensile side of the right angle positions.

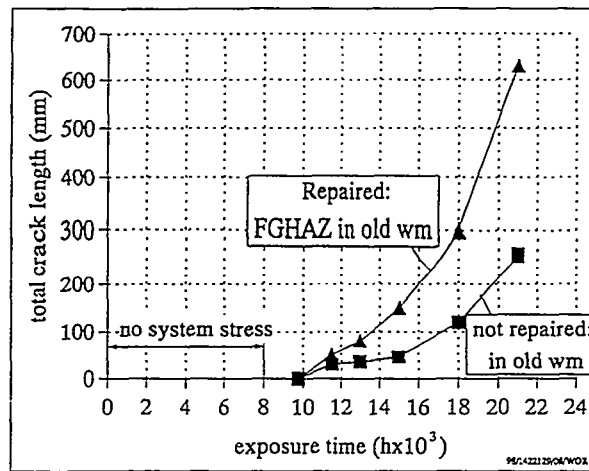


Figure 6. Creep crack growth evolution on the outer surface of the repaired and unrepaired T-joint, determined with MPI.

5 Finite Element Creep Calculations

5.1 Finite Element Model

The finite element model of the test component was three-dimensional utilising the symmetries in the geometry and the loadings. The model included base material and weld material with the aim to evaluate the effect of different creep rates. The heat affected zones were not included in the model.

The material creep data were measured on small specimens machined from parts of the header (Table 3). The FE calculations used a calibrated Norton law for the base material. The constants in the Norton law were chosen to fit the measured change in component diameter. The calibrated Norton law was within the scatter band of the measured Norton law.

Table 3. 2¼Cr1Mo service-exposed material creep laws.

Norton creep law: $\dot{\epsilon} = A\sigma^m$ Units: MPa,h		Base material	Weld material
Measured	A	$9.48 \cdot 10^{-21}$	$3.95 \cdot 10^{-15}$
	m	8.33	5.65
Calibrated	A	$1.0771 \cdot 10^{-19}$	
	m	8.00	

The finite element model was loaded with the same temperature and pressure as the full-scale component. System loads were applied after 8000 h as in the component test.

5.2 Results of Creep Analysis

Using the calibrated Norton law constants good agreement is found between measured and calculated diameter deformations up to about 13.000 hours (Figure 7). For longer test times, until 21000 h, better agreement would require taking into account the effects of crack formation and propagation.

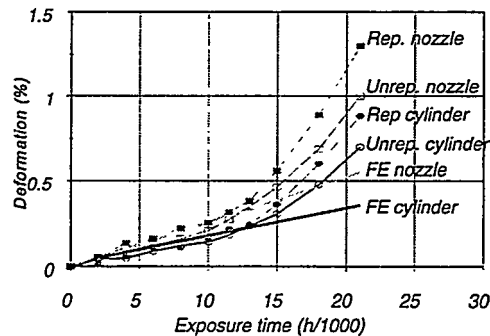


Figure 7. Comparison between numerical and experimental displacement.

At the high temperature used in the component test, stress relaxation occur very fast after load changes. As an example, the Tresca stress at outside nodes on the interface between base material and weld relaxes within 500 hours after load changes (Figure 8).

6 Calculations of Creep Damage

6.1 Prediction of Crack Initiation in Service

The stresses used in these predictions were calculated in a one-material finite

element model, the material data being taken from DIN 17175. The damage predictions also were based on DIN 17175 creep-rupture data. System loads were not included in the analysis.

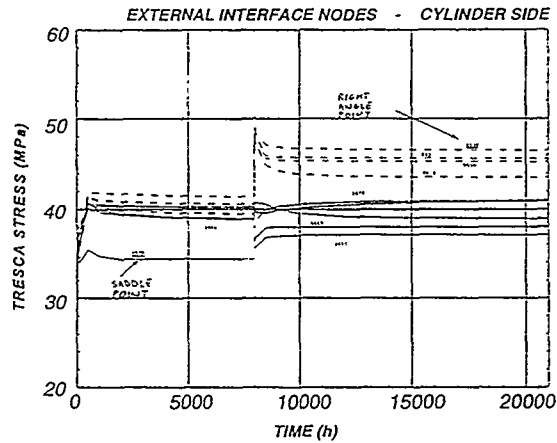


Figure 8. Tresca stress (MPa) vs. time (h) for outside nodes on cylinder side of the interface between base material and weld.

All the predicted times to crack initiation were much higher than the observed life for the real header (Table 4). Possible explanations for the discrepancy are:

- The header could have been subjected to large system loads.
- The one-material finite element model could be too simple to model actual creep behaviour and stress redistribution, especially at the heat affected zones.

Table 4. Predicted time to crack initiation and predicted damage after 130000 h.

Method of analysis	Saddle point		Right angle point	
	Outside t_i (h)	Outside $D_{130000 h}$	Outside t_i (h)	Inside $D_{130000 h}$
Sdobyrev [1]	474000		$2.7 \cdot 10^6$	
CEGB [2]	477000		$2.6 \cdot 10^6$	
Kachanov [3]		0.05		0.23
Kachanov-Lemaitre [4]		0.17		0.13
Rice-Tracey [5]		0.02		0.03

6.2 Predictions of Crack Initiation due to Test Exposure

Stresses versus time in key positions were calculated in a two-material (base metal and weld metal) finite element model. Creep rupture data used in damage calculations were measured on cross-weld specimens from repaired welds.

Predicted times to crack initiation are listed in Table 5. All the predictions include the effects of system loads applied after 8,000 h of testing. All the models for damage development predict that damage develops faster in the (new) HAZ in the old weld than in the base material.

Table 5. Time to crack initiation for the repaired weld at test conditions.

<i>Procedure</i>	<i>Saddle point</i>	<i>Right angle point</i>
Test observation	15.000-18.000	8.000-11.500
Sdobyrev [1]	13.500	14.200
Kachanov [3]	>15.000	14.300
Kachanov-Lemaitre [4]	8.500	3.400
Mixed [6]	13.600	8.700

Considering the fact that the scatter in the measured material data was large and also the fact that the finite element model of the weld was a crude approximation of the real weld, then the good agreement between observation and calculation for some of the procedures should be viewed with some precaution.

6.3 Prediction of Creep Crack Growth

Creep crack growth was calculated using the R5 procedure [7]. Initial cracks of 1 mm depth were assumed to be present in the right angle point and crack growth was assumed along the boundary between weld and base material of the cylinder i.e. in the radial direction of the nozzle. To account for the material inhomogeneity at a HAZ the calculated stresses were multiplied with 1.37 as recommended in R5.

For comparison the measured creep crack growth in the test component at the right angle position between 18.000 and 21.000 hr of testing was also used to calculate a time for penetration assuming constant creep crack growth rate.

The predicted time for the creep crack to penetrate the pipe wall agree reasonably well with the time estimated from measurements of crack growth (Table 6).

Table 6. Prediction of creep crack growth.

Procedure	Location	Type of crack	Load	Time for crack to penetrate (h)
R5	saddle point	type IV in HAZ	pressure	10.600-11.000
R5	saddle point	coarse grain zone	pressure	6.000-11.000
R5	right angle position	coarse grain zone	pressure + system load	6.200-8.900
Estimate from measurement	right angle position	type IV (HAZ in old Weld)	pressure + system load	8.000

7 Metallographic Examinations

Metallographic examinations were performed after 21.000 hours of component testing in order to determine the creep damage development through the wall thickness and to compare the non destructive creep crack depth measurements with the real crack depth.

The header was extensively examined at the right angle points and the saddle points of both the repaired and the unrepaired nozzle. An evaluation of the creep damage was performed based on the degree of creep cavitation according to VGB-TW 507. Figures 9 and 10 show macrographs taken from the welds.

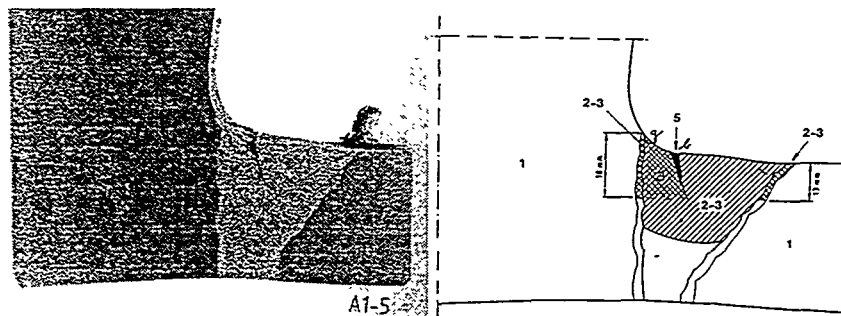


Figure 9. Right angle macrograph of the unrepaired nozzle.

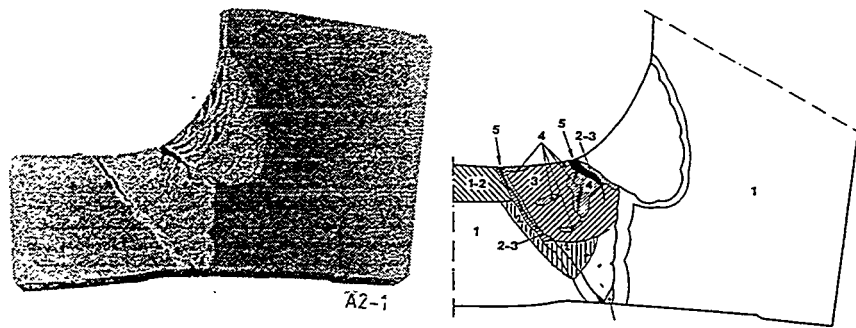


Figure 10. Right angle macrograph of the repaired nozzle.

The main findings from the examinations were:

- The level of creep damage (cavities and cracks) found in the repaired nozzle and in the unrepaired nozzle were almost comparable although the damages were observed in different positions.
- In the **unrepaired nozzle** the creep damage was mainly developed in the HAZ and the weld metal. Isolated and aligned cavities were found in the weld metal over half the wall thickness.
- In the **repaired nozzle** the creep damage was mainly located in the fine grained HAZ between the original weld and the weld repair. The creep damage in the original weld extended from aligned cavities to microcracks and extended to a larger depth. No creep damage was found in the repair weld.

Table 7. Crack depths measured on cross sections compared with potential drop measurements.

Crack id.	Depth measured on cross section	Depth measured with ACPD	Remarks
P1	6mm	3mm	narrow crack
C	15mm	6mm	narrow crack
A	15mm	1.2mm	narrow crack
K	23mm	26mm	wide crack
D	17mm	13mm	wide crack
P2	17mm	<1mm	extremely narrow crack

Crack depth evolution determined with potential drop. During the intermediate stops the crack depths were established with potential drop, without

knowing the reliability of the method. The final inspection showed that the potential drop measurements may severely underestimate the real cracks depths, especially for narrow cracks (Table 7). Care has to be taken by using the ACPD method for the determination of crack depth in practice.

8 Conclusions

The main results of the project are:

- The creep damage observed in the header could not have been caused by pressure loading only. System stresses have played a major role.
- Headers made of 2¼Cr1Mo are damage tolerant. Creep crack growth is slow and stable up to depths of more than half the wall thickness. It takes a long time from the moment a macrocrack is formed until it becomes critical.
- The effectiveness of weld-repair is questionable because a Fine-Grained Heat-Affected-Zone with low creep strength is created in the service-exposed weld material.
- The time to creep crack initiation and the header body deformation may be predicted quite accurately using one- or two-material finite element models.
- Predictions of creep crack growth based on the R5-procedure from Nuclear Electric (GB) are satisfactory.

9 References

- [1] V.P.Sdobyrev, *Izv.Akad.Nauk.SSSR, Otd.Tekh.Nauk*, Vol.4, p92, 1958.
- [2] R.A.Ainsworth et.al., "CEGB Assessment Procedure for Defects in Plant Operating in the Creep Range", *Fatigue Fract.Eng.Mater.Struc.*, Vol.10, No.2, 1987, pp 115-128.
- [3] L.M.Kachanov, "Time of the Rupture Process under Creep Conditions", 1958, *Izv.Akad.Nauk.SSR, Otdl Tech Nauk*, No. 8, pp 26-31.
- [4] J. Lemaitre, "A course on Damage Mechanics", Springer Verlag, 1992.
- [5] J.R.Rice, D.M.Tracey, "On the Ductile Enlargement of Voids in Tri-axial Stress Fields", *J.Mech.Phys.Solids*, 1969, Vol.17, pp 201-217.
- [6] R.Wu, R.Sandström, J.Storesund, "Through-Thickness Creep Damage in a Service-Exposed Header of 2.25Cr1Mo Steel". *Materials at high Temperatures*, No.3 Vol.10, 1992, pp 154-163.
- [7] R5 Assessment Procedure for the High Temperature Response of Structures, Nuclear Electric, 1992.

Predicting the Creep Life and Failure Mode of Low-Alloy Steel Weldments

J M Brear, C J Middleton and P F Aplin
ERA Technology Ltd.
Leatherhead, UK

Abstract

This paper reviews and consolidates experience gained through a number of research projects and practical plant assessments in predicting both the life and the likely failure mode and location in low alloy steel weldments. The approach adopted begins with the recognition that the relative strength difference between the microstructural regions is a key factor controlling both life and failure location. Practical methods based on hardness measurement and adaptable to differing weld geometries are presented and evidence for correlations between hardness ratio, damage accumulation and strain development is discussed. Predictor diagrams relating weld life and failure location to the service conditions and the hardness of the individual microstructural constituents are suggested and comments are given on the implications for identifying the circumstances in which Type IV cracking is to be expected.

1 Introduction

The creep life of components is frequently dominated by the behaviour of the welds. The association of microstructural complexity with the interaction between local and global stresses makes life prediction more difficult than for the regions of the component where the material is homogeneous and the geometry simpler. Preliminary calculation based on inverse use of design codes normally allows for welds by means of a straightforward efficiency factor. Inspection based methods rely on evaluation of damage accumulation and microstructural degradation. Both these approaches have their weaknesses; safety factors assume trends in long-term rupture behaviour which may not hold beyond design life and condition based methods require knowledge of the controlling physical parameters and access to the most critical areas for inspection.

In previous work (ref. 1) a mechanistic model for predicting creep life was presented which took account of both microstructural coarsening and creep cavitation. The cavitation was incorporated using a Kachanov approach whilst microstructural degradation was modelled in terms of interparticle spacing. As this combined model is quite complex, subsequent developments have tended to

treat damage and degradation individually. This present paper majors on the effects of precipitate strengthening effects.

The marked heterogeneous nature of particle dispersions in low alloy ferritic steels gives rise to difficulties when trying to obtain a non-subjective representative measure of the interparticle spacing. Consequently a non-subjective approach using hardness measurements was proposed for use in conjunction with the mechanistic model for creep life prediction (ref. 1).

A second line of work (ref. 2) specifically addressed Type IV failures in double-V preparation seam welded pipework. Here, a clear relationship was observed between the hardness difference between weld and parent metals and the susceptibility to creep cavity nucleation in the cusp region at the centre of the pipe section. Reasonable success was obtained in using surface hardness measurements to predict relative sub-surface damage levels and thus prioritise pipe spools for further inspection. Core samples could then be taken from critical positions to allow small specimen cross-weld tests to predict life. However, when attempts were made to extend this approach to other weld geometries - single-V, U and parallel sided - it was found to be unsuccessful. In these situations, the cavity nucleation rate was not dominated by local strength mismatch, but by larger scale stress controlling factors such as pipe ovality and system loads. For practical assessment purposes, full section cross-weld tests at mildly accelerated temperatures are used, with local strain gauges fitted and periodic, automated cavity density measurements.

Clearly there is a need to reconcile these approaches and to develop an integrated methodology for weld life prediction. The original creep model approach (ref. 1) has been extended to treat welds (refs. 3,4), and these developments have yielded some success at predicting weld life and failure location prior to the onset of Type IV cracking. This paper continues this line of research.

2 Modelling

2.1 Development of the model

The model is based on a Norton creep law, with a threshold stress term, σ_0 , which has its physical origin in the interaction between moving dislocations and precipitate particles:

$$\dot{\epsilon} = A \cdot \exp(-Q/RT) \cdot (\sigma - \sigma_0)^n \quad (1)$$

where σ is the applied stress, $\dot{\epsilon}$ the creep rate and A , Q and n are constants (refs. 1,5). The threshold stress is inversely proportional to the interparticle spacing, λ , but since this is problematic to measure directly, a relationship between threshold stress and hardness, H , is commonly accepted:

$$\sigma_0 = \alpha' \mu b / \lambda = K \alpha' (H - H_{SS}) \quad (2)$$

where α' is a geometric term, μ the shear modulus and b the Burgers vector.

H_{SS} is the contribution to the hardness due to solid solution strengthening and K defines the (well established) relationship between hardness and tensile strength. As the precipitates coarsen with time, t , at temperature, the hardness and threshold stress decrease in a manner which may be approximated, in the continuum limit, by the Lifschitz-Slyozov-Wagner-Greenwood kinetic:

$$\sigma_0 \sim (H - H_{SS}) \sim 1 / \lambda \sim t^{-1/3} \quad (3)$$

Subsequently the model was extended, for parent material, to yield an expression for the creep rate which included the effects of primary hardening - both kinematic and isotropic - and tertiary softening through both thermal and strain based mechanisms. If the applied stress, σ , is taken as the stress acting on a grain, rather than that on the specimen or component, then the normal Kachanov-Rabotnov type relationships for creep cavitation can be included, as can increases in stress due to overall changes in geometry consequent on deformation. Good agreement between the model predictions and experimental data has been demonstrated (refs. 3,4).

It would be possible, and informative, to calibrate the model separately for weld metal, the various regions of the heat affected zone and the parent material and use it within a finite element program to model weld behaviour in detail. This would, however, be prohibitively expensive as a routine assessment method and some practical simplification is required. The following approach has been adopted (refs. 3,4):

Assuming a Monkman-Grant relationship:

$$\dot{\epsilon}_m \cdot t_r = \epsilon_s \quad (4)$$

and making some bold but realistic assumptions as to the minimum value, ϵ_m , of the creep rate, the rupture life can be approximated by:

$$t_r \approx (\epsilon_s / \dot{\epsilon}_0) \cdot (\sigma / KH)^{-n} \quad (5)$$

where H is the initial hardness. This simplified treatment thus generates a relationship between rupture life (which may be temperature compensated) and the ratio of stress to strength. It is simply a modification of the conventional stress rupture plot with the data points normalised according to the hardness of the individual heats of material.

2.2 Experimental validation

Various heats of virgin, laboratory aged and ex-service 2.25Cr1Mo steels were procured for this work so as to allow testing of welds in the virgin condition, ex-service welds and 'repair' welds in ex-service material. Some of the virgin welds were laboratory aged to simulate service. In all cases matching 2.25Cr1Mo filler material and current welding practices were used. The majority of welds studied had been sub-critically stress relieved. A few renormalised welds were included among the ex-service samples.

All materials were fully characterised metallographically. Tensile and creep testing of parent and weld metals was performed and cross-weld creep tests were carried out on both small (10-15 mm diameter) and large (30-60 mm square) specimens, the latter being equipped with local strain gauges. Small specimens were tested under vacuum and the large cross-weld tests were interrupted periodically to allow replication. All hardness measurements reported were obtained using a conventional Vickers indenter, at 30kg load, on surfaces prepared to replication standard finish.

3 Results and Discussion

3.1 Rupture life and creep rate

Figure 1 shows data from a variety of parent, intercritical and coarse grained heat affected zone and weld metal specimens, over the ranges 20-125 MPa, 575-720°C and 50-27000 hours, plotted according to equation 5 (with temperature compensation of the rupture lives). A two-slope Kachanov model fit to the parent material data is shown, the different slopes corresponding to the flow controlled and damage controlled regimes. Stress sensitivities of 7 and 4 respectively and a common apparent activation energy of 440900 J/K/mol are in accordance with previous work and imply a true creep rate stress dependence of 4, a true activation energy of 25200 J/K/mol and a primary hardening coefficient of 1.75 (ref. 6).

The rupture data for the constituent microstructures of weldments were obtained from simple tests on weld metal, coarse grained or intercritical heat affected zone material and from small cross-weld specimens showing weld metal failure. They thus represent the behaviour of the individual microstructures, uninfluenced by interactions or constraint effects. The results fall into two groups. For sub-critically heat treated welds, there is no discernible difference between weld metal and coarse grained heat affected zone material; the data from these seem adequately represented by a simple transposition of the parent material lines. Rupture lives of intercritical heat affected zone material lie on the parent material line. Examination of the data reveals that, throughout the range of available information, equal rupture strengths for weld and parent metals are achieved at a hardness ratio of weld/parent of 1.423. By contrast, data for renormalised weld

metal and renormalised coarse grained heat affected zone material fall on the parent material line, implying equal strengths at equal hardnesses.

As a further illustration of the difference in behaviour between sub-critically heat treated and renormalised welds, and as a confirmation that the simplified rupture life model (equation 5) is adequate, Fig. 2 shows comparative strain rate information. The curves represent the fully developed creep rate model (refs. 3,4); the data points are obtained from local strain gauges affixed to the larger cross-weld specimens. Though the restricted range of test conditions (resulting from the requirements of the plant assessments for which these tests were carried out) leads to the data being somewhat clustered, the points do lie broadly on the model lines. The difference in hardness ratio for equal creep strength between the two post weld heat treatment conditions is clear.

Having noted this difference between sub-critically heat treated and renormalised welds, the remainder of this paper addresses the former only.

3.2 Failure location

From the separation between the parent and weld metal rupture lines in Fig. 1, it is possible to construct a weld predictor diagram, Fig. 3, showing the equal strength condition as a diagonal line on a weld versus parent hardness plot. On either side of this line, the relatively weaker component is predicted to fail first. Points defining an individual weldment may be plotted on this graph and from their position the failure location may be predicted. A weldment is shown as a vertical line representing the weld metal and coarse grained heat affected zone hardnesses (vertical axis) plotted against the parent material hardness (horizontal axis). Points above the line indicate that the weld metal is stronger than the parent metal and therefore failure in the parent material is to be expected. The converse applies below the line. Where the weld metal and coarse grained heat affected zone differ significantly in hardness, or show marked internal variation, it is the relatively weakest region that dominates.

All the cross-weld data from specimens that show clear parent, coarse grained heat affected zone or have been plotted on this diagram and it is seen that (with one borderline exception) all failures have occurred in the region predicted. The graph as shown is stress and temperature independent. At a specific pair of conditions, rupture life contours can be added to enable life and failure location prediction for a given weldment.

At longer times, the situation is complicated by the occurrence of Type IV cracking (in the intercritical region of the heat affected zone). By its long-term nature, this failure mode is difficult to achieve in laboratory testing, however a mix of research and plant assessment work has generated some results at 600 and 620°C. Even in programmes where this failure mode has not been directly observed, the tests performed have, nevertheless, enabled some progress to be made in estimating the temperature dependence of its onset.

Figure 4 replots the cross-weld data of Fig. 3 on a temperature time plot and adds results from those tests that failed by Type IV cracking. The actual Type IV failures at 600 and 620°C and their absence in the timescales achieved at 575, 585, 595°C serve to pin the Type IV failure boundary more or less exactly, at least in the temperature range 575 - 620°C. From this graph, a time-temperature parameter for the onset of Type IV failures can be derived. It is interesting that the value of activation energy is almost exactly $Q/4$, where Q is the same as that required for equation 5 and Fig. 1. The significance of the factor 4 in the temperature dependence of Type IV failures is not understood.

A second type of weld failure predictor diagram can now be constructed, it is shown in Fig. 5. Here, the vertical axis represents weld to parent metal hardness ratio. Thus the diagonal equal strength line of Fig. 3 becomes a horizontal line. The abscissa is the time-temperature parameter derived from Fig. 4. Three regions are generated. At shorter times, the failure location varies from parent to weld metal (or coarse grained heat affected zone), dependent solely on the relative hardnesses. At longer times, Type IV failures occur, independent of hardness ratio. In all three regions, stress (at least in the range studied) controls life, but not failure location. There are insufficient results at present to construct a rupture life plot for the Type IV failures.

4 Conclusions

The findings of the present work confirm the validity of the hardness based creep model and the application of a simplified version to weldments. The role of relative strength difference in controlling short-term failure location can now be considered well established and appropriate use made of the predictor diagram.

So far as Type IV failures are concerned, the strong time-temperature dependence and lack of hardness ratio effects for most weld geometries seem clear, but require further validation and a fuller understanding of the details needs to be developed. It is also necessary to explore the boundary between the behaviour observed in the present work and the role of hardness previously reported in the more highly constrained double-V welds.

The approach suggested here also requires extension to other materials, low alloy steels such as 1Cr0.5Mo and 0.5CrMoV and, perhaps more importantly, the standard and advanced 9Cr and 12Cr steels.

5 Acknowledgements

This paper is published with the permission of ERA Technology Ltd. Thanks are due to numerous colleagues, at ERA and several collaborating organisations, for stimulating discussions and for access to test material and data.

6 References

- 1) Cane, B J., Aplin, P F and Brear, J M
A probabilistic approach to remanent creep life assessment of low alloy ferritic components
4th Int Conf on 'Creep', JSME, IMechE, ASME, ASTM, Tokyo, April 14-18, 1986, p447
- 2) Bissell, A.M., Cane, B.J. and Delong, J.F.
Remanent life assessment of seam welded pipework
Int Conf 'Life assessment and Extension' VGB, KEMA, CRIEPI, EPRI
The Hague, June 1988
- 3) Tack, A.J., Brear, J.M. and Seco, F.J.
Mechanistic creep modelling for weldment life prediction
Fifth Int Conf 'Creep of Materials', Orlando, Florida, May 1992
- 4) Brear, J.M., D'Angelo, D., Seco, F.J. and Tack, A.J.
Mechanistic creep models for 2.25CrMo welds and parent metal
ERA European Conf 'Life Assessment of Industrial Components and Structures'. Cambridge, October 1993, Paper 4.3
- 5) Cane, B J., Brear, J M and Aplin, P F
Condition Assessment of High Temperature Plant
Third Int Conf 'Creep and Fracture of Engineering Materials and Structures'
Swansea, April 1987, Published Inst Metals, London 1987, pp 853-868
- 6) Brear, J.M. and Aplin, P.F.
Rationalisation of high minimum creep rate stress exponents and activation energies in the Norton creep law through incorporation of primary and tertiary creep effects
Proc. Fifth Int Conf 'Creep and Fracture of Engineering Materials and Structures'.
Swansea, April 1993, Published Inst Metals, London 1993, pp 73-79

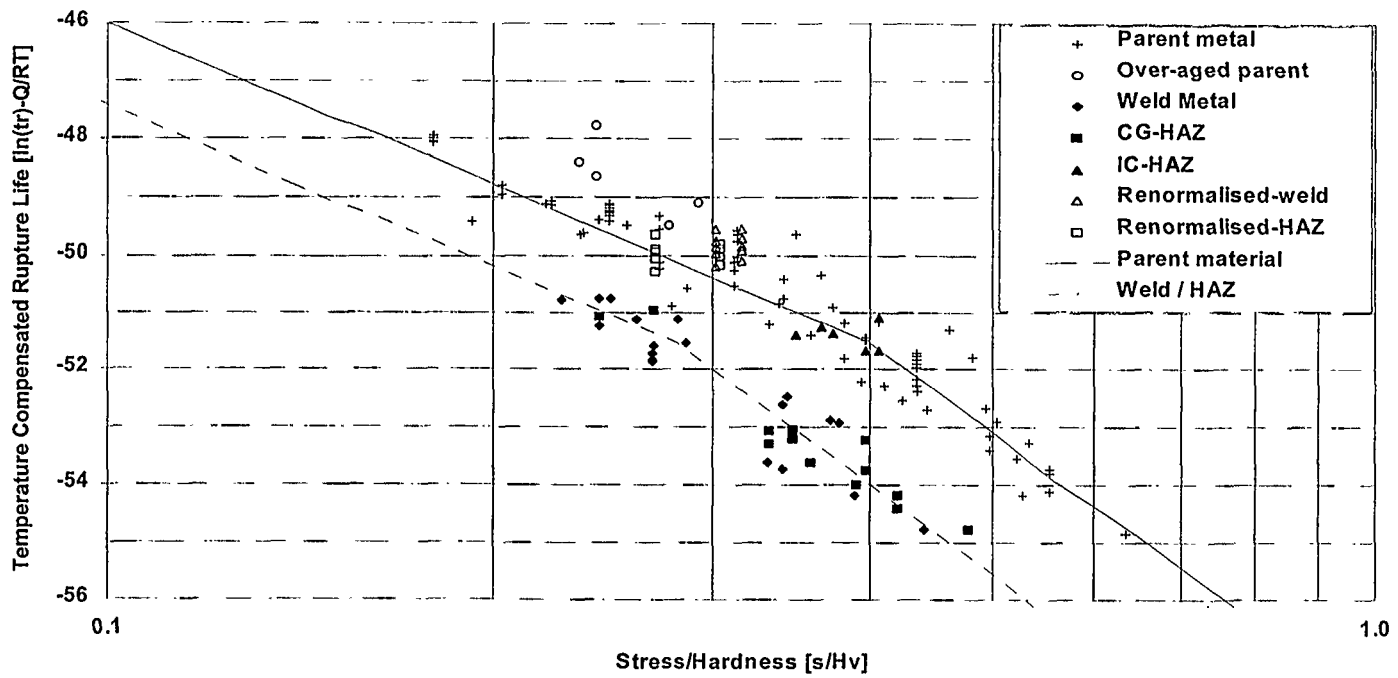


Fig. 1. Hardness compensated creep rupture data for 2.25Cr1Mo steels tested in vacuum.

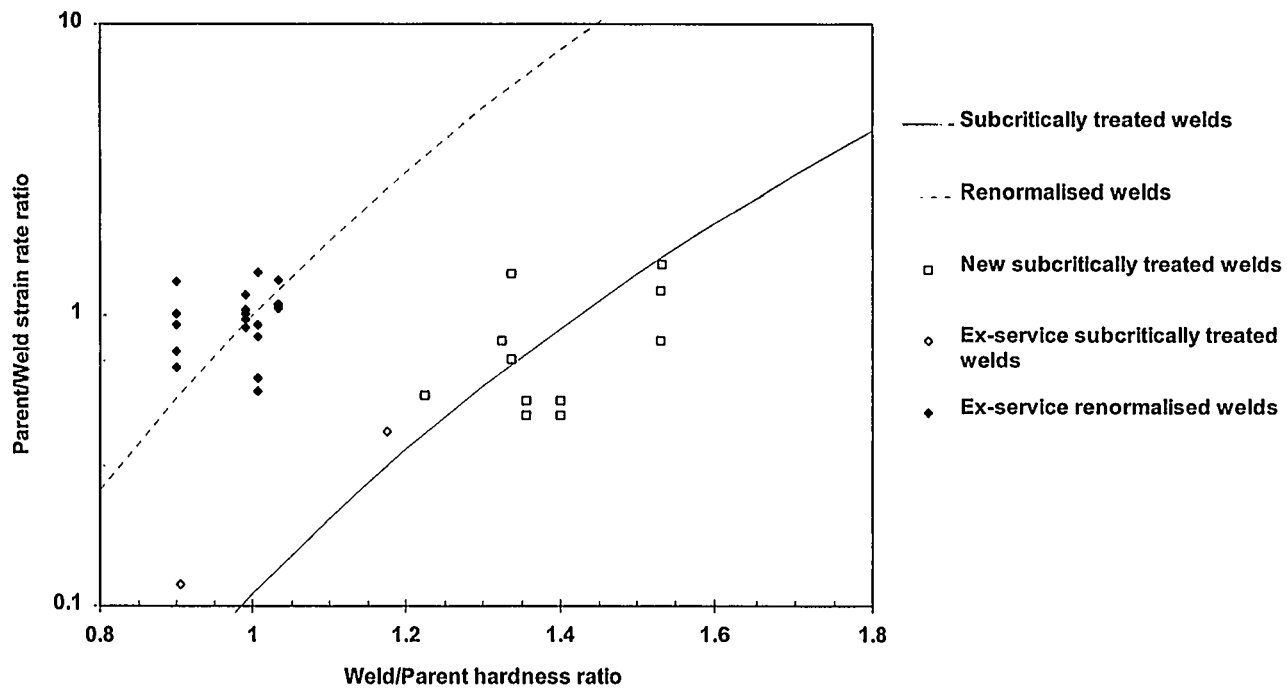


Fig. 2. Relationship between creep rate ratio and hardness ratio for large cross-weld specimens of 2.25Cr1Mo steel.

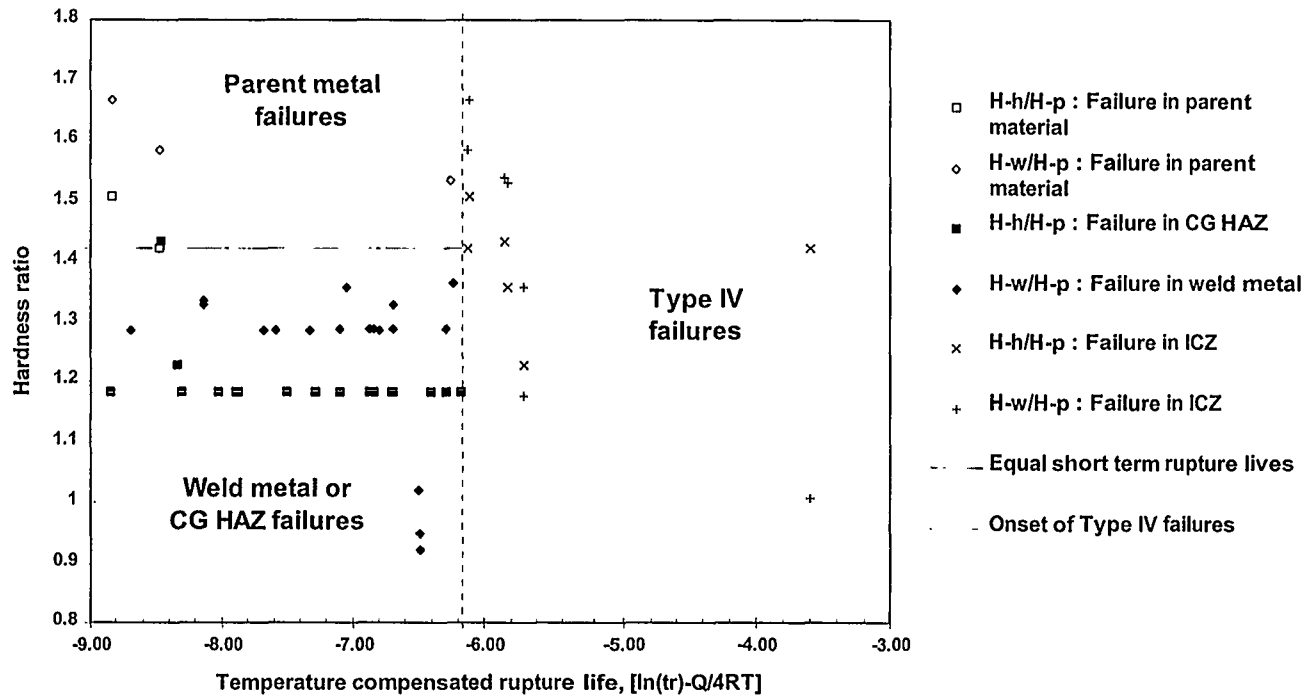


Fig. 5. Weld failure location predictor diagram, including the Type IV cracking regime, for 2.25Cr1Mo steel.

Type IIIa Cracking at 2CrMo Welds In ½CrMoV Pipework

S J Brett and P A Smith,
National Power plc, Swindon, UK.

Abstract

The most common form of in-service defect found today on the welds of National Power's ½CrMoV pipework systems is Type IV cracking which occurs in intercritically transformed material at the edge of the heat affected zone. However an alternate form of cracking, termed IIIa, which occurs close to the weld fusion line in fully grain refined heat affected zones, has also been observed. The incidence of Type IIIa cracking has increased in recent years and these defects now constitute a significant part of the total recorded crack population. This paper describes Type IIIa cracking and compares and contrasts it with the better documented Type IV cracking. Particular reference is made to the role of carbon diffusion at the weld fusion line in promoting Type IIIa damage in preference to Type IV.

1 Introduction

National Power currently owns and operates approximately 12 000 MW of coal-fired plant in the UK with high temperature steam pipework systems manufactured from ½CrMoV steel welded with 2CrMo weld metal. Typical operating conditions are 565°C and 175bar, with the oldest units having been in service for 180 000 hrs.

During the 1960s and 1970s welds on CrMoV pipework systems in the UK were frequently associated with reheat or stress relief cracking problems. With increasing age of plant however this form of cracking has given way to longer term creep mechanisms, sometimes referred to as "mid-life" cracking [1][2]. The most familiar form, termed Type IV after the classification system first introduced by Schüller et al [3], occurs in material intercritically annealed by the weld heating cycle at the limit of the parent heat affected zone (HAZ) and has been well documented.

However a second form has also been encountered, occurring close to the weld fusion line in HAZ that have been fully grain refined by the welding process (Fig. 1). While initially these cracks were classified as Type III they were later called Type IIIa in order to distinguish them from the earlier reheat cracks which could also be found at this location.

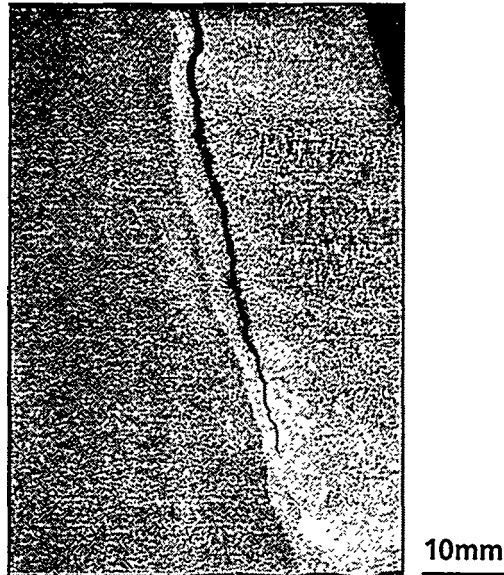


Fig. 1. Type IIIa crack in a $\frac{1}{2}$ CrMoV butt weld.

Reheat cracking was shown to be a result of high residual welding stress caused by inadequate stress relief. Type IIIa cracks, like Type IV cracks, are considered to be largely unaffected by residual welding stress and to be driven primarily by long range pipework system stresses. However, whereas Type IV cracking can be explained in terms of the weak creep properties of intercritically transformed material at the limit of the HAZ, Type IIIa cracking has remained more difficult to explain. In particular it has never been clear why the Type IIIa region should ever be weaker than the Type IV region in the same parent.

2 Type IIIa Cracking Incidence

The $\frac{1}{2}$ CrMoV systems on coal-fired stations operated by National Power contain about 7600 large butt welds with approximately 300 large branches, and thousands of small branches and attachments. Over the years a detailed hierarchical weld inspection strategy has been developed on the basis of observed cracking experience and pipework stress analysis. For the purposes of this paper however the butt weld population can be divided into two broad

groups, high inspection category welds, which are mainly terminal welds at the ends of pipework runs, and low inspection category welds, which are mainly plain butt welds in the middles of pipework runs. There are approximately 1000 high category welds and 6600 low category welds.

In the following table the observed incidence of weld repairs for Type IIIa defects is compared with those for Type IV defects for National Power's current coal-fired plant. Only repairs which have been confirmed by metallurgical investigation to be caused by either Type IV or IIIa defects are included. Repairs for other reasons are ignored. A total of 335 repairs recorded to date are included which constitutes just over 4% of the weld population. It should be emphasized however that the table is a summary and masks significant variation in the cracking patterns between stations and, in some cases, between units within stations.

Table 1. Weld repairs for Type IV or IIIa cracks and pre-crack damage.

Reason for Weld Repair	High Category eg terminal welds	Low Category eg plain butt welds	Totals
Type IV cracks	60	27	87
Type IV damage	84	92	176
Total Type IV	144	119	263
Type IIIa cracks	13	23	36
Type IIIa damage	0	36	36
Total Type IIIa	13	59	72
Total repairs	157	178	335
Total cracks	73	50	123
Total damage	84	128	212

In the table a distinction is made between repairs for fully developed cracks, usually found by standard non-destructive testing methods (ultrasonics or magnetic particle) and pre-emptive repairs for pre-cracking damage, usually found by metallurgical replication. (A more detailed discussion of this aspect is given in Section 3).

The table shows that repairs for Type IIIa cracks or damage tend to be more prevalent in low inspection category welds. 33% of the repairs carried out on this weld category have been a result of Type IIIa cracks or damage, whereas only 8% of repairs to high inspection category welds have been caused by Type IIIa. If cracks alone are considered 64% of Type IIIa cracks found have

been found in the low inspection category welds, compared to 31% of Type IV cracks. Almost half the cracks found in low inspection category welds (46%) were Type IIIa.

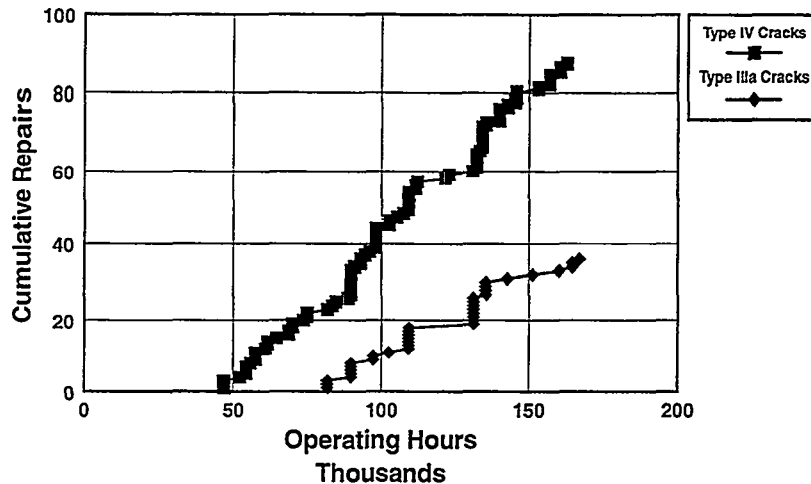


Fig. 2. Butt weld repairs for Type IV and IIIa cracks as a function of operating hours (current coal-fired plant).

Fig. 2 compares the relative incidence of Type IV and IIIa cracks in terms of the operating hours at which each crack was discovered. It can be seen that whereas Type IV cracks have been found from approximately 50 000 hrs onwards, Type IIIa cracks have tended to be found somewhat later. It should be noted however that this is partly a result of less frequent inspection of low category welds for the weld population being considered. Within the wider UK experience the earliest examples of Type IIIa cracks were observed about the same time as the first Type IV cracks.

3 Type IIIa Crack Morphology

The progression from cavitation to cracking is similar for both Type IV and IIIa defects. Cavitation initiates and increases in density leading to the formation of micro-cracks, each individually orientated perpendicular to the axial pipe direction, ie the maximum stress direction where significant system stress is present. The micro-cracks grow until they overlap and are able to link up to form macro-cracks. Type IIIa cracks are similar to Type IV cracks in that they tend to initiate just below the surface of a weld at the first weld bead below the surface capping bead. At this location the fusion line, and hence the Type IIIa zone, is orientated nearly perpendicular to the axial stress direction and it is easier for cavitation damage to progress to micro-cracking and subsequent macro-cracking. At the capping bead itself the fusion line intersects the surface

at a shallow angle, ie at a high angle to the axial stress direction where micro-crack formation and link up is more difficult.

Once initiated Type IIIa cracks, like Type IV cracks, may grow to substantial size before breaking out to the surface (often through the capping bead rather than along the fusion line). Approximately two thirds of Type IIIa cracks found on National Power's current plant were still subsurface when discovered and the largest subsurface crack had reached 64% through-wall extent.

Type IIIa cracks occur at, or very close to, the weld fusion line in HAZ that have been fully refined by the welding process. The local grain size is typically $5\ \mu\text{m}$. It is ironic that such fine grained structures, which are highly desirable in terms of their resistance to reheat cracking and are the basis of the welding techniques developed for this purpose, should have apparently resulted in increased vulnerability to an alternative cracking mechanism in the longer term.

In some respects Type IIIa cracks represent a "mirror image" of reheat cracking. Whereas reheat cracks tended to originate in the coarsest HAZ grain structures and were often observed to become inhibited when they grew into adjacent fine grained regions, Type IIIa cracks tend to exhibit the opposite behaviour. Where mixed HAZ structures are present the cracks initiate in the fine grained regions but may arrest as they grow into coarser regions.

Peak levels of Type IIIa creep cavitation are usually found in a distinct band extending from the fusion line up to approximately $100\ \mu\text{m}$ into this refined grain structure (Fig. 3).

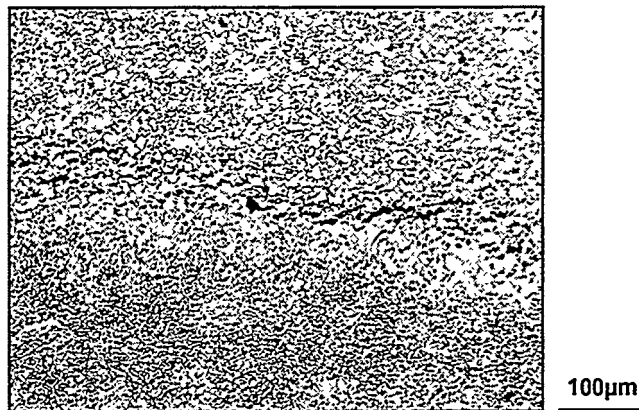


Fig. 3. Type IIIa cavitation and micro-cracking adjacent to the fusion line.

Micro-cracks and subsequent cracks usually form within this band, parallel to the fusion line and displaced a few grains into the HAZ.

Occasionally the defects are found at the fusion line itself, (Fig. 4) particularly where particles of welding slag are present to act as points of initiation. It should be noted however that slag particles are not a pre-requisite for cracks to develop. The majority of Type IIIa cracks found have not been associated with any observable slag at the fusion line.

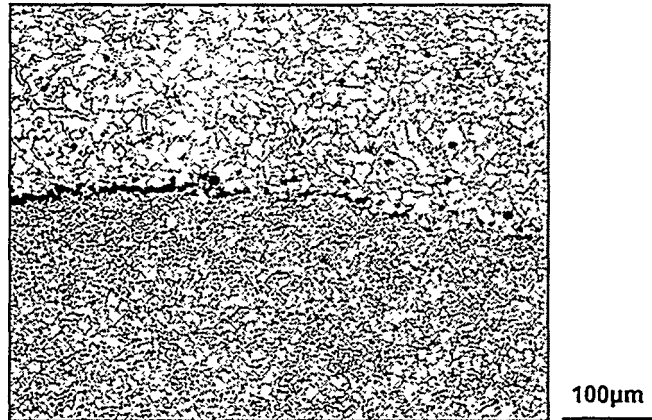


Fig. 4. Type IIIa cavitation and micro-cracking at the fusion line.

A high proportion of Type IIIa defects are found at the micro-cracking stage, in sharp contrast to the experience with Type IV cracks. For the purposes of this analysis micro-cracking is defined as a through-wall extent less than that of a weld bead (~2mm on a typical butt weld sidewall). This corresponds broadly to a distinction between those cracks which can be reliably found by standard ultrasonic inspection techniques and those for which specialised ultrasonic probes or metallurgical replication techniques are required. The appearance of significant numbers of Type IIIa micro-cracks suggests that some barrier exists to crack development beyond a weld bead dimension. Once Type IIIa cracks develop beyond this point however they appear to behave indistinguishably from Type IV cracks. This is illustrated in Fig. 5 which compares the through-wall dimensions of Type IV and IIIa cracks (micro-cracks are not included). While a difference exists at the smallest size, it can be seen that both varieties of crack exhibit the same size profile thereafter.

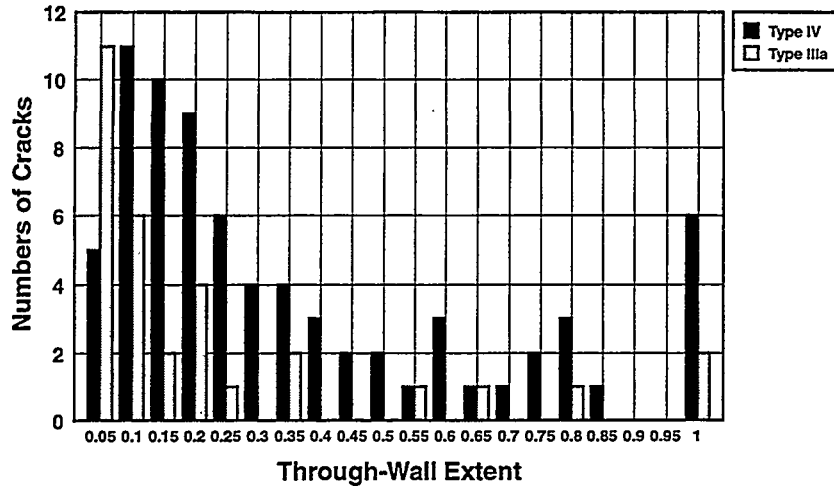


Fig. 5. The through-wall size distributions of Type IV and IIIa cracks found on current coal-fired plant

In terms of crack growth rate it appears that once Type IIIa cracks develop beyond the micro-cracking stage they grow at the same rate as Type IV cracks. The mean through-wall growth rate has been estimated to be 1mm/1000hrs for an average crack increasing to 3mm/1000hrs for the fastest growing cracks.

4 Carbon Diffusion Investigations

Historically within the UK Electricity Supply Industry CrMoV parents have been welded with 2CrMo weld metal. While these welds have not usually been regarded as dissimilar metal welds, a significant compositional difference is present. Work by Kimmins and Longley [4] demonstrated that Type IIIa cracks found in welds after long term service at high temperature were associated with depletion of carbon near the fusion line.

Subsequent investigation by Smith [5] demonstrated that the depletion could occur over an unexpectedly long range. A neutron microprobe carbon profile taken from a 2CrMo/½CrMoV test weld typical of welds in service is shown in Fig. 6. The test weld was given a normal post weld heat treatment and an artificial ageing to simulate service operation. Significant carbon loss extends to well beyond the HAZ. Another important feature shown is a distinct carbon peak just within the weld metal. The resulting mismatch in properties at the fusion line was cited as a further important factor in the initiation of Type IIIa damage.

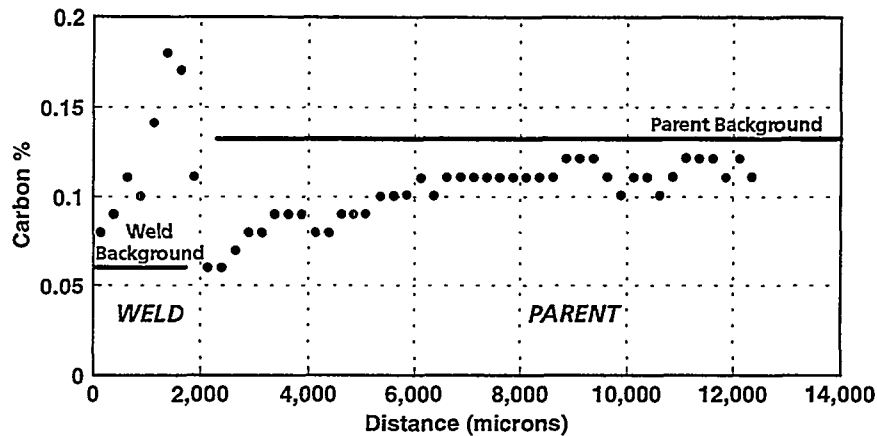


Fig. 6. Carbon profile for a 2CrMo weld in $\frac{1}{2}$ CrMoV pipe after post weld heat treatment and ageing for 884 hours at 642°C (measurements by neutron microprobe).

A survey of carbon contents was carried out on a wide range of samples taken from National Power's $\frac{1}{2}$ CrMoV pipework to establish whether such long range diffusion was typical of welds in service. The results are illustrated in Fig. 7.

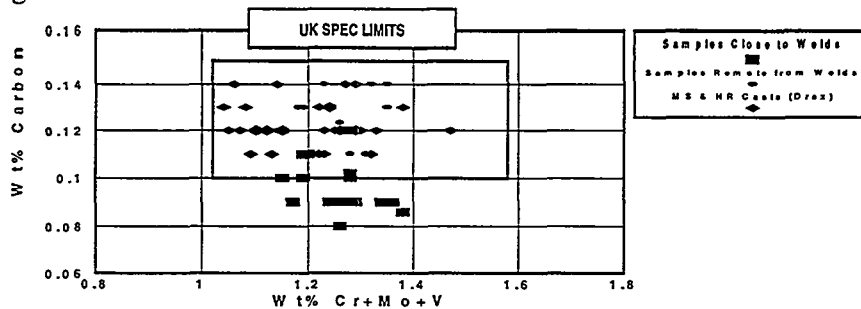


Fig. 7. Compositions of National Power $\frac{1}{2}$ CrMoV pipe.

Carbon measurements obtained away from welds, either from manufacturing records or from samples known to be taken on parent material remote from welds, showed levels within the UK specification range for wrought pipe (0.1-0.15%). Measurements on boat samples obtained at welds however, even when confined to parent material at the edges of the samples (typically 5-10 mm away from the fusion line) showed consistently lower values. In some cases the values were lower than the minimum specification level. It was concluded that long range carbon diffusion was widely present and that the boat samples were not sufficiently large to escape the effects.

The survey indicated the need for more detailed analyses of individual welds. The existence of diffusion on such a scale made possible the use of standard industrial techniques, more flexible and convenient than the neutron microprobe. It was found possible to cut thin slices of material at progressively increasing distance from the fusion line and to analyse them for carbon by combustion followed by infra-red detection of CO₂. Using this approach care has to be taken to avoid intersecting the fusion line during sectioning, since the carbon enrichment just within the weld metal (as shown in Fig. 6) will give rise to anomalously high carbon. The technique is therefore limited to investigation of the parent.

Table 2. Ex-service welds investigated for carbon depletion.

Weld	Operating Hours (565°C)	Pipe System	Comment
Station A Unit A Weld 1	89,700	Main steam	Large Type IIIa crack
Station A Unit A Weld 2	109,200	Main steam	Large Type IIIa crack
Station A Unit B	105,300	HP loop	Type IIIa micro-crack
Station B	123,000	HP loop	Undamaged - weld repaired as part of flange replacement
Station C	176,800	Main steam	Undamaged - weld repaired as part of header replacement
Station D	106,500	Hot reheat	Undamaged - weld repaired as part of pipe replacement

A total of six ex-service welds were available for this exercise, as detailed in the above table. All were ½CrMoV wrought pipe which had operated at 565°C. Three of the welds had experienced Type IIIa cracking to a greater or lesser extent, the other three had not. The six welds were taken from a total of five units distributed across four stations and represent several different types of pipe system.

The carbon profiles obtained from welds taken out of service are shown in Fig. 8. All show a systematic fall in carbon level as the fusion line is approached.

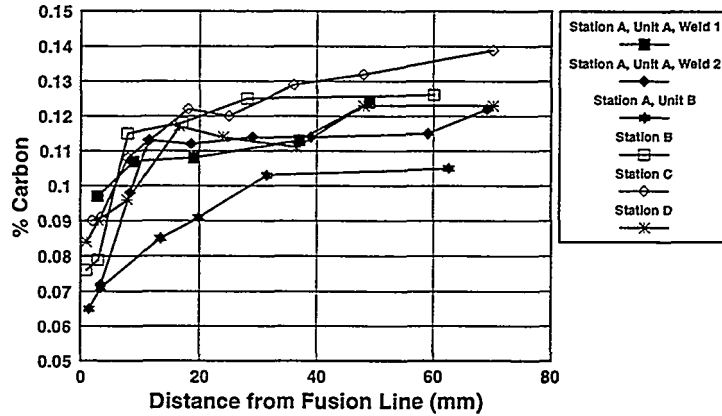


Fig. 8. Carbon profiles obtained adjacent to six ex-service welds (measurements by combustion followed by infra-red detection).

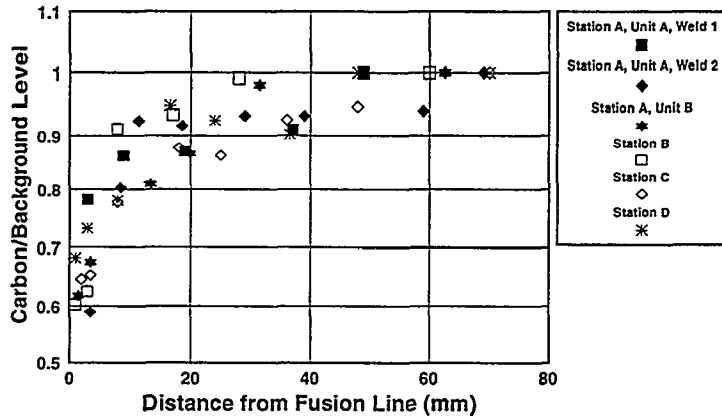


Fig. 9. Normalised carbon profiles (values divided by background for each parent).

In Fig 9 the profiles are each normalised by the remotest measurement available in each case, ie the measurement taken furthest from the fusion line. It can be seen that carbon level has fallen to 90% of background at approximately 20mm from the fusion line and 80% of background at a little under 10mm.

The normalised value of carbon level at a set distance of 10mm from the fusion line, taken from each profile, is plotted against operating hours in Fig. 10. No carbon loss is detectable at this location (using the analysis techniques adopted here) for welds entering service. An additional normalised carbon level of 1.0 has therefore been incorporated at zero time. While considerable scatter is present, there appears to be a tendency for the values to decrease with time, ie for carbon depletion to increase with length of time in service.

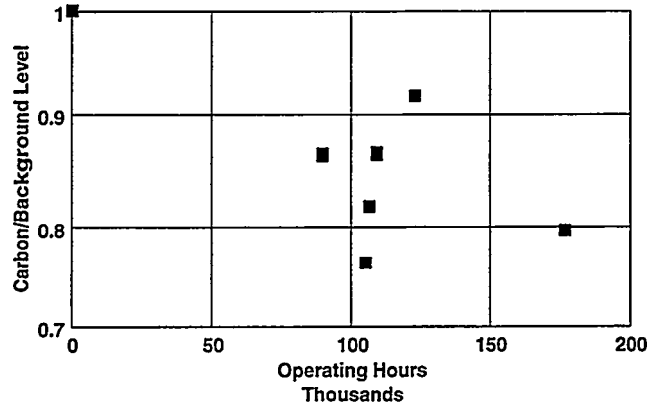


Fig. 10. Normalised carbon level at 10mm from the fusion line with time at 565°C

5 Implications for Future Operation

In the as-welded and/or post weld heat treated condition maximum HAZ hardness and, by implication, strength level, occurs immediately adjacent to the fusion line. The observed carbon loss can therefore be expected to significantly reduce the creep strength of this zone. Damage accumulation will be exacerbated by the development of a carbon rich zone just within the weld metal which will increase the local mismatch of properties at the fusion line [5]. The resulting increased triaxiality at this location will enhance Type IIIa cavitation while an increasingly wide depletion layer will promote the subsequent development of Type IIIa cracking.

While the extent of diffusion is sufficient to affect the Type IV region also, the consequences are not likely to be as great. Because the Type IV zone is so weak in the as-welded condition, any further weakening caused by carbon loss will be less significant. The mismatch in properties between the Type IV microstructure and the adjacent parent material will also not be as great as that at the weld fusion line. In fact the loss of carbon may reduce this difference as the parent grows weaker.

It can be concluded therefore that in the long term the carbon diffusion will promote Type IIIa at the expense of Type IV, giving rise to a greater proportion of Type IIIa cracks.

When weld repairs are carried out on National Power plant for Type IV or IIIa cracks it is normal to remove both the old weld metal and a margin of additional parent material. This is done in order to remove parent cavitation adjacent to the HAZ and usually involves 10mm of parent beyond the old fusion line, more extensive parent removal not being practical. The carbon profiles show however that, for welds that have been in service for long periods, this margin will not be sufficient to remove the carbon depleted layer completely. Welds repairs of this kind are therefore likely to be prone to eventual re-cracking.

6 Conclusions

Type IIIa cracks constitute a significant proportion of defects found at 2CrMo welds in ½CrMoV pipework systems.

Extensive carbon diffusion has been identified adjacent to such welds following service at 565°C, and is concluded to be the primary cause of Type IIIa cracking.

Carbon depletion increases with time at 565°C. This is likely to promote Type IIIa cracking relative to Type IV.

Repairs to such welds necessitate welding onto carbon depleted material and subsequent re-cracking of weld repairs may be accelerated because of the carbon depletion.

Acknowledgements

The authors would like to acknowledge the contributions of numerous colleagues to the work reported here. This has involved extensive data acquisition, metallographic investigation and technical discussion.

References

1. D J GOOCH and S T KIMMINS

Type IV Cracking in $\frac{1}{2}\text{Cr}\frac{1}{2}\text{Mo}\frac{1}{4}\text{V}/2\text{CrMo}$ Weldments.
Proceedings of the International Conference on Creep and Fracture of
Engineering Materials and Structures, Swansea, April 1987.

2. S J BRETT

Cracking Experience in Steam Pipework Welds in National Power.
VGB Conference "Materials and Welding Technology in Power Plants
1994", Essen, March 15 and 16, 1994.

3. H J SCHÜLLER, L HAGN and A WOITSCHECK

Cracking in the Weld Region of Shaped Components in Hot Steam Pipe
Lines - Materials Investigations.
Der Machinenschaden 1974 47 p1.

4. S T KIMMINS and E L LONGLEY

Unpublished work within National Power

5. P A SMITH

Investigation into Fusion Boundary Carbon Diffusion in $\frac{1}{2}\text{Cr}\frac{1}{2}\text{Mo}\frac{1}{4}\text{V}$
Weldments.
MSc Thesis, Cranfield University, September 1994.

Recent Advances in Condition Assessment of Components based on Strain Monitoring

J D Parker, Director – Engineering Doctorate Centre - Wales
University of Wales, Swansea, GB

Abstract

Service experience indicates that creep cavitation and cracking can develop in components operating at high temperature and pressure. Life optimisation programmes for power generating plant require periodic evaluation of plant condition. Instrumentation to measure component deformation provides information regarding operating practices which lead to excessive loading and data which can be related to damage state. Indeed, even near weldments, where creep cavitation and cracking can develop with low overall strain, significant levels of deformation have been recorded in local regions. Thus, knowledge of strain accumulation allows identification of the factors affecting damage accumulation and provides a basis for predicting remaining life.

1 Introduction

Increasingly, it is apparent that fossil fuelled stations have a useful service life of greater than 20 years, e.g. it is estimated that 77% of the fossil powered stations in the USA were built before 1975 (1). However, the continued operation of a high pressure system in power generating plant requires a strategy which integrates safe and reliable operation with economic production. Clearly, the primary considerations regarding production costs relate to the cost of fuel and fuel transportation. However, particularly for high efficiency units, plant availability is also important.

Moreover, as new regulations regarding emissions come into force, operators are faced with critical decisions regarding economic life optimisation. Thus, for example, it may be possible to retrofit an old plant to significantly reduce NO_x levels and to increase capacity. Whilst the cost per KW of these upgrades may be attractive, prudent asset management demands that the risks involved are also evaluated. It is therefore essential that a meaningful assessment of plant condition is undertaken as an integral part of this decision-making process.

The most effective plant assessment methodology is based on a systematic approach to component inspections, instrumentation and data analysis, with

the evaluation performed in a number of phases (2). For a wide range of components operating in the creep regime, it is generally accepted that a three phase assessment is appropriate. The procedures used at each level permit a conservative estimate of remaining life to be made for assumed operating conditions. If this estimate is too short, the next phase of the procedure is conducted, utilising progressively more rigorous evaluation techniques only if the desired remanent life is not shown from the lower level. As the assessment level increases, more detailed data are required allowing the accuracy of the calculated life to be improved. However, the more rigorous the assessment, the greater the time and cost required. Thus, it is implicit in the phased approach that resources are targeted, i.e. the right inspection methods are applied to high risk locations at the correct time.

Level 1 – This analysis is effectively a design reappraisal. Plant operating information and component geometry are used to calculate a stress or stress range. Condition is assessed by applying these values to appropriate minimum materials data to obtain a conservative estimate of life expended. This conservative analysis is performed to identify components and component locations most at risk of failure.

Level 2 – More accurate information regarding operating conditions may be required, e.g. through the installation of additional instrumentation, and the calculation procedures of Level 1 repeated. Furthermore, component specific information is obtained through non-destructive examination of high risk locations. These inspections are used to verify component specific data, e.g. dimensions, alloy type etc, and to identify physical evidence of distress. The specific inspection methods vary for different plant components.

Level 3 – If the component specific information demonstrates that significant damage is present, even more detailed inspection, instrumentation and analysis methods are required. These methods may be supplemented by removal of material samples so that critical material properties can be measured for the actual components. The life estimates made should be accurate since they are based on detailed operating data as well as specific component and materials information.

The assessment process should therefore be able to quantify the current plant condition and establish the principal factors leading to damage development. Thus, if high system loads have resulted in crack formation, mitigation of the operating factors causing these additional stresses will greatly improve subsequent performance. The present paper describes techniques for on-line measurement of displacement, reviews the high temperature strain behaviour of components and weldments and gives examples of how strain monitoring can be used to assess performance.

2 Monitoring Methods

Continuous monitoring of creep displacement is routinely undertaken during laboratory, uniaxial testing programmes to establish material strain:time characteristics for selected regimes of stress and temperature. These programmes normally involve attaching an extensometer to the specimen gauge length and measuring the change in position of the extensometer legs using transducers which remain under ambient conditions. The gauge length is then defined as the distance between the attachment positions on the specimen, with data recorded from each side of the sample allowing an evaluation of non-uniform deformation, e.g. due to bending.

Measurements made from the surface of laboratory specimens or components are more complicated since the instrumentation used must be able to withstand the elevated exposure temperatures involved. The issues associated with successful data collection will be illustrated by considering two specific capacitance based devices.

2.1 Planer Strain Gauges

These gauges were developed at the Central Electricity Research Laboratories and were widely used in British power plants. The devices operate up to about 700°C and have an effective gauge length of 20 mm (3). The gauges consist of two arches each with a central plate. The ends of the arch are attached to the substraight and as displacement occurs the curvature changes and the capacitance measured across the plates varies. Typically a calibration curve is established for each gauge at room temperature and the gauge is then spot welded to the appropriate location on the component surface. To accommodate dimensional differences due to the temperature change, it is normal to select a gauge manufactured from material with a coefficient of expansion which matches that of the component. The relatively small gauge length involved allows local deformation to be recorded and in piping situations it is normal to monitor strains in the hoop and axial direction.

2.2 SJB Sensors

One practical difficulty with the Planer gauges is that once fixed to a surface the device could not be easily repositioned. An alternative range of sensors which can be re used has been developed by SJB Engineering. These devices also operate on the basis that the capacitive reactance is directly proportional to the separation between two plates. Thus, the basic sensor comprises two parallel plates electrically insulated from ground. However, in practical applications, this type of insulation may not be

possible so that a 'positive phase' generation of sensors has been developed. As shown in Figure 1, this sensor involves a guard ring capacitance transducer focussed on a blank target, i.e. only one cable is required. However, satisfactory operation requires that good electrical insulation is maintained between both signal and guard, as well as guard to ground.

The attachment lugs of the sensor and target can be spot welded to the surface at any desired location, with the gauge length defined as the distance between location points, Figure 1. Output is normally recorded using a computer based logging system which also calculates displacement values using a sensor specific calibration curve.

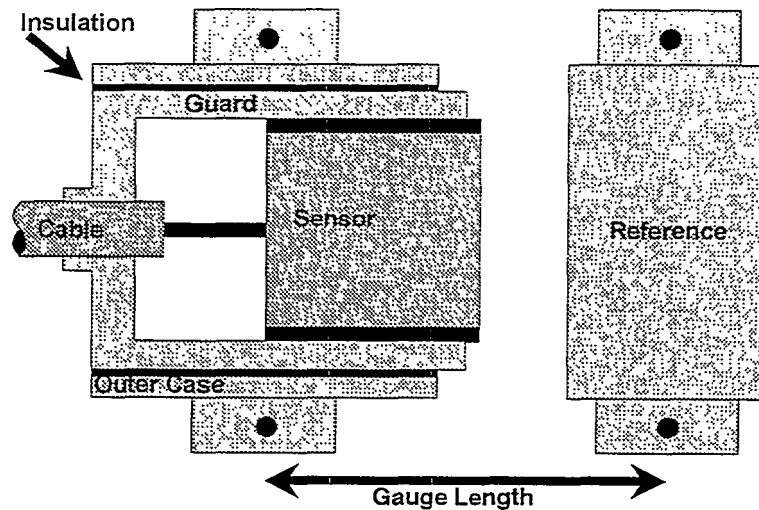


Fig.1. Schematic diagram of an SJB positive phase sensor.

3 Deformation Characteristics

Studies of the high temperature deformation behaviour of components and weldments have been undertaken to

- i. provide information regarding component stresses during normal and transient operating periods,
- ii. establish the long-term strain characteristics of cylindrical components, and
- iii. examine the effects of metallurgical and/or geometric heterogeneities on local strain accumulation.

The following examples have been selected to illustrate the benefits of strain monitoring to evaluation of structural integrity.

3.1 Loading Behaviour

A series of programmes have been reported which evaluated the high temperature deformation and fracture behaviour of welded components (e.g. 4,5). The pressure vessels were fabricated from full-sized piping sections by the manufacture of purpose designed pipe to pipe and pipe to end cap welds. During the experiments the vessels were raised to test temperature and then the pressure was increased incrementally to the required level. A brief hold period followed each pressure increase and this allowed displacement measurements to be made from pairs of hoop and axially oriented Planer gauges.

Typical loading relationships for strain against pressure are presented in Figure 2 for pipe to pipe and pipe to end cap locations. In all cases, a linear relationship between strain and pressure was observed indicating that deformation was elastic. Hoop and axial strains in the pipe to pipe weldment and in the parent were similar, giving a hoop to axial strain ratio of about 4. In the end cap situation, the hoop strain was reduced and the axial strain enhanced so that these strains were approximately equal.

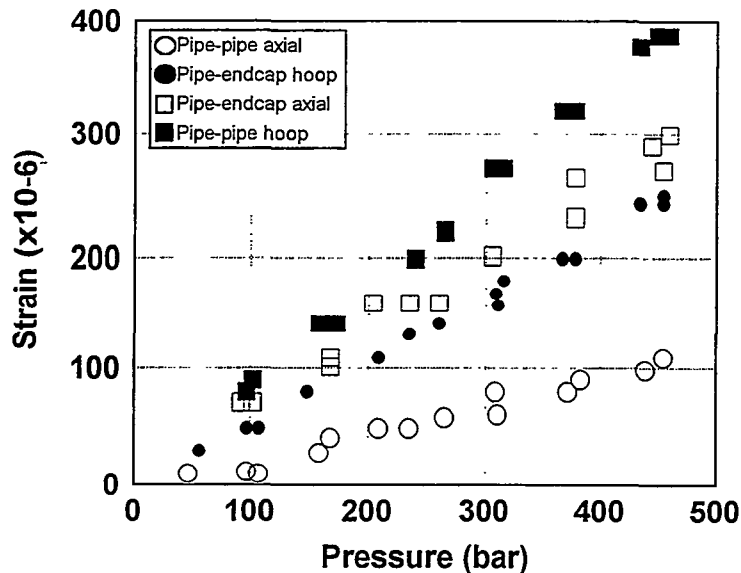


Fig. 2. The increase in hoop and axial elastic strain with pressure for pipe - pipe and pipe - end cap locations in a high temperature vessel.

The hoop to axial strain ratio on the outer surface of an elastically loaded cylinder, where the radial stress, σ_R , is zero, is given by:

$$\frac{\text{hoop strain}}{\text{axial strain}} = \frac{\sigma_H - \nu\sigma_A}{\sigma_A - \nu\sigma_H} \dots\dots\dots(1)$$

Where σ_H and σ_A are the hoop and axial stresses respectively and ν is Poisson's ratio. Using the measured hoop to axial strain ratio of 4 in equation (1) indicates that, in agreement with theory, the hoop stress is twice the axial stress. However, in the end cap situation, the hoop and axial elastic stresses are approximately equal. These data thus demonstrate that the geometry of a component can significantly modify the stress distribution established simply from pressure loading. The enhancement of the axial stress with certain end cap geometries can be sufficient to promote Type IV cracking in the weldment heat affected zone (6).

Problems of damage development in plant have also been studied using SJB devices. Application of eight sensors around the circumference of a weld adjacent to a steam chest, Figure 3, allowed the pattern of deformation during service to be established. The data produced indicated that each time the operating temperature of the piping system was changed, severe bending movements were developed. The sensors thus provided a diagnostic tool to determine the source of the systems loading. This information was sufficient for the plant operator to take remedial action and thus mitigate the driving force for a long standing problem.

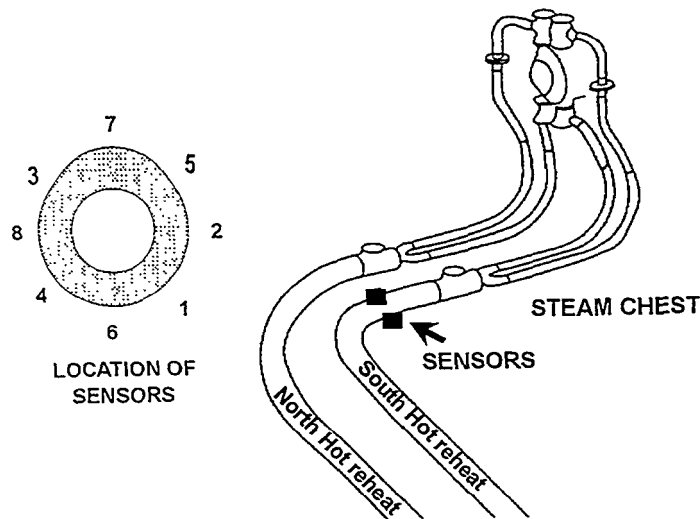


Fig. 3. Schematic diagram of plant showing the location of monitoring using SJB sensors.

3.2 Component Creep Performance

Strain:time data from cylindrical components have been recorded during controlled laboratory experiments and from plant. Where monitoring has been undertaken using intermittent measurements at selected reference points and high temperature strain gauges, in general, the results are in good agreement. Thus, for selected piping geometries, data are available from short to medium term tests, durations up to 50,000 hours, as well as from in-service monitoring, over 100,000 hours. For example, information for CrMoV low alloy steel components indicates that the stress dependence of the minimum creep rate is similar to that recorded from uniaxial laboratory tests, Figure 4.

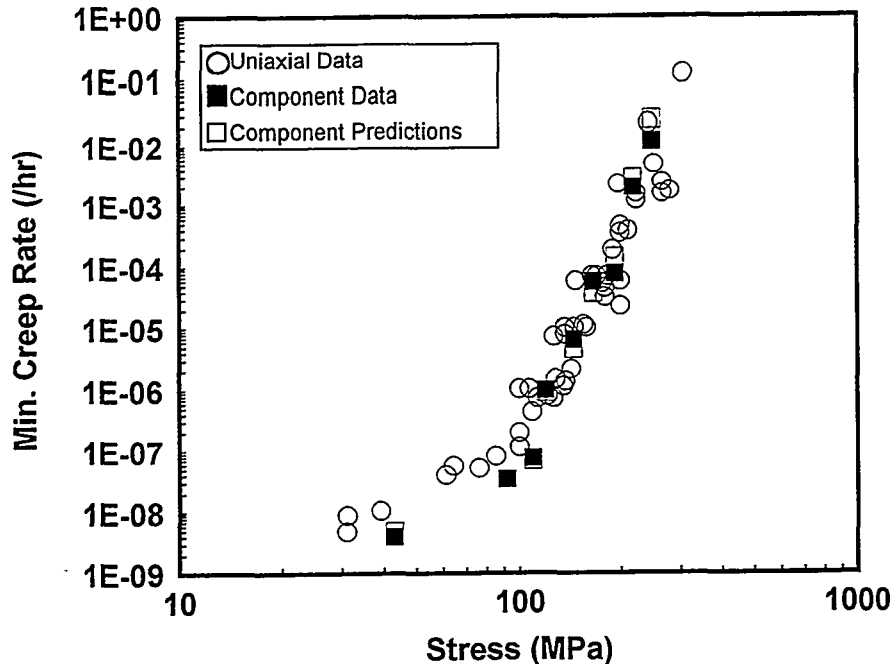


Fig. 4. Stress dependence of the minimum creep rate for CrMoV steel.

Where extension:time results are available, the creep curves are also similar to trends established in uniaxial tests, i.e. the creep rate initially decreases during primary before accelerating in a tertiary stage, e.g. Figure 5. Analysis of these creep curves using the θ projection approach (7) has demonstrated that excellent fits to the measured data are obtained. Indeed, the level of agreement is demonstrated by the solid line shown in Figure 5 which was generated using the θ analysis. It has thus been possible to derive relationships between the four theta parameters and stress. The general applicability of these expressions has been assessed by calculating minimum creep rates for the data given in Figure 4. As shown, the agreement between the measured and predicted values is good so that, at

least for CrMoV steel piping, knowledge regarding the change of creep rate with time is available.

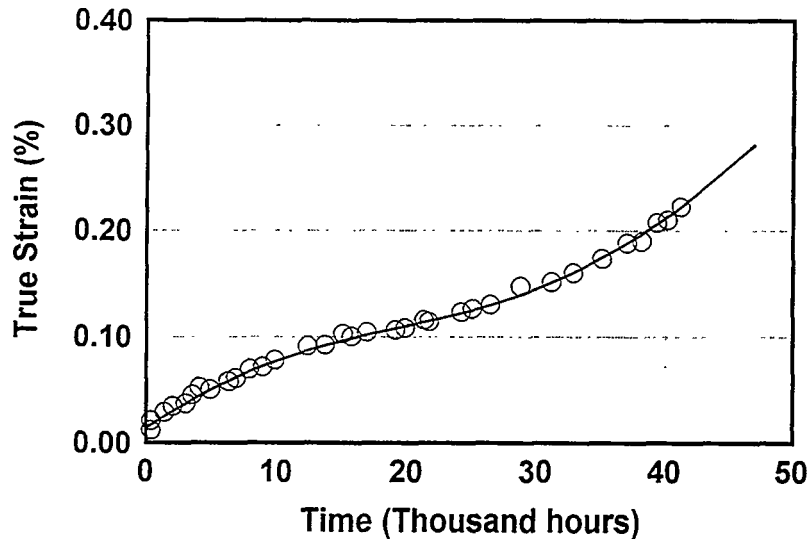


Fig. 5. Creep curve for a CrMoV steel component showing the agreement between measurements (o) and predictions made using the θ method (line).

3.3 Weldment Behaviour

Monitoring of weldments has demonstrated that for loading by internal pressure the deformation behaviour of the constituent zones will influence the stationary state stresses established (4). Thus, a compatibility of hoop strain rate will be developed so that using a weld metal of lower strength than the parent will lead to stress redistribution. In this case, the weld is required to sustain a stress below the average for the parent. Life estimates made on the basis of these redistributed stress values were accurate whereas calculations using a simple mean diameter approach were ultraconservative.

In-service experience indicates that cracking frequently develops at weldments. Thus, approaches have been developed to link the level of cavitation present to life fraction. However, whilst it has been observed that damage forms in a relatively brittle manner, it is well established that the nucleation and growth of creep cavities are linked to deformation behaviour (7). Recent monitoring programmes have demonstrated that creep damage present in weldment heat affected zones (HAZ) is a consequence of local creep deformation.

Creep cracking in transition welds manufactured between low alloy and stainless steel, frequently occurs in the HAZ of the ferritic material in weldments fabricated with austenitic consumables. Accelerated damage development in these joints appears to be related to the mismatch in coefficient of thermal expansion between weld and low alloy steel and diffusion of carbon from the ferritic steel to the weld. To overcome these difficulties this type of joint is now frequently made using nickel-based electrodes. However, improved creep performance has also been found using buttering techniques to control local gradients in composition, microstructure and strength (8).

These weldments achieve longer creep lives than traditional joints but long-term failure still occurs by cracking in the HAZ with low overall ductility. Thus, as shown in Figure 6 the total extension measured from the 75 gauge length was only 1.26 mm, i.e. about 1.7% strain. However, local displacement measurements were also performed using SJB sensors in the low alloy steel HAZ and the adjacent buttered layer. These results indicate that for the first 90% of the life, i.e. prior to crack propagation becoming significant, 70% of the total deformation occurred in these local regions. Thus, the strain to failure where the cracking developed was approximately 10%. These data therefore confirm that creep cracking is linked to deformation. However, even cavitation in the bainitic regions of the HAZ adjacent to the weld interface requires sufficient strain to offer the potential for in-plant assessment of these welds.

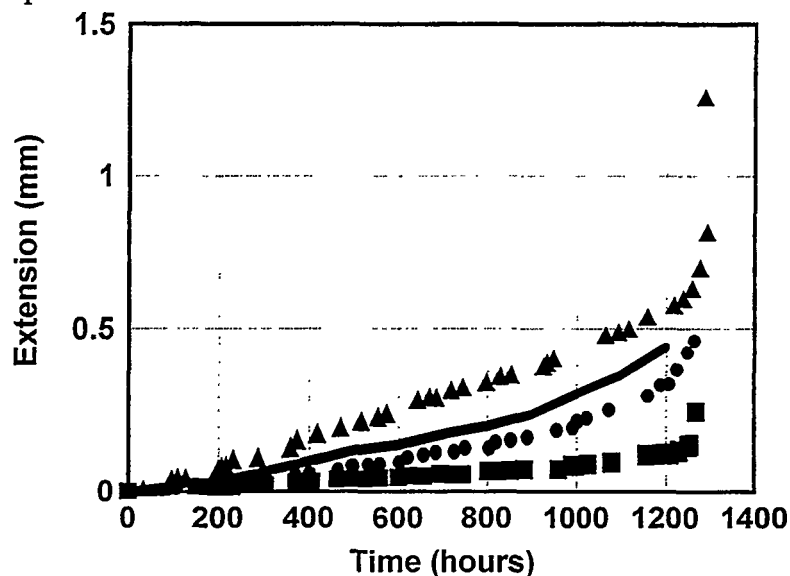


Fig. 6. Extension:time curves recorded from the extensometer (▲) and local sensors across the low alloy HAZ steel (●) and the adjacent 2CrMoNb buttered layer (■) of a transition weldment. The sum of the displacements from the local sensors is shown as the solid line (8).

In a similar manner, Type IV cracking in the intercritical region of weldment HAZ's frequently occurs with low overall displacement. However, detailed research has demonstrated that this damage is a consequence of high levels of local strain, up to about 20%, which develops in a narrow microstructural band, Figure 7. This example further illustrates the care which must be exercised in defining a meaningful gauge length for calculating the strain in weldments. Indeed, knowledge of the local deformation behaviour improves overall understanding of factors affecting weldment performance and offers the potential for strain based assessment of condition provided the appropriate instrumentation is applied in the correct location.

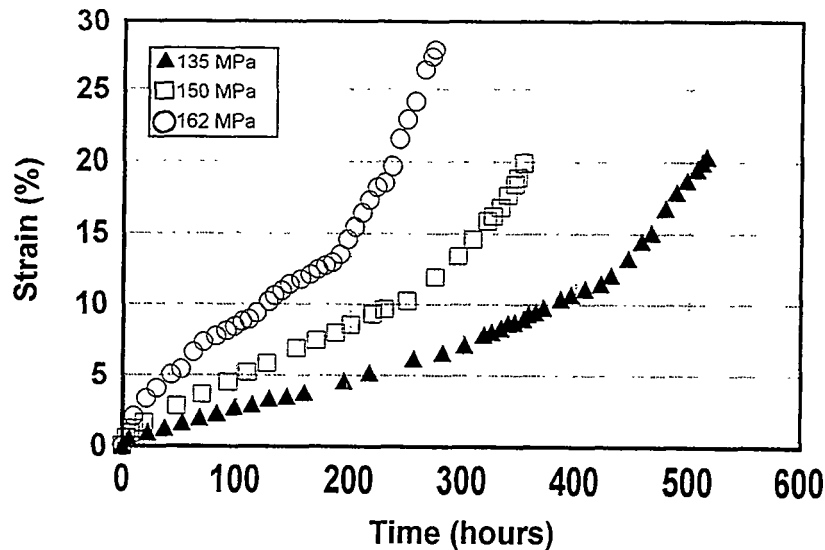


Fig. 7. Strain:time behaviour for the intercritical region of the HAZ in low alloy steel weldments which failed by Type IV cracking.

4 Discussion

There is an ongoing need to evaluate the condition of electricity generating plant as part of an integrated asset management programme. Indeed, not only must power producers evaluate the performance of existing plant, but should undertake structural integrity assessments prior to the acquisition of additional facilities. In circumstances where implementation of the phased approach to assessment justifies in-service monitoring, measurement of deformation behaviour should provide important information.

It is well established that creep deformation and fracture are highly dependent on stress and temperature. Under normal conditions the operation of piping systems should be carried out within design limits. Similarly, control of internal pressure should be such that the overall stresses present are known. Thus, short or medium term cracking problems suggest that, in the absence of serious fabrication difficulties, additional stresses due to temperature transients or systems loads are present. The application of appropriate sensors should allow the operational factors responsible for the excess loading to be established so that the necessary remedial action can be implemented.

In situations where long term behaviour needs to be considered, monitoring creep strain accumulation with time is of benefit since data can be obtained non-destructively, either under ambient conditions or on-line. Clearly, for piping components, θ analysis of creep curves has allowed accurate predictions of minimum creep rate to be made for a wide range of stresses, Figure 8. This approach also allows strain:time behaviour to be calculated so that it is possible to develop relationships between creep strain and remaining life. Consideration of Figure 8 indicates that for service conditions a hoop strain of 10% occurs at about 70% of the creep life with about 4% strain representing 90% life. These values are in excellent agreement with strain limits suggested for condition assessment following evaluation of plant experience.

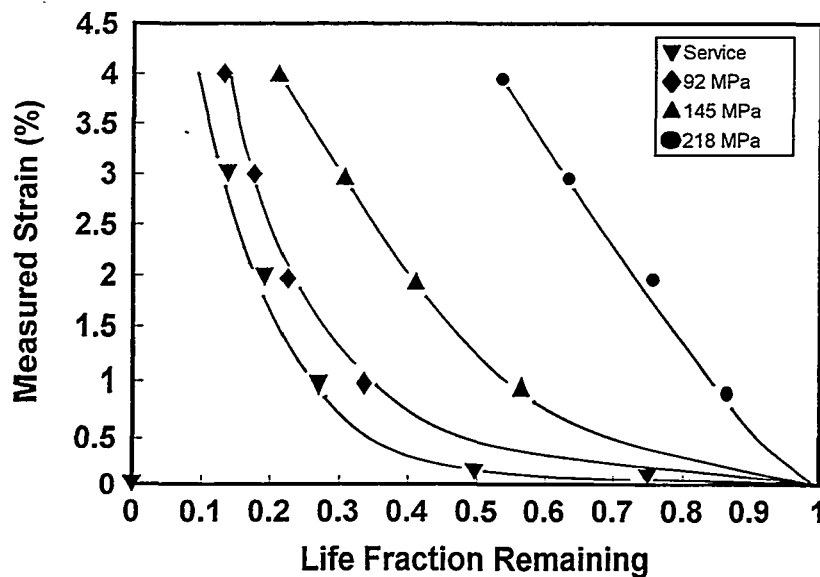


Fig. 8. Relationships between accumulated creep strain and life fraction for piping components at different hoop stresses.

The condition of components operating under high stress and temperature can be evaluated through knowledge of creep deformation behaviour. Indeed, similar approaches can be applied to evaluate weldment performance provided the basic relationships linking strain to life fraction have been established. However, in cases where the total displacement accumulated cannot be established since monitoring is initiated during life, it is possible to perform assessments on the basis of the change of creep rate with time.

5. Conclusions

Advanced sensors have been developed to allow displacement to be measured under high temperature conditions. The data available can be analysed to identify the factors affecting damage accumulation and to provide a basis for assessing current conditions as well as future performance.

6 References

1. Armor, A.F. 'Overview of the Power Generation Business in the United States', Int. Conf. On Advanced Heat Resistant Steels for Power Generation, 1998, Institute of Materials.
2. J. D. Parker *et al*, 'Condition assessment guidelines for fossil fuel power plant components', EPRI GS-6724, 1990.
3. B.E. Noltingk, D.F.A. McLachlan, C.K.V. Owen and P.C. O'Neill, Proc. IEE, Vol. 119, 7, 1972, pp. 897-903.
4. M.C. Coleman, J.D. Parker and D.J. Walters, 'The behaviour of ferritic weldments in CrMoV steel pipe at elevated temperature' Int. J. PVP, Vol. 18, 4, 1985, pp. 277-310.
5. M.C. Coleman, 'High Temperature Behaviour of Ferritic: Pipe Welds: Experience of Long-Term Testing', Int. J. PVP, 39, 1989, pp. 109-118.
6. M. Steen, M. de Witte and C. Coussement, 'Creep properties of 12% Cr Weldments, Part 2 : Component tests and design implications' Proc. of the 4th Int. Conf. On Creep and Fracture of Engineering Materials and Structures (Eds. B. Wilshire and R.W. Evans), IoM, 1990, pp. 679 – 690.
7. R.W. Evans and B. Wilshire, 'Creep of Metals and Alloys', IoM, 1985.
8. J.D. Parker, 'Creep and Fracture Behaviour of English Electric Mark III Transition Welds', Int. J. PVP, to be published.

LIFE MANAGEMENT OF POWER PLANT BASED ON STRUCTURAL DAMAGE TESTING

Tallermo H., Klevtsov I. Thermal Engineering Department of Tallinn
Technical University; Arras V., Eesti Energia
Tallinn, Estonia

Abstract

Presented here life management system is based on the valid nowadays in Estonian power plants regulation documentation. The system allows to estimate stress distribution in components, find computational assessment of cumulated creep damage, determine when and where it is necessary to cut off the particular number of microsamples or take replicas. Finally, the real metal condition may be assessed on the basis of metallographic specimen research and reasonable 3-R decision - run, repair, replacement - made on further component use.

1 Introduction

Power equipment developed and entered into operation in decade 1960-1970 was designed for the term of operation about 100 thousand hours. The thickness of a wall of power plant components and admitted operational pressure were designed also for the same life. In spite of the fact that a lot of power plant components have operated to the present time 200-250 thousand hours and work out their design life, they are still in a satisfactory condition [1]. Such phenomenon is caused by work on lowered steam temperature, duly realization of inspection of metal condition, repairs and partial replacements. Nowadays such power plant components require continuous inspection not only for components under maximum stress, but also for these operating within the admitted stress limits.

If not to take into account defects of manufacturing and repair, reliability of component is defined by changes in structure of metal, caused mainly by creep. Ultrasonic testing and superficial defectoscopy as well as monitoring of creep rate by measuring component's deflection cannot reveal any damages of structure before occurrence of cracks. Practically the sole

method of revealing of structure damages is a metallography research. We consider, that the most authentic criterion for estimation of metal serviceability in given circumstances is condition of its structure, mainly the level of cumulated changes in microstructure. Knowing dependence between the level of cumulated changes and life consumption, it is possible to accept the decisions on realization of more extensive inspection, repair or replacement of component in the certain time.

2 Computational determination of life consumption and testing sections

The Standard Document [2], valid nowadays in Estonian power plants in the area of the metal testing of power equipment components, prescribes check of outside and inside surfaces of thick-wall elements by non-destructive testing methods and microstructure analysis on the basis of the microsamples which has been cut out from a surface of a researched element.

The testing procedure and set of devices is presented in Figure 1. From Figure 1 it is visible, that before taking into operation of new, repaired or replaced component, the presence of the necessary documentation on all elements is supposed, where the geometrical sizes necessary in the further accounts on revealing of the most stressed sites of power equipment's component should be specified.

Simultaneously with start-up of the newly took into operation equipment, the monitoring of operational parameters begins as well as operational history (database) formation. According to Standard Document [3] all new power plant equipment should be equipped with automatic system for monitoring of operational parameters and accumulation of a database on a history of operation.

The estimation of stresses in components of a steam pipe and collectors is made for first time after consumption of a design life on 80-90%. The computer programs "RAMPA" or "TOTU", based on the Standard Document [4], are applied to estimate stresses in elements of steam pipe (straight parts and elbows) and program "Collector" is applied to estimate stresses in collectors. On the basis of found stresses the program assesses

cumulated life consumption (so named computational creep and fatigue damage) for the most loaded elements. Program "RESKU" takes into account also the amount of installation's start-ups and shut-downs. The similar assessments are carried out for collectors. The further actions depend on the level of found damage. For example, with computational creep and fatigue damage $D_c > 0.9$ for the highly loaded elbows further investigation must be conducted with the help of the program "ELBOW" to provide stress distribution along the elbow length and perimeter. Only on the basis of these estimations it is possible to determine a precise placement of cutting of microsamples or taking replicas. Let's note, that in our opinion the determination of microstructure damage by using metallographic specimen is more representative, than using replica.

Cutting off microsamples (as a rule, from stretched zones of elbow, where the maximal stresses are usually located) with thickness about 0.2-0.3 mm and diameter about 10-12 mm is provided by the mechanical cutting tool developed and manufactured in TTU. While cutting off, a cold-work hardening and overheating of metal and microsamples are not admitted. Our tool allows completely exclude these phenomena.

The necessary amount of cut off microsamples depends on value of computational creep and fatigue damage for the particular element as well as on stress level. For example, for elbow of steam pipe with outside diameter ≥ 133 mm under $D_c=95\%$ according to Standard Document [2] it is prescribed the following order of cutting and amount of cut off microsamples:

- in area, where $\sigma=\sigma_{max}$, 3 samples must be cut off;
- in area, where $\sigma=0.9\sigma_{max}$, 2 samples must be cut off;
- in area, where $\sigma=0.75\sigma_{max}$, 1 sample must be cut off.

If elbow computational damage $D_c=80-90\%$, the necessary amount of cut off samples decreases.

3 Assessment of actual life consumption on the basis of metallographic research

The microstructure of the metallographic specimen, prepared by using cut off microsample, is investigated ordinarily under an optical microscope.

Microstructure analysis may be provided directly under an optical microscope or by using its portrait received by traditional photographing or by computer scanning. In the latter case it is able to apply the computer programs, which allows to execute some integrated transformations of a portrait:

- alignment of light exposure;
- increase of contrast;
- smoothing of high-frequency noise.

It is also able in this case to provide the formal analysis of microstructure on the basis of gray tone gradation to determine the following quantitative characteristics:

- average size of grain;
- density of distribution and average size of carbides;
- amount, maximal and average size of pores, specific porosity;
- divide microstructure into two phases on tone level (can be applied to allocation of structure pearlitic component).

The conformity of qualitative and quantitative parameters of researched metal structure with its analogue allows establishment of a degree of its actual damage.

In absence of pores, the degree of microstructure damage of alloys 12Ch1MV and 15Ch1M1V is defined by the scale of structures [5], with presence of pores it is defined by the scale of the professor T. Berezina [6]. This scale subdivides creep damaged microstructures of pearlitic alloys into 5 degree as follows:

- 1 - pores in amount of 1-2 in a field of microscope sight under blow-up 800 no more, than in two fields from 20 researched. The value of pores volumetric share may be assessed here as $f \leq 0.15\%$ and actual life consumption or cumulated damage as $D_r \leq 0.65$.
- 2 - pores in amount 3 or more in a field of sight, or less than 3 in single field but with 3 or more fields, in which pores is found out. The value of pores volumetric share may be assessed here as $f = 0.15-0.20\%$ and actual cumulated damage as $D_r \approx 0.65-0.74$.

- 3 - chain of pores at least in one field of sight. The value of pores volumetric share may be assessed here as $f=0.20-0.30\%$ and actual life consumption or cumulated damage as $D_r \approx 0.74-0.81$.
- 4 - chain of pores and their association in microcracks within the size of a grain. The value of pores volumetric share may be assessed here as $f=0.30-0.40\%$ and actual life consumption or cumulated damage as $D_r \approx 0.81-0.87$.
- 5 - critical damage, microcracks are united into macrocracks. The value of pores volumetric share may be assessed here as $f=0.40-0.80\%$ and actual cumulated damage as $D_r \approx 0.87-0.96$.

Preliminary assessments of value of pores volumetric share may be found on the basis of computational life consumption by using of the professor T. Berezina empirical equation:

$$f = \frac{f_{cr}}{\exp(a - \sqrt{1 - D_c})} \quad (1)$$

where

f_{cr} - critical value of pores volumetric share, for pearlitic alloys
 $f_{cr}=2\%$;

D_c - computational life consumption;

a - coefficient depending on structure of alloy; $a=4.4$ for ferrite-sorbite and ferrite-carbide structure; and $a=4.8$ for structure with tempered bainite.

4 Assessment of component serviceability

The serviceability of power plant component and admitted duration of its operation until the following metal testing is nominated on the basis of results of the structural analysis as follows:

- Pores are not revealed. Suitability of component with given structure is judged on the basis of conformity of its qualitative and quantitative characteristics to the alloy standards [5].

- Pores are revealed. Residual life factor k_τ should be estimated on the basis of microstructure damage degree that allow assessment of component residual by using the following governing equation:

$$\tau_{res} = \tau \cdot k_\tau \quad (2)$$

where τ_{res} is residual life in hours (until the following testing, repair or replacement of component); τ - current operational time in hours.

For alloy 12Ch1MoV, values of residual life factors depending on degree of actual cumulated damage are presented in Table 1:

Table 1. Residual life factors depending on cumulated damage.

Damage degree	1	2	3	4	5
Residual life factor	0.3	0.15	0.03	0	0

Usage of residual life factor k_τ is based on the following assumption. When life consumption $D = \tau / [\tau]$, defined as fracture of admitted life $[\tau]$, exceeds value $D = 0.85$, the further creep damage cumulating process become be unpredictable and this component further operation become be unreliable and inexpedient. It means that finally life factor k_τ may be estimated on the basis of actual cumulated damage by using the following empirical equation:

$$k_\tau = \frac{0.85}{D} - 1 \quad (3)$$

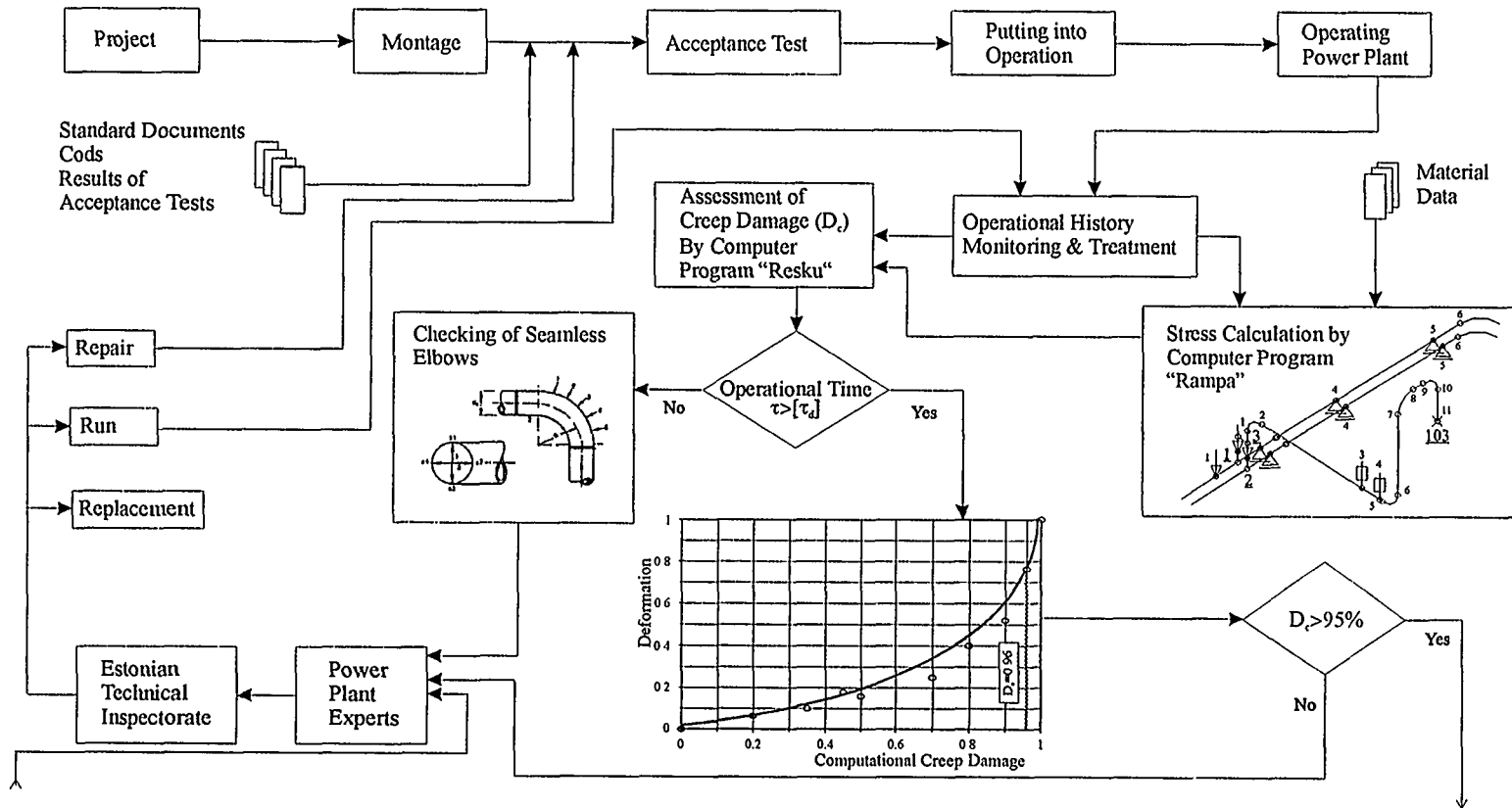
References

1. Tallermo H., Klevtsov I., Arras V., Gorohhov J. Trends In Life Management Of "Eesti Energia" Power Plants, Proceedings of Baltica III International conference on plant condition & life management, Helsinki-Stockholm, June 6-8, 1995, Vol. 2, p. 621-627.

2. The Standard for Testing of Metal Condition of Power Plant Components Under Inside Pressure / H. Tallermo, I. Klevtsov, Tallinn, 1997, pp. 54 (In Estonian, unpublished).
3. Standard Document for Estimation of Life Consumption of Metal of Steam Pipes and Headers Operating Under Elevated Temperature ($>450^{\circ}\text{C}$) and Pressure ($>9.0\text{ MPa}$) / H. Tallermo, I. Klevtsov, T. Lausmaa et al. // Tallinn, 1995, p. 17 (In Estonian and Russian, unpublished).
4. Standard Document for Energy Equipment's Strength Estimation. RTM 24.038.08-72, Moscow, 1972, pp. 67.
5. Scales of Microstructure of Boiler Tubes of Alloys 12Ch1MV and 15Ch1M1V. Appendix to MRTU 14-4-21-67, Dnepropetrovsk, 1968, pp. 31.
6. Berezina T., Bugay N., Trunin I. Diagnosis and Prognosis of Energy Equipment's Metal Life. - Kiev, Tehnika, 1991, pp. 120.



THE SYSTEM FOR TESTING OF CUMULATED METAL CREEP DAMAGE



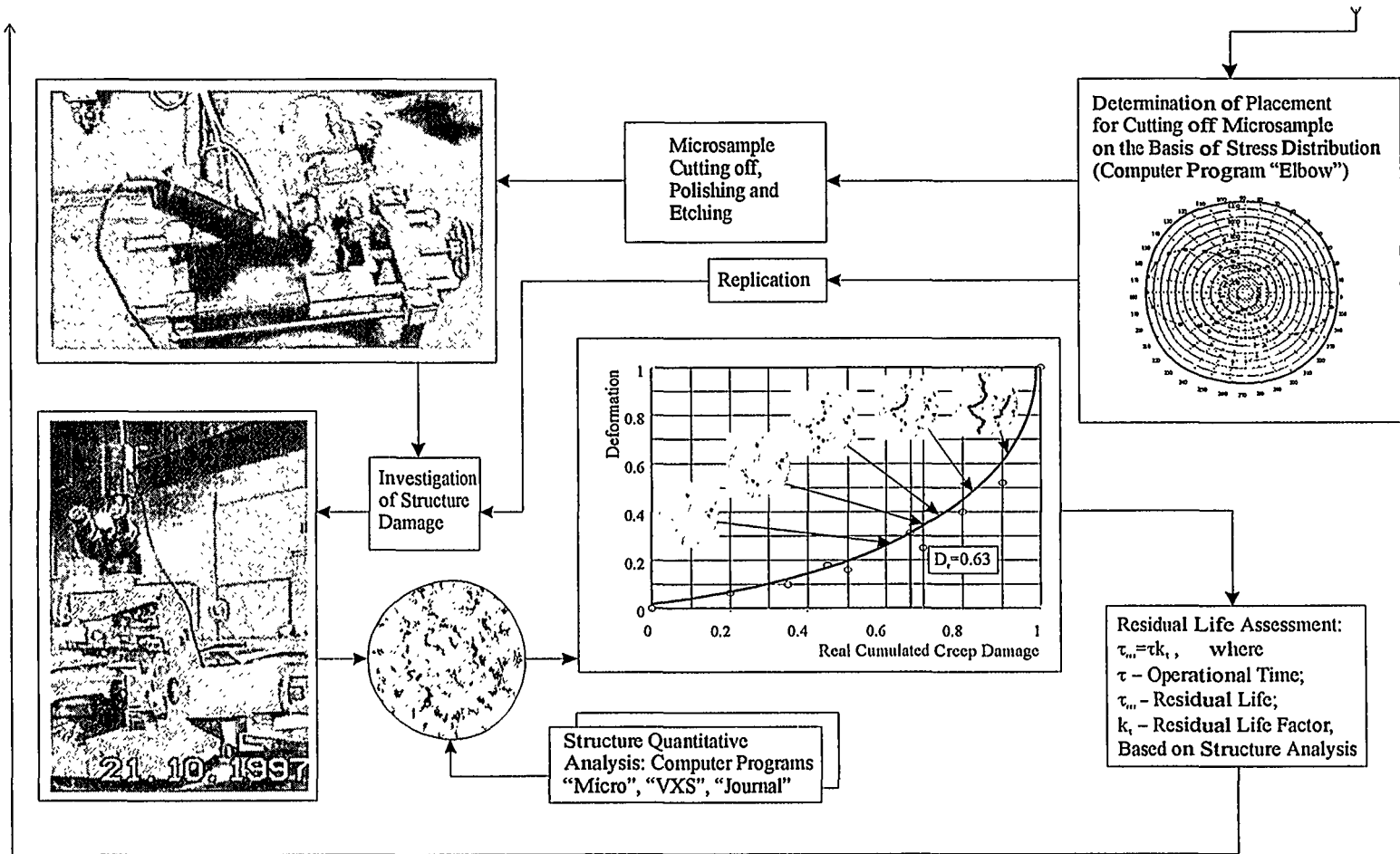


Figure 1. Schematic Presentation of Components of the System for Testing of Cumulated Metal Creep Damage.

Can the lifetime of the superheater tubes be predicted according to the fuel analyses? - Assessment from field and laboratory data

Keijo Salmenoja, Senior R&D Engineer
Kari Mäkelä, Chief Metallurgist
Kvaerner Pulping Oy
PO Box 109, FIN-33101 Tampere, Finland

Abstract

Lifetime of the superheaters in different power boilers is more or less still a mystery. This is especially true in firing biomass based fuels (biofuels), such as bark, forest residues, and straw. Due to the unhomogeneous nature of the biofuels, the lifetime of the superheaters may vary from case to case. Sometimes the lifetime is significantly shorter than originally expected, sometimes no corrosion even in the hottest tubes is observed. This is one of the main reasons why the boiler operators often demand for a better predictability on the corrosion resistance of the materials to avoid unscheduled shutdowns.

1 Introduction

Corrosion is one of the most important factors preventing the increase of thermal efficiency of modern steam rising boilers. Due to corrosion, steam outlet temperatures are limited usually below 560 °C. In incinerators and municipal solid waste (MSW) combustors the steam outlet temperatures are relatively low, typically between 400 - 440 °C. In the recent years, also biomass fired boilers have encountered severe, unexpected corrosion problems, even at steam outlet temperatures of 480 °C. The trend towards higher steam outlet temperatures, demand for longer plant lifetimes and reduced maintenance costs, enforce the boiler manufacturers to gain better understanding on the behavior of biofuels. This is also to reduce unexpected guarantee costs.

The behavior of the fuel and ash can be predicted relatively well in coal firing. Several different parameters and factors exist to predict the slagging and fouling behavior of different coals [1]. In biomass firing, however,

these parameters do not usually apply. Therefore, it is also very difficult to predict the corrosiveness of different types of biofuels.

The use of different iron (Fe) based alloys in power and steam production has a long and successful history. Low alloyed Fe-Cr alloys have mainly been used due to the combination of low price, high strength properties at elevated temperatures, and high scaling resistance. However, the use of conventional Fe-2Cr and Fe-12Cr alloys in boilers burning high chlorine (Cl) and potassium (K) containing fuels have in some cases resulted in corrosion rates higher than 1.0 mm/month [2]. High steam outlet temperatures in addition to the aggressive fuels have stipulated the emerge of new materials. The use of highly chromium (Cr) and nickel (Ni) alloyed Fe based steels have therefore increased, too. In some cases, austenitic stainless steels have performed well in highly corrosive environments [3].

In this paper the predictability of the corrosiveness of biofuels is evaluated, based on several probe and full scale tests.

2 Assessment of test data

2.1 Fuel analyses

The evaluation of the corrosiveness of a specific fuel generally starts from fuel analyses. To be able to predict the behavior of the fuel in a particular boiler ultimate analysis is needed in addition to the proximate analysis. According to experiences, the most important elements from the corrosion point of view are Cl, sulfur (S), sodium (Na), potassium (K), and calcium (Ca).

Chlorine in biofuels is mostly in the form of organic chloride compounds or is inorganically bound to alkali chlorides, mostly as potassium chloride (KCl). During the combustion organic chloride is released as gaseous hydrochloric acid (HCl). Alkali chlorides can be vaporized directly into the gas phase. The release of alkalis during combustion of biofuels may also be rather high. Measurements with straw have shown that around 20% of K and around 70% of Cl is released during combustion [4].

Due to the different mineral compositions in the fuel ash, the deposit formation properties of the fuels are also divergent. Even small changes in the temperature and other conditions in the furnace may result in different behavior of the fuel. Therefore, it is exceedingly important to know the

characteristics of the particular fuel. Several meaningful fuel parameters can be calculated from the fuel analyses; sulfur to chlorine ratio (S/Cl), chlorine to alkali ratio (Cl/Alk), and sulfur to alkali ratio (S/Alk). Table 1 shows the content of Cl, S, Na, K, and Ca in some biomass based fuels with the calculated fuel parameters.

Table 1: Concentration of Cl, S, and alkalis in different biofuels (wt.-%). Calculated fuel parameters are also shown (mol/mol).

Fuel	Cl	S	Na	K	Ca	S/Cl	Cl/Alk	S/Alk
Bark+sludge	0.07	0.1	0.05	0.1	1.1	1.6	0.06	0.10
Peat	0.0	0.4	0.04	0.04	0.53	high	-	0.78
Straw	0.2	0.1	0.01	0.24	0.19	0.55	0.50	0.28
Wood	0.0	0.1	0.00	0.03	0.15	high	-	0.69
Salix	0.0	0.0	0.01	0.31	0.57	-	-	-

Sulfur and chlorine are competing from alkalis to form either alkali chlorides or alkali sulfates. Thermodynamics favor the formation of sulfates. If an excess amount of alkalis is available some free chlorine may be available to form alkali chlorides. Alkali chlorides are known to decrease the first melting temperature (T_0) of the deposits. In combined bark and sludge combustion the lowest T_0 observed has been around 530 °C [5].

Sulfation of alkali chlorides in the deposits may also introduce rapid corrosion in the superheaters. Therefore, the degree of sulfation prior to the heat transfer surfaces should be as high as possible. The S/Cl ratio may give an indication whether the fuel is corrosive or not. A value higher than 4.0 has been regarded as beneficial in refuse firing [6]. In biofuels the sulfur content is generally very low, except in peat, and consequently the S/Cl ratio is very low. Since the S/Alk ratio is also very low in biofuels, all biofuels can therefore be regarded to be more or less corrosive. Wood, on the other hand, is non corrosive since it does not usually contain considerable amounts of chlorine.

2.2 Deposit probe tests

According to experiences, basically the same fuel has in some cases produced different types of deposits in two boilers with different design. This example shows that not only the furnace conditions but also other factors associated to the boiler layout may be important. Therefore, sometimes the only way to find out the effects of the fuel in a particular boiler is to make in situ deposit probe tests.

Deposit formation and fouling properties of different biofuels have been evaluated with air-cooled probes, as schematically shown in Fig. 1. The probe is cooled with pressurized air to the desired temperature. The temperature of the probe is controlled by an automatic control unit. Collected deposits are generally analyzed with scanning electron microscope (SEM) and energy dispersive X-ray (EDX) analyzer. Bulk analysis of the deposits is also made by wet chemical methods.

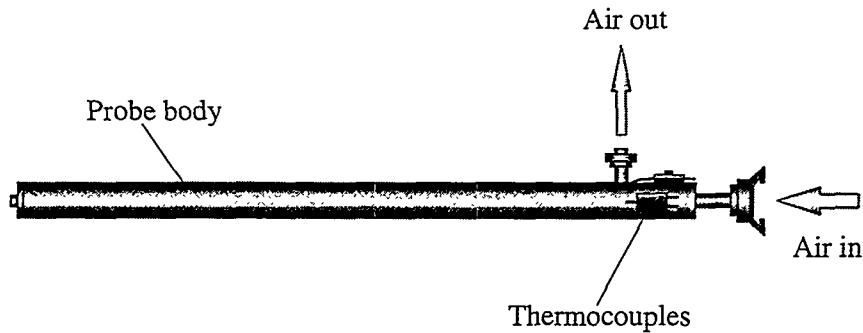


Figure 1: Schematic view of the air-cooled deposition probe.

Comparing the compositions of the long and short term deposits may give indications on the fouling propensity of the fuel. Typically, alkali chlorides have the lowest condensation temperatures and are deposited first [7]. Therefore, a thin layer of alkali chlorides may be found on the tube surface below the deposit. Sulfur content in the deposit is on the contrary increasing towards the surface. This may also be due to the increase in the surface temperature when the deposit is growing. At a certain temperature, alkali chlorides stop condensing on the surface. The result is a deposit with a chlorine free outer surface.

Fig. 2 shows an example of the results obtained in deposit probe tests in a biomass fired boiler. Considerable differences between the short and long term deposits in this case was observed. The Cl/Alk ratio indicates how high percentage of the particles are depositing in a alkali chloride form. In this case a large portion of alkalis is either depositing as small KCl particles or condensing directly from the gas phase. The disappearance of Cl from the deposits in the long run suggests that sulfation of alkali chlorides is occurring after deposition.

In some cases, this kind of behavior has been related to severe corrosion problems in the superheater area. The sulfation of alkali chlorides by gaseous sulfur dioxide (SO_2) is a well known phenomenon, especially in

recovery boilers [8]. This reaction releases chlorine in a gaseous form (HCl or Cl₂) directly near the tube surface. Released chlorine gases may then be available for subsequent reactions with different metals in the alloy and induce the corrosion process.

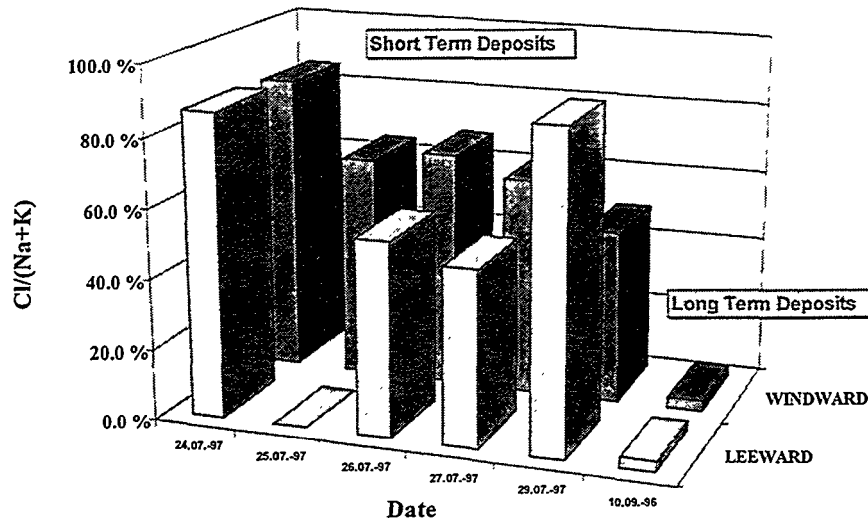


Figure 2: Measured behavior of short and long term deposits in a biomass boiler. Duration of the short and long term test is 12-24 and 1000 hours, respectively.

2.3 Material probe tests

The only way to find out the corrosion resistance of different materials in certain atmospheres is to make in situ tests in the boilers. This usually gives an overview on things like how the material behaves in the particular environment and what is the effect of temperature on corrosion rate. As was mentioned earlier, boiler design and local conditions may have a crucial effect on the corrosiveness of a fuel. Therefore, any generalizations made from separate results may lead to totally misleading conclusions.

Several probe tests have been accomplished during the last five years at Kvaerner Pulping Oy to study the behavior of different iron (Fe) based alloys in various environments. Tests have been done in bubbling fluidized bed (BFB) and circulating fluidized bed (CFB) boilers. Fuels have varied from bark, peat, and sludges to refuse derived fuels (RDF). The aim has been to test the materials in different atmospheres with a wide range of fuels.

Air-cooled probes, as shown in Fig. 3, have been used in the tests. Replaceable metal inserts of different alloys are installed into the probes. Alloys evaluated in the tests can be divided into four general categories; 1) alloys containing less than 5% Cr such as 10 CrMo 9 10 (10CrMo), 2) alloys with Cr content in the range from 5% to 15% including X 20 CrMoV 12 1 (X 20), 3) standard austenitic stainless steels such as AISI 304 and AISI 310, and 4) high Cr and Ni alloys such as Sanicro 28 and X5 NiCrCeNb 32 27 (AC 66). The test temperature ranges from 400 °C up to 600 °C depending on the case and the material. Table 2 shows the composition of some of the alloys tested in several boilers.

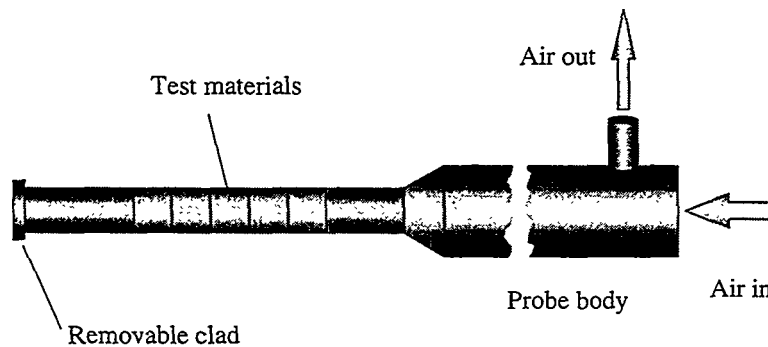


Figure 3: Schematic view of the air-cooled material probe.

Table 2: Nominal composition (wt.-%) of Fe based alloys tested in various probe tests.

Alloy	Cr	Ni	Fe	Others
10 CrMo 9 10	2.25	-	Balance	Mo, C
X 20 CrMoV 12 1	12.0	-	Balance	Mo, V, Cu
AISI 304	18.0	9.0	Balance	-
AISI 347H	18.0	11.0	Balance	Mn, Nb
AISI 316L	17.0	12.0	Balance	Mo
AISI 310	25.0	21.0	Balance	Mn, Si
Sanicro 28	28.0	30.0	Balance	Mo, Mn, Cu
AC 66	27.0	32.0	Balance	Ce, Nb

After dismantling, metal inserts from the probes are immediately placed in a desiccator to avoid scale blistering. Due to the hygroscopic nature of the scales, even moisture from air could destroy the samples. Inserts are then dry cut, dry cleaned and polished. Water is not used during the whole preparation procedure. Polished metal inserts are first evaluated with optical microscopy (OM) to detect visually possible corrosion layers. Scanning

electron microscopy (SEM) is used for more detailed evaluations. Spot analyses, elemental maps, and line profiles are prepared for each sample. The same procedure is also applied to tube samples from actual superheaters.

Two types of results is typically obtained with the probes; 1) corrosion rate as function of temperature, or 2) relative corrosion rates of different alloys. Fig. 4 shows one example of relative rates according to probe measurements. Actual corrosion rate of the superheater tubes (AC 66/SH) is also shown in the figure. The temperature in the superheater case is the steam outlet temperature which corresponds to material temperatures between 560-570 °C.

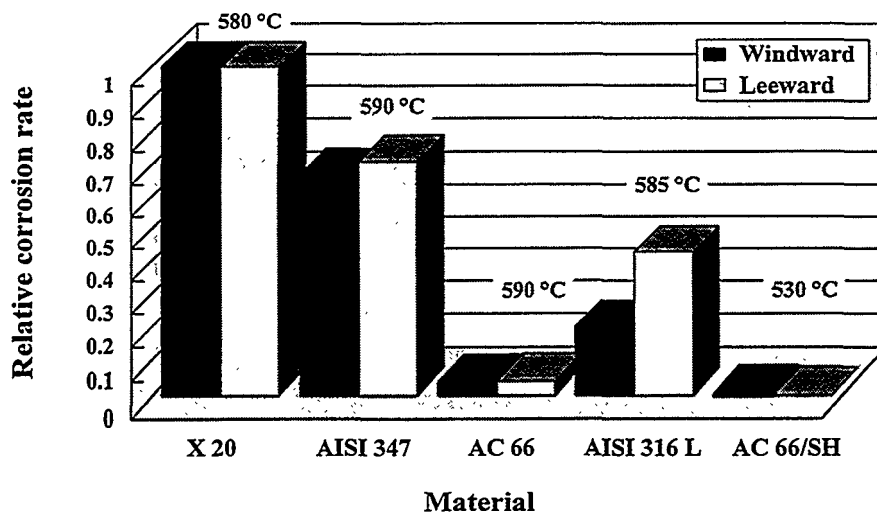


Figure 4: Relative corrosion rate of different alloys according to probe tests. Temperatures represent probe metal temperatures, except with AC66/SH, which is the result obtained from a real superheater tube. In this case the temperature refers to the actual steam outlet temperature (530°C), not the material temperature.

Measured corrosion rate of the original superheater material (X 20) was around 10 mm/year. Predicted corrosion rate of the alloy AC 66, according to Fig. 4, would be around 0.3-0.5 mm/year. Inspection made after two years of operation at 530 °C, however, revealed that the corrosion rate has been only around 0.05 mm/year, which is an order of magnitude lower than the predicted rate.

Usually, corrosion rates obtained from probe tests are lower than the actual observed rates in the superheater tubes. Since the length of the probe is only 1.8 m, the material inserts may experience a somewhat different environment than the superheaters in the middle of the boiler. Flow characteristics and flue gas temperatures near the furnace walls are also different than in the middle of the pass.

3 Discussion

Generally, an increase in the Cr content increases the oxidation resistance of the alloy. Nickel content in the alloy, as well as some minor alloying elements, also has beneficial effects on the oxidation and corrosion resistance. Full scale tests have proven the same trend. Increase in the alloy Cr content boosts the corrosion resistance of the superheaters. However, a certain content of Cr is needed to form a fully protective oxide scale on the alloy. In many occasions, only those alloys having a Cr content of over 25% are able to effectively resist corrosion and keep the corrosion rate below the design limit (0.1 mm/year).

The example shown in Fig. 4, which presents relative corrosion rates obtained with probe tests in a BFB boiler burning a mixture of bark and sludge, shows also that a clear improvement in the tube lifetime is achieved by increasing the alloy Cr content over 25%. Due to the brittleness of high Cr steels Ni is also added to these alloys. In fact, no clear evidence is available which one of the components, Cr or Ni, is actually increasing the corrosion resistance of the alloy in this case. However, some experience from earlier studies have shown that Cr seems to be quite stable and does not diffuse to a large extent in the alloy. Nickel, on the other hand, seems to diffuse along with Fe through the oxide scale [9].

The selection of proper materials or the prediction of corrosion resistance of different alloys, necessitates the knowledge on the fuel characteristics, furnace conditions and reactions, fly ash formation rates and reactions, and boiler layout (see Fig. 5). The boiler is a chemical reactor and several competing reactions are proceeding at the same time. Especially, sulfur and chlorine are competing from the same elements. Therefore, it is essentially important to know every single step in the chain from fuel analysis to deposits and fly ash before the proper materials can be selected.

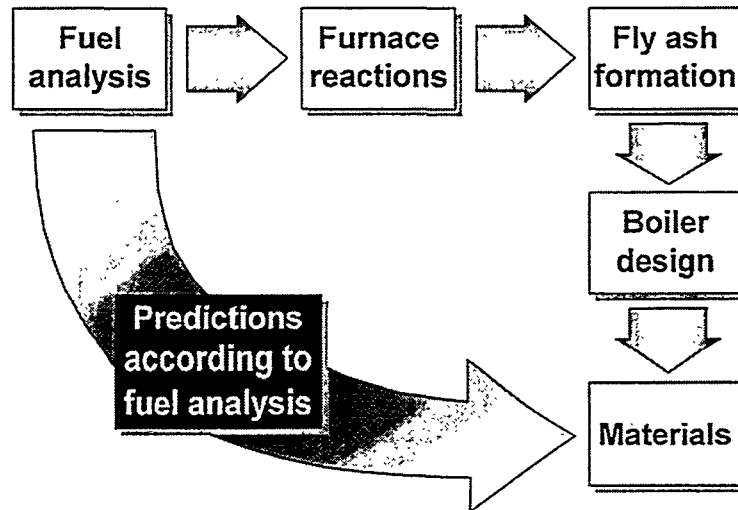


Figure 5: Prediction of the corrosiveness of a fuel is not usually a straightforward procedure. Materials can not in most cases be readily chosen according to the fuel analysis. Several different steps between the fuel analysis and material selection must be taken into account.

4 Summary and recommendations

Today, the ability to predict the corrosiveness of a certain biofuel is still based on experiences. Therefore, unpredicted failures occasionally occur in the hottest superheaters. To avoid this, the boiler manufacturer should have a wide experience on different biofuels and superheater materials. The fact is that every boiler is corroding and therefore the real know-how lies in the measures how to limit the rate below the design limit (0.1 mm/year).

Corrosion of materials is typically a temperature related process. Limiting the maximum material temperatures longer lifetimes can be achieved. This may also sometimes be the only way to limit the corrosion rate. To choose the best (and the most expensive) high alloyed material is another approach to the problem. Unfortunately, only few can afford this measure.

One feasible and a relatively low cost way to find out the corrosion resistance of different alloys is to make in situ probe measurements in the boiler. This assures that the conditions are proper for the particular case. However, the results obtained are generally only valid in that specific boiler and may give misleading guidelines if applied to other cases. Probe studies are recommended if a totally new fuel with relatively high alkali and chlorine content is considered.

5 References

1. Alekhnovich, A. N., Bogomolov, V. V., "Slagging property indices of coals and their use when designing boilers", in *The Impact of Ash and Deposition on Coal Fired Plants* (Williamson, J., Wigley, F., eds.), Taylor&Francis, 1994, pp. 725-732.
2. Salmenoja, K., Mäkelä, K., Backman, R., "Corrosion in Bubbling Fluidized Bed Boilers Burning Chlorine Containing Fuels", *Proc. of the 8th Int. Symp. on Corrosion in the Pulp&Paper Industry*, May 16-19, Stockholm, Sweden, 198-206, 1995.
3. Salmenoja, K., Mäkelä, K., "Corrosion in Bubbling Fluidized Bed Boilers Burning Potassium and Chlorine Containing Fuels", *Proc. of the 1996 TAPPI Engineering Conference, September 16-20*, Chicago, Illinois, USA, 707-713, 1996.
4. Christensen, K. A., "The formation of submicron particles from the combustion of straw", Ph.D. Thesis, Technical University of Denmark, Lyngby, Denmark, 1995.
5. Salmenoja, K., Mäkelä, K., Hupa, M., Backman, R., "Superheater Corrosion in Environments Containing Potassium and Chlorine", *Journal of the Institute of Energy* 69: 155-162 (1996).
6. Krause, H. H., "Corrosion by Chlorine in Waste-Fuelled Boilers" in *Incinerating Municipal and Industrial Waste* (Bryers, R. W., editor), Hemisphere, 1991, pp. 145-159.
7. Bishop, R. J., Cliffe, K. R., "Condensation of sodium chloride vapour from a moving gas stream", *J. Inst. Fuel* 42 (7): 283-285 (1969).
8. Adams, T. A., Frederick, W. J., "*Kraft Recovery Boiler Physical and Chemical Processes*", American Paper Institute, New York, 1988.
9. Salmenoja, K., Mäkelä, K., "Studies on the corrosion of Fe based alloys for superheater applications", presented at the 9th International Symposium on Corrosion in the Pulp and Paper Industry, May 26-29, Ottawa, Ontario, Canada, 1998.

Neural Network for Prediction of Superheater Fireside Corrosion

Pasi Makkonen, Research Engineer / Lic. Tech.
Foster Wheeler Energia Oy, Karhula R&D Center
Karhula, Finland

Abstract

Superheater corrosion causes vast annual losses to the power companies. If the corrosion could be reliably predicted, new power plants could be designed accordingly, and knowledge of fuel selection and determination of process conditions could be utilized to minimize of superheater corrosion. If relations between inputs and the output are poorly known, conventional models depending on corrosion theories will fail. A prediction model based on a neural network is capable of learning from errors and improving its performance as the amount of data increases. The neural network developed during this study predicts superheater corrosion with 80 % accuracy at early stage of the project.

1. Introduction

The material loss in superheaters is one of the most expensive phenomena as far as the maintenance costs of commercial boilers are concerned. Superheater corrosion is a common reason for boiler shutdown. A shutdown and consequent superheater repair significantly increase the operating costs of a boiler. The factors which cause corrosion in combustion are not fully known. Neural networks are an effective prediction method when the relations which affect the result are uncertain. The use of neural networks is based on teaching the network with existing data, and, after a sufficient prediction accuracy has been achieved, utilizing the network by feeding new input data to achieve a solution for the problem. The decision chain behind the answer does not have to be known, and a result can be derived with little data. However, in order to create a reliable device for prediction, a large amount of data has to be available for the learning process.

The factors which have to be taken into account when creating a neural network model for the superheater corrosion are:

- Fuel Characteristics
- Bed Material Characteristics
- Temperatures in Combustion Zone and in Superheater Area
- Boiler Design.

2. Neural Networks

The idea of neuron was introduced by Ramón y Cajál in the middle of the 20th century, but at that time devices for utilizing the theory in practice were unavailable (Haykin /1/). The first applications utilizing neural network for prediction were adaptive linear filters in the middle of the 1980's. The idea behind neural networks is the similarity to the action of brain cells: the neural network allows complex, nonlinear, and multitasking function.

A neuron is a simple derivation element consisting of several inputs and one output. A neuron is shown in Figure 1. The operation of the neuron can be presented with equations

$$u_k = \sum_{j=1}^p w_{kj} x_j \quad \text{and} \quad y_k = \varphi(u_k - \theta_k) \quad (1)$$

where u result of linear combiner
 j, k, p indexes
 w synaptic weight
 x input signal
 φ activation function
 y output signal
 θ threshold / bias.

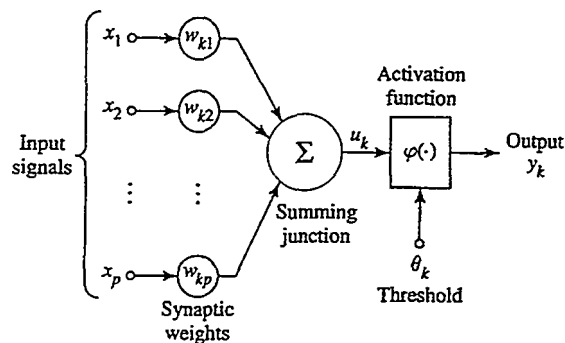


Figure 1. Model of a neuron (Haykin /1/, page 8).

The activation functions can be divided into three basic types:

- Threshold Function
- Piecewise-Linear Function
- Sigmoid Function.

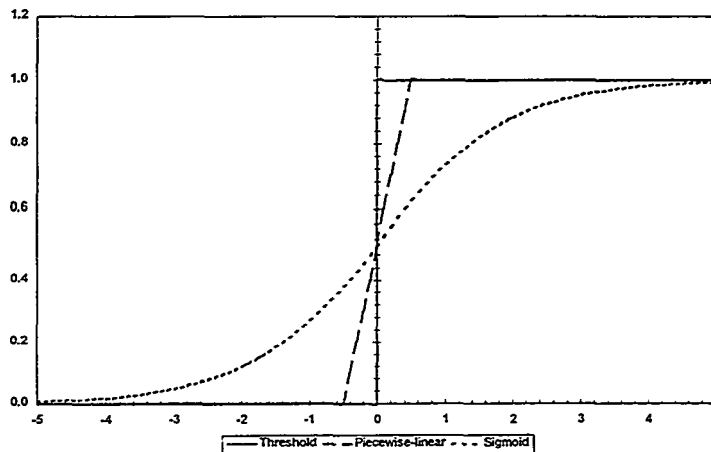


Figure 2. Responses of different activation functions.

A neural network is a combination of one or more neurons which are connected according to the desired operation. Two examples are illustrated in Figure 3. When one or more outputs are connected as a feedback, the neural network type changes to *recurrent*. This allows the network output to be used as an input, which in many cases assist the learning process. A *lattice* structure is a feed-forward neural network, in which the outputs are arranged in rows and columns, allowing a matrix-like layout.

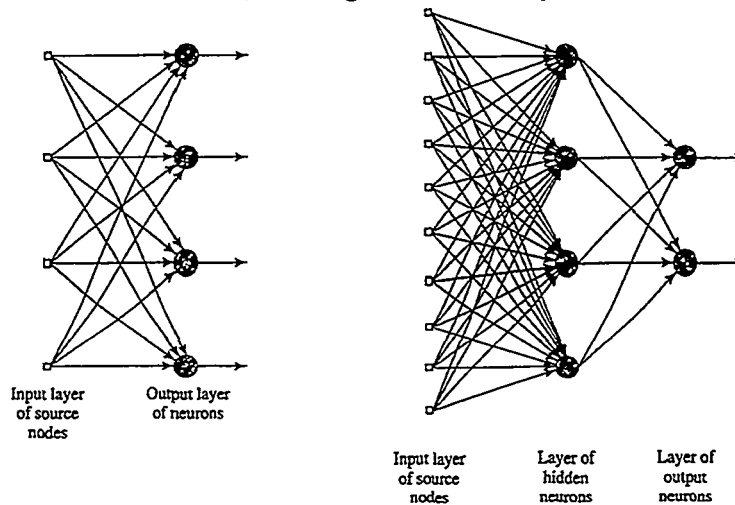


Figure 3. Two examples of feed-forward neural networks (Haykin /1/, pages 18 and 19).

2.1 Learning Procedures

The learning process is the initial function when working with neural networks. Undergoing changes is an essential part of the learning process. The changes can take place in the synaptic weights, biases, and even in the activation functions. However, the larger the number of neurons in the network is, the more data have to be used for the learning process. If we consider one linear neuron, the network operation can be presented with matrix operations, equation

$$y = WX + \theta \quad (2)$$

where W array of network weights
 X array of network inputs.

If it is possible to determine X^{-1} , W can easily be solved.

By Haykin [1], for each neuron it is possible to write an equation

$$e_k(t) = d_k(t) - y_k(t) \quad (3)$$

where $e_k(t)$ error of neuron k at time t
 $d_k(t)$ desired response of neuron k at time t .

The network error can then be minimized according to the sum of squared errors by adjusting the synaptic weights according to equation

$$\Delta w_{kj}(t) = \zeta e_k(t) x_j(t) \quad (4)$$

where ζ learning rate.

The signal-flow graph of error correcting learning is shown in Figure 4 and the corresponding learning process is shown in Figure 5.

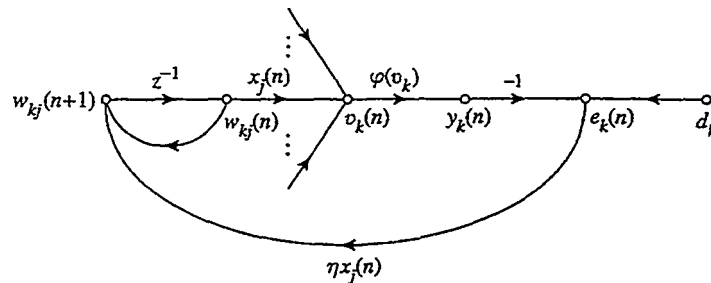


Figure 4. Error correction learning (backpropagation) (Haykin [1], page 48).

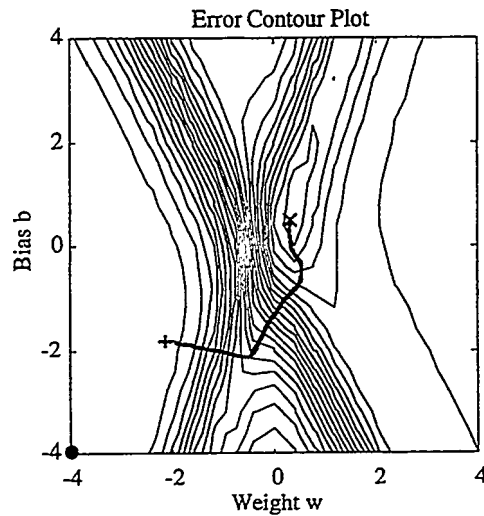


Figure 5. Black line shows the progress of the learning process on the error contour plot, "+" refers to the start and "x" to the end (Demuth and Beale /2/, page 5-13).

2.2 Applications

The amount of neural network applications is increasing all the time. The variety of possible subjects is vast, and only the difficulties in teaching the network and in some cases the high number of neurons required set the limits to the target applications. Examples of the use of neural networks in Finland are listed by Bulsari and Saxén /3/. These applications include:

- Image Compression
- Non-Linear Modeling
- Self Organizing Maps
- Conscious Machines.

3. Superheater Fireside Corrosion

Fireside corrosion is often a very complicated process. Metal wastage of superheater can occur due to oxidation, sulfidation, erosion-corrosion, or a combination of these. Chlorine-containing deposits may also be one of the crucial factors causing metal loss. In order to evaluate the risk of superheater fireside corrosion, one has to be aware of the main corrosion types and their effects. The risk evaluation is often done by examining the fuel characteristics, but the role of combustor type must not be neglected (Jia-Sheng /4/). The occurrence of many corrosion types is accelerated by a reducing gas environment.

3.1 Corrosion Mechanisms

The most common metal degradation mechanism encountered in combustion is oxidation. Oxidation takes place when the oxygen in the flue gas gets in contact with the superheater steel surface. Due to the need for elevated strength at high temperatures, the steels used in superheaters are often chromium and/or nickel containing alloys. The oxidation of the alloy surface creates a protective iron or chromium oxide layer which prevents diffusion of oxygen. Because of the decreased diffusion, the oxidation rate slows down, and a stable oxide layer is formed on the steel surface. This type of oxidation is called selective, and the mechanism is widely used for protection against corrosion. Oxidation can seldom be presented with only one equation, combinations of rate laws are common. The oxidation rate constants depend on metal, temperature, and diffusion coefficient of oxygen through the oxide layer. If the diffusion rate through the oxide layer is high, the oxide forms no protection against further oxidation.

Sulfur corrosion, often referred to as sulfidation, is a very common phenomenon in coal combustion, but it can also occur with other fuels. In the combustion process, the sulfur in fuel reacts with oxygen in the combustion air forming SO_2 , and, if the residence time and O_2 content are sufficient, also SO_3 . The reaction seldom continues so as to result in internal sulfidation of the metal. Some parabolic oxidation and sulfidation rate constants are listed in Table 1.

TABLE 1. Oxidation and sulfidation rate constants for parabolic oxidation and sulfidation (Mrowec /5/, page 373).

Metal or alloy	Sulphidation		Oxidation	
	Temperature C	kp $\text{g}^2\text{cm}^{-4}\text{s}^{-1}$	Temperature C	kp $\text{g}^2\text{cm}^{-4}\text{s}^{-1}$
Cu	650	$8,45 \cdot 10^{-4}$	900	$1,3 \cdot 10^{-8}$
Ni	620	$1,1 \cdot 10^{-6}$	1000	$9,1 \cdot 10^{-11}$
Co	720	$6,67 \cdot 10^{-6}$	950	$1,6 \cdot 10^{-9}$
Fe	800	$8,1 \cdot 10^{-6}$	800	$5,5 \cdot 10^{-8}$
Al	800	$1,0 \cdot 10^{-9}$	1000	$1,0 \cdot 10^{-14}$
Zn	600	$2,0 \cdot 10^{-8}$	800	$6,4 \cdot 10^{-10}$
Cr	1000	$8,0 \cdot 10^{-7}$	1000	$4,5 \cdot 10^{-12}$
Fe-20Cr	1000	$9,8 \cdot 10^{-6}$	1000	$2,0 \cdot 10^{-11}$
Fe-20Cr	900	$1,8 \cdot 10^{-6}$	900	$1,7 \cdot 10^{-12}$
Ni-20Cr	1000	$8,8 \cdot 10^{-6}$	1000	$5,0 \cdot 10^{-11}$
Co-20Cr	800	$2,7 \cdot 10^{-7}$	800	$8,3 \cdot 10^{-13}$
Fe-25Cr-5Al	1000	$1,1 \cdot 10^{-6}$	1000	$2,7 \cdot 10^{-13}$
Ni-20Cr	800	$1,0 \cdot 10^{-7}$	800	$2,0 \cdot 10^{-12}$

Chlorine-induced corrosion is a common corrosion type in waste combustion. This type of corrosion can also take place in combustion of other chlorine-containing fuels, for example biofuels and high-chlorine coals. Chlorine corrosion is often accelerated by alkaline components in the fuel. At low temperatures, chlorine corrosion can take place as hydrochloric acid corrosion, but in the case of superheater corrosion, the mechanism is initiated when the fuel contains sufficient amounts of chlorine, and the superheater tube temperature is sufficient for chlorides to form molten eutectics. If there are sulfur-containing components present, the chlorine corrosion can cause very rapid metal loss. The highest rates of superheater tube degradation reported have been about 3 mm/1000 hours of operation. Chlorine corrosion has mostly been studied in connection with waste combustion.

Vanadine, and especially vanadine pentoxide (V_2O_5) can cause a fast increase in the material loss rate in sulfur corrosion environment. The role of vanadine in this corrosion case is not fully agreed on: some researchers claim that the vanadine pentoxide acts as a catalyst, while others think that the role of vanadine is more complex (Evans /6/).

In erosion-corrosion, the protective oxide layer or the created corrosion product is removed from the tube surface by erosion. The erosion is due to particles colliding with the metal surface. The erosion rate depends on the particle velocity and characteristics, as well as the metal surface properties (Barkalow, Goebel and Pettit /7/).

3.2 Measurement of High-Temperature Corrosion

Several measurement methods of high-temperature corrosion have been developed to be used in a laboratory scale (Haynes and Baboian /8/). However, few of these give results which could be directly applied to field use. The problem lies in the changing flue gas atmosphere, which is very hard to create in a laboratory. Results achieved in metal tests at laboratories can only be used with caution for material selection, and that is why field tests are considered to be the only reliable method of achieving a basis for lifetime estimation of a material. The superheater corrosion can be evaluated directly by measuring the material loss on a time basis. This, however, requires a boiler shutdown. Other ways of measuring the corrosion rate and determining the corrosion mechanism are more or less indirect. The corrosion rate can be evaluated by measuring the material loss by using a special probe. The corrosion probe can be of a type that utilizes electrical phenomenon taking place in a corrosion attack (Barrett /9/), or a type which contains cooled steel coupons which are weighed and analyzed.

3.3 Ways Of Preventing Superheater Corrosion

If the fuel is harmful enough, superheater corrosion can seldom be totally prevented. However, there are methods of reducing the corrosion rate. Several factors can be taken into account in the superheater design. The concentration of harmful impurities in the flue gas can be reduced by limiting the fraction of the worst fuel component. The boiler can be designed so that the corrosion risk is reduced. The superheater materials can be selected according to the presumed corrosion risk. The superheaters can be placed so that the fouling and corrosion are minimized. Hein /10/ has presented some possible means for reducing high temperature corrosion:

- Dilution of Sulfur Oxides
- Change of Tube Material
- Change of Tube Temperatures
- Shielding of Tubes
- Change of Fuel or Fuel Blends.

4. Experiments

A neural network was selected as the method for prediction, because the factors contributing to superheater corrosion in atmospheric fluidized bed combustion are not evident. Development of a theoretical calculation model for the phenomenon necessitates several assumptions. However, a neural network which is taught with existing field data provides a solution which gives a good estimate with a few input parameters. The teaching was based on the data achieved from field studies and laboratory measurements of superheater corrosion. The methods used for the measurements and analyses included measurements of metal thickness, microscopic studies and SEM/EDS analyses. Several neural networks were tested and evaluated. The final model was evaluated by statistical means and by comparing it to corrosion cases not included in the learning data.

4.1 Corrosion Evaluation

Means used for corrosion evaluation during this work can be listed as follows:

- SEM/EDS Analyses
- Optical Microscopy
- Chemical Analyses of Deposits and Corrosion Products
- Both Thermodynamical and Thermochemical Calculations
- Probe Tests
- Tube Thickness Measurements.

In order to be able to utilize the information achieved from the field and laboratory tests, a database of corrosion cases was constructed. The database was built upon an existing fuel database. The fuel database was supplemented with corrosion and process data so that the factors contributing to superheater corrosion could be evaluated. The database consisted of boiler type, size, steam parameters, bed and tube material, fuel characteristics, and corrosion data.

4.2 Prediction Of Corrosion With A Neural Network

The corrosion database was further developed by creating a neural network program which was taught to provide an estimate of the predicted corrosion potential of a known fuel and bed material with certain flue gas and steam temperatures. The number of data sets was 92, evenly distributed between laboratory and field tests, and commercial projects. The fuel data was imported from a fuel database, and the tube material and bed characteristics were gathered from separate databases. Several different networks were constructed for the task. The testing was started with a simple approach, and the complexity of the solution was increased as the knowledge about the system behavior increased. The generated networks were improved by testing different activation functions during the study in order to find the optimal solution for the problem at hand. The outlook of the output and result windows of the user interface are shown in Figures 6 and 7.

Data Input

INPUT VALUES:

Boiler Type: C-BFB Selected Type: CFB Boiler Size, MW: 100

Project Name: Test 1

Available Fuels:

Fuel	LHV	Volatile	Ash	C	H	N	O
Coal Anthracite	29.55	18.15	10.05	77.70	3.01	1.43	6.66
Coal Bituminous	29.72	25.80	17.10	72.30	4.18	1.09	4.79

ADD SELECTED FUEL

Selected Fuels:

Fuel	Fraction	LHV	Volatile	Ash	C	H
Coal Bituminous	100%	29.72	25.80	17.10	72.30	4.18

REMOVE FUEL

Flue Gas Residence Time: 112

Temperatures, C:

Combustion: 880

Flue Gas: 850

Steam: 500

Inlet Quench, mm/s: 10.08

Available Bed Materials:

Sand
Limestone
Dolomite

SELECT BED

Selected Bed Material: Limestone

Available Steels:

10CrMo910
9Cr1Mo
X12

SELECT STEEL

Selected Steel: 10CrMo910

RUN END

Figure 6. Data input window for the corrosion prediction model.

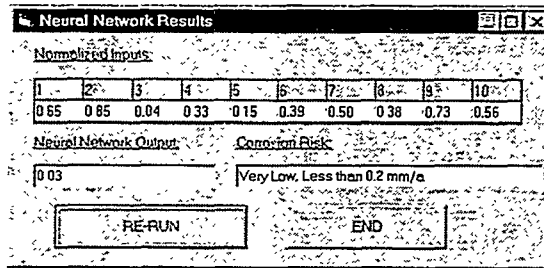


Figure 7. Result output window for the corrosion prediction model.

5. Results

The neural networks were taught with backpropagation. The quality of learning was evaluated by monitoring the calculated sum of squared errors (SSE) for the learning data and by monitoring the risk of relative overfitting. The dependence of the SSE on the number of neurons as tested with the Levenberg-Marquardt algorithm is shown in Figure 8. It may be noted that the increase in the number of neurons decreases the SSE until the number of neurons is 6, after which the SSE is almost constant, if a sufficient amount of epochs is used for the learning. However, while increasing of the number of neurons improves the accuracy, the risk of overfitting also increases, as can be seen from Figure 8.

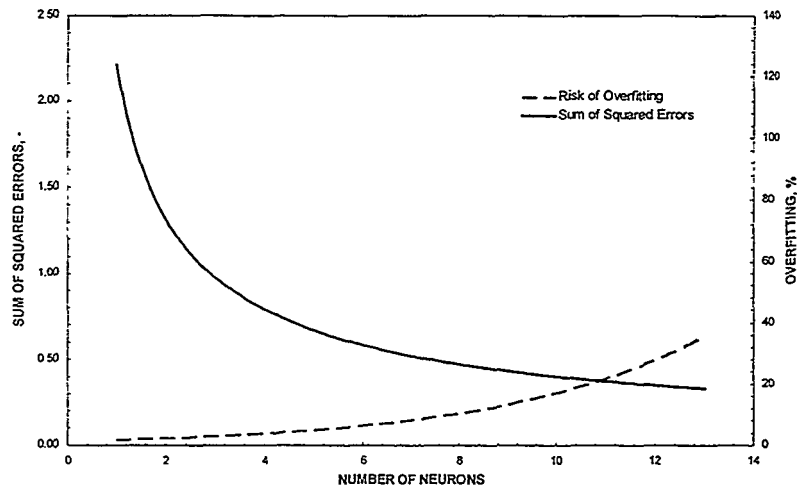


Figure 8. Dependence of SSE and overfitting on the number of neurons, Levenberg-Marquardt learning algorithm.

The network layout selected for the model contained two hidden layers. The first layer was formed by five *tansig* neurons, the second had five *logsig* neurons and the output layer had one linear neuron. The calculated corrosion risk versus the measured corrosion risk is shown in Figure 9.

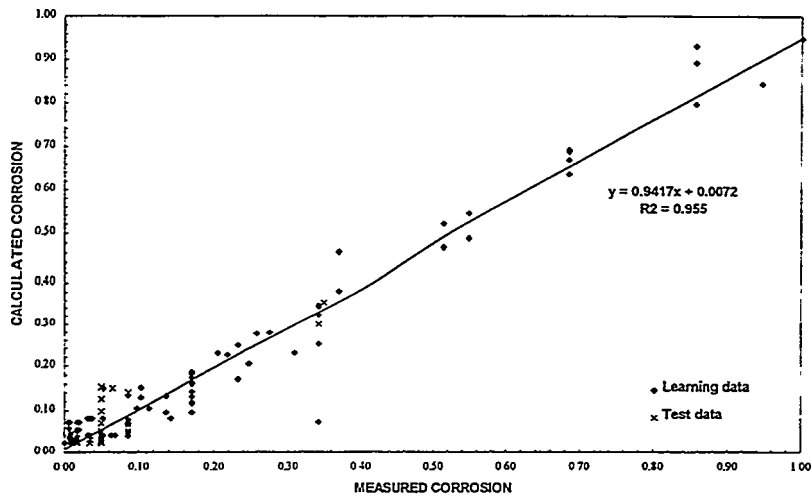


Figure 9. Calculated corrosion versus measured corrosion, normalized values.

6. Conclusions

At the beginning of a project, only little information about the fuel characteristics is available. Further, the boiler design is known only in principle. However, with this small amount of information a skilled professional can say if there is a risk of corrosion. The challenge of this study was to put this information into a form that can be used in a computer program. The generated model for corrosion prediction was based on the data gathered from field and laboratory measurements. The neural network is based on two non-linear hidden layers and a linear output layer. The total number of neurons was 11, five in both hidden layers and one for the output. The network was implemented into the user interface so that the weight and bias arrays can easily be changed as the amount of learning data increases and the network can be re-taught. The generated tool for corrosion prediction can be further improved by generating more reliable methods for fuel, bed material, and boiler quality evaluation.

7. References

1. Haykin S., *Neural Networks, a Comprehensive Foundation*, Macmillan Publishing Company, New York, 1994.
2. Demuth H. and Beale M., *Neural Network Toolbox For Use with Matlab*, User's Guide, The Math Works Inc., Massachusetts, 1996.
3. *Neural Network Research in Finland*, Bulsari A. and Saxén B. (Ed.), Publications of the Finnish Artificial Intelligence Society - no 10, Åbo Akademi, Turku, 1993.
4. Jia-Sheng L., *Corrosion Mechanisms in Fluidized Bed Combustion Environments*, Ph.D. Thesis, Stanford University, Department of Materials Science and Engineering, 1988.
5. Mrowec S., *Mechanism of High-Temperature Sulphide Corrosion of Metals and Alloys*, Werkstoffe und Korrosion Vol. 31, n:o 5, Verlag Chemie GmbH, Weinheim, 1980.
6. Evans U. R., *The Corrosion and Oxidation of Metals: Scientific Principles and Practical Applications*, Edward Arnolds (Publishers) LTD., London 1960.
7. Barkalow R. H., Goebel J. A. and Pettit F. S., *High Temperature Erosion-Corrosion by High Velocity (200 m/s) Particles*, in Materials Problems in Fluidized-Bed Combustion Systems, Electric Power Research Institute, Pratt&Whitley Aircraft Group, Connecticut, 1980.
8. *Laboratory Corrosion Tests and Standards*, Haynes G. S. and Baboian R., (Ed.), ASTM Special Technical Publication 866, Texas Instruments, Incorporated, Philadelphia, 1983.
9. Barrett J., *Cool Probe Measures High Temperature Corrosion*, Eureka Transfers Technology, November 1993.
10. Hein K. R. G., *Fuel Related Problems in Boiler Operation*, in Fuels Utilization and Environment, Volume 1, International Flame Research Foundation, Prague, 1991.

Cracking and Corrosion Recovery Boiler

Heinrich Suik

Tallinn Technical University – Horizon Pulp & Paper

Tallinn, Estonia

Abstract

The corrosion of heat surfaces and the cracking the drums are the main problems of the recovery boiler. These phenomena have been appeared during long-term operation of boiler “Mitsubishi - 315“ erected at 1964. Depth of the crack is depending on the number of shutdowns and on operation time.

Corrosion intensity of different heat surfaces is varying depend on the metal temperature and the conditions at place of positioning of tube. The lowest intensity of corrosion is on the bank tubes and the greatest is on the tubes of the second stage superheater and on the tubes at the openings of air ports.

1 Introduction

Recovery boiler “Mitsubishi - 315“ erected at 1964 has worked more than 220 000 hours. Boiler consists of two drums connected with bank tubes, furnace with waterwalls, the first and the second stages of superheater and the vertical economizer with its headers. Some basic elements of boiler have been changed during operation - the economizer tubes due to corrosion problems - two times, also the second stage of superheater, and the lower part of waterwalls in the furnace has been taken reconstruction. The fin tubes on the level below the second oil burners have been changed tubes with smooth tubes so that one upper tube has been connected with two tubes by Y-joints. Original basic part are drums with bank tubes, the first stage of superheater, upper waterwalls in the furnace and most of headers.

Long-term operation has been ascertained two problems - corrosion of heating surfaces and cracking in the drums. The main safety problem of boiler is developing of cracks

and also intensity of corrosion during the operation. The reason of forming and developing of cracks and rate of corrosion are the subject for this paper.

1.1 Operation conditions

Operation pressure of steam is 3.3-3.5 MPa and temperature 430 - 450 °C. Operation regime of boiler has been cyclic. It was varied liquor and oil burned cycles. During 4-30 days it was burned black liquor with one oil burner, and during 1-3 days only oil. Usually recovery boiler was stopped during operation in every month due to different reasons, for example for cleaning, for technological reasons and so on. Duration of such outages was 48 - 72 hours. One of the longest shutdown in year for the repair the boiler continued for a month. The number of all shutdowns are about 350 - 380.

2 Cracking

2.1 Drum material

In the table 1 the consist of drum metal is given. Material used for the drums of boiler Mitsubishi-317 is STB49B. The other materials shown in table 22K and 16THM are given for the comparing.

Table 1

Materials used in boiler drums.

Material	Composition, %					Mechanical properties	
	C	Si	Mn	Si	P	Tensile stress, MPa	Yield stress, MPa
STB49B	0.24-0.27	0.20-0.26	0.84-1.27	0.009-0.013	0.011-0.013	560-580	380-400
22K	0.18-0.26	0.17-0.40	0.7-1.0	<0.04	<0.04	510	250
16THM	0.12-0.18	0.12-0.26	0.7-1.0	<0.04	<0.04	560	400

As seen in table 1 the materials STB49B and 16THM according to mechanical properties are similar. Investigation showed that intensity of stress in the eyes of tubes in the drum of steel 16THM is equal 40-60 kg/mm² after of few ten thousand hours operation, i.e. limit of creep-rupture strength in the temperature of 350 °C. Cracking drums manufactured from steel 16THM is observed in operation of 10-30 thousand hours. /1/. Examinations the drums of Mitsubishi-317 showed two type cracks: The crack in the welding between the head and cylindrical part of drum inside surface. It appeared after the fifteen years operation. The depth of crack was 5 - 7 mm and the length was three quarters of perimeter the drum. This crack was observed in the water drum. After sharpening on a grindstone the crack has been not developed further to depth. The second type cracks were developing around tube holes in the steam and water drums. The bank tubes were rolled in the drums, and besides this the tube ends on the border rows in the three side (in Fig. 1 bold line) were welded too.

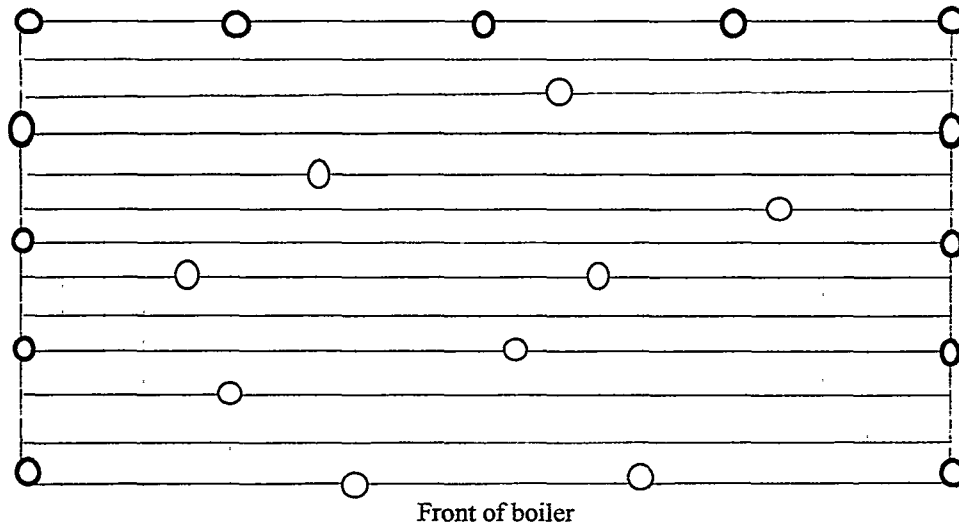


Fig. 1. Layout of bank tubes board in steam and water drums. Bold line shows welded rolled eyes.

The first cracks in this welded eyes were observed after 20 years operation ,about 160 000 h and after 220-240 shutdowns. Most of formed cracks had been aligned in two towards: radial and concentric of tube holes. Some cracks had more complicated shape. Cracks with different shapes are represented in Fig. 2.

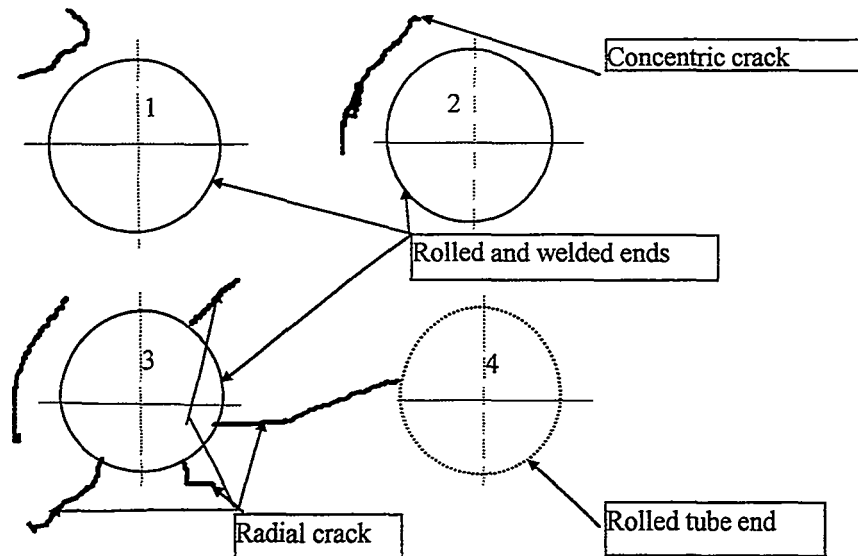


Fig. 2. Cracks with different shape.

Tube eyes Nr. 2 and 3 have concentric cracks. Tube eye Nr. 1 has crack. with complicated shape. Tube eye Nr. 3 has the both cracks - radial and concentric. After 240 000 hours operation the radial crack beginning from eye Nr. 3 has penetrated through ligament between eyes Nr-s.3 and 4. In the table 2. are given cracks marked in the investigated 92 tube eyes.

Table 2

Nature of cracks,

Nature	Number of tube eyes	
	Depth 3-8 mm	Depth 9-40 mm
Concentric	40	7 (9-16 mm)
Radial	2	1 (10mm)
Complicated	11	2 (30-40mm)

As seen in Table 2 the most cracks are concentric and are lesser than 8 mm, but one of complicated cracks is through cracks.

The drums were investigated by different laboratory, and the results also were different. Some researchers were not marked the little concentric cracks (with depth 1-5 mm). The crack begins from welded seam and develop through seam to body of drum. In every year the drums were checked and found cracks were removed by sharpening on a grindstone and the formed pit was filled with welding. It was observed by checking that with aging the metal the cracks formed more and more. After 176 00 hours operation was observed crack in 1 tube eye, after 208 000 h-in 3 tube eyes, 216 000 h,-in 8 tube eyes, 232 000 h in 63 tube eyes.

Through crack

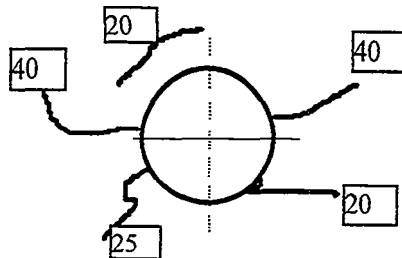


Fig. 2. Through crack in water drum. Number in the box show the depth of crack.

The first crack in this tube eyes is observed after 176 000 hours operation. The depth was measured 5 mm. After checking 32 000 hours the depths of crack were 7 and 8 mm, and in additional again 8 000 hours (216 000 hours) the depths increased to 12 mm, and after 232 000 h operation some cracks run through the wall (40 mm) of water drum.

Probably the developing of through crack was the next:

The first crack with depth 5 mm observed after 176 000 h has not sharpened on a grindstone to peak of crack and the crack continued to penetrate deep. So it is repeated in every year, and after 232 000 hours operation the crack run through the wall of drum.

2.2 Kinetic of developing of crack

In ref. /1/ developing of thermal-mechanical crack is described occurring in two stage: beginning of the initial crack and growth of formed crack. Conventionally it is taken so at the beginning stage the initial crack from the both stresses - the thermal and the mechanical stress started at the same number of cycles of the heat changes at present shutdowns of boiler. Coefficient of damage (N_0) is taken the number of shutdowns being appeared the first crack. In the case of penetrating crack the coefficient of damages is equal $N_0=264$. Kinetic of developing of crack at the initial stage is expressed as following:

$$L = K \times N_0, (1)$$

where, L is depth of crack, mm

K is coefficient of intensity, main parameter characterizes intensity of the crack growth.

Coefficient of intensity (K) of initial crack is equal $K=1.16 \times 10^{-3}$ mm/cycle.

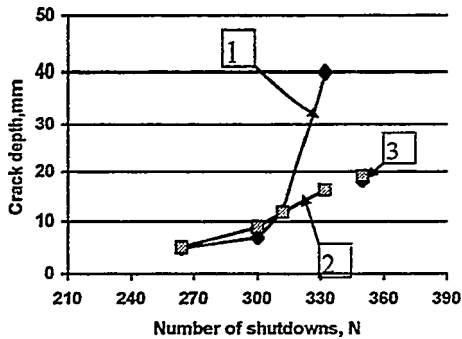


Fig.3. Development of penetrating crack.

1 - current crack. 2 - calculated crack.
3 - crack formed during one year after 240 000 hours operation.

	264	300	312	332	330	350
L	5	7	12	40		18
L(calc)	5.16	9	11.82	16.25		19.06

It is known that depth of crack depend on the number of heat change cycles and on operation time, $L = f(N, \tau)$. On the basis of these data the equation (2) expresses the depth of crack as follows: (in the following form)

$$L=4.35^{-1}(\tau \times 10^{-5})^{2.9} \times N^{1.5} \times 10^{-3}, (2)$$

where τ is operation time, h,

N is number of shutdowns.

As seen in Fig. 3, the calculated crack depth (line 2) corresponds to the current depth at first stage of the crack forming. Obviously these crack are formed and developed due to thermal fatigue.

In time depending on the cycles of shutdown and operation time, the mechanical stress exceeded the thermal stress and development of crack is due to mechanical fatigue. At this stage the intensity of crack growth induced by mechanical fatigue is much more than intensity induced by thermal fatigue.

Minimum required thickness of shell plate of drum is 26.56 mm, and it was actually taken equal to 29 mm. At same time the calculated thickness of tube plate in drum equals to 44.25 mm, actually and it was determined equal to 46 mm. It is seen that if the depth of crack in the ligament equals to more than $46 - 26.65 = 19.35$ mm then residual thickness of plate is less than required minimum thickness. Obviously it is time of increasing the intensity of crack developing due to mechanical stress. It is shown by the current data (Fig.3 the upper part of line 1) as well.

Point 3 in Fig.3 shows the depth of crack formed in boiler drum during one year after 232 000 h operation and 336 shutdowns, i.e. the crack formed after these conditions. After that, boiler worked extra 8000 hours and had 14 shutdowns.

Calculated by the equation (2) under conditions $\tau=240\ 000$ h and $N=350$ shutdowns depth is equal to 19.06 mm. As seen in Fig.3, the difference between depth of actual crack (18 mm) and calculated value (19.06 mm) is equal to 1.06 mm.

2.3 Discussion of Cracking

Operating cyclic loads in the drum are classified into low-cyclic load resulting from starting, shutdowns, accident removal boiler from service and hydrotests, for example 15 times during in year at the present, and high-cyclic load concerned with long term operation of drum at optimal regime.

Fluctuation of temperature in the wall of drum is about 15-20 C° with periodicity 20 - 50 sec and 5 - 12 °C with periodicity 3 - 6 sec. Thermal stresses under these conditions are equal to respectively 60 - 80 and 20 - 50 MPa at cyclic recurrence 5×10^6 - 5×10^7 and 5×10^7 - 5×10^8 /1/. In near the eyes of tube in the drum the additional stress from the heat changes are much more than the value far from holes.

Mechanical loads under transient regime may be considerable. Mechanical loads during transient regime may be extent to 300 MPa /3/.

Cyclic thermal stress arising from nominal regime of drum influences with static extending stress from internal pressure and together they exceed the yield limit at the edges of holes.

In current case it must be mentioned the effect of welding on the developing of cracks. Cracks formed in the eyes of tubes welded in the drums. So far the forming of cracks in the eyes of tubes rolled in the drums has not observed.

Long-term operation with low-cyclic and high-cyclic loads is a reason of forming of cracks in the welded rolled eyes in tube plates of drum.

One year operation of boiler after long term working with frequent shutdowns (12 - 16) is sufficient time to forming crack with dangerous crack (more than 18 mm in present case).

3 Corrosion

3.1 Heat surface material

Carbon steels are the construction materials for the heat surfaces.

Table 3

Material used for heat surfaces.

Material	Elements, %							
	C	Si	Mn	Cr	Mo	P	S	Cu
STB-35	0.08- 0.18	0.10- 0.35	0.30- 0.60	-	-	<0.035	<0.035	0.20
STB-39	0.10- 0.20	0.10- 0.50	0.30- 0.80	-	0.45- 0.65	<0.03	<0.03	0.20
STB-42G	0.15	0.50- 1.00	0.30- 0.60	1.00- 1.50	0.45- 0.65	<0.03	<0.03	

Throughout the operation some heat surfaces were changed due to corrosion. The corrosion process was different on the heat surfaces. It was most intensive on the tubes of the secondary superheater and of furnace wall in the level primary air openings and of smelt.

The decreasing of wall thickness of tube was measured on the front of the tubes, i.e. the values of corrosion showed maximum corrosion rate on the circumference of tube. In the table 4 shown below some of the maximum of corrosion depths on the front of tubes are given after operation at different time at the same metal temperature. The corrosion depths on the superheater tubes are given for different metal temperature at two different operation time.

Table 4

Corrosion depth on front of tube.

Primary superheater

Temperature, °C	Time, h		
	24 000	224 00	248 000
	Corrosion depth, mm		
300	0.62; 0.65	2.2; 2.5	2.5; 2.5
360		2.3; 1.89	
400		2.3; 2.5	2.5; 2.5
Wall tube in the level of smelt			
Temperature, °C	Time, h		
	16 000	96 000	112 000
	Corrosion depth, mm		
270	0.68; 0.78; 0.53	1.27; 1.45; 1.63	2.02; 2.03; 2.13
Wall tube at the level higher than primary air ports			
Temperature, °C	Time, h		
	16 000	96 000	112 000
	Corrosion depth, mm		
270	0.47; 0.51; 0.45	1.30; 1.16; 1.16	1.41; 1.43; 1.27

Wall tube at the level of primary air ports			
	Time, h		
Temperature, °C	16 000	96 000	112 000
Temperature, °C	Corrosion depth, mm		
270	0.65; 0.60; 0.45	2.0; 1.9; 1.8	1.70; 1.8; 1.65
Bank tube			
	Time, h		
Temperature, °C	16 000	224 000	248 000
Temperature, °C	Corrosion depth, mm		
270	0.35; 0.3; 0.28	1.07; 1.09; 1.08	1.08; 1.07; 1.06

As seen in the table 4. at metal temperature 270 °C the corrosion intensity is the highest in the furnace at the level of air ports in operation of 96 000 h and it is equal 2.00 mm. At same metal temperature (270 °C) the most lowest intensity of corrosion is at bank tubes. After operation 224 000-248 000 h corrosion depth not exceed 1.09 mm. Primary superheater had leakage in the lower bend of tube coil. Superheater plate is formed by two tubes bend to parallel external and internal coils. There are four two-tubes coils in the plate. Leakage on the front of the external bend of coil and on the both side of the internal bend of tube coil. Data of superheater given in the table 2 show corrosion depth of tube bend which had leakage. Original wall thickness of superheater tube is 4 mm. Maximum of the corrosion depth on the superheater tube at temperature 400 °C is 2.5mm after operation 224 000 h and 248 000 h.

3.2 Discussion of Corrosion

Results of corrosion at the tubes of evaporation heat surfaces are presented in fig. 4. All evaporation heat surfaces have the same metal temperature it's 270 °C. As seen at this metal temperature the highest corrosion is on the tubes level of air ports – shown by line air ports. The intensity of corrosion of tubes at the level of smelt is very nearly the same –as line at smelt.

Corrosion of tubes in the furnace higher than primary air ports is being intermediate in intensity between the highest (air ports) and the lowest corrosion (on the bank tubes) – as line air ports. The lowest intensity of corrosion is on the bank tubes shown by line bank tube.

On the basis of operation test data of bank tubes by applying the theoretical method in the /5/ the next equation has been obtained for calculating the corrosion depth on the tubes of bank.

$$\ln \Delta S = -2.333 - \frac{2450}{T} + 0,51 \times \ln \tau \quad (3)$$

Where

- ΔS is corrosion depth, mm,
- T is metal temperature, °K,
- τ is operation time, h

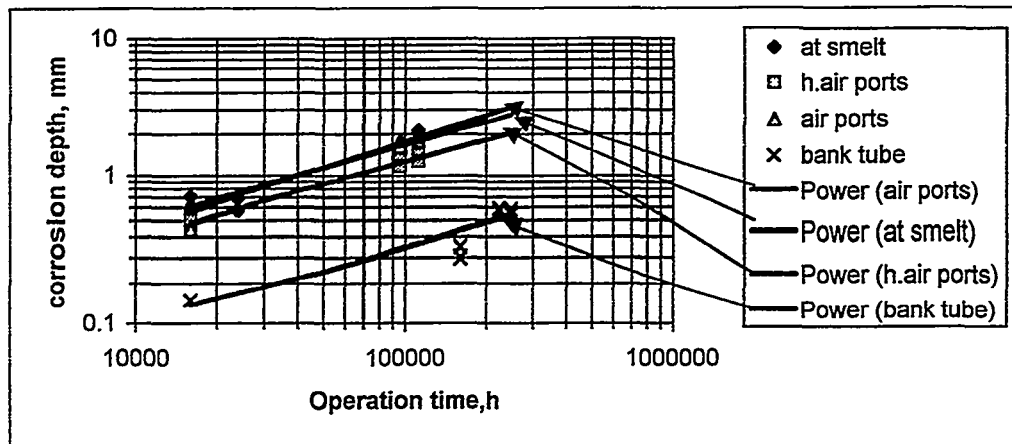


Fig.4. Corrosion depths on the tubes depend on time in the different places of boiler at metal temperature 270°C.

By modification equation 3 with data at the level higher than primary air ports the equation is obtained for calculation the corrosion depth on waterwall tubes:

$$\ln \Delta S = -1.145 - \frac{2450}{T} + 0,51 \times \ln \tau \quad (4)$$

For calculation corrosion depth on waterwall tubes at level of smelt spouts and at level of primary air sports corresponding equation is:

$$\ln \Delta S = -0.8038 - \frac{2450}{T} + 0,51 \times \ln \tau \quad (5)$$

On the Fig.5 the presented line is showing the corrosion depths at different metal temperatures – at 300 °C, 340 °C and 400 °C. It is seen that the corrosion depths are not different in considerable extent. Accordingly the increasing of metal temperature from 300°C to 400°C no effects to corrosion intensity.

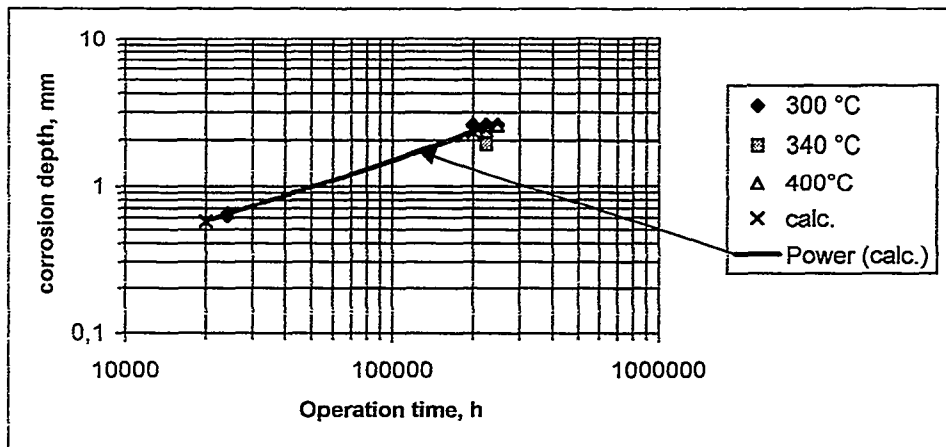


Fig.5. Corrosion depths on the superheater tubes depend on time at the different metal temperature.

Usually corrosion intensity is described by Arrhenius equation /5/

$$\Delta S = A \times e^{B/T} \times \tau^n$$

n is power of oxidation, $n(T) = C \times T$. It is obtained $C = 0.939 \times 10^{-3}$ at metal temperature 270 °C. The mean metal temperature of superheater tubes is 340 °C, and power of oxidation $n = 0.57$.

Calculated depth of corrosion on the superheater tube according the equation 6 is shown on the fig. 5 by line calc. The metal temperature is 340 °C.

$$\ln \Delta S = -1.819 - \frac{2450}{T} + 0,57 \times \ln \tau \quad (6)$$

Black liquor contains about 25 % inorganic material, making it one of the highest ash-containing industrial fuels used in boilers. The formation of massive ash-derived fireside deposits on the heat transfer surfaces in the boiler is inevitable. Deposits consists of more than 99.8 wt% water-soluble compounds, mainly sodium sulfate (Na_2SO_4) and sodium carbonate (Na_2CO_3), with small amounts of sodium chloride (NaCl), sodium hydroxide (NaOH), and reduced sulfur compounds such as sodium sulfide (Na_2S). Potassium is also present as a substitute for some sodium sulfide (Na_2S). Potassium is also present as a substitute for some sodium. According to H. Tran the composition of smelt consists mainly of 20- 30 % Na_2S , and 60-70 % Na_2CO_3 . The carbonate content in deposits decreases dramatically toward the back side of boiler. In deposit of boiler bank content of Na_2CO_3 is below 5 %. Main component is Na_2SO_4 /3/. Composition of deposit at the level of superheater consists of Na_2SO_4 , Na_2CO_3 and Na_2S correspondingly 60 %, 10 % and 25 %.

The melting temperatures in a salt mixtures of sodium and potassium sulfates, carbonates, chlorides, and sulfides ranges from 710 °C to 760 °C, and the lowest solidus temperatures to be reached 520 °C /4/.

As seen above the most intensity of corrosion was at the level of smelt spouts and at the level of air ports, and lowest intensity in the region of bank tubes. That means corrosion rate is the greatest by deposits with the greatest content of Na_2CO_3 , and the lowest by the greatest content of Na_2SO_4 .

The corrosion intensity was influenced by flushing liquid smelt waterwall tubes at the level smelt spouts.

Literature

1. G. A. Tuljakov, Termicheskaia ustalocit v teploenergetike, Moskva Mashinostrojenija, 1978, p.199. (in Russian).
2. P. Auerkari, J. Verho, The service performance of steam drum material, Int. Symposium on Life and Performance of High Temperature Materials and Structures, Baltica II, 1992, p. 1-12.
3. Kraft Recovery Boiler Plugging and Prevention. Honghi Tran, 1992 Kraft Recovery Operations Short Course, 209-218, TAPPI Notes.
4. Sodium and Sulphur Chemistry in Combustion Gases, Rainer Backman. Academic Dissertation, ABO Akademi, 1989.
5. A. A. Ots, Korrozija i iznos poverhnostei nagreva kotlov, Moskva, Energoatomizdat, 1987, p.272. (in Russian).

PECULIAR HIGH TEMPERATURE CORROSION OF MARTENSITE ALLOY UNDER IMPACT OF ESTONIAN OIL SHALE FLY ASH

Tallermo H., Klevtsov I., research scientists
Thermal Engineering Department of Tallinn Technical University
Kopli tn. 116, EE0017, Tallinn, Estonia
Uus M., engineer, Eesti Energia AS
Estonia pst. 1, EE001, Tallinn, Estonia

Abstract

The superheaters' surfaces of oil shale steam boiler made of pearlitic and austenitic alloys, are subject to intensive corrosion, mainly due to presence of chlorine in external deposits. The applicability of martensitic alloys X10CrMoVNb91 and X20CrMoV121 for superheaters is examined here and empirical equations allowing to predict alloys' corrosion resistance in the range of operational temperatures are established. Alloy X10CrMoVNb91 is found been most perspective for superheaters of boilers firing fossil fuel that contain alkaline metals and chlorine. The abnormal dependence of corrosion resistance of martensitic alloys on temperature is revealed, namely, corrosion at 580°C in presence of oil shale fly ash is more intensive than at 620°C.

1 Introduction

The Estonian oil shale is local low-grade fuel having calorific value $Q^r \approx 8.4$ MJ/kg, contents of ashes $A^d \approx 51.3$ % and moisture content $W^r \approx 11.7$ %. It is fired in pulverised condition on two power plants where is produced about 99% of Estonian electricity. The heating surfaces of oil shale steam boilers nowadays are made of pearlitic and austenitic alloys. Their fouling by ash deposits sharply accelerates high-temperature corrosion of metal, mainly due to presence KCl. The periodic clearing of high-temperature heating surfaces from external ash deposits additionally accelerates corrosion process.

Because of metal intensive corrosion, the volumes of repair of superheaters' heating surfaces are great. For example, after 3 years of 100 MW_e boiler operation, about 3300 sections of superheater tubes should be replaced among them about 600 sections of austenitic tubes. Earlier carried out laboratory and industrial researches of corrosion resistance of various alloys did not reveal more suitable alloys that would be able longer resist to aggressive impact of external oil shale ash deposits.

As the strength properties of martensitic alloys under high temperatures are rather high, it seems expedient to investigate suitability of application of these alloys in superheaters of oil shale boiler. Determinative parameter is here alloy's corrosion resistance. Even in the worse case, with identical corrosion intensity of austenitic and martensitic alloys, the preference should be given to martensite because to reduction of expenses for repair of superheater.

In connection with opening of western market and purchasing by Eesti Energia AS of pipes made according to DIN 17175, there was necessity to research corrosion resistance of such alloys as 13CrMo44, 10CrMo910, X10CrMoVNb91, X20CrMoV121, X8CrNiMo1613, X8CrNiMoNb1616 under impact of PF oil shale ashes.

2 Experiments

The laboratory corrosion tests of alloys were carried out using known technique [1,2]. Experiments were performed in electrically heated furnaces under temperatures 540, 580 and 620°C with the ground plate samples by the size 3x10x40 mm. Each 10 hours samples were covered with a layer of fly ash of Estonian PF oil shale. The samples in furnaces were washed by products of combustion of natural gas containing O₂ ~ 4% and CO₂ ~ 10%. The velocity of gases in furnaces made 1.5-1.8 m/s. The contents of chlorine in oil shale ash made approximately 0.60%.

After corrosion testing samples were cleaned off products of corrosion under 400°C by using an electrochemical method to determine the losses of their weights. As an electrolyte the mixture of 60% of calcinated soda and 40% of caustic soda was used. The results of laboratory corrosion tests are presented on Fig. 1 (alloy X20CrMoV121) and Fig. 2 (alloy X10CrMoVNb91). From figures may be noted that most heavily both alloys corrode under temperature 580°C. Exceptions are made by two samples (Fig. 1) under temperature 540°C and duration of test 600 hours. These samples were covered with friable oxide layer poorly cohered with the basic metal. The surface of metal under oxide layer was very rough.

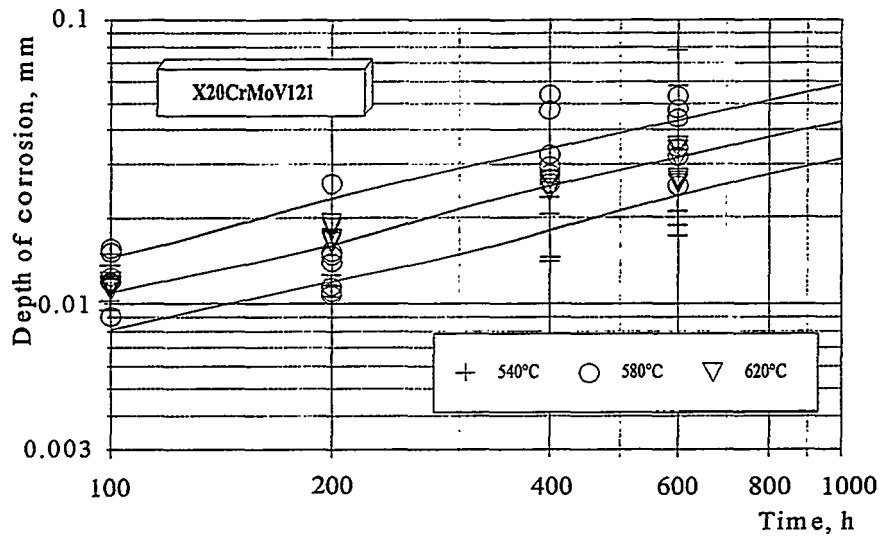


Figure 1. Experimental data and regression of corrosion depth of alloy X20CrMoV121 under impact of Estonian PF oil shale fly ash.

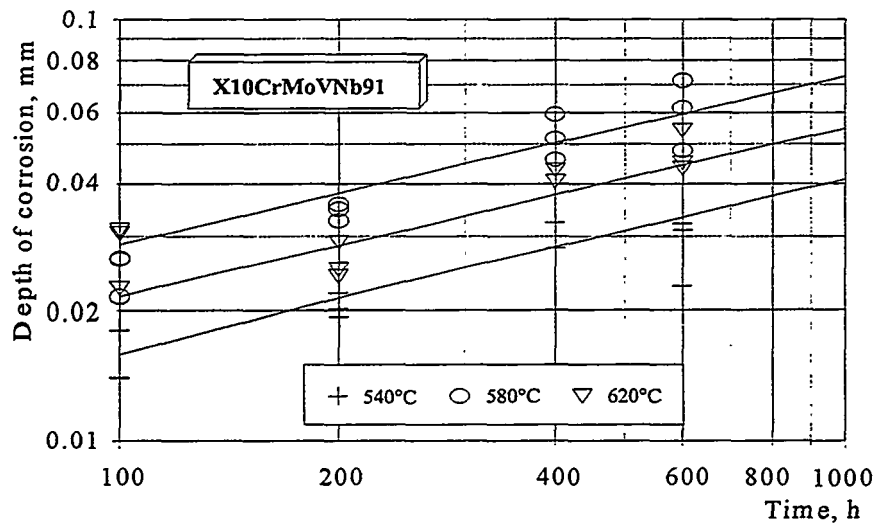


Figure 2. Experimental data and regression of corrosion depth of alloy X10CrMoVNb91 under impact of Estonian PF oil shale fly ash.

3 Results

The received results do not correlate with the well-known characteristics of corrosion process (Arrhenius law), where increase of temperature leads to increase of corrosion intensity. It is necessary to note that similar abnormal

behaviour was found when earlier corrosion tests of alloy 11Ch11W2MoV (or ЭИ-756, Russian alloy manufactured according to ТУ-14-3-460-75) were performed. Our tests of ferritic, pearlitic and austenitic alloys provided in the same conditions do not display such abnormal behaviour under temperatures 580°C and 620°C.

In this connection it seems unreasonable to approximate the received results by using empirical equations of general type $\Delta S=f(\tau, T)$ for predicting depth of corrosion for a long period of operation τ under given temperature T . More reasonable in this case seems to represent entire set of tests' results in tested range of temperatures 540-620°C approximated by using least squares method with equation:

$$\ln \Delta S = a + b \ln \tau, \quad (1)$$

where ΔS is depth of corrosion;
 τ is test duration;
 a and b are constants.

For temperature interval 540-620°C values of corrosion depth predicted by using equation (1) are presented on Fig. 1 and 2 by average line. In these Figures the top and bottom straight lines with probability 67% characterise standard deviation of regression.

It is necessary to note that regression analysis provided for each level of temperatures separately and for temperature range 540-620°C in whole has shown in the first case much greater standard deviation. In opinion of the authors, it means that for alloys having abnormal dependence of corrosion on temperature we deal with the factors whose nature till now is not found out but which impact to corrosion process is more significant than temperature. In this case generalised estimation of corrosion depth for interval 540-620°C as a whole is more precise than separately for each particular temperature level.

Table 1. Prediction of corrosion depths of martensitic alloys under impact of Estonian PF oil shale fly ash.

Alloy	Depth of corrosion, mm		Standard Error
	10 000 h	100 000 h	
X10CrMVNb91	0.14	0.36	±0.29
X20CrMoV121	0.17	0.64	±0.31
11Ch11W2MoV	0.23	0.58	±0.59

In Table 1 predictions of corrosion depths of alloys X10CrMVNb91 and X20CrMoV121 for terms 10^3 and $100 \cdot 10^3$ hours are presented. Predictions of corrosion depths of alloy 11Ch11W2MoV are presented here for

comparison. These data were established earlier on the basis of tests provided in the same conditions and processed by using the same method. It may be noted that predicted depth of corrosion of alloy X20CrMoV121 on the term $100 \cdot 10^3$ h of operation in temperature range 540-620°C is approximately 1.8 times higher than of alloy X10CrMoVNb91. Corrosion depth of alloy 11Ch11W2MoV for the same period is 10% lower than of alloy X20CrMoV121 but it is 60% higher than of alloy X10CrMoVNb91.

4 Discussion

The most probable reason of abnormal behaviour of the three examined martensitic alloys under temperature 580°C is, in authors' opinion, in the change of structure and protective properties of oxide layer under impact of KCl contained in PF oil shale fly ash.

To check of the given assumption, the corrosion tests of the specified alloys in environment of products of combustion of natural gas without presence of oil shale ash were performed. The depth of corrosion was determined in this case by measuring of increase of samples' weight after 100, 200, 400 and 600 hours. This increase is due to oxygen combined with basic metal in corrosion process so amount of corroded metal may be easily estimated knowing the type of compounds in oxide layer. The maximal estimations of corrosion depth will be found here in assumption that oxide layer consists entirely from FeO. The minimal estimations correspond to assumption that oxide layer consists entirely from Fe₂O₃. The results of tests of alloy X10CrMoVNb91 with duration 600 hours in various environments are given in Fig. 3. It may be noted that at the presence of PF oil shale fly ash the expressive maximum of corrosion depth is observed under temperature 580°C, in the absence of fly ash abnormal behaviour of corrosion does not reveal. The roentgen-structural analysis of oxide layer has shown that irrespective of temperature and corroding environment the layer consists basically of Fe₂O₃ and slightly of Fe₃O₄¹. Thus the depth of corrosion in the absence of fly ash with high degree of reliability can be presented by the bottom border of the appropriate area rather than by entire area shown in Fig. 3.

With the purpose of revealing of influence of chlorine on corrosion process its contents in oxide layer was determined on the basis of chemical analysis, see Table 2. It may be noted that with increase of temperature the contents of chlorine in oxide layer decreases. Increase of test duration affects in the same direction.

¹ measurements were performed by Prof. U. Kallavus, Centre for materials research, TTU

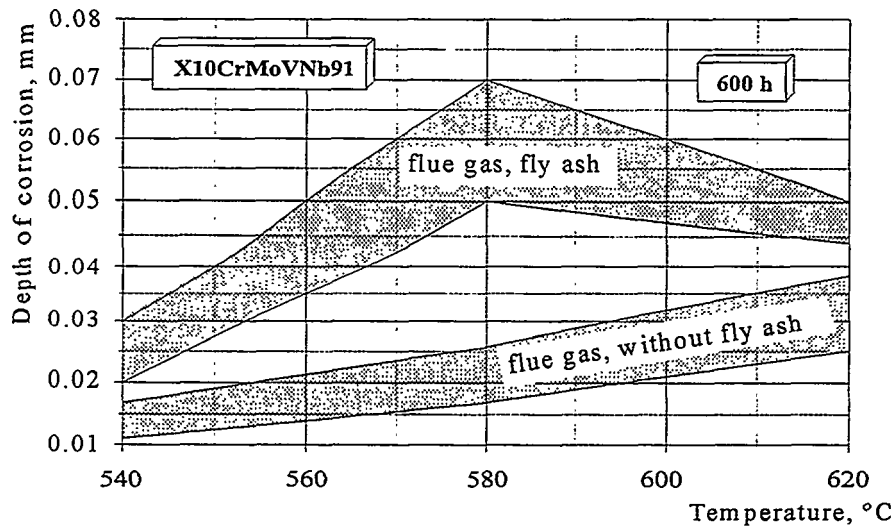


Figure 3. Corrosion depth of alloy X10CrMoVNb91 in various environment.

Table 2. Contents of chlorine in oxide layer of various alloys, %.

Alloy	540°C		580°C		620°C	
	400 h	600 h	400 h	600 h	400 h	600 h
X10CrMVNb91	0.87	0.72	0.05	0.02	0.04	-
X20CrMoV121	1.4	1.08	0.1	0.06	0.03	0.03
11Ch11W2MoV	1.33		0.45	0.82	0.17	0.02
	150 h		150 h	500 h	150 h	500 h
	545°C					

In Fig. 4 the dependence of corrosion depth of alloy X10CrMoVNb91 on test temperature is presented for various duration of tests. It may be noted that the abnormal behaviour of alloy under 580°C does not reveal for test terms shorter than 150-200 hours. It is very important phenomenon that allow to reduce corrosion degree by appropriate correction of periodicity of superheater clearing from external deposits. However on the basis of the stated results it is impossible to explain the reason of abnormal behaviour of martensitic alloys under impact of oil shale ash under temperature 580°C therefore the following step was research of distribution of alloying elements in oxide layer.

It is known that alloying elements migrate from the basic metal into oxide layer. Their concentration there depends, in general case, on concentration of alloying elements in metal and on temperature. In ideal case distribution of alloying elements along layer thickness is uniform. Compounds of

chlorine in external ash deposits, according to our research, react with iron and chromium with formation of volatilising compounds. It leads to counter migration (the chlorine migrates from deposit through oxide layer towards tube metal, alloying elements migrate from tube metal towards oxide layer) and outside oxide sub-layer should be depleted of alloying elements.

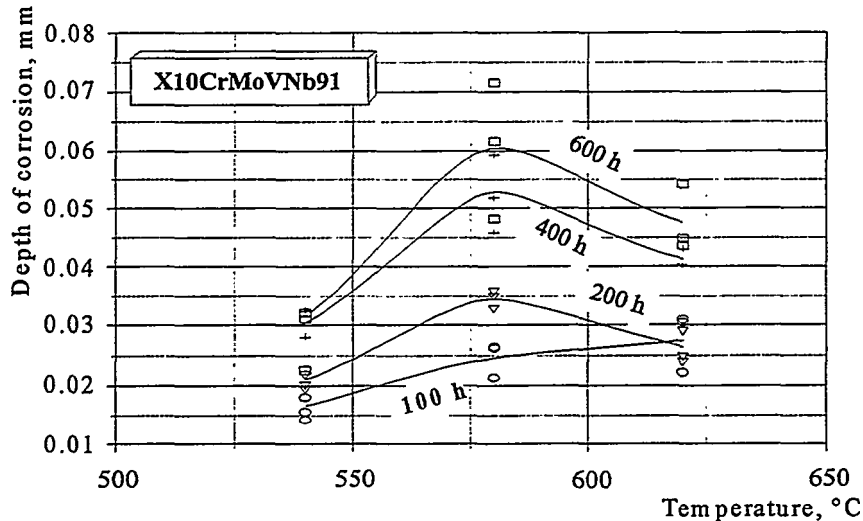


Figure 4. Corrosion depth of alloy X10CrMoVNb91 under impact of Estonian PF oil shale fly ash.

To research the distribution of alloying elements in oxide layer¹ there were used an optical microscope MIKROPHOT FX, scanning electronic microscope JXA 840A with an accelerating voltage 20 kV and X-ray spectrometer AN 1000, the time of scanning of entire spectrum made 20-3600 seconds depending on alloying element concentration. The results of research allow to observe relative distribution of alloying elements along oxide layer thickness. As an example in Fig. 5 the distributions of alloying elements along oxide layer cross-sections of samples from alloy X10CrMoVNb91 subjected to corrosion tests within 600 hours in environment of products of combustion of natural gas in absence (a) and at presence (b) of PF oil shale fly ash are presented. On X-ray maps at the left there are presented scanned cross-sections' portraits (above) accompanied with appropriate distributions of elements Fe, Cr, Mo, Cl (below) that are characterised by gradation of grey tone. On linescans at the right the distributions of the same elements are presented as graphs against a background of scanned cross-sections' portraits, scanning was performed along central lines (white).

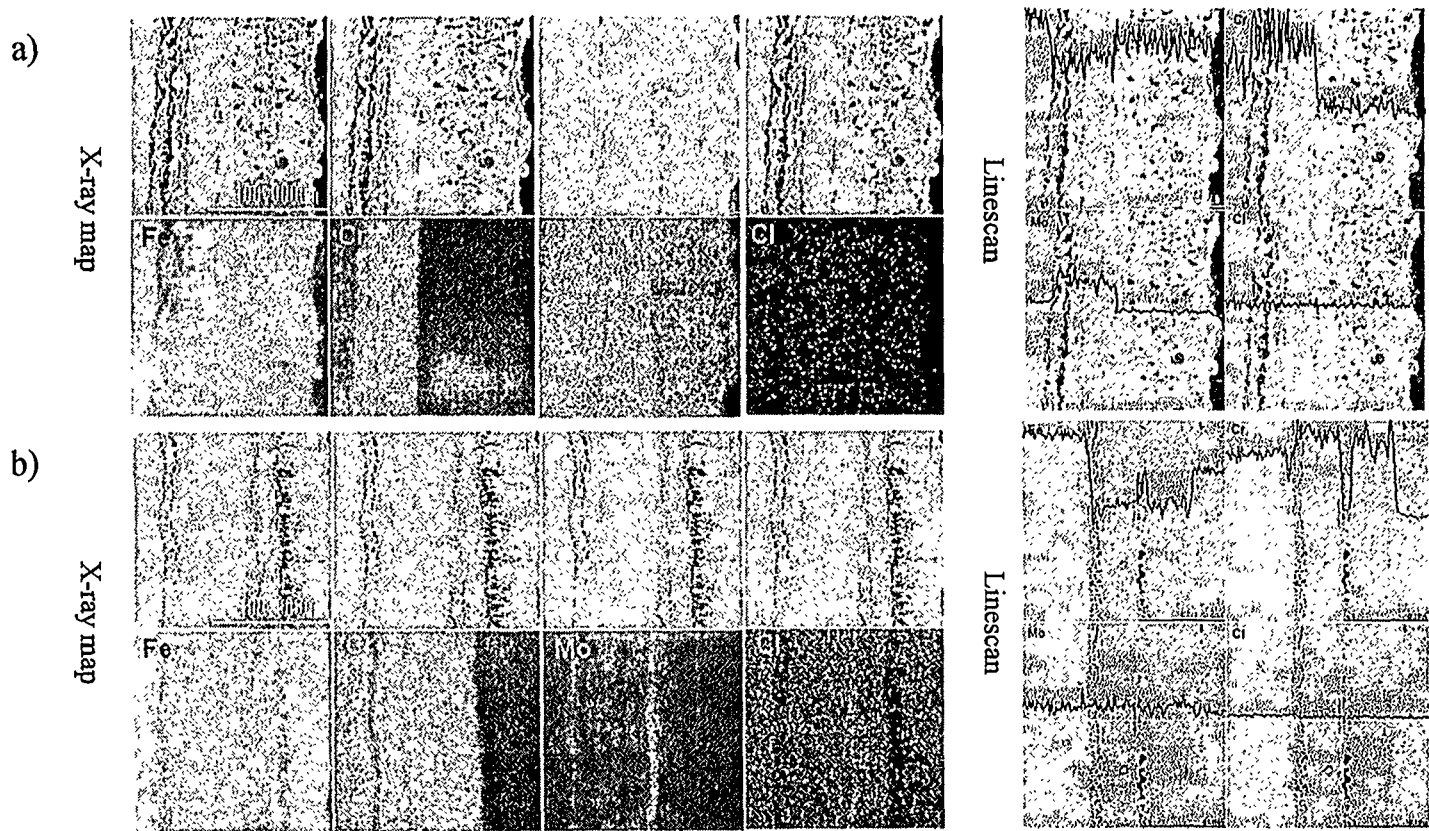


Figure 5. Distributions of alloying elements in oxide layer of alloy X10CrMoVNB91. Corrosion at 580°C within 600 h in environment of natural gas combustion products in absence (a) and in presence (b) of oil shale ash.

There was found that oxide layer of martensitic alloys consists of two sub-layers divided by expressive border from cracks and pores, especially on samples tested at the presence of ash. The contents of chromium in internal sub-layer remains at the level of its contents in the basic metal (some rise of curves is explained by difference of density) and sharply decreases to zero in outside sub-layer. The contents of molybdenum in sample tested in absence of fly ash is distributed in a similar way. In presence of fly ash the little bit increased contents of molybdenum is observed on the map as a light strip on border between sub-layers. The contents of iron falls already on border between metal and internal sub-layer. Such distribution of elements in oxide layer confirms the assumption of occurrence (at the presence of chlorine) of volatilising compounds leading to depletion of outside sub-layer of alloying elements. However under temperatures 540 and 620°C the distributions of elements do not differ from given in Fig. 5 so significantly that anomaly of dependence of corrosion process on temperature could be comprehended. It is necessary to assume, that with identical concentration of elements various chemical compounds could be formed depending on temperature. Various compound sets have different diffusion permeability and chemical activity that leads to distinctions in corrosion intensity. Unfortunately authors did not have opportunity to investigate what kind of chemical compounds are formed in oxide layers and what is their contents so the reasons of abnormal corrosion of martensitic alloys at the presence of fly ash of PF Estonian oil shale remain non comprehended. It does not diminish by no means, however, the reliability of empirical equations established for prediction of corrosion depth of martensitic alloys at the presence of fly ash.

Main conclusion that would be reasonably made on the basis of corrosion test results is following: alloy X10CrMoVNb 91 shows the best corrosion resistance under impact of fly ash of PF Estonian oil shale and it seems been the most appropriate material for superheaters of boiler burning fuels containing alkaline metals and chlorine.

References

1. Standard Rules for Determination of Corrosion Resistance of Boiler Alloys at Elevated Temperature.-RTM 108.030.116-78 (in Russian).
2. Steam Boilers. Standard Technique of Corrosion Testing.-OST 108.030.01-75 (in Russian).

Formation of Thermal Fatigue Cracks in Periodic Rapid Quenching of Metal

Arvo Ots, professor
Tallinn Technical University
Thermal Engineering Department
Tallinn, Estonia

Abstract

Water lancing is an effective technique for cleaning boiler heating surfaces from ash deposits by burning low-grade fuels with complicated composition of mineral matter. In water cleaning cycles of boiler's heat transfer surfaces due to rapid quenching destruction of corrosion protective oxide film and formation of thermal fatigue cracks on the outer surface of the tube's metal occur. The criterion of the thermal fatigue cracks' formation and their growth intensity depend on the character of temperature field in the tube's metal outer layer. The solution of non-stationary heat conductivity equation for metal rapid quenching conditions is given. The convective heat transfer coefficients from hot metal surface to water jet were established experimentally. Thermal fatigue crack growth intensity was investigated in real boilers' heat transfer surfaces' tubes as well as in laboratory conditions. The formula for predicting thermal fatigue cracks' depth depending on the number of cleaning cycles.

1 Introduction

One effective method for ash deposit removal from boiler's heat transfer surfaces is periodic water cleaning. In water cleaning cycles besides ash deposits' removal from heat transfer surfaces also destruction of corrosion protective oxide film in tube surface and rapid quenching of metal take place. In certain conditions the latter will cause formation of thermal fatigue cracks in the outer surface of tubes' metal of boiler's heat transfer surfaces.

Thermal fatigue cracks' formation criterion and their growth intensity depend mainly on character of temperature field in the outer layer of metal. For determination of thermal stresses in the boiler tube wall the non-stationary heat conductivity equation for metal rapid quenching conditions

was solved. The convective heat transfer coefficient from hot metal surface to water depends on the water jet character. Two different water jet types exist in water cleaning practice of boiler's heat transfer surfaces from ash deposits. These are the compact and the sprayed jet. The different water jet types have also different convective heat transfer coefficient values from the heat transfer surface to jet. The convective heat transfer coefficient for determination of temperature fields and thermal stresses in tube wall was established experimentally.

Thermal fatigue cracks on the outer surface of metal do not arise immediately but only after a certain amount of quenching cycles. That incubation period is characterized by the amount of quenching cycles to spring up the first thermal fatigue crack. The amount of quenching cycles in the incubation period to form the first cracks is a complicated function of temperature drop on the outer surface of tube, type of metal, period between the quenching cycles, et al.

In the second stage the growth of thermal fatigue cracks with decreasing intensity takes place. The cracks' growth dynamics was investigated in real boilers' heat transfer surfaces' tubes as well as in laboratory conditions. Mathematical formula for prediction of thermal fatigue cracks' depth depending on the number of quenching cycles is presented.

2 Non-Steady Temperature Field in Tube Wall

In water cleaning cycles of steam boiler's heat transfer surfaces besides ash deposits' removal also destruction of corrosion protective oxide film in tube surface and rapid quenching of metal take place. These originate from the temperature gradient in tube wall and are the parents of additional thermal stresses. Thermal stresses cause destruction of the corrosion protective oxide film and act as acceleration factor on corrosion-erosion wear of heat transfer surfaces' metal [3] and is a starting-point for formation of thermal fatigue cracks on the outer surface of tubes.

The temperature field in the tube wall in water quenching condition is described by the following non-steady heat conductivity (one-dimensional) equation:

$$\frac{\partial T(r;\tau)}{\partial \tau} = a \left(\frac{\partial^2 T(r;\tau)}{\partial r^2} + \frac{1}{r} \frac{\partial T(r;\tau)}{\partial r} \right). \quad (1)$$

The initial and border conditions (the third order of border conditions):

$$T(r;0) = T_0 = \text{const}; \quad (2)$$

$$\lambda \frac{\partial T(r_2; \tau)}{\partial r} = \alpha [T(r_2; \tau) - T_w], \quad (3)$$

where: a - thermal diffusivity; λ - thermal conductivity; α - convective heat transfer coefficient; r - radius; r_2 - outside radius of tube; T - temperature; T_0 - steady temperature of metal; T_w - temperature of water.

In most cases the solution results of the heat conductivity equation (equation type (1)) is presented as an infinite Fourier row. In case of very fast temperature drop on metal surface and high heat fluxes (Fourier number is low), as it occurs in water cleaning conditions of boiler's heat transfer tubes for getting appropriate accuracy, very large amounts of terms in Fourier row should be taken into account. It is more rational to use the simplified analytical formulas for determination of temperature field in the tube wall [1]. The temperature field in tube wall in rapid quenching conditions is expressed by the following formula:

$$\begin{aligned} T(x; \tau) = T_0 - \sqrt{\frac{r_2}{r}} & \left[\operatorname{erf} \left(\frac{2s-x}{2\sqrt{a\tau}} \right) - \operatorname{erf} \left(\frac{x}{2\sqrt{a\tau}} \right) - \exp \left(\frac{a\alpha^2\tau}{\lambda^2} + \frac{\alpha}{\lambda} x \right) \times \right. \\ & \times \operatorname{erfc} \left(\frac{\alpha}{\lambda} \sqrt{a\tau} + \frac{x}{2\sqrt{a\tau}} \right) + \exp \left[\frac{a\alpha^2\tau}{\lambda^2} + \frac{\alpha}{\lambda} (2s-x) \right] \times \\ & \left. \times \operatorname{erfc} \left(\frac{\alpha}{\lambda} \sqrt{a\tau} + \frac{2s-x}{2\sqrt{a\tau}} \right) \right] (T_0 - T_w), \end{aligned} \quad (4)$$

where: $x = r_2 - r$ - distance from the outside surface of tube, $s = r_2 - r_1$.

The latter formula was derived for conditions when the convective heat transfer coefficient from tube surface to water jet does not depend on time and the thermo-physical parameters of metal are constant.

Formula for calculation of temperature on the outer tube surface is derived from the equation (4):

$$\begin{aligned} T(o; x) = T_0 - \left[\operatorname{erf} \left(\frac{s}{\sqrt{a\tau}} \right) - \exp \left(\frac{a\alpha^2\tau}{\lambda^2} \right) \operatorname{erfc} \left(\frac{\alpha}{\lambda} \sqrt{a\tau} \right) + \right. \\ \left. + \exp \left(\frac{a\alpha^2\tau}{\lambda^2} + \frac{2\alpha s}{\lambda} \right) \operatorname{erfc} \left(\frac{\alpha}{\lambda} \sqrt{a\tau} + \frac{s}{\sqrt{a\tau}} \right) \right] (T_0 - T_w). \end{aligned} \quad (5)$$

3 Experimental Determination of Temperature Field in Tube Wall

For analytical calculation of the temperature fields in the tube wall (e.g. by the formula (4)) besides thermo-physical properties of the metal we should also know convective heat transfer coefficient from the outer surface to water jet. At experimental determination of convective heat transfer coefficient from hot metal surface to water jet the temperature field in tube wall as function of time was also experimentally investigated.

On the basis of the measured temperature at the fixed distance (fixed point) from the outer tube surface in cooling cycle of metal depending on time it is possible to re-establish temperature field history in the tube wall. Starting point for solving inverse heat conductivity problem is the experimentally established temperature change history at the fixed point of tube wall. This allows getting convective heat transfer coefficient and then, after solving direct conductive heat transfer equation by established heat transfer coefficient, the full temperature field in the tube wall. Consequently, for determination of temperature field history on the tube wall it is sufficient to measure temperature at one point of the tube wall versus time.

Exact experimental establishment of the non-steady temperature in the tube wall in case of water quenching of tube surface is a very complicated problem due to high heat conductivity and low specific heat capacity of boiler steels. The basic parameters influencing the result of temperature measurement by thermocouple are the hole diameter for thermocouple, distance from thermocouple's soldering point to the outer surface of the tube and diameter of thermocouple wire. Increase in the distance of soldering point of thermocouple from tube's outer surface will decrease the error from thermocouple position as well as thermoelectric voltage. For investigation of temperature field in the tube wall and determination of the influence of thermocouples' holes at accurate temperature measurement in rapid quenching conditions the experimental block was erected proceeding from these theoretical conclusions [4]. The experimental block was made of boiler steel 12Cr1MoV with the outer diameter 32 mm and wall thickness 6 mm. The block consists of two symmetric semi-sides. One-electrode 0.05 mm copel thermocouples are located in the first block side. Cable type two electrode copel-chromel thermocouples with 0.2 mm wire diameter and 1.5 mm cable diameter are located in the other block side.

The outer surface of block was quenched by compact water jet.

Starting from tube's outer surface distance of $x > 0.4-0.5$ mm the temperatures measured by one-electrode or cable-thermocouples were

practically the same. Also there were no differences between the measured and calculated temperature distribution on the tube wall in the region $x > 0.4-0.5$ mm.

In Figure 1 the established temperature of the tube wall depending on distance x for three different times is given. Steady temperature of metal was 500°C . The tube surface was washed by the compact water jet. Dynamic pressure on the contact point of water with surface was 0.6 Pa. It is obvious that the experimentally established temperature measured by 0.05 mm one-electrode thermocouples corresponds well to the calculated temperatures, but the temperatures measured by the cable-thermocouples up to distance $x < 0.4-0.5$ mm had a remarkable error.

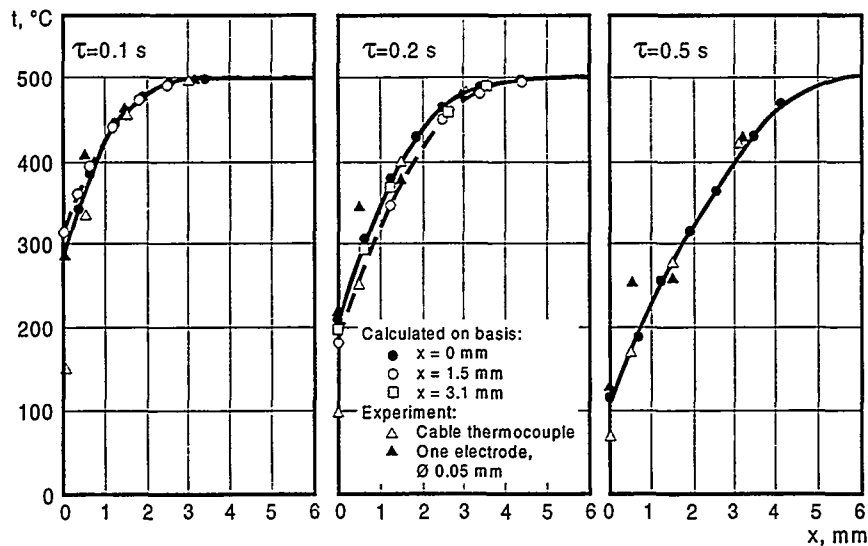


Fig. 1. Temperature field in the $\text{O}32 \times 4.5$ mm tube wall made of 1CrMoV steel. Steady temperature – 500°C .

Using experimentally determined dependence $T = T(t; x = \text{const.})$ it is possible to establish the average convective heat transfer coefficient from surface to water jet by solving reverse heat conductivity equation. As the equation (4) got on the precondition that convective heat transfer coefficient is constant, solution of reverse heat conductivity equation in condition $T = T(t; x = \text{const.})$ gives the average value of the heat transfer coefficient in the range of time $0 - \tau$.

Typical dependence of the average values of the heat transfer coefficient from metal surface to water jet is given in Figure 2. Curve 1 was established by washing the tube surface by compact water jet in laboratory conditions

(that correlate with experiment results given in Figure 1). Curve 2 describes dependence of the average convective heat transfer coefficient on real boiler conditions when washing tube wall by the sprayed water jet. The steady temperature of the outer surface of the water wall tube was 427°C.

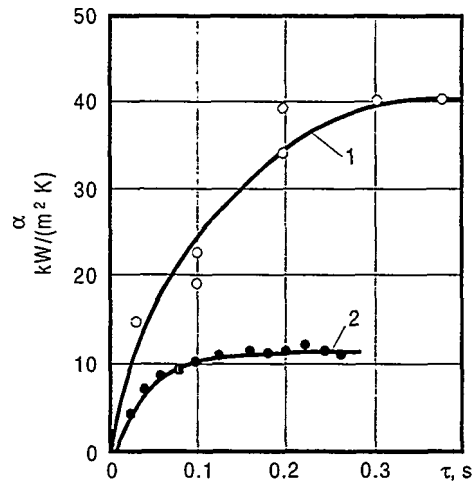


Fig. 2. The average heat transfer coefficient from the outer tube surface to water jet depending on time. 1 - compact water jet, steady temperature – 500°C, 2 - sprayed water jet, steady temperature – 427°C.

It is typical that the average convective heat transfer coefficient from the hot tube surface to water jet first increases very rapidly and afterwards stabilizes at the fixed level. The heat transfer coefficient from the hot metal surface to compact water jet is remarkably higher than that to sprayed jet.

In Figure 3 the convective heat transfer coefficient from superheater and water wall tube surface to water jet in cleaning conditions of real boiler's heat transfer surfaces depending on distance from water nozzle is given. The temperature of tubes' outer surface was in the range 420-460°C. Experimental points in Figure 3 were got using the long distance rotating blower or the scanning blower.

The maximum temperature drop on the outer tube surface Δt_M and duration of the quenching cycle τ_c characterizes the cleaning regime of the heat transfer surface by water.

It is very difficult to establish experimentally the maximum temperature drop on the outer tube surface in real boiler conditions. It is easier by using calculation methods based on the measured temperature at the fixed point on the tube wall depending on time.

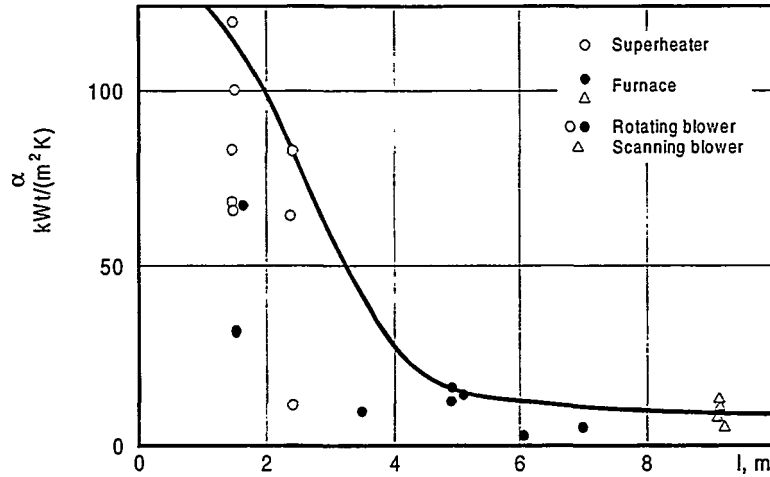


Fig. 3. The average heat transfer coefficient from outer tube surface to water jet in real boiler water washing condition depending on distance from nozzle. Temperature of tube's outer surface - 430-470°C.

In Figure 4 the measured temperature characteristic (curve 1) of the water wall tube of a real boiler with 4.5 mm wall thickness made of 12Cr1MoV steel at 0.41 mm distance from the outer tube surface is shown. We can see that the temperature change depending on time has a non-linear character. First the temperature falls very intensively but afterwards the temperature change is braked. In this case the quenching duration is $\tau_c=0.3$ s and the temperature at distance from outer tube surface $x=0.41$ mm falls from 427 to 322°C. Temperature on the outer tube surface (curve 2) was calculated via the obtained convective heat transfer coefficient (curve 2 in Figure 2). Temperature field in the tube wall is given in Figure 5. The maximum temperature drop was $\Delta t_M = 129$ K.

The maximum temperature drop in the tube wall at water cleaning of heat transfer surfaces of boiler is determined by the contact duration of a water jet with surface in cleaning cycle, structure of water jet, characteristics of ash deposits on heat transfer surfaces etc. In practice the maximum temperature drop Δt_M for water wall tubes is in the range 70-130 K and the contact time $\tau_c=0.2-0.3$ s.

In Figure 5 the calculated temperature field in the wall of water wall tube on basis of measured temperature at the fixed point (Figure 4) is given.

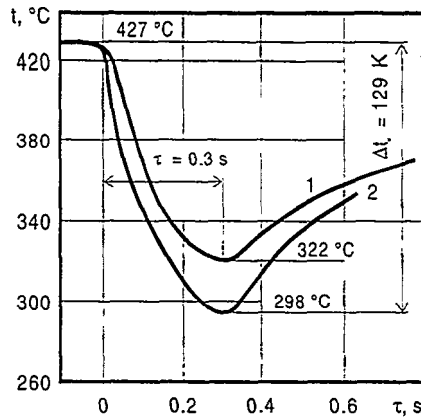


Fig. 4. Change of the measured temperature at 0.41 mm from outer surface (1) and calculated temperature on outer surface (2) of tube $\varnothing 42 \times 4.5$ mm made of steel 11Cr1MoV depending on time. Steady temperature on the outer tube surface – 427°C.

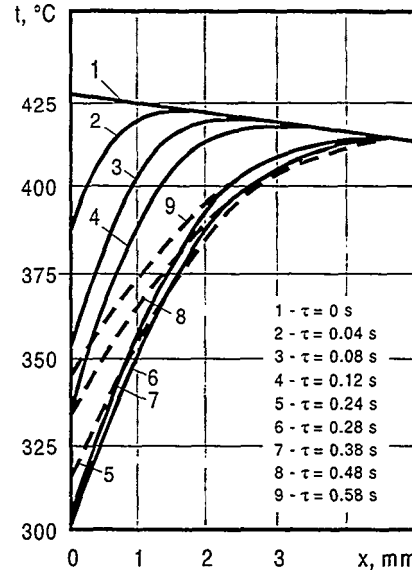


Fig. 5. The calculated temperature field in the water wall tube of boiler.

4 Thermal Stresses in Tube Wall

On basis of established temperature fields the axial thermal stress in the tube wall was calculated as the highest compared to radial and tangential thermal stresses. The axial thermal stress with pressure-induced stress component is expressed by the following well-known equation:

$$\sigma_z = -\frac{\beta E}{1-\mu} \left[\Delta t(r) - \frac{2}{r_2^2 - r_1^2} \int_{r_1}^{r_2} r \Delta t(r) dr \right] + \frac{r_1^2 \left(1 + \frac{r^2}{r_2^2}\right)}{r_2^2 - r_1^2} p. \quad (6)$$

In Figure 6 the axial thermal stresses in the wall of tube $\varnothing 42 \times 4.5$ mm made of 12Cr1MoV steel correspondingly to temperature fields in Figure 5 are given.

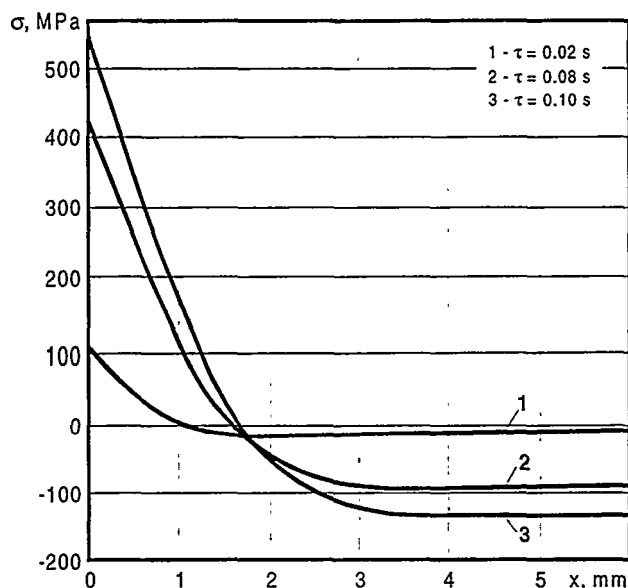


Fig. 6. The axial thermal stress field in the wall of tube $\varnothing 42 \times 4.5$ mm made of 12Cr1MoV steel (corresponds to Figure 4). Steady temperature – 427°C.

The tensile stresses arisen in the tube wall in water cleaning cycle of heat transfer surface are maximal in the outer surface, diminish very rapidly in thin metal layer near the outer surface and afterward transform into compressive stresses. Consequently thermal fatigue cracks occur only in the very thin layer of metal and after a certain amount of cleaning cycles will stabilize on the extent level.

5 Formation of Thermal Fatigue Cracks on Tube Surface

Formation of the thermal fatigue cracks on the outer tube surface of boiler's heat transfer surfaces could be divided into two following stages.

1. *The incubation (initial) period.* It is the time from the first quenching cycle to the formation of the first thermal fatigue crack on metal surface. In this stage the gathering of the micro-damages in the surface occur. The incubation period is characterized by the amount of cleaning cycles' m_0 or amount of the quenching cycles N_0 .

2. *The growth period of cracks.* It is the time from the formation of the first crack to the crack of given depth. This period is characterized by the amount of cleaning cycles m_1 or amount of quenching cycles N_1 .

Comment. One cleaning cycle may consist of several quenching cycles. The total amount of cleaning cycles $m=m_0+m_1$ or quenching cycles $N=N_0+N_1$.

For estimation of the quenching cycles' amount in the incubation period N_0 depending on the maximum temperature drop on the metal in the quenching cycle and on the mechanical properties of the metal in [3] the following formula is recommended:

$$N_0 = \frac{\mu \delta^2}{8 \left(\beta \Delta t_m - 2\nu \frac{\sigma_{0.2}^{20}}{E} \right)^2}, \quad (7)$$

where: μ – parameter depending on duration of quenching period; δ – plastic deformation endurance limit at working temperature; β – thermal expansion coefficient; Δt_M – maximum temperature drop in the metal; $\nu = \sigma_{-1}^{20} / \sigma_{0.2}^{20}$; σ_{-1}^{20} – fatigue endurance limit at temperature 20°C; E – modulus of elasticity.

According to formula (7) the amount of quenching cycles in the incubation period strongly depends on the plastic deformation endurance limit. The latter is determined by metal type, temperature and time and it may be calculated by the formula:

$$\delta = \delta_0 \exp(-\gamma N_0 \tau_0) + \delta_1, \quad (8)$$

where γ , δ_0 and δ_1 are the coefficients describing the function $\delta = \delta(\tau)$; τ_0 – period between quenching cycles.

Plastic deformation endurance limit for the austenitic steels depending on time drops very intensively in the high temperature conditions compared to perlitic steels.

The coefficient λ is expressed by the formula:

$$\zeta + \exp(-\zeta \lambda) = (1 + \zeta) \sqrt{\lambda}, \quad (9)$$

where: $\zeta = \gamma N_0 \tau_0$; $\zeta = \delta_1 / \delta_0$.

The amount of quenching cycles in the incubation period calculated on basis of formula (7) for austenitic steel 18Cr12NiTi by temperature drop $\Delta T=180$ K shows that due to the low plastic deformation endurance limit the first thermal fatigue cracks form only after several tens of quenching cycles. Ferritic steel 12Cr1MoV has higher deformation endurance plastic limit than austenitic steel and endures much more of quenching cycles until cracks' formation.

Experimental research shows that thermal fatigue cracks on the real boiler water wall tubes' ($\varnothing 42 \times 4$ mm) outer surface made of steels 12Cr1MoV and 12Cr2MoV form approximately after the 50 cleaning cycles in water cleaning conditions. Temperature of the outside tube surface was 370-400°C and the maximum temperature drop on it – 120-130 K. Period between cleaning cycles was $\tau_0=54$ h.

Experiments in laboratory conditions show that in water washing conditions in case of short period between quenching cycles $\tau_0=6$ min thermal fatigue cracks form after the 1500 quenching cycles on the outer tube surfaces ($\varnothing 32 \times 4$ mm) made of steel 12Cr1MoV (at steady metal temperature 500°C and temperature drop on the outer tube surface 250-280 K). Newton et al also obtained results of the same kind [2]. These results allude to the very complicated mechanism of thermal fatigue cracks formation in incubation period where the period between quenching cycles plays an important role. If duration between water cleaning cycles increases the amount of quenching cycles to form the first thermal fatigue crack will decrease. The influence of period between the quenching cycles on the formation of the first crack can be explained by the relaxation of stresses in thermal state of metal [3].

Growth of thermal fatigue cracks' depth dependence on washing cycles was investigated in real water cleaning conditions of boiler's furnace wall tubes [3,5, et al].

Furnace wall superheater tubes in pulverized oil shale boiler TP-101. Steam output of boiler is 320 t/h and boiler inside pressure 15 MPa. Temperature of the outside surface of superheater tube 370-400°C; the maximum temperature drop on outside tube surface in cleaning cycles $\Delta t_M=120-130$ K; the period between cleaning cycles $\tau_0=54$ h; contact time of water jet with tube surface $\tau_c=0.3$ s. Duration of experiments for tubes made of steel 12Cr1MoV was 2,949; 10,921; 14,721; 16,583; 19,532; 38,500; 53,800 h and for tubes made of steel 12Cr2MoV – 2,949; 10,921; 11,772; 14,721; 16,583 and 19,532 h.

Occurrence of the first damages on the tube surface with depth of 0.05 mm was mentioned after the first 50 cleaning cycles.

Thermal fatigue cracks with maximum depth of 0.08 mm (steel 12Cr1MoV) and 0.1 mm (steel 12Cr2MoV) appeared after 200 cleaning cycles on the outer tube surface. Growth of cracks was broken after approximately 54,000 cleaning cycles. Expansion of cracks due to corrosion processes was observed.

Experimental furnace wall superheater tubes in pulverized oil shale boiler BK. Steam output of boiler is 75 t/h, boiler inside pressure is 4 MPa. Temperature of the outside surface of tube 345-415°C; the maximum temperature drop on outside surface of tube in cleaning cycles $\Delta t_M=170-180$ K; the period between cleaning cycles $\tau_0=0.5-3.7$ h; contact time of water jet with tube surface $\tau_c=0.08-0.14$ s. Duration of experiments with tubes made of steel 12Cr1MoV was 1,030; 1,775; 4,245 and 6,020 h and for tubes made of steel 12Cr2MoV – 2,949; 10,921; 11,772; 14,721; 16,583 and 19,532 h.

Furnace wall tubes in pulverized brown coal boiler P-49. Steam output of boiler is 800 t/h, boiler inside pressure is 22 MPa. Temperature of the outside surface of tubes 400-460°C; the maximum temperature drop on outside surface of tube $\Delta t_M=120-130$ K; the period between cleaning cycles $\tau_0=54$ h; contact time of water jet with tube surface $\tau_c=0.3$ s. Duration of experiments for tubes made of steel 12Cr1MoV was 6,500 and 17,000 h.

In Figure 7 the established general character of dependence of the thermal fatigue cracks' depth on the amount of the cleaning cycles is given. This dependence has an effaced character, i.e. the cracks' growth intensity will decrease if quenching cycles' amount increase. Because of crack's depth growing the crack top moves to the less thermal stress zone due to very intensive drop of temperature in the tube wall. Therefore thermal fatigue cracks has very intensive development in the initial period (at low number of cleaning cycles) when temperature drop (thermal stresses) on top of the crack has maximum value.

Certain influence on the character of the development of thermal fatigue cracks has also their amount in the linear unit or the space between cracks. The space between cracks could have remarkable influence on the plastic stresses on top of the cracks. Consequently, due to decrease of spaces between the cracks the crack's growth intensity must decrease.

Development of the mechanical fatigue cracks is usually expressed by the following formula:

$$\frac{da}{dN} = c (\Delta K)^v, \quad (10)$$

where da/dN - crack development intensity; ΔK - coefficient of mechanical stresses intensity; c, v - coefficients.

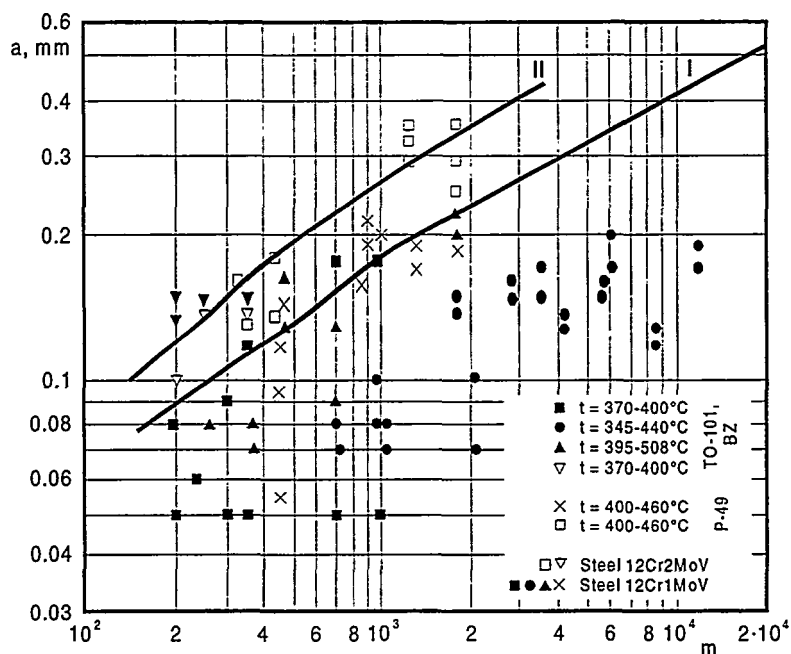


Fig. 7. Thermal fatigue crack depth depending on cleaning cycles. I – steel 12Cr1MoV, II – steel 12Cr2MoV.

According to formula (10) and experimental data (Figure 7) the maximum depth of thermal fatigue cracks depending on cleaning cycles is expressed by the formula:

$$a = \gamma (m - m_0)^{\nu} . \quad (11)$$

According to the experimental data: $\nu=0.36$ (12Cr1MoV and 12Cr2MoV steels), $\gamma=0.0015$ for steel 12Cr1MoV and $\gamma=0.023$ for steel 12Cr2MoV.

Starting from 2,000 cleaning cycles the growth of thermal fatigue cracks is braked or very slow.

References

1. A. Luykov. Theory of Heat Conductivity, Moscow, 1967, p. 592 (In Russian).
2. J. Newton, M. Melksham. An Analysis Of Thermal Fatigue Crack Growth in 2.25% Cr 1% Mo Steel Superheater Tubes Caused by On-Load Water Deslagging, Ash Deposits and Corrosion Due to Impurities in Combustion Gases, Washington-London: Hemisphere Publishing Corporation, 1977, pp. 369-386.
3. A. Ots. Corrosion and Wear of Boiler Heat Transfer Surfaces, Moscow, 1987, p. 272 (In Russian).
4. A. Ots, U. Soodla, R. Touart. The Measurement of Temperature Fields in the Wall of the Tube by Rapid Quenching, Transaction of Tallinn Technical University, N°579, 1984, pp. 29-38 (In Russian).
5. A. Ots, V. Pella, R. Touart. Water Washing of Oil Shale Boiler Water Wall Tubes, Oil Shale, Vol.5, No. 3, 1988, pp. 266-278 (In Russian).

Life Extension of Boilers Using Weld Overlay Protection

George Lai and Philip Hulsizer
Welding Services Inc.
2225 Skyland Court
Norcross, GA 30071
U. S. A.

Rick Brooks
Welding Services Europe LLC
Elementenweg 18
3201 LG. Spijkenisse
The Netherlands

Abstract

The present paper describes the status of modern weld overlay technology for refurbishment, upgrading and life extension of boilers. The approaches to life extension of boilers include field overlay application, shop-fabricated panels for replacement of the worn, corroded waterwall and shop-fabricated overlay tubing for replacement of individual tubes in superheaters, generating banks and other areas. The characteristics of weld overlay products are briefly described. Also discussed are successful applications of various corrosion-resistant overlays for life extension of boiler tubes in waste-to-energy boilers, coal-fired boilers and chemical recovery boilers. Types of corrosion and selection of weld overlay alloys in these systems are also discussed.

1 Introduction

Corrosion and/or erosion problems are quite common for boilers in a variety of industries, such as, waste incineration, fossil energy and pulp and paper. Proper management of these corrosion/erosion problems is essential for reliable, efficient, and safe operation of a boiler. As plant operators are under pressure to operate their plants longer and at lower cost, more and more boilers are relying on weld overlay technology for corrosion/erosion protection and life extension. Weld overlay is now considered to be a reliable, long-term solution to corrosion/erosion problems in boilers.

In many waste-to-energy boilers, weld overlay with the nickel-base alloy 625 has been widely used to protect waterwalls, superheaters and generating banks against chloride attack. With recent installation of low NO_x burners in coal-fired boilers to reduce NO_x emissions, weld overlay with alloy 625 or type 309 SS has been proven to be successful in protecting waterwalls against sulfidation attack. Also successful with weld overlay in protecting boiler tubes are recovery boilers in pulp and paper mills.

The present paper describes modern weld overlay technology for applying weld overlay for corrosion/erosion protection and life extension of boilers. The paper also highlights some of the successes in waste-to-energy boilers, coal-fired

boilers and kraft recovery boilers. Also discussed in the paper is selection of proper weld overlay alloys for these industrial systems.

2 Overlay Approaches to Life Extension

Three approaches are used to effectively provide life extension for boilers using weld overlay technology. They are (a) field overlay application of the waterwall, (b) shop-fabricated overlaid panels for replacement of the worn, corroded waterwall, and (c) shop-fabricated overlay tubing for replacement of individual tubes in superheaters, generating banks and other areas.

2.1 Field Overlay Application

The Unifuse[®] overlay welding system currently in use by Welding Services Inc. (WSI) is in its eighth generation. The welding process utilizes pulse spray gas metal arc welding. The system is fully automatic capable of depositing weld beads in a vertical down mode starting typically from the membrane and then moving to the tube section following a preprogrammed weld bead sequence to achieve a uniform coverage of the waterwall (i.e., membranes and tubes). In order to cover a large surface area of the boiler's waterwall, the overlay welding process requires a mechanized system to yield a consistent quality over a large overlaid area, typically thousands of square feet (hundreds of square meters) or more. The quality of the weld overlay is dependent upon welding system, welding method, welding parameters, weld bead sequence and profile, overlay microstructure, weldability of the overlay alloy, QA/QC programs, and welding operator, among other factors.

Development of the optimum welding procedures is critical for ensuring a weld overlay with free of cracks and microfissures, low dilution in overlay chemistry, optimum microstructure, sound metallurgical bond and minimal lack of fusion, minimal distortion, and minimal heat-affected zone in the substrate. And, to ensure that the overlay is homogeneous and consistent in quality over a large area, the system is equipped with real-time digital readouts displaying the essential welding parameters, such as current, voltage, wire speed, travel speed, etc., during the entire welding operation. The field overlay job generally follows the following sequence of tasks: mobilization, site set-up, scaffolding, gritblasting, boiler tube mapping, overlay welding, final inspection, site clean-up, and demobilization. It is common to employ a number of welding machines simultaneously in order to reduce the total project time. Figure 1 shows multiple weld overlay machines for overlaying the waterwall in the field.

Unifuse is a registered trademark of Welding Services, Inc.

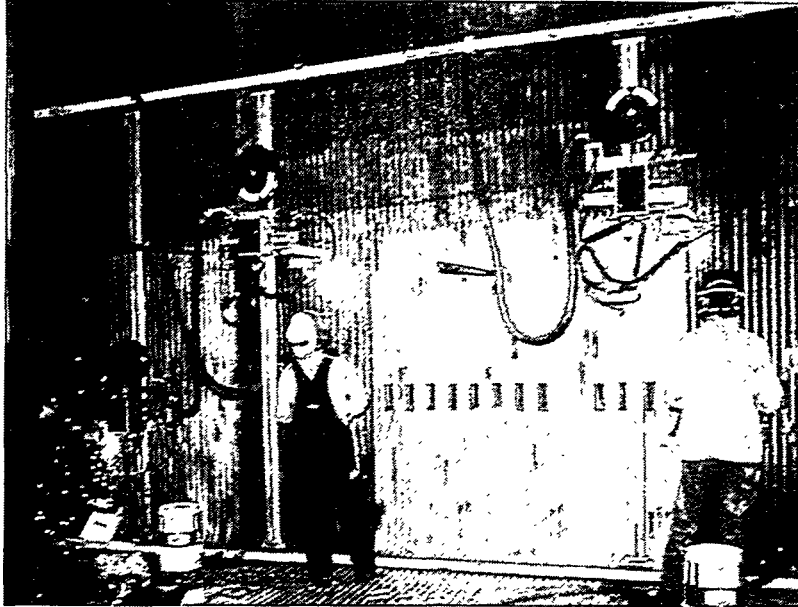


Fig. 1. Three weld overlay machines are shown in overlaying the waterwall in the field.

During overlay welding, some weld penetration into the substrate steel can occur, which tends to result in slight dilution in overlay chemistry. Dilution in chemistry of approximately 10% or less has been routinely achieved by the field overlay process. The thickness of a field-applied overlay is typically 0.070" (1.8 mm) minimum. Table 1 shows typical chemical composition of the field-applied type 309 stainless steel overlay on carbon steel.

Table 1. Typical overlay chemical composition of the field applied type 309 SS overlay (wt.%).

<u>Cr</u>	<u>Ni</u>	<u>Fe</u>	<u>Mn</u>	<u>Si</u>	<u>C</u>
22.3	12.2	Bal.	2.0	0.8	0.05

2.2 Shop-Fabricated Overlay Panels

When the waterwall is badly damaged and is beyond repair by field overlay, the damaged section can be removed and replaced with shop-fabricated overlay panels. Overlay panels are fabricated by simply applying overlay to regular carbon steel panels in a stand using a vertical down welding mode. This shop overlay of panels is illustrated in Fig. 2. The weld overlay panel can also be constructed out of individual overlay tubes. Panels of sizes up to 4 ft (1.2 meters) wide and 40 ft (12 meters) long can be handled in the shop, with common sizes of panels being up to 1.2 meters wide and 6 meters long.

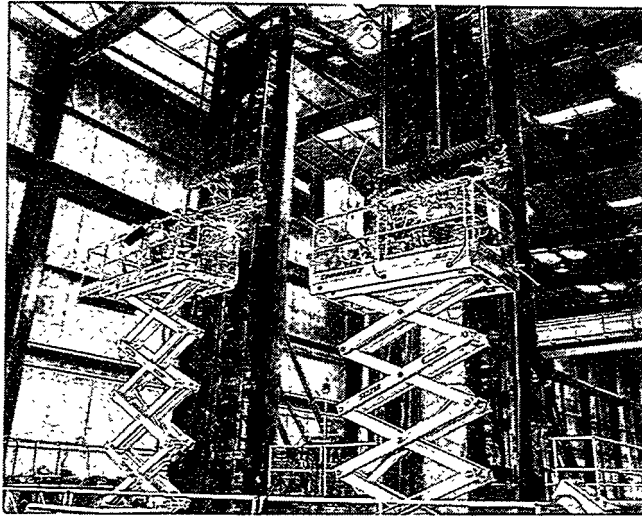


Fig. 2. Stands for weld overlaying of panels in shop.

2.3 Shop-Fabricated, Proprietary Overlay Tubing

WSI's proprietary welding process is especially designed for depositing weld overlay continuously around the outer diameter of the boiler tube as the tube is rotating. The weld metal deposit is produced by a fully automatic welding system with real-time digital readouts of major processing parameters to ensure constant welding parameters during the production run. This unique patent-pending tube overlay process involves pulse spray gas metal arc welding along with proprietary processing techniques to deposit a uniform weld overlay with unique microstructure and properties. In general, this welding process results in about 5 to 7% dilution in weld overlay chemistry. Typical overlay chemistry for the alloy 625 overlay tubing is shown in Table 1. Also tabulated in the table are chemical specifications for AWS ERNiCrMo-3 filler metal and ASTM B443 alloy 625 plate/sheet product for comparison. The overlay chemistry is within both AWS filler metal and ASTM plate/sheet product specifications for all the elements except Fe. Iron content in the overlay is only slightly higher than the specification limit because of some iron pick up from the substrate steel tube.

Tubes up to 45' (13.5 meters) in length are processed in production runs with excellent reproducibility in product quality. Tube diameters from 3/4" (19 mm) to 5" (127 mm) with wall thickness as thin as 0.100" (2.54 mm) can be processed on a routine production basis. Some of the most common tube sizes being processed are 2-1/2" (63.5 mm) and 3" (76 mm) OD.

The overlay produced by this unique proprietary process exhibits tremendous ductility. The overlay tubes in the as-overlaid condition can be cold bent at 180° routinely with a bend radius of 2D (2 times tube diameter) without cracking. A bend radius of as small as 1.5D can sometimes be performed in cold forming

successfully for some tubes. Figure 3 shows a cross-section of alloy 625 overlay tubing (2-1/2"OD x 0.265"wall SA210 A-1 internally ribbed carbon steel base tube) along with samples from the same overlay tube after flattening tests at room temperature with a bend radius being equal to 1/2 thickness of the tube wall. The middle sample, shown in Fig. 3, was as-overlaid and flattening tested, while the right-hand sample was as-overlaid, normalized at 900 C/20 min/air cool, and flattening tested. Normalizing at 900 C was to eliminate the residual tensile stresses in the overlay in the as-overlaid condition. The properties and microstructures of this unique alloy 625 overlay tubing are described in detail elsewhere (1)

Table 2. Typical 625 overlay chemical composition (wt.%)* of the alloy 625 overlay tubing.

	<u>Ni</u>	<u>Cr</u>	<u>Mo</u>	<u>Nb**</u>	<u>Fe</u>	<u>Ti</u>	<u>Al</u>	<u>C</u>
625 Overlay*	61.1	20.6	8.3	3.3	5.8	0.3	0.2	0.02
AWS-SFA5.14‡	58.0+	20.0-	8.0-	3.15-	5.0	0.4	0.4	0.10
ERNiCrMo-3		23.0	10.0	4.15				
ASTM B443‡	58.0+	20.0-	8.0-	3.15-	5.0	0.4	0.10	
625 plate/sheet		23.0	10.0	4.15				

* Overlay chemical composition was analyzed on overlay surfaces after grinding off 20 mils (0.5 mm) or less from the surface.

** Plus Ta

‡ Single values are maximum, + means minimum values

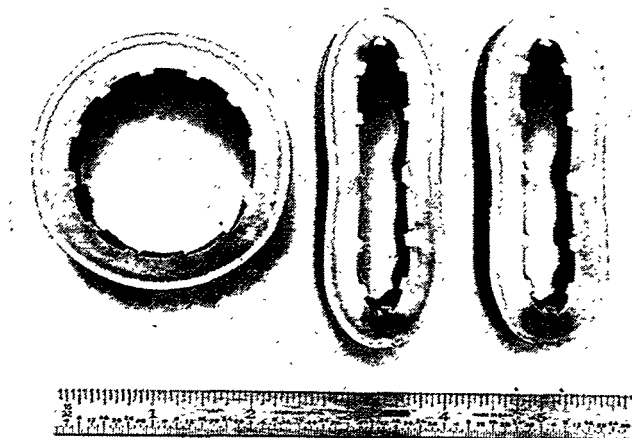


Fig. 3. Cross-sections of alloy 625 overlay tube samples in the as-overlaid condition (left-hand sample), and two flattening tested samples. The middle sample was as-overlaid and flattened while the right-hand sample was overlaid, normalized at 900 C (1650 F)/20 min/air cool and flattened.

3 ASME & NBIC Requirements

The boilers are normally constructed to the American Society of Mechanical Engineers (ASME) Section VIII Code requirements. Any repairs and alterations of pressure-retaining components, such as boiler tubes, are permitted by the National Board Inspection Code (NBIC) under specific conditions. These conditions are highlighted in the NBIC; and the contractor who performs the welding work requires to hold a valid "R" certificate issued by NBIC. In addition, NBIC allows for repairs of wasted areas by welding, provided the procedures and the personnel who perform the work are qualified in accordance with ASME Section IX.

When the boiler tube wall is corroded to below the minimum wall thickness allowed by the ASME Code, the Code allows the subject area(s) to be restored to the required thickness by using weld metal buildup with a filler metal composition matching that of the boiler tube. This can, then, be followed by applying a corrosion-resistant weld overlay for corrosion protection.

4 Boiler Tube Protection and Life Extension

4.1 Waste-To-Energy Boilers

Municipal waste contains corrosive constituents and impurities, such as chlorine, sulfur, sodium, potassium, zinc, lead, and others. During combustion of this fuel at temperatures in excess of 1200 C, vapors of corrosive compounds, such as, chlorides, sulfates, HCl and SO₂, are formed in the combustion zone. Chloride and sulfate vapors, along with ash and slag, condense and deposit on cooler surfaces, such as waterwalls surrounding the combustion zone as well as superheaters, reheaters and the generating bank in the convection zone. The corrosion problems for waterwalls and superheater tubes are very well documented in the literature. (2-6) Corrosion takes place on the outer diameter of the tube exposing to the combustion gas, thus often being referred to as "fireside" corrosion as opposed to the water or steam side corrosion in the internal diameter of the tube. Wastage rates of 50-80 mpy (mils per year), or 1.3-2.0 mm/yr, have been observed for carbon steel waterwall tubes. It is now generally agreed by researchers and materials engineers in the waste-to-energy boiler industry that chloride attack by chloride deposits and gaseous HCl is mainly responsible for the wastage (corrosion) of waterwall boiler tubes.

In 1984, WSI pioneered the field overlay welding of alloy 625 (Ni-21.5Cr-9Mo-3.7Nb alloy) to the waterwall of a waste-to-energy boiler in Lawrence, MA. The alloy 625 overlay had proven to be so successful against fireside corrosion that approximately 280,000 lbs (127,000 kg) of alloy 625 weld metal had been applied by WSI by 1990 for 15 waste-to-energy plants. (7) A list of those plants

is shown in Table 2. Today, alloy 625 overlay continues to play a very significant role in managing the corrosion and erosion problems in waste-to-energy boilers. Up to date approximately 800,000 lbs (363,000 kg) of alloy 625 overlays have been applied by WSI in waste-to-energy boilers in the U.S. In Europe, weld overlay approach is increasingly becoming acceptable as a reliable, long-term solution to corrosion/erosion problems in waste-to-energy boilers. Welding Services Europe has applied alloy 625 overlays to many boilers in such countries as the Netherlands, United Kingdom, Germany and France.

Table 3. Alloy 625 weld overlay jobs performed by WSI up to 1990 on waterwalls in waste-to-energy boilers in the U. S.

<u>Location</u>	<u>No. of Boilers</u>	<u>Alloy 625 Overlay, kg (lbs)</u>
Hartford, CT	3	25,302 (55,780)
Detroit, MI	3	29,312 (64,620)
Ewa Beach, HI	2	21,920 (48,324)
Poughkeepsie, NY	2	1,222 (2,695)
Biddeford, ME	2	3,887 (8,570)
Portsmouth, VA	4	6,635 (14,627)
Niagara Falls, NY	2	11,703 (25,800)
West Palm Beach, FL	2	1,219 (2,687)
Orrington, ME	2	4,672 (10,300)
Rochester, MA	2	4,401 (9,702)
Rochester, NY	1	454 (1,000)
Oxford, NJ	1	879 (1,938)
Lawrence, MA	1	9,526 (21,000)
Barberton, OH	1	680 (1,500)
Islip, NY	2	5,262 (11,600)

Superheater tube failures with less than two years of service due to accelerated wastage have also been frequently encountered. Tube shields made of austenitic alloys, such as, Type 310 SS, 309 SS, etc., have also been used to mechanically attach to the tubes to mitigate the corrosion/erosion problems. The problem with this approach is that the shields tend to be overheated and then suffer sulfidation/chloride attack, resulting in premature failure. Furthermore, using a mechanical means to fasten the shields to the tubes also presents a reliability problem. Application of a corrosion/erosion-resistant overlay on carbon steel or Cr-Mo superheater tubes provides a more "permanent" solution. Alloy 625 overlay tubing has been used successfully in superheaters, generating banks and other areas. Approximately 50,000 linear feet (15,000 meters) of alloy 625 overlay tubes were supplied to different waste-to-energy plants in 1997. Figure 4 shows alloy 625 overlay tubes used as superheater tubes in a waste-to-energy plant in the Netherlands.

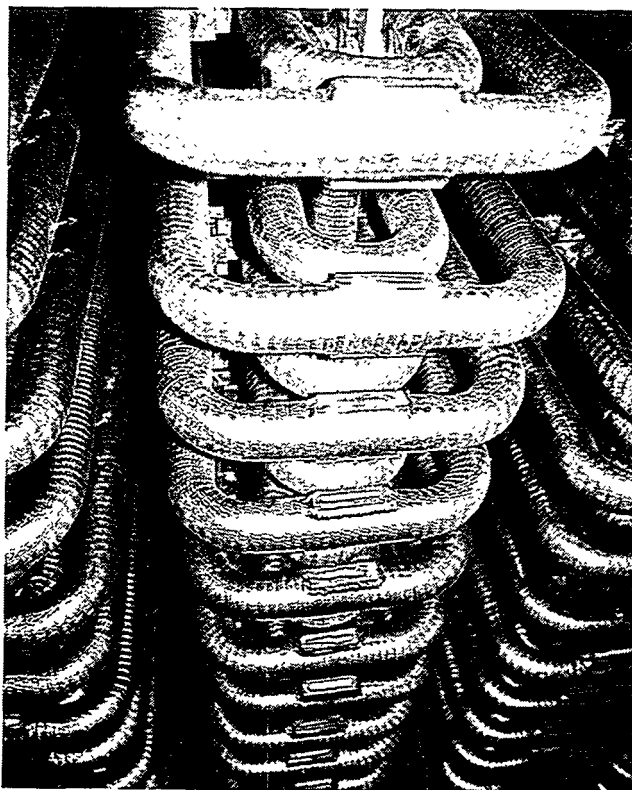


Fig. 4. Alloy 625 overlay tubes used as superheater tubes in a waste-to-energy plant in the Netherlands.

4.2 Coal-Fired Boilers

Recent installation of low NO_x burners in pulverized coal-fired boilers has resulted in accelerated boiler tube wastage. Wastage rates of 50-60 mpy (1.3-1.5 mm/yr) on carbon steel and Cr-Mo steel waterwalls have been observed. It is believed that the accelerated wastage was attributed to the formation of reducing environments which resulted in sulfidation attack. (8-10) The weld overlay approach has proved to be very successful in solving boiler tube wastage problems in these boilers. In a Midwest supercritical coal-fired boiler, the carbon steel waterwall has been suffering a wastage rate of 25- 35 mpy (0.6-0.9 mm/yr). A section of the waterwall, where the wastage was the worst, was weld overlaid with alloy 625 in 1991. Recent inspection of the overlay area revealed that the weld beads were still visible with no evidence of corrosion attack or cracking after six years of operation. In another supercritical unit, the waterwalls suffered wastage rates of more than 50 mpy (1.3 mm/yr) on the sidewalls after installing low NO_x burners. An area was weld overlaid with type 309 stainless steel for testing. After 18 months of operation, type 309 SS weld beads were still clearly visible when the overlay area was inspected, showing no evidence of corrosion attack or cracking.

To further illustrate the excellent performance capability of the Unifuse overlay, a case of type 309 SS overlay applied to 1-1/4Cr-1/2Mo (SA213-T11) waterwall in the wall blower region after service for about seven years in a supercritical unit with low NO_x burners is illustrated here. Prior to the application of the weld overlay, bare SA213-T11 boiler tubes lasted for only about 18 months with approximately 80-90 mpy (2.0-2.3 mm/yr) of wastage rates. The wastage was the result of erosion/corrosion due to sootblowing. The outer tube metal temperature was estimated to be in the range of 800 to 900 F (427-482 C). After seven years of operation, the weld beads of type 309 overlay were still visible, with no evidence of corrosion attack. Furthermore, no thermal fatigue cracking was observed at either the overlay surface or the interface between the overlay and the substrate steel. More and more utility coal-fired boilers are relying on either type 309 SS or alloy 625 overlays for waterwall protection against corrosion attack under low NO_x combustion conditions. Table 4 shows a partial list of the overlay jobs performed by WSI up to 1997 on the coal-fired boilers in the U.S.

Table 4. Partial listing of coal-fired boilers with waterwalls overlaid by WSI.

<u>State</u>	<u>Plant/Boiler</u>	<u>Overlay Area m²(ft²)</u>	<u>Alloy</u>	<u>Date Performed</u>
Alabama	"A"	93 (1000)	309	2/94
Florida	"A"	37 (400)	309	3/95
	"B"	47 (500)	309	6/96
Georgia	"A"	65 (700)	309	4/93
	"B"	93 (1000)	309	12/94
	"C"	28 (300)	309	9/96
Illinois	"A"	47 (500)	625	10/93
Indiana	"A"	93 (1000)	309	10/94
	"B"	93 (1000)	309	10/94
	"C"	465 (5000)	625	3/96
	"D"	79 (850)	625	5/96
	"E"	930 (10000)	625	10/96
Maryland	"A"	47 (500)	309	10/93
	"B"	47 (500)	309	10/96
New Jersey	"A"	149 (1600)	625	5/96
Ohio	"A"	93 (1000)	309	10/96
Pennsylvania	"A"	47 (500)	622	9/87
	"B"	56 (600)	625	9/95
	"C"	595 (6400)	625	10/95
	"D"	470 (5000)	309	11/95
	"E"	84 (900)	625	3/96
	"F"	140 (1500)	625	5/96
	"G"	930 (10000)	625	9/96
	"H"	140 (1500)	625	3/97

4.3 Kraft Recovery Boilers

The recovery boiler in pulp and paper mills is used to recover chemicals from spent cooking liquor. Black liquor coming from spent liquor, discharged from digesters and followed by a series of evaporators to increase its concentrations, is fed into the boiler for combustion. The black liquor generally contains about 50% or more of organic solids and approximately 6% total sulfur in the form of Na_2SO_4 and $\text{Na}_2\text{S}_2\text{O}_3$, along with some NaCl . (11) Combustion takes place in reducing conditions, transforming sodium sulfate to sodium sulfide and forming sodium carbonate. Organic compounds are burned to generate steam for various processing applications within the mill. The combustion heat melts the inorganic solids, such as, sodium sulfide, sodium hydroxide, sodium carbonate, sodium sulfate, thiosulfate, sodium chloride and others. This melted material (smelt) stays in the furnace bed. The furnace is constructed with waterwall tubes in the furnace floor as well as on the sidewalls. The furnace floor tubes are covered with a layer of solidified smelt, which protects the tubes quite well under normal conditions. However, corrosion of carbon steel can still be a problem. Thus, co-extruded composite tubes with austenitic stainless steels, such as, 304L, as an outer tube cladding, have been used for floor tubes in many recovery boilers. Many of these composite floor tubes have suffered severe cracking in recent years. Singbeil, et al. (12) provided an excellent review on the cracking of the 304L cladding, concluding that the mechanism of cracking to be a form of environmentally assisted cracking. Alloy 625, known to be highly resistant to environmentally assisted cracking and to thermal fatigue cracking, is a potentially excellent candidate overlay for floor tube applications. WSI's unique alloy 625 overlay tubing offers a potential solution to the composite tube cracking problems. Initial experience and performance of these alloy 625 overlay tubes for recovery boiler floor tubes and smelt openings are extremely encouraging. These applications as floor tubes and smelt openings, which are summarized in Table 5, have shown no cracking or other degradation since installations.

Table 5. Some of the applications of alloy 625 overlay tubes as floor tubes and smelt openings in recovery boilers in the U.S., Canada and South America.

<u>Mill Location</u>	<u>Application Description</u>	<u>Year Performed</u>
South	One floor panel made with 625 overlay tubes	1995
Canada	Half a floor made with 625 overlay tubes	1996
Southeast	Floor membranes overlaid with alloy 625	1995
South	One 625 overlay tube in a smelt spout wall	1994
Canada	Smelt opening	1987
Southeast	Smelt opening	1994
South America	Smelt opening	1996

For waterwall tubes in the lower part of the furnace above the smelt bed, corrosion is primarily due to sulfidation. (13). Wastage rates of carbon steel tubes have been reported to be 8-32 mpy (0.2-0.8 mm/yr). (14) Application of type 309 SS weld overlay has been very successful in protecting the carbon steel waterwalls above the smelt bed against sulfidation attack. There have been approximately seven boilers in the U.S. with type 309L SS overlays applied by WSI that have had more than one year of operation. These boilers include one in Midwest since 1989, two in South since 1995 and 1996, respectively, and four boilers in Southeast since 1995 for one boiler and the rest since 1996.

5 Summary

Weld overlay technology, particularly the Unifuse overlay technology developed by Welding Services Inc., has been used successfully in protecting industrial and utility boilers against corrosion and/or erosion. The technology is briefly described. Successful applications of this technology in mitigating corrosion/erosion problems in waste-to-energy boilers, coal-fired boilers with low NO_x burners, and kraft recovery boilers are summarized. Some of the successful weld overlay alloys used by WSI in solving corrosion/erosion problems in the aforementioned systems are highlighted. Field overlay or shop-fabricated overlay panels using alloy 625 has been extremely successful in protecting waterwalls in waste-to-energy boilers. Also successful in waste-to-energy boilers is the use of alloy 625 overlay tubing in superheaters and generating banks, and also as screen tubes. Both alloy 625 and type 309 SS have been used for weld overlays of waterwalls successfully to resist sulfidation attack in low NO_x combustion conditions in pulverized coal-fired boilers. Also successful in initial trials in kraft recovery boilers are alloy 625 overlay floor tubes and smelt openings. This unique alloy 625 overlay tubing may provide a potential solution to the current type 304L composite floor tube cracking problems in kraft recovery boilers. For corrosion protection in lower furnace waterwalls above the smelt bed, field overlay with type 309 SS has been proven to provide satisfactory performance in kraft recovery boilers.

6 References

1. G. Lai, M. Jirinec and P. Hulsizer, "The Properties & Characteristics of Unifuse 625 Overlay Tubing for Recovery Boiler Floor Application", to be presented in the 1998 TAPPI Engineering Conference, Sept. 14-17, 1998, Miami, FL, and will be published in the conference proceedings.
2. G. Y. Lai and G. Sorrel, Eds., Materials Performance in Waste Incineration Systems, NACE International, Houston, TX, 1992.
3. E. Haggblom and J. Mayrhuber, in High Temperature Materials for Power

Engineering 1990, Part I, E. Bachelet, et al. Eds., Kluwer Academic Publishers, Dordrecht, 1990, p. 91.

4. H. H. Krause and I. G. Wright, Paper No. 561, Corrosion/95, NACE International, Houston, TX.

5. I. G. Wright, H. H. Krause and R. B. Dooley, Paper No. 562, Corrosion/95, NACE International, Houston, TX.

6. J. L. Blough, G. J. Stanko, W. T. Bakker and T. Steinbeck, in Heat-Resistant Materials II, K. Natesan, P. Ganesan and G. Lai, Eds., ASM International, Materials Park, OH, 1995, p. 645.

7. P. N. Hulsizer, Paper No. 246, Corrosion/91, NACE, Houston, TX.

8. S. F. Chou, P. L. Daniel and D. Eskinazi, "Fire-Side Corrosion in Low NOx Combustion Systems," EPRI/EPA Joint Symposium on Stationary Combustion, RDTPA 85-36, Boston, MA, May 1985.

9. S. C. Kung and L. D. Paul, Paper No. 65, Corrosion/91, NACE, Houston, TX.

10. S. C. Kung and C. F. Eckhart, Paper No. 242, Corrosion/93, NACE, Houston, TX.

11. "Corrosion in the Recovery Boiler", in Metals Handbook, Ninth Edition, Vol. 13. Corrosion, ASM International, Materials Park, OH, 1987, p. 1198.

12. D. Singbeil and R. Prescott, J. Keiser, and R. Swindeman, in the 1997 TAPPI Engineering & Papermaking Conference Proceedings, TAPPI Press, Atlanta, GA, 1997, p.1001.

13. W. B. A. Sharp, in 7th International Symposium on Corrosion, TAPPI Proceedings, p. 23.

14. D. F. Bowers, in Pulp and Paper, Vol. 61, No. 7, 1987, p. 118.

Failure Analyses and Weld Repair of Boiler Feed Water Pumps

R. van Vulpen, Welding Engineer

Kema Power Generation

Arnhem, The Netherlands

Abstract

During a regular inspection of the Boiler Auxiliaries at one of the Dutch Electricity Production Companies serious cracks were found in the cover and casings of the feed water circulation pumps in two units after 108.000 and 122.000 hours of boiler operation. Kema Laboratories carried out Failure analyses on boat samples at the cracked areas. Corrosion fatigue cracking was found on the inner side of the GS-24CrNiMo325 casing. Shop Weld repairs were carried out using a newly developed mechanized Plasma Welding Technique. The repaired feed water circulation pumps showed no problems after several years of operation. The costs of repair were substantially lower than the costs of replacement.

1. Introduction

During plant scheduled shut down of a 180MW Gas Fired Unit for electricity production one of the two feed water circulation pumps was visually inspected after 122.000 hours of boiler operation. It was planned to run the unit for at least 3 years more. The Boiler is a Benson circulation type and was in service since 1968. A large number of cracks were found at the inside of the pump cover and casing. The pumps were fabricated from the 3/4Cr-1/2Ni-1/2Mo casting steel GS-24CrNiMo325. The casing outside diameter is about 700 mm with a wall thickness of about 70mm. The service temperature of the water varies with a maximum estimated deviation of 225 °C.

According to the original pump manufacturer weld repair possibilities were very poor and it was advised to replace the casing. Because of plant availability the plant maintenance group decided to analyze the cause of the cracks and to identify the feasibility for weld repair. Boat samples were taken from the cracked areas and were microscopically examined. A dedicated repair shop was found to perform a weld repair.

2. Failure Analyses

Figure 1 shows the pump casing. The cracks were located at the inside surface of the cylindrical parts as well as on the inner radius. Penetrant Testing showed a large number of axial cracks at the cylindrical parts and circumferential cracks at the main part of the inner radius. Figure 2 shows the casing inside. Ultrasonic testing indicated that crack depth was not exceeding 10mm. The cover of the casing was penetrant tested also and showed a number of axial cracks at the corner of the sealing section.

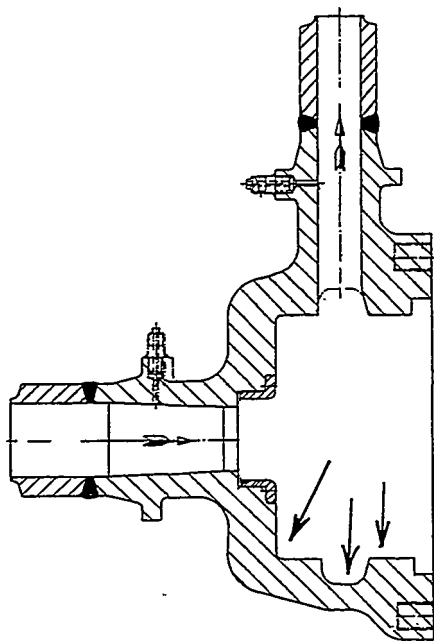


Figure 1. Crack locations at the pump casing inside.

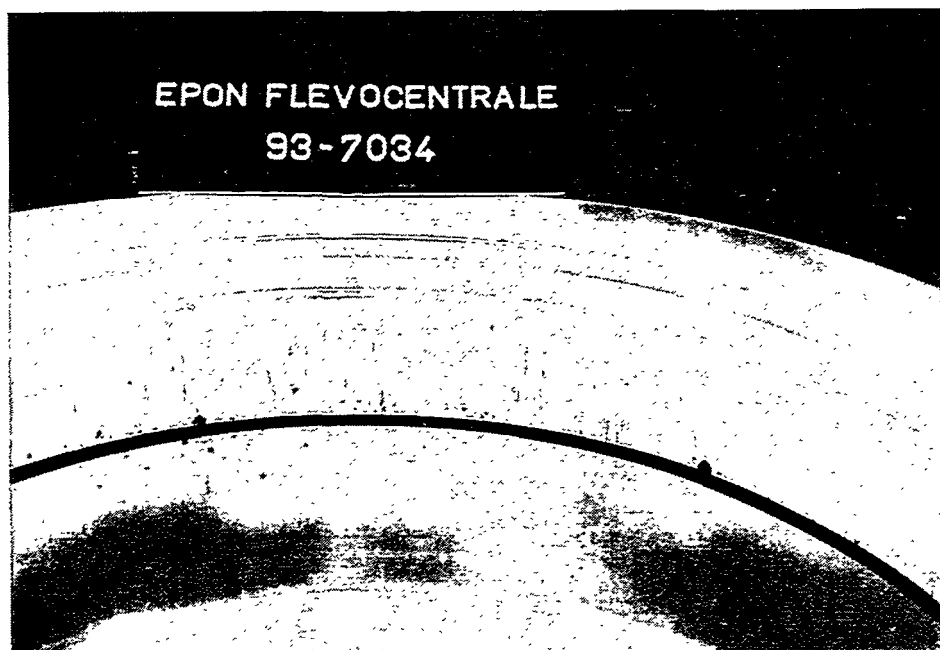


Figure 2. View of the cracked area of the pump casing after Penetrant Testing.

Two boat samples were taken at the inside of the casing. A small one at the tip of an axial crack to analyse the failure mechanism and an other one to analyse the actual chemical composition of the pump casing steel as an indicator for the weldability. Cross sections of the boat sample were microscopically examined and show multiple, mainly transgranular cracks, filled with oxides (see figure 3). The crack profiles are irregular. Small corrosion holes can be observed at certain stages of the cracks, which might indicate a larger shut down period. It has been recognised as corrosion fatigue, a type of stress corrosion cracking, due to strains generated by large thermal variations of the boiler water.

Due to this type of service induced failure the other circulation pumps became suspicious, and resulted in actions to inspect the second circulation pump of this unit and at a later stage two identical circulation pumps from the second 180MW unit as well. Damage was observed in all cases, however not at a higher level.

According to [1] and [2] the crack growth rate would be small and not lead to a detrimental situation in this case within 3 years of operation, and Leak Before Break is expected. However, for plant availability reasons it was decided to have one of the two circulation pumps per unit in optimal condition. When leakage might occur, the boiler still can continue to operate. The feasibility for a Weld Repair in the next major plant outage was studied.

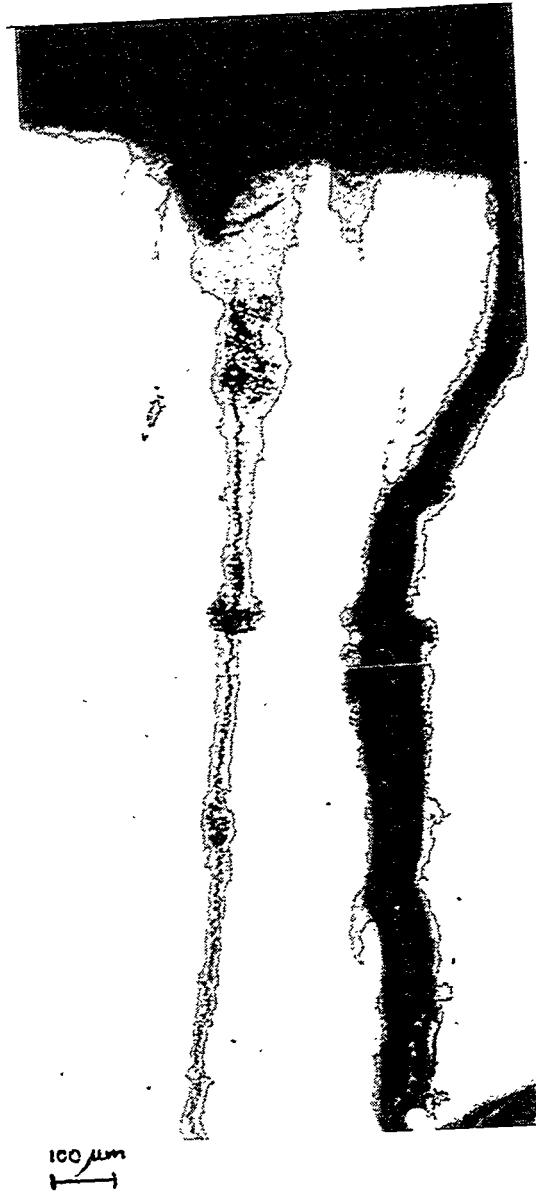


Figure 3. Microscopic view of the cracks in the pump casing.

3. Weld Repair

To identify the actual weldability of the pump casing material the chemical composition was analysed. The results are shown in table 1 and confirmed that the casting steel is of the type GS-24CrNiMo325 according to the material sheet VdTUV 252

Table 1. Results of the chemical analyses of the pump casing.

		Weight %							
		C	Si	Mn	P	S	Cr	Mo	Ni
Pump Casing		0.25	0.34	0.72	0.022	0.009	0.85	0.35	0.48
VdTUV 252	Min.	0.20					0.7	0.4	0.4
	Max.	0.28	0.50	0.90	0.035	0.025	1.0	0.6	0.6

3.1 Weldability

To minimise the risk of cold cracking and eliminate high hardness values after weld repair of the pump casing, Preheat and Post Weld Heat Treatment conditions were estimated. Based on the actual chemical composition as listed in table 1 the maximum hardness was predicted. It was estimated according to [3] that an acceptable As Welded hardness level of 350 HV could be established by welding with parameters (Heat Input and Preheat Temperature) which realise a cooling time of about 50 seconds between 800 and 500°C (see figure 4). Using a Heat Input of about 13 kJ/cm this cooling time was translated to a recommended Preheat Temperature of at least 300°C (see figure 5). Stress relieving is required according to the material sheet VdTUV 252. The Post Weld Heat Treatment Temperature should be within the range of 660-720°C, which might result in maximum hardness values of 260 HV. It was concluded that weld repair is metallurgically feasible.

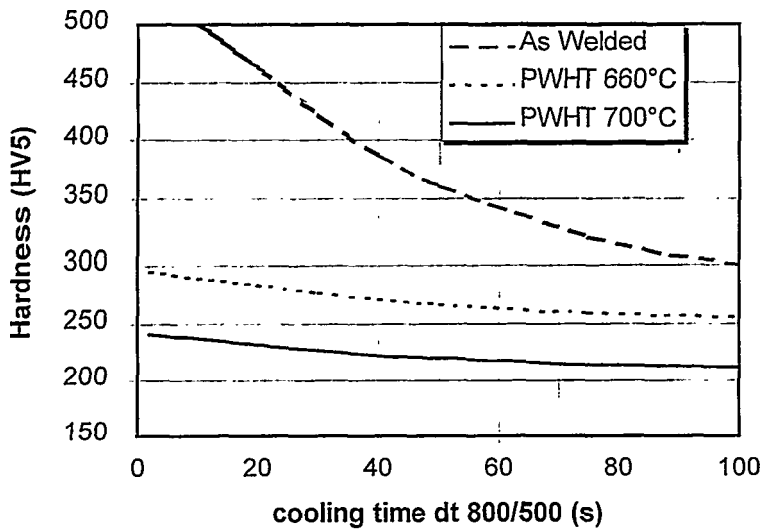


Figure 4. Maximum predicted HAZ hardness of GS-24CrNiMo325 [3].

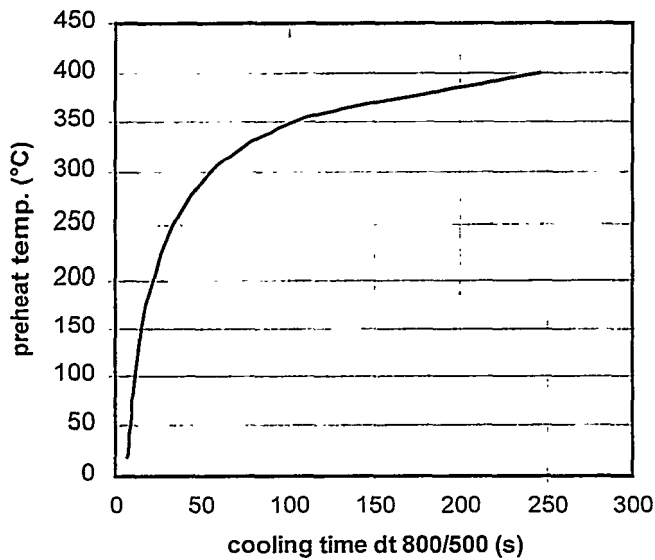


Figure 5. Recommended Preheat Temperatures related to weld cooling times.

3.2 Repair Procedure

Based on the above mentioned metallurgical recommendations a welding procedure was developed and performed in the next major plant outage. In co-operation with a weld repair shop the Plasma Arc Welding process was selected, because of excellent quality, available welding procedure qualification (ASME IX) and shop experiences. Before removing the damaged areas the pump casing was X-rayed and stress relieved to reduce the risk of unexpected bad sections. No severe porosity was found except for some local porosity at the casing outside. At the casing inside surface all cracks were removed by milling and checked by penetrant testing. To minimise unfavourable distortion the welding process was mechanised using a manipulator. So continuous welding in the horizontal position was realised. The creep resistant filler metal type CrMo2 (\varnothing 1.2mm) was selected. The casing was preheated in a furnace and maintained during welding at 340°C. The welding current was about 200 Amp. The welding head oscillated 15mm. The welding speed was about 175mm/min. Figure 6 shows the plasma-welding torch at the inside of the pump casing, welding several layers with a total thickness of about 10mm.

To minimise the risk of grain coarsening the maximum interpass temperature was maintained below 400°C. The local repairs at the casing outside were performed with the conventional Shielded Manual Arc Welding technique. A Post Weld Heat Treatment was carried out at 660-700°C for three hours holding time. The cooling rate was limited to 100°C/hr. After glass blasting the casing no defects were found at the penetrant testing X-ray examination. Final machining was performed and penetrant testing showed a successful weld repaired casing. In the same way the cover was successfully repaired. Hardness measurements showed acceptable levels of 180 HV for the base metal and 218 HV for the weld metal. Frequent shop surveillance prevented unnecessary failures and time delay.

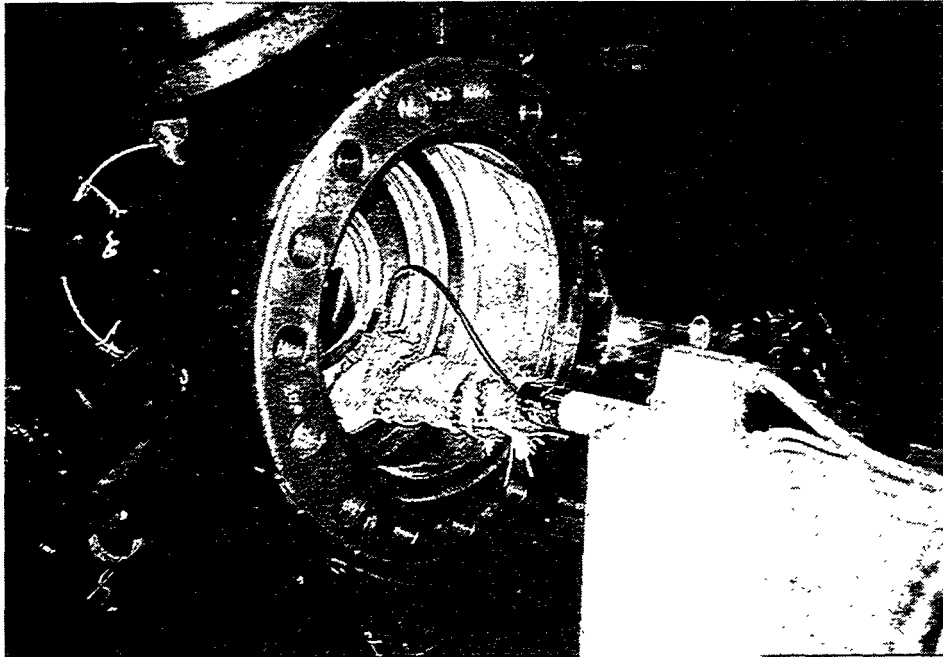


Figure 6. View of the Plasma Arc Weld repair process.

During a major outage of the second unit after 108,000 boiler operating hours one of the other circulation pumps was successfully repaired in the same way. After two and a half years of operation no problems occurred at the repaired feed water pumps. The weld repair delivery time and costs were beneficial compared to replacement. The costs of these weld repairs were about one third of the costs of replacement.

4. Conclusions

Corrosion fatigue damaged feed water circulation pumps of the casting steel GS-24CrNiMo325 have been successfully repaired by using a specially developed Plasma Arc Welding Procedure. The benefits of repair were substantially higher than of replacement.

References

- [1] T. Sakon, F. Masaharu, T. Sada, Residual life assessment of pump casing considering thermal fatigue crack propagation. Thermomechanical fatigue behavior of material, STP 1186, H. Sehitoglu, American Society for testing and materials, Philadelphia, 1993, pp239-252
- [2] T. Endo, Progress in life assessment and design methodology for fossil power plant components. Int. J. Pres. Ves. & Piping 57 (1994) 7-20.
- [3] M. Okumura, N. Yurioka, T.Kasuya, H.J. Cotton. Prediction of HAZ hardness after PWHT.

Published by



Vuorimiehentie 5, P.O.Box 2000, FIN-02044 VTT, Finland Series title and number
Phone internat. +358 9 4561
Fax +358 9 456 4374

VTT Symposium 184

Author(s) Seija Hietanen and Pertti Auerkari (eds.)			
Title BALTICA IV Plant Maintenance for Managing Life & Performance Vol. 1			
Abstract BALTICA IV International Conference on Plant Maintenance Managing Life & Performance held on September 7-9, 1998 on board M/S Silja Symphony on its cruise between Helsinki-Stockholm and at Aavaranta in Kirkkonummi. The BALTICA IV conference provides a forum for the transfer of technology from applied research to practice. This is one of the two volumes of the proceedings of the BALTICA IV International Conference on Plant Maintenance Managing Life & Performance. The BALTICA IV conference focuses on new technology, recent experience and applications of condition and life management, and on improvements in maintenance strategies for safe and economical operation of power plants.			
Keywords power plants, maintenance, boilers, turbines, condition monitoring, life management, evaluation, performance			
Activity unit VTT Manufacturing Technology, Operational Reliability Kemistintie 3, P.O.Box 1704, FIN-02044 VTT, Finland			
ISBN 951-38-4577-X		Project number	
Date September 1998	Language English	Pages 340 p.	Price K
Name of project Baltica IV		Commissioned by Commission of the European Communities CEC	
Series title and ISSN VTT Symposium 0357-9387		Sold by VTT Information Service P.O.Box 2000, FIN-02044 VTT, Finland Phone internat. +358 9 456 4404 Fax +358 9 456 4374	

VTT SYMPOSIUM

- 166 Väsytymismitoitus 1996. Hämeenlinna, 29. - 30.5.1996. Toim. Asko Kähönen & Eila Moring. Espoo 1996. 319 s.
- 167 Selection and Safety Criteria of Probiotics. 1st Workshop. FAIR CT96-1028, PROBDEMO. Helsinki, Finland, 15 November 1996. Ed. by Minna Alander & Tiina Mattila-Sandholm. Espoo 1996. 55 p.
- 168 Integrated numerical and experimental methods in ship design. Espoo, Finland, 27 March, 1996. Ed. by Antti Rantanen. Espoo 1996. 141 p.
- 169 SIHTI 2. Energia- ja ympäristöteknologia. Tutkimusohjelman vuosikirja 1995. Projektiesittelyt. Toim. Maija Korhonen & Rabbe Thun. Espoo 1997. 564 s. + liitt. 29 s.
- 170 SIHTI 2. Energia- ja ympäristöteknologia. Tutkimusohjelman vuosikirja 1996. Projektiesittelyt. Toim. Maija Korhonen & Rabbe Thun. Espoo 1997. 346 s. + liitt. 6 s.
- 171 COMADEM '97. 10th International Congress and Exhibition on Condition Monitoring and Diagnostic Engineering Management. Vol. 1. Espoo, Finland, 9 - 11 June, 1997. Ed. by Erkki Jantunen. Espoo 1997. 553 p.
- 172 COMADEM '97. 10th International Congress and Exhibition on Condition Monitoring and Diagnostic Engineering Management. Vol. 2. Espoo, Finland, 9 - 11 June, 1997. Ed. by Erkki Jantunen. Espoo 1997. 584 p.
- 173 Novel Methods for Probiotic Research. 2nd Workshop. Demonstration of the Nutritional Functionality of Probiotic Foods. FAIR CT96-1028, PROBDEMO. Cork, Ireland, 3 October 1997. Ed. by Minna Alander, Tiina Kauppila & Tiina Mattila-Sandholm. Espoo 1997. 70 p.
- 174 Moisture measurement in concrete constructions exposed to temperature and moisture variations. Nordic Mini-seminar of the Nordic Concrete Federation. Espoo, Finland 22.8.1997. Ed. by Heikki Kukko & Hemming Paroll. Espoo 1997. 118 p.
- 175 Käyttöturvamus kilpailutekijänä. Espoo, 18.11.1997. Toim. Kenneth Holmberg. Espoo 1997. 151 s.
- 176 Maritime Safety '97. Espoo, Finland, March 19, 1997. Ed. by Matti Hellevaara. Espoo 1997. 127 p.
- 177 Biotechnology in the food chain. New tools and applications for future foods. Helsinki, Finland, 28 - 30 January, 1998. Ed. by Kaisa Poutanen. Espoo 1997. 260 p.
- 178 Väsytymismitoitus 1997. Hämeenlinna, 15.9.1997. Toim. Asko Kähönen & Eila Moring. Espoo 1998. 136 s.
- 179 COST Action E5 Workshop on Fire Safety of Medium-Rise Timber Frame Residential Buildings. Espoo, Finland, June 2 - 3, 1997. Ed. by Monica Fernandez. Espoo 1998. 161 p.
- 180 COST 516 Tribology Symposium. Espoo, Finland, 14 - 15 May 1998. Ed. by Helena Ronkainen & Kenneth Holmberg. Espoo 1998. 457 p.
- 181 Fatigue design 1998. Vol. I. Espoo, Finland, 26 - 29 May, 1998. Ed. by Gary Marquis & Jussi Solin. Espoo 1998. 602 p.
- 182 Fatigue design 1998. Vol. II. Espoo, Finland, 26 - 29 May, 1998. Ed. by Gary Marquis & Jussi Solin. Espoo 1998. 274 p.
- 183 Euromicro Summer School on Mobile Computing '98. Oulu, Finland, August 20 - 21, 1998. Ed. by Tapio Seppänen. Espoo 1998. 189 p. + app. 4 p.
- 184 BALTICA IV. International Conference on Plant Maintenance Managing Life & Performance. Vol. 1. Helsinki-Stockholm-Helsinki, 7 - 9 September, 1998. Ed. by Seija Hietanen & Pertti Auerkari. Espoo 1998. 340 p.
- 185 BALTICA IV. International Conference on Plant Maintenance Managing Life & Performance. Vol. 2. Helsinki-Stockholm-Helsinki, 7 - 9 September, 1998. Ed. by Seija Hietanen & Pertti Auerkari. Espoo 1998. 307 p.